Investigation on Selectivity and Warhead Reactivity of Novel Cathepsin S Inhibitors

Dissertation

zur Erlangung des Grades

„Doktor der Naturwissenschaften (Dr. rer. nat.)“

im Promotionsfach Pharmazeutische und Medizinische Chemie

Fachbereich 09: Chemie, Pharmazie, Geographie und Geowissenschaften

der Johannes Gutenberg-Universität Mainz

Mergim Meta

geboren in Mainz

Submitted to the Faculty of Chemistry, Pharmacy, Geography, and Geoscience.

Dean: [redacted]

Name of the 1st reviewer: [redacted]

Name of the 2nd reviewer: [redacted]

Date of the doctoral examination: _____

Declaration of Authorship

I, Mergim Meta, declare that this thesis entitled, “Investigation on Selectivity and Warhead Reactivity of Novel Cathepsin S Inhibitors”, and the work presented in it are my own. I hereby declare that:

- I did this work entirely while in candidature for a research degree at this university.
- I have clearly stated which parts of this thesis have already been submitted for another degree or qualification at this university or other institutions.
- I always attributed clearly where I have consulted the published work of others.
- I always gave the source when I quoted from other works. Excluding those quotations, this thesis is entirely my work.
- I have acknowledged all primary sources of help.
- I have made clear exactly what was done by others and what I have contributed myself.

Place, Date: _____ Signature: _____

Für meine Familie

Acknowledgments

First and foremost, I am very grateful and wish to give a great thank you to my doctoral supervisor, [redacted] for giving me the opportunity of carrying out this doctoral thesis in her group. Her support and encouragement gave me the freedom to organize and plan my academic journey and prioritize my research effectively. She has been an invaluable mentor and played an important role in successfully completing this thesis; for that, I will always be thankful.

I owe [redacted] a large thank you, for all the fruitful and very interesting discussions which helped me tremendously in progressing during my PhD. I am very grateful for always cheering me up during difficult times and our joint supervision of the drug analysis lab course was always a pleasure.

I want to thank all my collaboration partners; I am indebted for their contributions to various projects. From the Organic Chemistry at Johannes Gutenberg-University I want to thank [redacted] and his co-workers [redacted] and [redacted], from the MPIP in Mainz, I thank [redacted] and her coworkers [redacted] and [redacted] and from the Universitätsmedizin in Mainz, [redacted] for the productive and fruitful collaboration during the Q5 project of the CRC1066. For the support in the warhead project, I want to thank [redacted] and [redacted] from the Institute of Physical and Theoretical Chemistry at the Julius-Maximilians-University of Wuerzburg for their contributions with quantum mechanics simulations and [redacted], [redacted], [redacted] and [redacted] from the Organic and Inorganic Chemistry Department at the University Jaume in Spain for helping to synthesize several inhibitors.

A special note of thanks goes to all colleagues and friends from the [redacted], firstly to [redacted], [redacted] and [redacted] who I had the opportunity of sharing a lab during the past years. There was always a good atmosphere, and I am grateful for the great time and productive conversations we had together! Special gratitude to [redacted] and [redacted] for their great support and helpful manner in scientific and organizational matters.

I want to thank my collaboration partners from the [redacted], without your help the great success in our projects would not have been possible. Therefore, I want to express my appreciation to [redacted] and [redacted] for the cooperation in the Q5 project and to [redacted] for the great teamwork in our catS project and the countless hours we spent together, debating on how to further improve our research. Special thanks to [redacted], [redacted], and [redacted] for the fruitful collaborative effort that guided us successfully through the warhead project and to [redacted] for being a great mentor and friend that helped and encouraged me at the beginning of this doctoral work.

To the students I had the privilege of supervising during my doctoral studies – [redacted] during his master thesis, [redacted] during their bachelor theses and [redacted], [redacted] and

[redacted] during their research modules – thank you for your great interest in learning new methods and your hard work. Your contributions were of great value for me and this thesis. Thank you for your support.

Finally, I want to express my greatest gratitude to my family and friends. The never-ending support, encouragement, and belief in me have been of great importance for me. Without this love and motivation, this thesis would not have been possible.

Again, from the bottom of my heart to every one of you: A big Thank You!

Table of Contents

Declaration of Authorship ..... **i**

Acknowledgments ..... **iv**

Table of Contents ..... **vi**

List of Abbreviations ..... **viii**

Abstract ..... **x**

Zusammenfassung ..... **xi**

1. Introduction **1**

1.1 Proteases in Drug Discovery 1

1.2 Cysteine Proteases 3

1.2.1 Catalytic Reaction of C1 Cysteine Proteases 3

1.2.2 Cysteine Cathepsins 6

1.2.3 Physiological Functions and Pathologic Involvement of CatS 7

1.2.4 CatS Binding Site and comparison with other cathepsins 12

1.2.5 Inhibitors of CatS 13

1.3 Protease-Inhibitor Interactions 19

1.3.1 Determining Affinity and Binding Mode of Reversible Binders 19

1.3.2 Covalent Enzyme Inhibition 21

1.3.3 Reversible vs Irreversible Binding 24

1.4 Nanocarrier-Mediated Delivery and Reversible Linker Strategies 29

2 Projects **32**

2.1 Project 1: Design and Functionalization of CatS-selective Inhibitors 32

2.2 Project 2: Reactivity and Selectivity of Protease Inhibitors with varying Warheads 33

3 List of Publications **35**

3.1 Publications as Part of this Doctoral Thesis 35

3.1.1 Project 1: Design and Functionalization of CatS-selective Inhibitors 35

3.1.2 Project 2: Reactivity and Selectivity of Protease Inhibitors with varying Warheads 35

3.2 Publications Beyond this Doctoral Thesis 35

3.2.1 Research Articles 35

3.2.2 Review Article 36

4 Project 1: Design and Functionalization of Cathepsin S-Selective Inhibitors 37

4.1 Subnanomolar Cathepsin S Inhibitors with High Selectivity: Optimizing Covalent Reversible α-Fluorovinylsulfones and α-Sulfonates as Potential Immunomodulators in Cancer 37

4.1.1 Context, Project Summary, and Own Contributions 37

4.1.2 Publication 38

4.2 Structural Modifications of Covalent Cathepsin S Inhibitors: Impact on Affinity, Selectivity, and Permeability 60

4.2.1 Context, Project Summary, and Own Contributions 60

4.2.2 Publication 62

5 Project 2: Reactivity and Selectivity of Protease Inhibitors with varying Warheads 108

5.1 Investigation of the Compatibility between Warheads and Peptidomimetic Sequences of Protease Inhibitors—A Comprehensive Reactivity and Selectivity Study 108

5.1.1 Context, Project Summary, and Own Contributions 108

5.1.2 Publication 110

6 Conclusions and Outlook 176

7 Bibliography 179

List of Abbreviations

[S]	substrate concentration
[I]	inhibtor concentration
ABP	activity-based probe
AMC	7-amino-4-methyl coumarin
APC	antigen presenting cells
Asp	aspartate
Blimp-1	B lymphocyte-induced maturation protein-1
c	concentration
catB	cathepsin B
catK	cathepsin K
catL	cathepsin L
catS	cathepsin S
CD	cluster of differentiation
CRC	collaborative research center
Cys	cysteine
DC	dendritic cells
DPPIV	dipeptidyl peptidase IV
EC	enzyme commission
ECM	extracellular matrix
EI	non-covalent enzyme inhibitor complex
EI*	covalent enzyme inhibitor complex
EPR	enhanced permeability and retention
ER	endoplasmatic reticulum
EWG	electron-withdrawing group
F	fluorescence intensity
FBDD	fragment-based drug design
FDA	U.S. Food and Drug Administration
FRET	Förster resonance energy transfer
GSH	glutathione
His	histidine
HPLC	high-pressure liquid chromatography
HTS	high throughput screening
HuR	human antigen R
I_a	allosteric inhibitor
IC_{50}	the concentration of inhibitor needed to reduce the enzyme activity by half

IF	induced fit
IFN	interferon
IL	interleukin
IRF-1	interferon regulatory factor 1
ISC	intersystem crossing
ISRE	IFN stimulating response element
K_d	dissociation constant/ binding affinity constant
K_i	inhibition constant
K_i^{app}	apparent K_i
K_M	Michaelis Menten constant
MDSC	myeloid-derived suppressor cells
MHC	major histocompatibility complex
MAPK/ ERK	Mitogen-activated protein kinase/ extracellular signal-regulated kinase
miRNA	micro-RNA
MMP	matrix metalloprotease
NBD	7-nitrobenz-2-oxa-1,3-diazol-4-amine
NHL	non-Hodgkin's Lymphoma
NMR	nuclear magnetic resonance
PDB	RASC Protein Data Bank
pNA	*p*-nitroanilide
PPAR-γ	peroxisome proliferator-activated receptor-γ
RIP-1	receptor interacting serine/threonine kinase 1
ROS	reactive oxygen species
SAR	structure affinity relationships
Ser	serine
TAM	tumor-associated macrophages
TCI	targeted covalent inhibitors
TFEB	transcription factor EB
TME	tumor microenvironment
TNF	tumor necrosis factor
Tregs	regulatory T cells
TTP	tristetraprolin
uPA	urokinase plasminogen activator
v	reaction rate/ turnover rate

Abstract

The resurgence of covalent drug development in various diseases since the beginning of the 21st century has led to the approval of several new agents, that interact with their target enzyme by forming a covalent bond. Nowadays most of these approvals are for kinase inhibitors in the targeted covalent inhibition strategy, but also proteases have shown to be attractive targets whose inhibition by covalent drugs is a promising strategy. After the successful drug development campaigns leading to the approval of several serine-, threonine- and metalloprotease-inhibitors, in 2021 the first drug targeting a cysteine protease has been approved by the U.S. Food and Drug Administration and the EMA. The covalent small molecule inhibitor nirmatrelvir targets the SARS-CoV-2 main protease with its mildly electrophilic nitrile warhead and has an emergency approval for the treatment of COVID-19 patients. This milestone reinitiated the development of potential cysteine-reactive inhibitors, since in many diseases, especially in several cancers, cysteine proteases like the human cathepsins play crucial roles. The successful downregulation of these cysteine proteases was demonstrated to be a powerful tool to counteract tumor growth. Especially cathepsin S seems to be involved in a plethora of different cancer types by altering the tumor microenvironment to promote conditions contributing to tumor growth and the inhibition of this protease promises to remodulate this immune-related microenvironment in many tumors towards an anti-tumor type.

In this work, several highly affine and selective cathepsin S inhibitors were designed, synthesized, and characterized. Enzyme kinetic analysis, molecular modeling and docking methods, and quantum mechanics calculations were used to help understand the binding modes and reaction mechanisms of the new inhibitors. Several new warheads against this protease were used for the development of the new inhibitors which resulted in a series of compounds with covalent reversible or irreversible binding modes. Reactivity studies of leucine as model amino acid decorated with these heterogenous warheads revealed preferred reactivities of specific warheads towards either ethanolate as a model for serine and threonine proteases or towards phenylethane thiolate as a cysteine protease model. Vinylsulfone and -sulfonate-based inhibitors together with 4-oxoenoates showed irreversible binding, whereas nitriles, several electron-deficient or electron-rich ketones and the fluorinated derivatives of the vinylsulfones and -sulfonates were found to reversibly inhibit cathepsin S. Additionally, high selectivity over several closely related cysteine proteases like cathepsins L and B but also over unrelated enzymes like the SARS-CoV-2 main protease or threonine and serine proteases as the human 20S proteasome and the urokinase-type plasminogen activator were retained. Especially the covalent-reversible inhibitors found during this work are promising due to the advantageous course of inhibition which is proven to lead to reduced off-target reactivity and toxicity. Two different approaches for further functionalizing the inhibitors with different linker systems were developed, by either using the warhead functionality as reversible linker position while simultaneously masking and protecting the electrophile, or by attaching the linkers on the P3-residue of the inhibitor.

Zusammenfassung

Das Wiederaufleben der Entwicklung kovalenter Wirkstoffe bei verschiedenen Krankheiten seit Beginn des 21. Jahrhunderts hat zur Zulassung mehrerer neuer Arzneimittel geführt. Die meisten dieser Zulassungen erfolgten für Kinase-Inhibitoren, aber auch Proteasen haben sich als attraktive Ziele erwiesen, deren Hemmung durch kovalente Wirkstoffe eine vielversprechende Strategie darstellt. Nach erfolgreichen Kampagnen, die zur Zulassung mehrerer Serin-, Threonin- und Metalloprotease-Inhibitoren führten, wurde 2021 das erste Medikament, das eine Cysteinprotease adressiert, von der US-amerikanischen *Food and Drug Administration* und der EMA zugelassen. Der kovalente Inhibitor Nirmatrelvir mit seinem elektrophilen Nitril hemmt die SARS-CoV-2 *main protease* und hat eine Notfallzulassung zur Behandlung von COVID-19-Patienten erhalten. Dies ist ein Meilenstein in der Entwicklung potenzieller cysteinreaktiver Inhibitoren, da bei vielen Krankheiten, insbesondere bei mehreren Krebsarten, Cysteinproteasen wie die humanen Cathepsine eine entscheidende Rolle für den Krankheitsverlauf spielen. Die erfolgreiche Herunterregulierung dieser Cathepsine erwies sich als wertvolles Werkzeug zur Bekämpfung des Tumorwachstums. Insbesondere Cathepsin S scheint an einer Vielzahl unterschiedlicher Krebsarten beteiligt zu sein, indem es das Tumormikromilieu verändert, was zum Tumorwachstum beitragen kann. Die Hemmung dieser Protease verspricht das immunologisch komplexe Mikromilieu so zu verändern, dass antitumoröse Bedingungen vorliegen.

In dieser Arbeit wurden mehrere hochaffine und selektive Cathepsin-S-Inhibitoren entworfen und charakterisiert. Enzymkinetik-Analysen, molekulare Docking-Methoden sowie Quantenmechanik-Berechnungen wurden verwendet, um die Bindemodi der neuen Inhibitoren zu untersuchen. Verschiedene *Warheads* wurden für die Entwicklung der neuen Inhibitoren verwendet, was zu einer Serie von Verbindungen mit unterschiedlichen Bindemodi führte. Reaktivitätsstudien mit Leucin als Modell-Aminosäure, die mit diesen heterogenen *Warheads* dekoriert wurden, zeigten bevorzugte Reaktivitäten entweder gegenüber Ethanolat oder Phenylethanthiolat als Modell für Serin- und Threonin- bzw. Cysteinproteasen. Vinylsulfon- und -sulfonat-basierte Inhibitoren und 4-Oxoenoate gingen irreversible Bindungen ein, während Nitrile, mehrere elektronenarme oder -reiche Ketone und die fluorierten Vinylsulfone und -sulfonate Cathepsin S reversibel hemmten. Darüber hinaus wurde eine hohe Selektivität gegenüber mehreren eng verwandten Cysteinproteasen wie den Cathepsinen L und B sowie gegenüber nicht verwandten Enzymen wie der SARS-CoV-2 *main protease* oder dem humanen 20S-Proteasom und dem *urokinase-type plasminogen activator* beibehalten. Insbesondere die kovalent-reversiblen Inhibitoren, die in dieser Arbeit gefunden wurden, sind aufgrund des vorteilhaften Inhibitionsmodus vielversprechend, der nachweislich zu einer Verringerung von *Off-Target*-Reaktivität und Toxizität führt. Zwei verschiedene Ansätze zur weiteren Funktionalisierung der Inhibitoren mit verschiedenen Linkersystemen wurden erprobt, durch Verwendung des *Warheads* als reversible Linkerstelle, um gleichzeitig das Elektrophil zu maskieren und zu schützen, oder durch Anbringen des Linkers an der P3-Position des Inhibitors.

1. Introduction

1.1 Proteases in Drug Discovery

Approximately 2% of the human genome code for the largest family of enzymes, namely the proteases.[1] These proteins catalyse the cleavage of other enzymes and polypeptides and regulate growth factors, cytokines, chemokines and cellular receptors leading to downstream intracellular signaling and gene regulation.[2,3] To date over 600 proteases are known and they can be divided into six classes, namely aspartate, cysteine, serine, metallo-, threonine and glutamate proteases depending on the hydrolysis mechanism inside the active site.[4] Initially perceived solely as resilient digestive enzymes, proteases play essential roles in various intricately controlled physiological mechanisms, such as development of the innate and adaptive immunity, cell cycle management, and apoptosis. It is evident that proteolysis constitutes a meticulously choreographed process in vivo, guaranteeing the precise cleavage of relevant substrates at specific times, sites, and within the appropriate cellular environments.[2] Upregulated and dysregulated proteolysis is associated with a variety of diseases, such as different cancers, inflammations, infectious and heart diseases.[5] This resulted in a constant interest in members of this enzyme class as a potentially attractive target for drug discovery.[6,7] The design and discovery of new modulators of proteases that selectively inhibit specific proteases is part of many medicinal chemistry campaigns.[8,9] Several successful drug discovery projects led to marketed drugs, some examples are angiotensin converting enzyme (ACE) inhibitors like captopril for the treatment of hypertonia, proteasome inhibitors as bortezomib for treatment of multiple myeloma or dipeptidyl peptidase IV (DPP-IV) inhibitors against type 2 diabetes.[10–12]

The classification of proteases is done according to the Enzyme Commission (EC) system as hydrolases (EC 3) more specifically peptidases (EC 3.4).[13] They can be further categorized as endopeptidases and exopeptidases. Endopeptidases cleave peptide bonds within a peptide chain, whereas exopeptidases either cleave bonds at the *C*-terminal end (carboxypeptidase) or at the *N*-terminal end (aminopeptidase). Additionally, proteases are classified based on the active site residue primarily responsible for catalysis, according to the EC and MEROPS systems (**Figure 1**).[14]

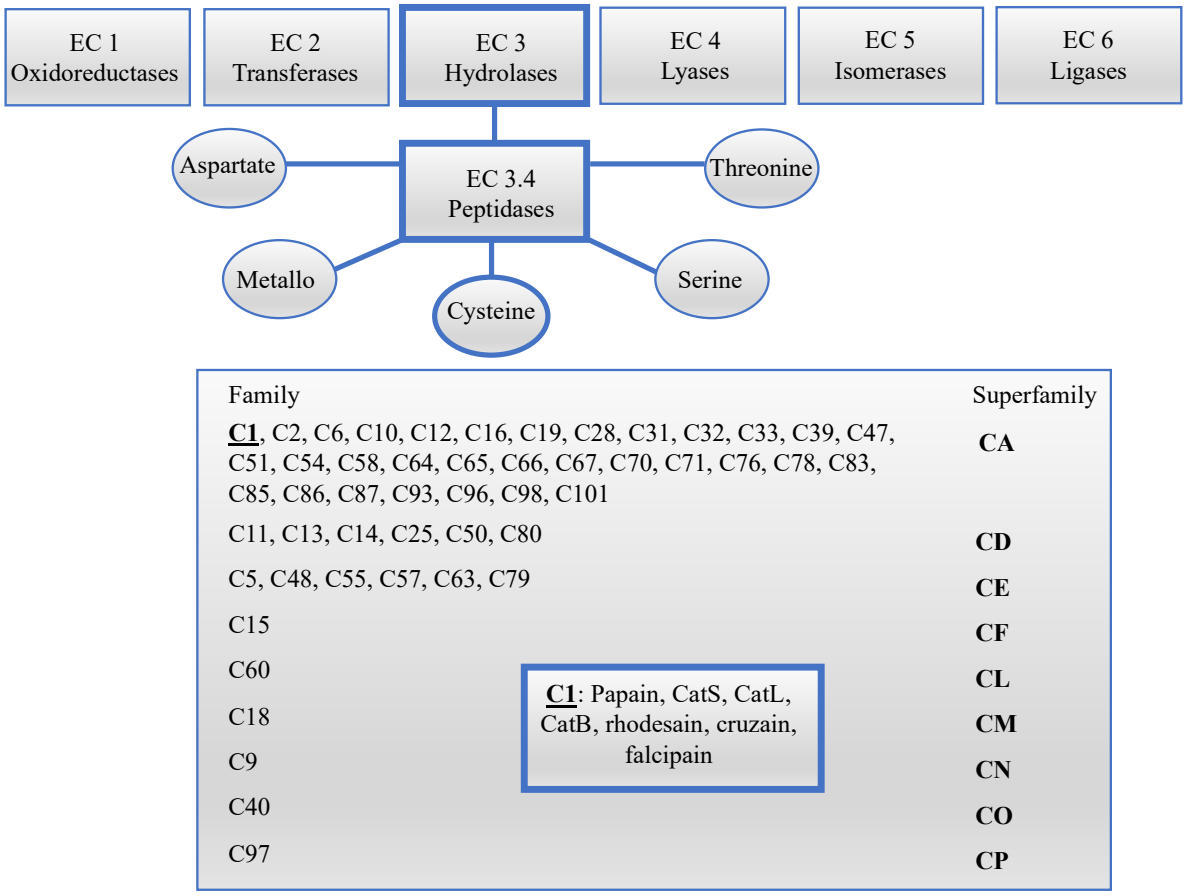

Figure 1: Classification of proteases according to the MEROPS and EC system.[14]

Three of the main classes are named after the amino acid which acts as a nucleophile in the active site of the corresponding enzyme, namely cysteine, serine, and threonine proteases. In the remaining two main classes (metallo and aspartate proteases) a water molecule functions as a nucleophile, since its nucleophilicity is enhanced by aspartate or a coordinated metal ion, respectively. Each class is further divided into superfamilies (clans) and families based on their evolutionary origin and their tertiary structure.[15]

The binding pockets of proteases can be labeled by the Schechter and Berger nomenclature according to the occupation of sub pockets by the amino acid side chains of substrates.[16] Approaching the *N*-terminus of the substrate from the cleavage site, the following residues are labeled P1 – Pn (non-primed site) and approaching the C-terminus, the residues are labeled P1' – Pn'.The corresponding pockets in the active site of a protease are labeled S1 – Sn and S1' – Sn', respectively (**Figure 2**).

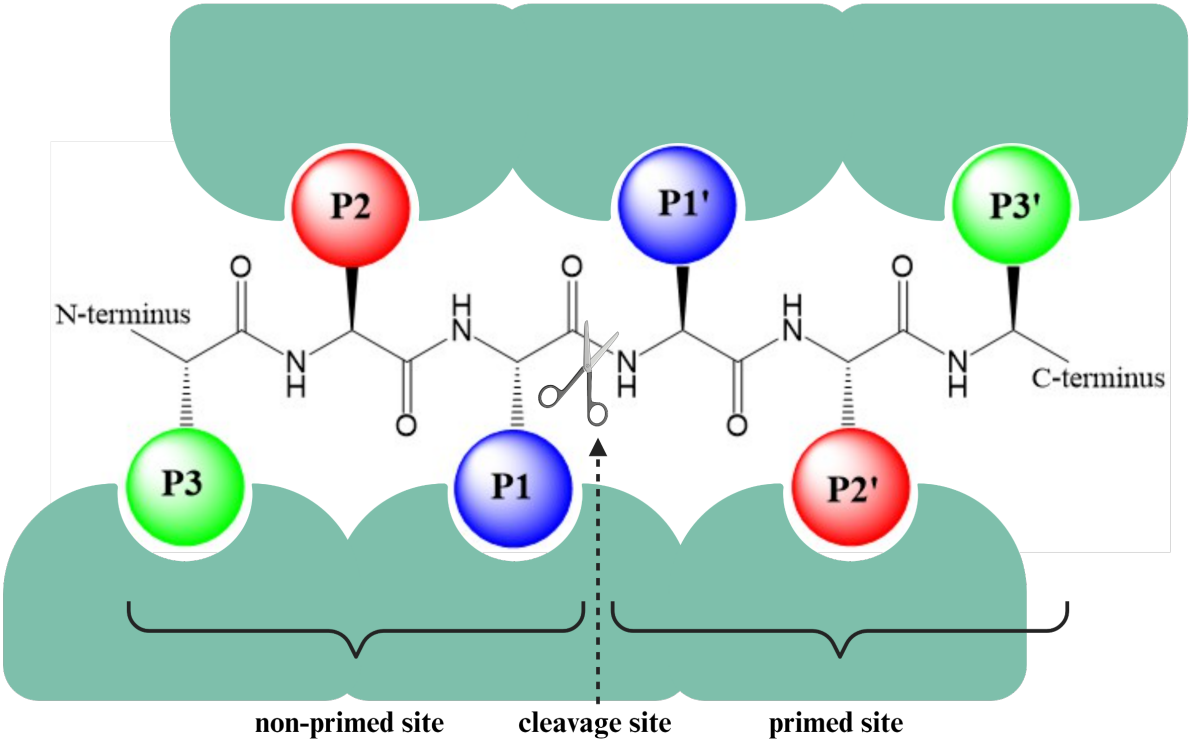

Figure 2: Illustration of the Schechter-Berger nomenclature used for substrate and protein active site labeling.[16] Created with Biorender.com.

1.2 Cysteine Proteases

1.2.1 Catalytic Reaction of C1 Cysteine Proteases

Enzymes belonging to the cysteine proteases, are encoded ubiquitously in viruses, bacteria, fungi, parasites, and mammals.[17] The three dimensional structures of most cysteine proteases have already been solved and in the protein data bank (pdb) there are over 50.000 entries for crystal structures of cysteine proteases.[18] As discussed in chapter 1.1 cysteine proteases are classified into nine clans and 69 families depending on their tertiary structure and evolutionary origin. Every protease in each superfamily contains a characteristic catalytic dyad (histidine, cysteine) or triad (histidine, cysteine, asparagine), but differs in the protein fold, and therefore emerged from convergent evolution of the catalytic mechanism.[19] The process of peptide cleavage orchestrated by cysteine proteases has undergone extensive scrutiny both through experimental and computational means (**Figure 3**).[20–25]

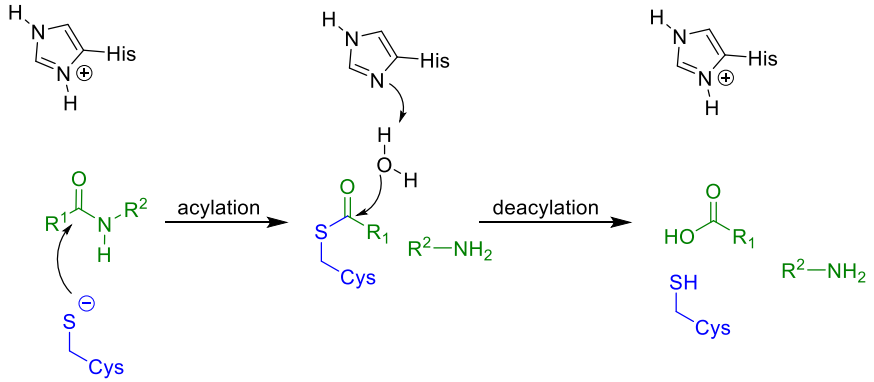

Figure 3: Peptide bond hydrolysis inside the active site of cysteine proteases (catalytic dyad consisting of histidine, His and cysteine, Cys).

The nucleophilicity of the cysteine residue in the active site of the protease is enhanced by the environment inside the pocket, involving a basic histidine residue which acts as a proton acceptor (catalytic dyad). The resulting ion pair consists of a highly nucleophilic and negatively charged thiolate and a positively charged imidazolium ion.[26] For clan CA cysteine proteases, the prevailing understanding leans towards the ion-pair mechanism, a concept supported by empirical data and computational research. Experimental validation of the ionic ground state was achieved through potentiometric assessments of ionization states at the active site of papain and corroborated by QM/MM studies indicating a strong preference for the ionic state within the enzymatic milieu.[23,27] In the majority of clan CA cysteine proteases, proper histidine orientation is secured via hydrogen bonding involving an asparagine or aspartate residue, constituting a catalytic triad crucial for maintaining the ion pair ground state.[21] Additional factors implicated in ion-pair stabilization include the dipole moment from nearby α-helices and a complex hydrogen bond network within the enzyme's active site environment.[20,28,29] Mechanistically, the hydrolysis of peptide bonds by cysteine proteases entails two principal stages: acylation and deacylation (**Figure 3**). During acylation, the cysteine thiolate executes a nucleophilic attack on the carbonyl carbon of the peptide bond, leading to the formation of an acyl-enzyme intermediate. Subsequently, deacylation ensues through a base-catalyzed reaction. The imidazole nitrogen of the catalytic histidine activates a water molecule, which then attacks the carbonyl carbon of the thioester intermediate, resulting in the production of the final cleavage products.

The more detailed mechanism of hydrolysis of substrates by cysteine proteases is schematically shown in **Figure 4**.

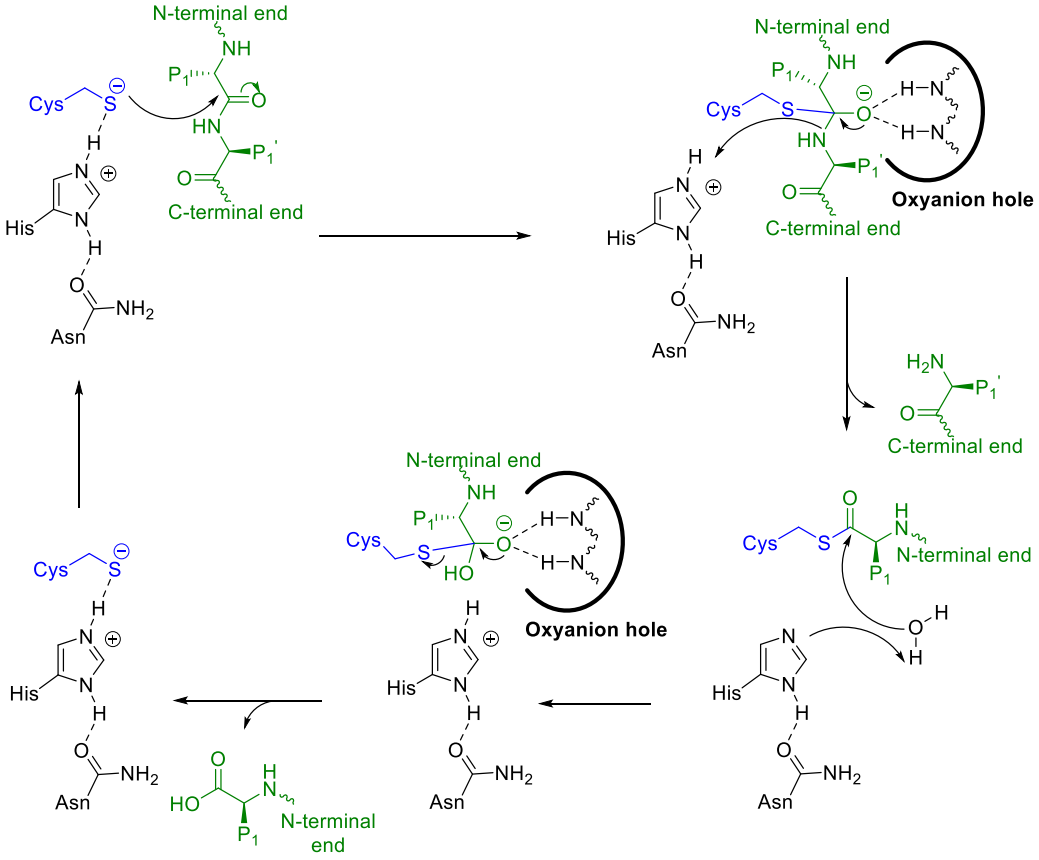

Figure 4: Mechanism of the catalytic hydrolysis of peptide bonds of substrates by cysteine proteases.

After a nucleophilic attack of the thiolate of the active site cysteine on the carbonyl of the peptide bond, a tetrahedral intermediate is formed. This intermediate is stabilized by an oxyanion-hole, which is formed through hydrogen bond interactions between the oxyanion and the amide backbone of the catalytic cysteine and a NH_2-gruop of a glutamine residue.[17,30] The symmetric distribution of charges helps to stabilize the oxyanion intermediate further. In the next step, the protonated histidine acts as an acid and protonates the nitrogen of the leaving group, whereas the oxyanion transforms back to a carbonyl moiety. The deacetylation step of the enzyme then follows as previously described through base catalysis: the imidazole nitrogen of histidine helps to polarize a water molecule, thus making it more nucleophilic enabling a nucleophilic attack of water on the carbonyl atom of the thioester intermediate. The resulting product is another oxyanion which is subsequently stabilized analogously to the previous oxyanion intermediate and a similar distribution of charges. In the final step a carboxylic acid of the *N*-terminal fragment is being released as the final product of substrate hydrolysis and the unchanged enzyme is regenerated.

1.2.2 Cysteine Cathepsins

The human genome encodes for 11 cysteine cathepsins (B, C, F, H, K, L, O, S, V, W and X) most of them being ubiquitously expressed in human organs and tissues.[31] They belong to the papain-like family C1 of clan CA cysteine peptidases and exert their proteolytic activity mainly, but not exclusively within the compartments along the endocytic pathway.[32] Among these, cathepsins K, S, V, and W exhibit a distinct localization pattern, presumably linked to their more specialized functions. Thus, cathepsin K (catK) is found primarily in osteoclasts and synovial fibroblasts, cathepsin S (catS) predominantly in immune cells, cathepsin V in the thymus and testis, and cathepsin W in natural killer cells and cluster of differentiation (CD) 8+ lymphocytes.[32,33] While most cathepsins are predominantly located in lysosomal compartments, there are exceptions like catS which has extracellular functions, like extracellular matrix degradation.[34] The upregulation and overexpression of certain cathepsins is connected to several diseases, such as osteoporosis, rheumatoid arthritis, and different cancers.[35–38] Cysteine cathepsins especially play critical roles in tumor progression and migration and extracellular matrix degradation leading to angiogenesis and metastasis. **Table 1** summarizes the physiological functions, and disease relevant alterations of several human and pathogen cathepsins.[38–40] Although there is no U.S. Food and Drug Administration (FDA) approved drug to date targeting one of the cathepsins, many investigations demonstrated tumor volume and invasion reduction, suggesting the use of small molecule cathepsin inhibitors against these targets.[41–45]

Table 1: Functions and related diseases of cysteine cathepsins.

Enzyme	Organism	Functions	Diseases
Cathepsin S	*Homo sapiens*	Antigen presentation and processing, ECM degradation	Auto-immune, cancer
Cathepsin L		Lysosomal protein degradation, antigen presentation	Cancer, hyperplasia
Cathepsin B		Lysosomal protein degradation, apoptosis	Cancer, pancreatitis
Cathepsin K		Bone resorption	Osteoporosis, bone cancer
Rhodesain (TbCatL)	*Trypanosoma brucei*	Host protein degradation, immune evasion	Human African Typanosomiasis
***T brucei* cathepsin B (TbCatB)**		Host protein degradation	
***S. mansoni* cathepsin B1 (SmCB1)**	*Schistosoma mansoni*	Host protein degradation, parasite development	Schistosomiasis

1.2.3 Physiological Functions and Pathologic Involvement of CatS

Parts of this chapter and of the following chapters 1.2.4 and 1.2.5 have been published in a review on catS (2020).[46]

Cathepsin S is a papain-like protease consisting of two domains, which is synthesized in vivo as an inactive precursor. Its pro-peptide is important for the activation and proper folding of the enzyme.[47,48] The pro-form of catS is distinctively recognized (among human cathepsins) for autocatalytic processing under neutral pH conditions, particularly in the presence of glycosaminoglycans.[49] The mature enzyme consists of 217 amino acid residues, the most important one being the catalytic cysteine-25 (Cys-25) which is located at the active site together with several residues forming the S1' – S3 sub-pockets that are essential for the binding specificity.[50,51] CatS differs from other cathepsins by its stability at neutral pH and its limited tissue distribution, since higher levels of the protease are found in the spleen and in the lymphatic system.[52,53] It is mainly expressed in dendritic cells (DCs), B cells and macrophages, that act as key antigen presenting cells of the immune system.[54] The main function of catS is the degradation of the invariant chain peptide (also known as li and CD74) occupying the major histocompatibility complex (MHC) II binding pocket. This degradation can promote antigen processing and the presentation of antigens to T cells via the MCHII pathway on antigen presenting cells (APC).[55]

In humans the catS gene is located on the 1q21 chromosome, and the expression of catS is regulated on the transcriptional and post-transcriptional level.[56] Inflammatory cytokines like interferon-γ (IFNγ) or interleukin-1β (IL-1β) and tumor necrosis factor-α (TNFα) can enhance catS expression before inflammation occurs, whereas anti-inflammatory cytokine IL-10 suppresses catS expression (**Figure 5**).[57–59] The catS promoter includes a functional IFN stimulating response element (ISRE) which induces catS transcription after binding of the transcription factor interferon regulatory factor-1 (IRF-1).[60] Dysregulation by micro-RNA (miRNA)-31 is a regulating factor in IRF-1 mediated catS expression.[61] PU.1 and transcription factor EB (TFEB) are other transcription factors that can also induce catS expression, while peroxisome proliferator-activated receptor-γ (PPARγ), B lymphocyte-induced maturation protein-1 (Blimp-1) and transglutaminase-2 (TG2) suppress catS expression.[62–65] After successful transcription of the catS gene, the following translation can be regulated by RNA-binding proteins. The catS mRNA can be stabilized by human antigen R (HuR) or destabilized by tristetraprolin (TTP).[66,67] While HuR binds on the 3′UTR of the catS mRNA, TTP destabilizes the catS mRNA and can be enhanced by protein phosphatase 2A (PP2A) and thus lead to an dysregulation of catS expression through the Mitogen-activated protein kinase/ extracellular signal-regulated kinase (MAPK/ERK)-pathway.[67–69] The influence of pathogens such as the mycobacteria *M. bovis* and *M. tuberculosis* can lead to an upregulation of miR-106b-5p, a miRNA that destabilizes the catS mRNA, leading to an increase in the pathogen survival.[70] After translation and biosynthesis of the pre-pro-catS, processing leads to an mannose-6-phosphate (M6P)-tagged, glycosylated pro-catS that binds to the M6P receptor and is transported to late endosomes.[71] Through an increase in the intracellular Ca^{2+}

concentration, catS is secreted by vesicular exocytosis.[72] The release of catS is mainly regulated by proinflammatory cytokines, such as IL-1β, TNFα, IL-4, and IL-13, which hints to the association of catS in inflammatory diseases. CatS is predominantly found in or secreted by immune cells and inflamed tissue.[58,73,74] Due to catS's strong proteolytic activity over a wide pH range, even at neutral pH, interactions with ECM components of glycosaminoglycans (GAG) can stabilize or change catS activity in the extracellular environment. Secreted catS remains bound to the plasma membrane or can be found in exosomes.[75,76] After secretion the pro-catS enzyme has a differing half-life, depending on the cell origin.[77] These variables can impact the activity and prevent inactivation of catS in the extracellular environment but at the same time limit catS inhibitor development.[78]

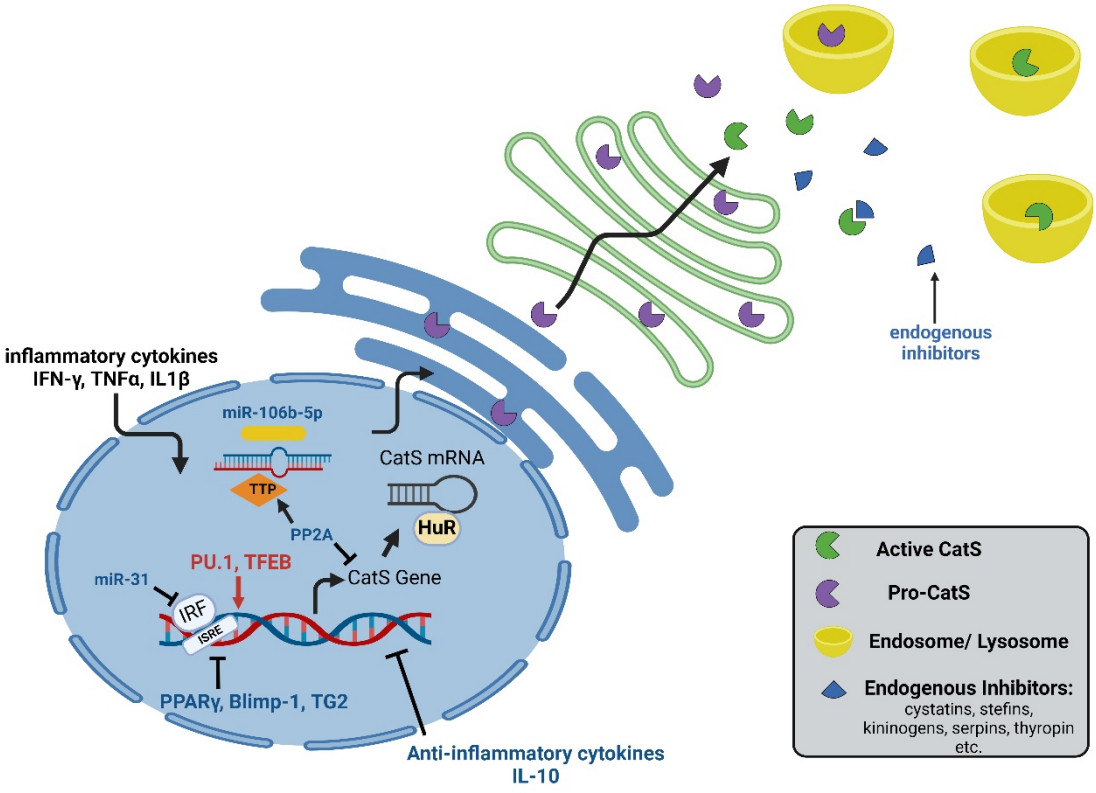

Figure 5: CatS expression and regulation. Inflammatory cytokines are mainly involved in catS expression regulation. Cytokines in black lead to upregulation of catS expression and cytokines in blue lead to downregulation of catS expression. Adopted from Yoo et al. Created with Biorender.com.[79]

After the final activation step, the mature catS enzyme is regulated by endogenous peptide and protein inhibitors. They bind tightly and reversibly to the orthosteric binding site and prevent substrate binding.[80] The biggest superfamily of C1 protease endogenous inhibitors are the cystatins, which include stefins, cystatins and kininogens. Among them cystatin C is the most potent endogenous inhibitor of catS. High concentrations of cystatins can neutralize high amounts of extracellularly secreted catS.[81,82] Additionally non-specific protein inhibitors also serve as potential inhibitors of catS, including serpins, thyropin and α2 macroglobulin.[80]

The pathologic involvement of catS consists mainly of auto-immune dysfunctions and several cancers by altering the tumor microenvironment (TME) to promote conditions contributing to tumor growth. In this chapter the focus will be on different cancer types which have been connected to catS as either the cause or a contributor.

Chronic inflammation plays a significant role in cancer development. Inflammatory factors and cytokines released during inflammation, along with extracellular matrix (ECM) remodeling and angiogenesis, modify the microenvironment, fostering a pro-tumorigenic milieu.[83] CatS mediates communication among various cell types within the inflammatory microenvironment of tumors and other inflammatory diseases, aiding disease progression. Abnormal expression of catS is common in multiple tumor types and together with increased levels of the enzyme, is associated with poor patient outcomes (**Figure 6**).[83–85] Tumor cells produce excessive catS, contributing to tumorigenesis through various mechanisms. However, catS is not solely derived from tumor cells but also from endothelial cells and infiltrating immune cells within the TME.[39,84,86–89]

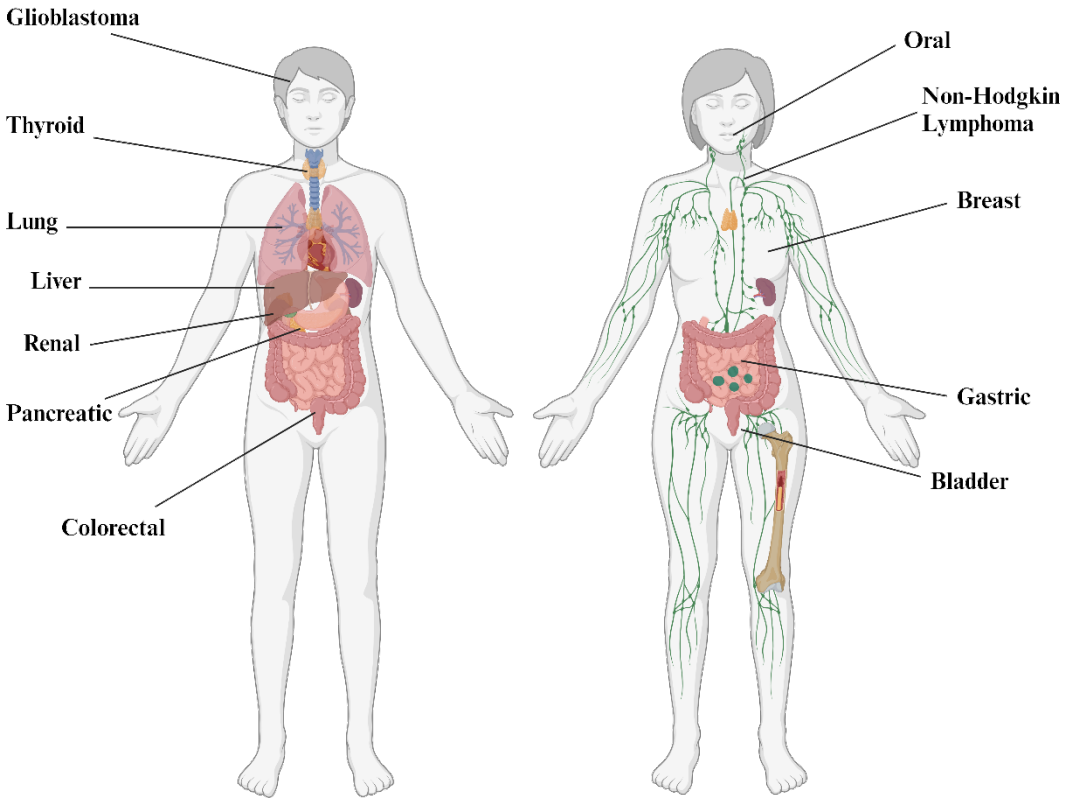

Figure 6: Illustration of different tumor types associated with CatS. Modified after McDowell *et al.*[90] Created with Biorender.com

The involvement of catS in many different tumor types and models is the basis of many research programs. For example, the role of catS in pancreatic cancer was first investigated by Joyce *et al*. in

2004, where they showed through gene expression analysis in a receptor interacting serine/threonine kinase 1 (RIP1)-Tag2 transgenic mouse model that an upregulation of the catS expression occurred during tumorigenesis.[88] By using activity-based probes (ABPs) the conclusion was, that infiltrating immune cells which were identified as tumor associated macrophages (TAMs) were the primary source of catS in the mouse model.[89] Further studies identified that a genetic ablation of catS led to a significant reduction of angiogenesis, tumor vascularization, tumor invasion and volume.[86,91] Wang and co-workers identified that catS regulated angiogenesis through the degradation of anti-angiogenic proteins to generate pro-angiogenic fragments.[91] CatS expression was also inducible by exposure to inflammatory cytokines and angiogenic factors.[92]

In the RIP1-Tag2 pancreatic mouse model, research on the regulation of cathepsin expression and secretion from TAMs revealed that IL-4, IL-6, and IL-10, which are Th2-associated cytokines, work together to stimulate the transcription and secretion of catS via a synergistic signaling pathway involving STAT3 and STAT6. While T cells produce more IL-4 than tumor cells, they constitute a minor fraction of infiltrating immune cells in the pancreatic-islet tumor studied, leading to the conclusion that tumor cells primarily supply IL-4, thereby driving the increased catS expression.[93]

CatS also seems to play an important role in the development of breast cancers, as shown with a xenograft MDA-MB231 model, where catS was ultimately overexpressed in primary tumors and TAMs and led to the development of brain metastasis. Inhibition of catS led to a reduction of brain metastasis in vivo if inhibition was prior to the development of metastatic tumors.[94] In a MCF7 breast cancer model tumor invasion and proliferation was promoted by catS and the use of a small molecule nitrile inhibitor of catS led to an increase in tumor cell apoptosis.[95] Another interesting finding was that whenever catS inhibition was carried out alongside chemotherapy treatment in vivo, the efficacy of the chemotherapy treatment of breast cancers was improved, demonstrating that targeting catS in the TME is potentially an attractive therapeutic strategy.[96]

In context of the colorectal carcinoma, several studies indicate elevated catS levels in tumor samples of patients compared to normal colon tissue.[97] A MC38 syngeneic study revealed that catS was expressed from both tumor and tumor-associated cells. By blocking either of the two sources for catS production, the tumor growth was effectively reduced and thus the importance of catS for driving tumorigenesis was demonstrated. Depletion of catS reduced tumor growth and vascularization, and exhausting catS from both tumor and tumor-associated cells had the biggest impact.[87] Inhibition of catS by a small molecule nitrile inhibitor similarly led to a decrease in tumor volume and invasion.[95]

CatS also plays a particularly important role in regulating cell activity and modifying antigen processing in the context of lymphomas.[44,45] In a group of non-Hodgkin's Lymphoma (NHL) patients, a hotspot mutation (Y132D) was identified in the binding pocket of catS which led to higher autocatalytic cleavage of the enzyme therefore making it overactive. In a follicular lymphoma study, this Y132D

mutation was shown to influence expression of inflammatory cytokines (IFN-γ), leading to tumor progression.[44] In a separate study the same Y132D mutation was also found and the expression of catS led to reduced CD8+ cytotoxic T-cells and an increase in the infiltration of CD4+ helper T-cells.[45] The T-cell receptor repertoire was severely diversified in catS knock-out tumors which led to an anti-tumor-immune response.[45] Overall these studies highlight the importance of catS mutations and expression profiles on the tumor microenvironment of aggressive forms of lymphoma, enhancing tumor growth through manipulation of T-cell populations.[45,90]

In glioblastoma patients, overexpression of catS is associated with poor prognosis and increased tumor progression. In an astrocytoma analysis, Flannery and coworkers correlated the highest catS expression with grade IV tumors.[98,99] Increased catS expression was even measured in human brain tumors in at least 50 % of samples taken from patients.[100] Additional examination of catS's mechanistic role in glioblastomas revealed its participation in intracellular signaling pathways. In U251MG and U87MG glioblastoma cell lines, the reduction of catS expression triggered the activation of two significant programmed cell-death pathways: mitochondrial apoptosis and autophagy. Both pathways are putatively mediated by reactive oxygen species (ROS) production.[101]

Gene expression analysis on Mdr-2 knockout mice also indicated that catS might be a potential therapeutic target in liver cancer.[102] Several studies showed that higher levels of catS expression are found in hepatocellular carcinoma compared to non-tumor liver cells, in some cases even up to 74-fold.[103] By silencing the catS gene, a decrease in tumor invasion and an increase in apoptosis was observed.[104]

In bladder cancer, catS is proposed to play a role in decreasing immunosuppressive functions of regulatory T cells (Tregs). Under normal conditions, catS inhibition resulted in increased immunosuppressive functions of Tregs, while in cancer, catS inhibition led to an increase in CD8+ cytotoxic T-cell proliferation and a decrease of CD8+ cytotoxic T-cell apoptosis. Dependent on the location and type of tumor, this indicates that inhibition of catS might lead to tumor reduction.[105,106]

In gastric cancer in vivo studies, a reduction of the tumor invasion and migration was directly linked to catS silencing. The involvement of catS in an inferred protein network which contributes to cellular movement is believed to be the mode of action which ultimately leads to an increase in tumor invasion and migration. This is often associated with poor patient prognosis.[107,108]

Overall, inhibition of catS seems to be a promising approach to help abrogate tumor growth or invasion and activate the innate anti-tumor immune response.[33,46,90]

1.2.4 CatS Binding Site and comparison with other cathepsins

The mature and active form of catS consists of 217 amino acid residues and has a high sequence homology with other cathepsins, especially K, L, and B, with some distinct differences in the S2 and S3 pockets. **Figure 7** comprises two crystal structures of catS with a vinylsulfone (1NPZ) and a nitrile inhibitor (2FQ9) respectively as co-crystallized ligands.[51]

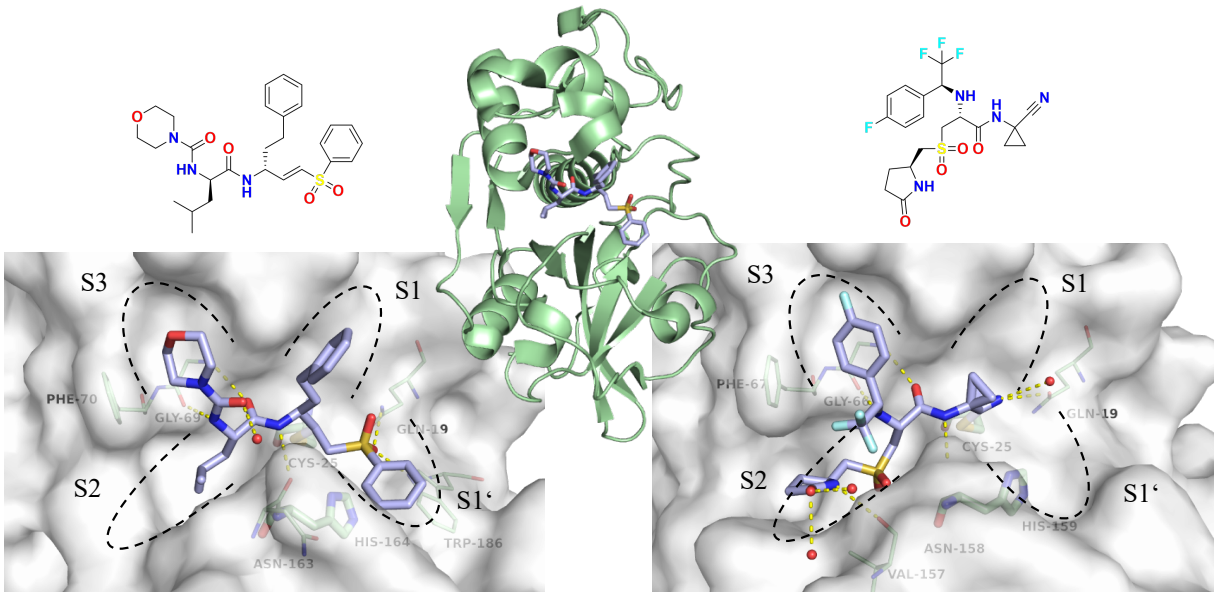

Figure 7: Crystallographic structures of catS with a vinylsulfone-inhibitor LHVS (middle) and the active site of catS with vinylsulfone-inhibitor LHVS (left, 1NPZ) and with a nitrile-inhibitor (right, 2FQ9).

The S2 pocket of catS contains Phe70, Gly137, Val162, Gly165 and a flexible Phe211 which is located at the bottom of the sub pocket. The Phe211 residue can, depending on the interactions with substrates or inhibitors with the S2 pocket, lead to an open conformation. The additional space between Phe211 and Phe70 can provide possible π-stacking interactions between ligands and either or both phenylalanine residues.[34,46] Phe211 is replaced by leucine in catK, making the S2 pocket tighter and shallower. Additionally, the two glycine residues Gly137 and Gly165 in catS are both alanine residues in catK, catL and catB and serve as “gatekeepers”, prohibiting bulkier residues from entering the S2 pocket. The missing methyl groups in the two glycine residues in catS enable the S2 pocket to be wider and deeper, therefore making the S2 pocket in catS addressable by larger substituents compared to the S2 pocket of the other cathepsins.[109] Other differences between catS and catK lay in the exchange of Lys64 in S3 (catS) to an aspartate (catK), and both phenylalanine residues in S2 are different in catK (tyrosine and leucine).[46] CatK (pdb: 1TU6) has a sequence homology of 58% with catS (pdb: 1NPZ) and a similarity of 72% (calculated with MOE). CatB differs significantly from catS due to its unique occluding loop and an additional glutamate residue blocking off the S1 pocket (**Figure 8**).

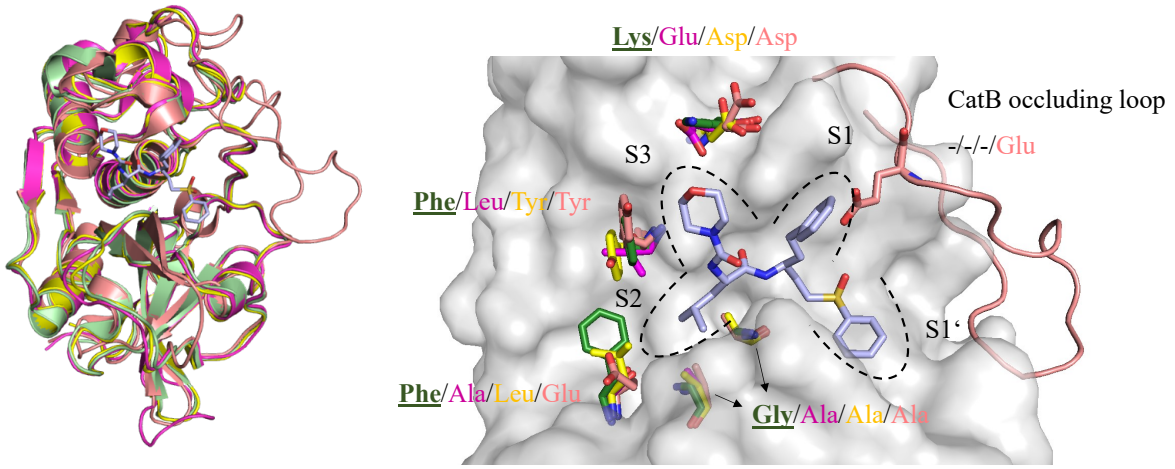

Figure 8: Left: superimposition of catS (green, 1NPZ), catL (magenta, 3OF8), catK (yellow, 1TU6) and catB (pink, 1GMY), right: active site of catS with corresponding amino acid residues in catL, catK and catB.[51,110–112]

Additionally, instead of Lys64 in S3, catB contains an aspartate and the phenylalanine residues of catS in S2 are tyrosine and glutamate in catB. CatS (pdb: 1NPZ) has the lowest sequence homology (31%) and the lowest sequence similarity (48%) with catB (pdb: 1GMY). CatL (pdb: 3OF8), which shares the highest similarity of 74% and a homology of 56% with catS (pdb: 1NPZ) has an aspartate in S3 instead of the lysine and the phenylalanines in S2 are leucine and alanine in catL (**Figure 8**).

1.2.5 Inhibitors of CatS

To date more than 1800 entries regarding catS inhibitors can be found in the ZINC15 database.[113] Most of these inhibitors are not very selective and inhibit several cathepsins and other off-targets. The most selective inhibitors comprise covalent and non-covalent inhibition types (**Figure 9**). While non-covalent inhibitors solely interact with the binding site of the target enzyme by interactions such as hydrogen-bonds and ionic interactions, covalent inhibitors are designed to additionally form a covalent bond with the catalytic cysteine.[114]

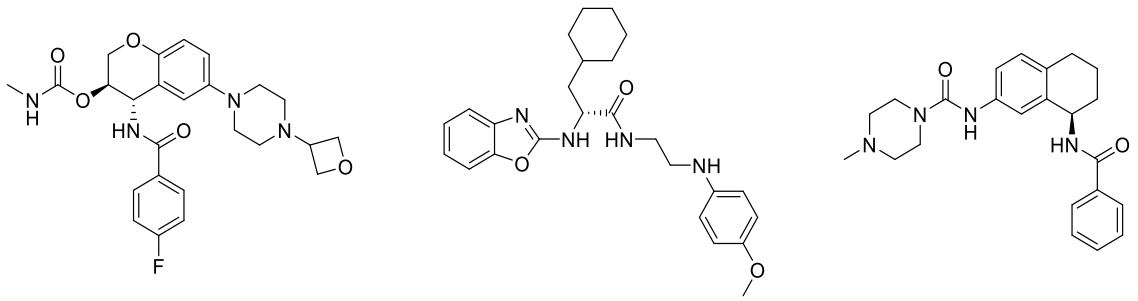

2FZ (**4P6G**)
IC_{50}: 7.7 nM

GNF (**2F1G**)
K_i: 29 nM

2FZ (**4P6E**)
IC_{50}: 1290 nM

Figure 9: Structures of three relevant non-covalent catS inhibitors with promising pre-clinical results with compound ID and pdb code of the co-crystallized structure in bold.[115,116]

Depending on the chemical structure, a small molecule inhibitor designed to inhibit a target enzyme covalently contains a so called 'warhead' functionality. This warhead is an electrophilic structural element of an inhibitor, which in proximity to basic amino acid residues in the binding pocket of cysteine proteases (e.g. catS) can be attacked by the deprotonated cysteine, resulting in the formation of a covalent adduct.[54]

Typically, inhibitors of catS and other cysteine proteases of the C1 family consist of a warhead attached to a peptidic or peptidomimetic recognition unit, which contributes to non-covalent interactions and helps placing the warhead functionality close to the active site cysteine, to which it can covalently bind. There are many different warheads which have been extensively studied and used in many different catS inhibitors.[46,109,114,117,118] One of the major drawbacks of covalent modulators containing a warhead can be a low selectivity for nucleophilic cysteines which are present in several enzymes. This can result in considerable off-target reactions with several proteins and is associated with toxicity and haptenization, which often prevented further development or the use as drug candidates.[119–124] A carefully fine-tuned reactivity to prevent off-target reactions is therefore crucial for the development of covalent inhibitors of catS.

The most prominent example of a widely used warhead in the development of covalently reacting catS inhibitors is the nitrile functionality. This covalently reversible warhead is not solely reactive towards cysteine proteases, but also it is part of many serine-protease targeting approved drugs like the gliptins which are used as antidiabetics.[125–127] Since 2021 there is an emergency approval for the first cysteine protease inhibitor (nirmatrelvir) in combination with ritonavir as short-term treatment of COVID-19 infections, which also contains a nitrile as warhead.[10,128,129] Another famous example is odanacatib, a small-molecule nitrile inhibitor, which entered clinical trials as a catK inhibitor for the treatment of bone metastasis and osteoporosis.[130] Due to toxicity concerns the development was halted, but the structure continues to serve as a basis for new nitrile inhibitors targeting several cathepsins.[131] The nitrile is a mild electrophile and reacts reversibly with the thiolate of cysteine in the active site of C1 proteases as catS to form a thioimidate adduct which is susceptible to hydrolysis, making this type of inhibition reversible. **Figure 10** comprises several examples of warheads commonly encountered in the field of cysteine protease inhibitor development.[54,109,118,132–135]

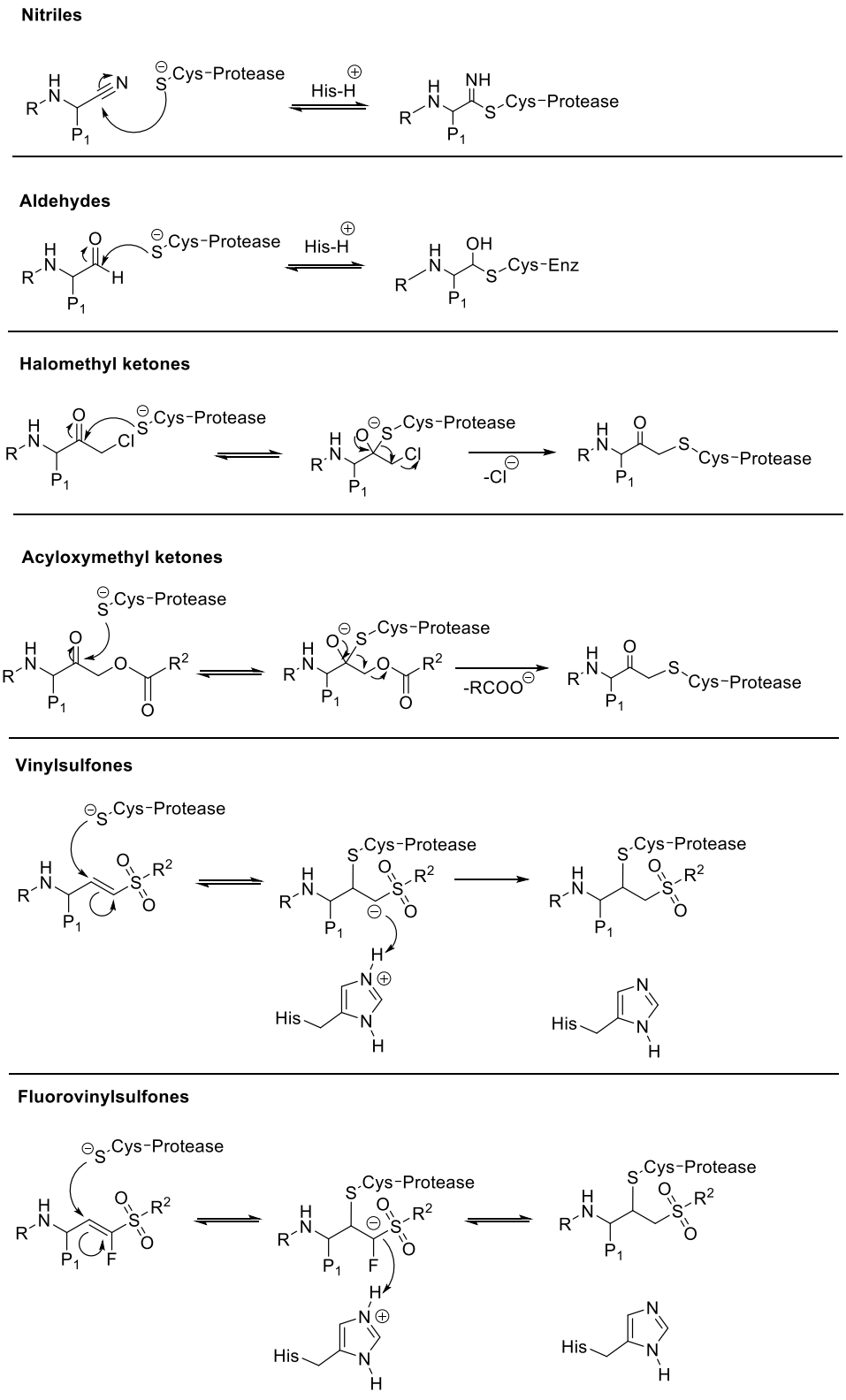

Figure 10: Examples of common warheads used in the design of cysteine protease inhibitors with the corresponding inhibition mechanism.

Aldehydes react similarly to nitriles in a covalent reversible mechanism, but due to the high reactivity and their tendency to form hydrates or hemiacetals, they are mostly used as experimental probes rather

than drug candidates.[136–138] Despite safety concerns due to the high electrophilicity and low metabolic stability of aldehydes, there have been studies, focusing on using masked aldehydes to prevent these drawbacks and potentially improve their pharmacokinetic properties.[139,140] Another class of well investigated warheads are α-substituted ketones like halomethyl ketones and acyloxymethyl ketones. Both warheads contain intrinsic leaving groups and ultimately lead to an irreversible inhibition of the protease.[141–143] While halomethyl ketones are known to react quickly in a concerted way due to the high reactivity, acyloxy methyl ketones are known for their use in quiescent affinity labeling, due to the slow inactivation step.[143–146] Both halomethyl ketones and acyloxy methyl ketones have similar reaction mechanisms, since both are initially attacked by the thiolate of cysteine at the ketone moiety, leading to the formation of a thiohemiketal, which after an rearrangement produces the corresponding thioether while the nucleofuge leaves the molecule. Another class of covalent warheads used as cysteine targeting groups are Michael acceptors, especially acrylamides, vinyl ester and vinyl sulfones, which in general react irreversibly.[147–151] They undergo a Michael-type addition to the active site cysteine and show high selectivity for cysteine over serine proteases and lower reactivity with endogenous thiol-nucleophiles like glutathione.[152] While acrylamides are more known for their use in targeted covalent inhibition strategies focusing on kinases, the use of vinyl sulfones has led to the development of compounds like K11777 against Chagas disease and was effective in animal models of schistosomiasis, hookworm infection, and cryptosporidiosis.[131] K11777 targets several cysteine proteases such as cruzain, rhodesain or catS.[153–155] The inhibitor was found to be safe in rodents, dogs, and nonhuman primates, but upon completing pre-clinical tests, no further data was provided on the current stage of drug development.[131] Substitutions of an H-atom in the α-position of vinyl sulfones led to inhibitors that can react covalently reversible, depending on the electron-withdrawing group (EWG) attached at this position. The fluorovinylsulfone warhead has shown to be an interesting alternative to the irreversible vinyl sulfones, leading to covalent reversible inhibitors of rhodesain.[156,157] Further variations include the exchange of the sulfone moiety with sulfonates, creating inhibitors with enhanced affinity, slower off-rates and even favorable selectivities towards off-target cathepsins.[118]

Several covalent inhibitors, targeting catS selectively, have been developed with many crystal structures already solved. **Figure 11** comprises a collection of covalent catS inhibitors containing the nitrile, vinylsulfone or aldehyde functionality with their inhibitory potencies disclosed.

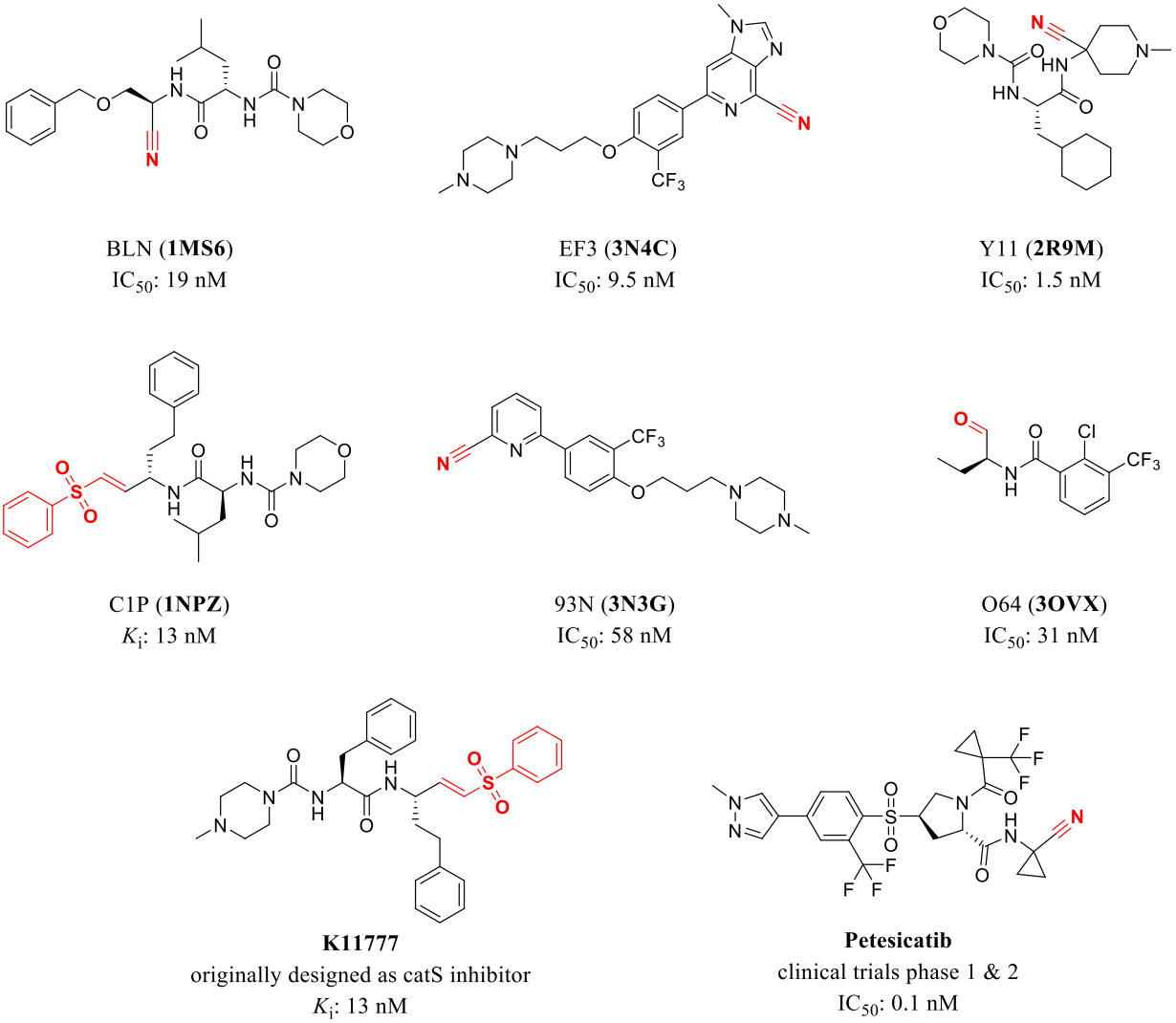

Figure 11: A selection of covalent catS inhibitors with compound ID and pdb code of the co-crystallized structure or the trivial name in bold. Warheads are depicted in red.[115,158–162]

Despite many efforts for producing a drug that targets catS, none of the drug discovery campaigns in the past have led to a drug approval, with all catS inhibitors in clinical trials being discontinued as of today (**Table 2**).

Table 2: Cathepsin S inhibitors in clinical trials.[90]

Inhibitor	Company	Disease	Phase	Clinical trial identifier	Year (completed)	Progress
Petesicatib (RG7625/RO5459072)	Hoffmann-La Roche	Sjogren's syndrome	II	NCT02701985	2017	Discontinued, no further details published
		Coeliac disease	I	NCT02679014	2016	
		Pharmacodynamic monitoring of healthy volunteers	I	NCT02295332	2015	
VBY-036	Virobay Inc.	Neuropathic pain Security studies of healthy volunteers	I	NCT01892891	2013	Company dissolved
VBY-891		Psoriasis Security studies of healthy volunteers	I	NCT01947738	2013	
LY3000328	Eli Lilly	Abdominal aorta aneurysm	I	NCT01515358	2012	No further progress reported
SAR114137	Sanofi	Pain	II	Not available	2011	Discontinued for pain treatment. Since 2015: Investigation for Chagas.
RWJ-445380	Johnson and Johnson	Rheumatoid arthritis	II	NCT00425321	2008	Showed lacking effectiveness. No further details published.
		Plaque psoriasis	II	NCT00396422	2007	
CRA-028129	Celera/ Bayer Schering	Psoriasis	I	Not available	2005	No further details published

1.3 Protease-Inhibitor Interactions

In the field of drug design, understanding the interactions between ligands and proteins is of crucial importance. These interactions play a pivotal role in determining various aspects of drug development, including binding affinity, conformational dynamics, binding mechanisms, and interaction sites. By delving into these foundational components, researchers can gain invaluable insights into the molecular basis of drug function and create innovative therapeutics with improved effectiveness and reduced side effects.[163–167]

Binding affinity, denoting the strength and stability of the bond formed between a ligand and its target protein, emerges as a fundamental factor influencing the potential efficacy of a drug candidate. Precise determination of binding affinity furnishes crucial data for pinpointing and refining compounds exhibiting high binding affinities.[164–168]

Examining the binding mechanism provides insights into how a ligand interacts with its target protein, including the binding mode, specific residues involved, and the interactions formed. Understanding the binding mechanism may help to enhance specificity and selectivity, to reduce the likelihood of off-target effects, and to facilitate the development of ligands that selectively bind to the target protein.[164,165,169,170]

1.3.1 Determining Affinity and Binding Mode of Reversible Binders

Fluorometric Enzyme Inhibition Assay.

The use of fluorometric enzyme assays is a common approach in drug design and the analysis of inhibitor protease interactions.[171,172] The utilization of fluorogenic substrates dates to 1973 in Förster resonance energy transfer (FRET) consisting of a quencher and a fluorophore, to enable protease activity measurements.[173] Due to higher sensitivity these substrates replaced the previously used *p*-nitroanilide (pNA) substrates.[174] The next milestone was the discovery of 7-amino-4-methyl coumarin (AMC) as a fluorescent molecule, and peptides that were known to be preferably cleaved by proteases were fused with this AMC moiety to produce new fluorogenic protease substrates. This helped reducing assay interferences in comparison to FRET or pNA substrates.[175] In general, AMC-based fluorometric protease assays operate similarly. The protease cleaves the peptide bond in the fluorogenic substrate, releasing the AMC fluorophore, which is then excited by a specific excitation wavelength inside a microplate reader (**Figure 12A**). The resulting fluorescence increase is then measured at a specific emission wavelength. The increasing fluorescence intensity over time corresponds to the enzymatic activity (**Figure 12B**). In presence of a competitive active site inhibitor, which competes with the substrate, the enzymatic reaction rate (v) is reduced depending on the concentration of the inhibitor, and the inhibitory activity can be assessed by different methods.[168,176–179]

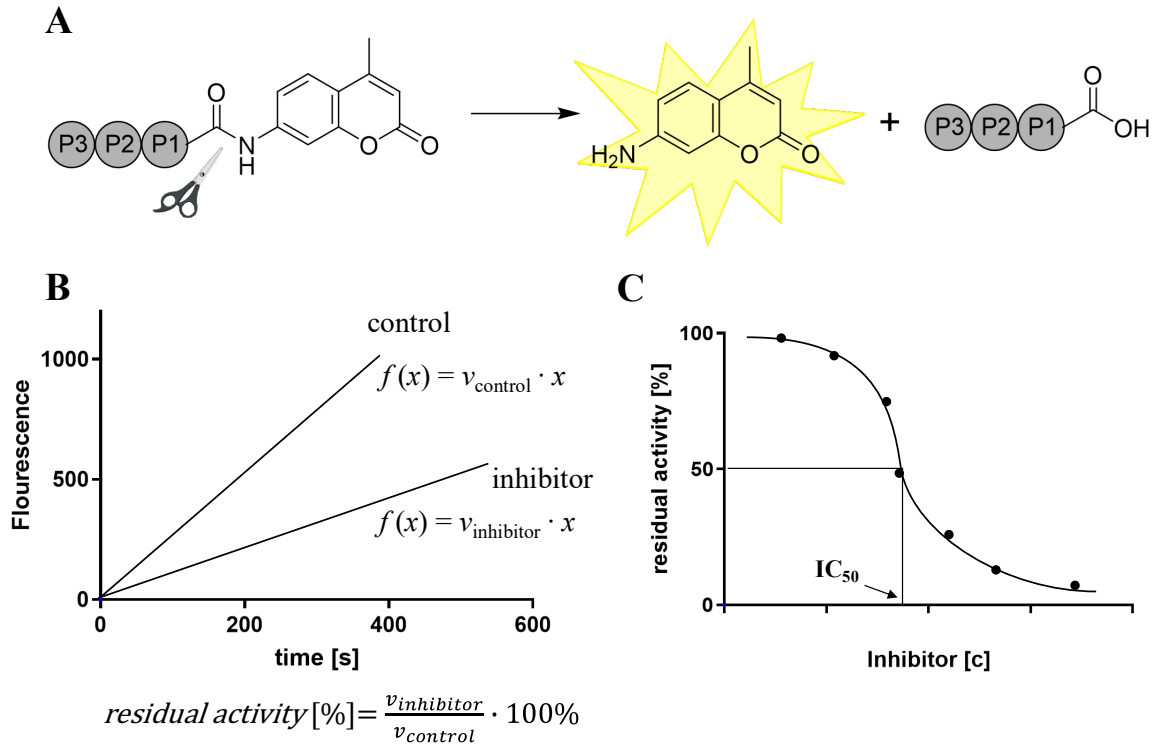

Figure 12: (A) Schematic representation of fluorogenic substrate hydrolysis by a protease to release the AMC fluorophore which can be detected by a fluorescence reader. (B) Graphical illustration of progress curves, obtained by plotting of the measured fluorescence during a typical protease assay measurement against the time. (C) Plotting the residual enzyme activity against the inhibitor concentration [I] gives access to the IC_{50} value of reversible inhibitors.

Inhibitory Potency

The commonly used parameters for assessing inhibitory potency of potential inhibitors are the inhibition constant (K_i) which is the equilibrium constant for the dissociation of the inhibitor-enzyme complex and the inhibitory concentration (IC_{50}) at which the enzymatic activity is reduced to 50 % (**Figure 12C**). While the IC_{50} value is strongly dependent on the substrate and the substrate concentration used in the assay, the K_i remains constant for a specific inhibitor and the corresponding enzyme.[180] The relationship between K_i and the IC_{50} and the mathematical transformation from one to another can be described by the Cheng-Prusoff relation (**Equation 1**), that applies for competitive inhibitor binding to free enzymes and inhibiting the catalytic enzyme reaction.[181]

$$IC_{50} = K_i \left(1 + \frac{[S]}{K_M}\right) \qquad \text{(Equation 1)}$$

The Cheng-Prusoff equation includes the dependency of the IC_{50} value of a competitive inhibitor on the K_i value, the substrate concentration ([S]), and the Michaelis Menten constant (K_M). The transformation of the IC_{50} to the K_i and vice versa via the Cheng-Prusoff equation is only possible for inhibitors with certain inhibition modes. For reversible competitive inhibitors, the Cheng-Prusoff equation is widely applicable. In case of covalent inhibitors, particularly for slowly reversible tight binders and irreversible

inactivators of enzymes, additional kinetic parameters other than the K_i value need to be determined or calculated with methods that will be discussed in the following.

1.3.2 Covalent Enzyme Inhibition

Traditional drug design efforts were focused on small molecule inhibitors that interact non-covalently and reversibly with their biological target. Contrarily, the covalent bond formed between an electrophilic group of covalent inhibitors and nucleophilic amino acids of target proteases like the active site cysteine in cysteine proteases is much stronger.[182] The list of covalent drugs that were being used in the clinic long before their mechanism of action was elucidated, includes aspirin, which was developed in the late 19th century, several penicillin antibiotics discovered in the first half of the 20th century, proton pump inhibitors like omeprazole and the antiplatelet agent clopidogrel which both act as prodrugs that need to be activated before covalently binding to their target structures (**Figure 13**).[183–185] Other covalent drugs include antibiotics like fosfomycin, which is used to treat bladder infections and contains a highly reactive epoxide ring or the antituberculotic isoniazid which effectively acts as a prodrug that inhibits the formation of the mycobacterial cell wall after the enzymatic formation of an acyl radical.[186–188] Around the end of the 20th century and the beginning of the 21st century, the first drug candidates were developed consciously containing electrophilic warheads, while prior most potential drugs containing highly reactive moieties were deliberately excluded from ongoing drug design projects due to toxicity and selectivity concerns.[189] Examples of successful covalent drugs purposefully developed to covalently interact with its target enzyme include the proteasome inhibitor bortezomib with approval for the treatment of multiple myeloma, several Hepatitis-C-Virus inhibitors like telaprevir and the gliptins as DPP-IV inhibitors against type 2 diabetes.[10,12,190]

The more recent clinical approval and success of targeted covalent inhibitors (TCIs) bearing moderately reactive electrophilic warheads, finally triggered the current resurgence of covalent drugs.[191–193] Through structure-guided covalent drug design, targeting catalytically active nucleophilic amino acids and with the TCI approach for targeting non-catalytically active amino acids, inhibition properties of ligands are frequently enhanced.[194]

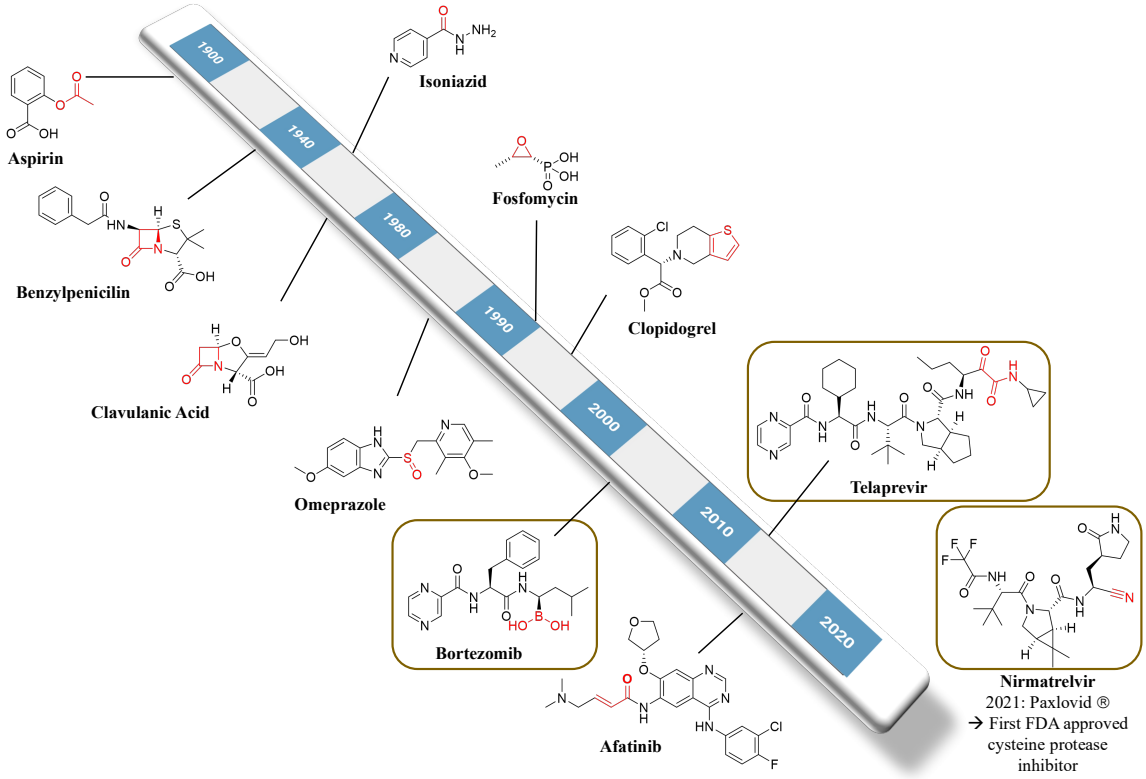

Figure 13: Timeline for covalent drug approvals since the late 19th century. Protease targeting drugs are highlighted in brown frames and the reactive warhead is highlighted in red in the corresponding structure.

The development of covalent inhibitors typically involves the identification of noncovalent inhibitors with a subsequent modification with a mildly electrophilic warhead to help improve selectivity and inhibition potency.[195,196] An alternative strategy is the finding of an electrophilic fragment that forms a covalent bond with a nucleophilic residue by covalent fragment-based drug design which is then combined with a suitable recognition unit with favorable non-covalent interactions.[197–199] The basic requirement for this is the presence of an nucleophilic amino acid (cysteine, serine, threonine, lysine) that is able to form a covalent adduct with the electrophile of the inhibitor.[200,201] Depending on the nature of the electrophilic warhead, the covalent adduct formed can either be reversible or irreversible.[202–204]

One of the biggest advantages of irreversible inhibition is the decoupling of pharmacokinetics and pharmacodynamics leading to an infinite target residence time and prolonged therapeutic efficacy even after the inhibitor has been eliminated from circulation. The resulting loss in enzyme activity can only be restored by protein resynthesis. One drawback is that the consequences of continuous target inhibition are poorly understood, making this property a potential risk issue.[205]

Modern approaches try to combine the advantages of both reversible and irreversible inhibition types by designing inhibitors with covalently reversible binding modes where the target residence times is tunable due to the choice of warheads with varying electrophilicities.[203,206,207]

Inhibitor Binding Kinetics

Since the enzyme-inhibitor binding kinetics may differ quite significantly, depending on the nature of the inhibitor, the possibly occurring binding kinetics will be discussed in the following.

The formation of a noncovalent complex (EI) and subsequent inhibition of the enzymatic activity by reversible noncovalent inhibitors generally occurs in a single reaction step (**Figure 14A**). For fast-binding reversible inhibitors, the steady-state equilibrium between free inhibitor and unbound enzyme on one hand and the inhibitor-bound enzyme complex EI on the other hand will be reached almost instantly since both the association rate constant k_1 and the dissociation constant k_2 are fast. Contrarily to these classic fast-binding inhibitors, time-dependent or slow-binding inhibitors reach the steady-state or enzyme inactivation in case of irreversible binders relatively slowly.[208,209] This is often observed for covalently binding inhibitors and can therefore help to differentiate between a covalent and a noncovalent binder (**Figure 14B–D**).

Reversible covalent inhibition takes place in two steps consisting of a rapid initial association of the noncovalent EI complex, followed by the conversion into the covalent EI* complex after the covalent bond is formed (**Figure 14B**). The covalent EI* complex is at equilibrium with the noncovalent complex EI as the formation of the covalent bond is reversible ($k_4>0$) with the resulting inhibition constant K_i contemplating the initial noncovalent equilibrium and steady-state constant K_i^* reflecting the overall steady state equilibrium. Optimization of the overall affinity (reflected by low K_i^*) is preferred when developing new covalently reversible inhibitors. This can be achieved by slowing the dissociation rates since a slow off rate (k_{off}) leads to prolonged target residence time τ ($\tau = 1/k_{off}$).[210,211]

If the inhibition leads to a residence time that exceeds the resynthesis rate of the target enzyme, the binding is considered irreversible.[212] In contrast to covalently reversible inhibition, completion of the reaction does not lead to an equilibrium state, since the dissociation from the covalent EI* complex is negligible for irreversible inhibition types (**Figure 14C** and **D**). The obtainable kinetic parameters for ranking irreversible inhibitor potency differs from inhibitors with reversible binding modes as the IC_{50} may vary depending on the preincubation time of the inhibitor with the enzyme.[193,212] For two-step irreversible inhibitors with a noncovalently formed EI complex in the first step and the formation of an irreversible EI* complex in the second step, the noncovalent affinity is reflected by the inactivation constant K_I, whereas the maximum rate of inactivation can be described by the kinetic constant k_{inact} (**Figure 14C**). The general accepted method for comparing inactivation potencies of two step irreversible inhibitors is the determination of the rate constant k_{2nd} which can be calculated by k_{inact}/K_I.[193,212–214] Finally for irreversible inhibitors with highly reactive warheads, the equilibrium of the noncovalent step is non-existent, effectively changing the binding kinetics to a one-step irreversible binding, where the inhibitory potency can be described with the rate constant k_{chem} or $k_{obs}/[I]$ (**Figure 14D**).[213,215]

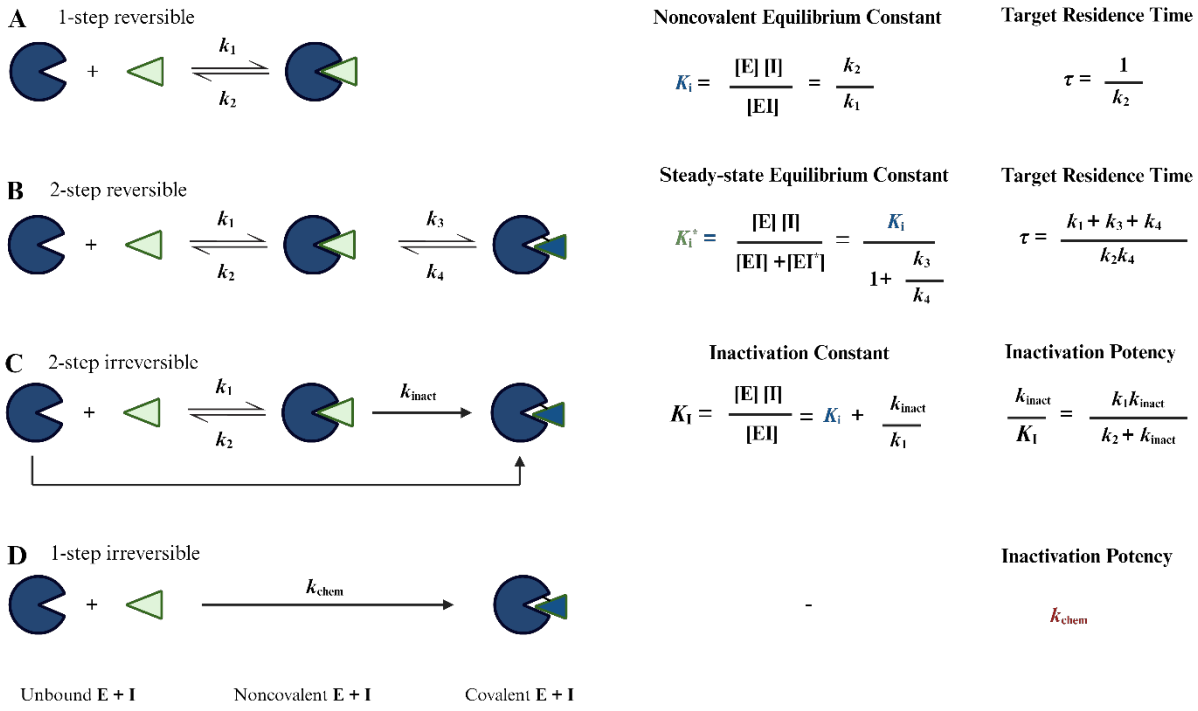

Figure 14: Schematic representation of inhibitor binding modes and kinetic parameters which can be used to rank inhibitor potencies. Adopted from Mons et al.[205] Created with Biorender.com.

1.3.3 Reversible vs Irreversible Binding

Most covalent drugs comprise two-step reaction mechanisms. Subsequently, their design is more complicated compared to their noncovalent counterparts.[17] The stability (ΔG_B) of the noncovalent EI complex formed in the first inhibition step and its geometrical arrangement is generally dictated by the noncovalent interactions formed by the recognition unit of the inhibitor with the enzymatic environment (**Figure 15**). This energy (barrier) must be overcome and equals the energy required to dissociate the enzyme-inhibitor interactions. If a favorable orientation of the inhibitor inside the active site of a target enzyme is possible and the electrophilic warhead gets in close proximity to the nucleophilic amino acid (e.g., cysteine, serine, threonine), the covalent bond formation can occur.[156] The free reaction energy, ΔG_R, of this subsequent chemical reaction is heavily reliant on the chemical properties of the warhead. This primarily determines whether the covalent inhibition step is reversible or irreversible (**Figure 15**). The reaction barrier of the reverse reaction (k_4) is often the critical issue deciding on the reversibility of the covalent bond formation. Covalent bond formations with highly exergonic reaction energies ($\Delta G_R < -25$ kcal/ mol) generally lead to an irreversible bond formation, whereas reversible bonds are mostly formed if the reaction barrier is to a lower degree exothermic (in the range of –20 kcal/mol or lower).[156] For the successful design of covalent drugs, optimization of both the recognition unit and the warhead must occur simultaneously.[216]

From the kinetic viewpoint, the formation and stability of the noncovalent EI complex is mainly determined by the microscopic rate constants k_1 and k_2.[213] In the second step of a two-step reaction mechanism, the kinetics for the covalent bond formation are described by k_3, which is dependent on electrophilicity of the warhead and nucleophilicity of the amino acid in the active site. Depending on the kinetic constant k_4 the inhibition type is either reversible (k_4>0) or irreversible (k_4≈0).

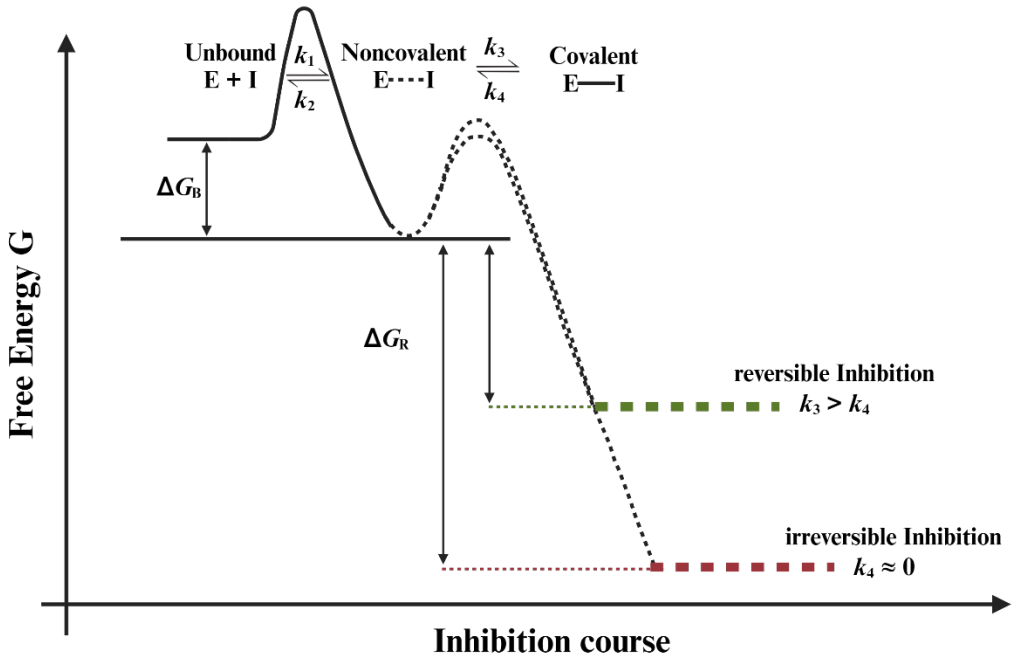

Figure 15: Free energy diagram of the mechanism of covalently reacting inhibitors. Adopted from Schirmeister et al.[156] Created with Biorender.com.

For fast reversible inhibitors, the resulting progress curves in fluorometric enzyme assays show linearity (**Figure 16A**). Since reversible time-dependent inhibition often occurs in a slowly reversible manner (k_3>>k_4), the resulting progress curves display a biphasic behavior (**Figure 16B**), resembling the progress curves of irreversible inhibitors (**Figure 16C**) which are often heavily bent after initial linearity. This suggests a two-step (or a one-step irreversible) reaction mechanism and makes it difficult to distinguish between slowly (tight) reversible and irreversible binders. In many cases there is even an intermediate progress curve behavior, further complicating the distinction between irreversible and (slowly) reversible binding. An experimental method for the differentiation between reversible and irreversible binding is the jump dilution analysis.[217–219] For inhibitors displaying a time-independent dose-response relationship, inhibition of the target enzyme will lead to 50% inhibition at the IC_{50} and at 10-fold the IC_{50} value the target is inhibited by almost 91%. After pre-incubation of enzyme and inhibitor and subsequently diluting the 10-fold [I] by 100-fold into assay buffer, one would get a 0.1-fold [I] below the IC_{50} that will lead to around 9% inhibition of the target (**Figure 16D**).[140,220] The resulting progress curves differ, depending on the inhibition mechanism. The control without inhibitor containing

only solvent (typically DMSO) will lead to a linear progress curve, with a higher slope compared to a progress curve of a fast reversible inhibitor (**Figure 16E**). Irreversible inhibitors also show linear progress curves, but with a substantially smaller slope compared to the fast reversible inhibitors, thus making the distinction between reversible and irreversible binding possible (**Figure 16E**).[220] Finally slowly reversible inhibitors show progress curves with a slope between those of fast reversible and irreversible inhibitors, depending on how slowly the dissociation of the inhibitor enzyme complex takes place.

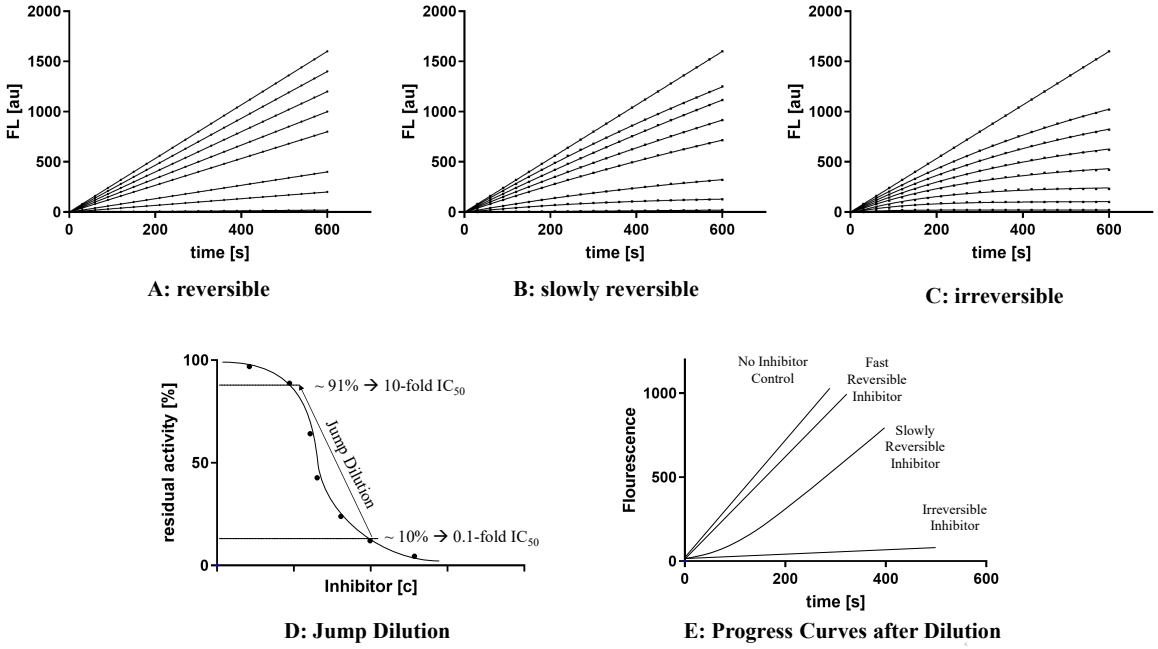

Figure 16: Exemplary progress curves of reversible inhibitors (A), slowly reversible inhibitors (B) and irreversible inhibitors (C). Principle of the jump dilution assay starting from [I] at 0.1-fold IC_{50} reaching 10-times IC_{50} of the inhibitor after 100-fold dilution (D). Resulting progress curves of control without inhibitor and fast reversible, slowly reversible, and irreversible inhibitors (E).

Another method often used for differentiating between reversible and irreversible binding and to quantify the degree of reversibility of selected inhibitors is the dialysis experiment. The enzyme is incubated with an excess of inhibitor ([I] of 10-fold the IC_{50} value) to ensure full inhibition.[221] A semi-permeable membrane separates an inner and an outer dialysis compartment which can only be passed by small molecules of a certain molecular weight. In the next step, the enzyme-inhibitor mixture inside the inner compartment is dialyzed against a continuous flow of buffer in the outer compartment. Inhibitor molecules not bound to the enzyme in the inner compartment will diffuse into the outer compartment until an equilibrium of the free inhibitor concentration between both compartments is reached.[222,223] Removing the free inhibitor from the outer compartment via a continual flow of fresh buffer prevents the system from reaching equilibrium, resulting in a concentration gradient of the inhibitor. Consequently, the free inhibitor in the inner compartment diffuses continuously along this gradient into the outer compartment. If the inhibitor binds reversibly to the enzyme, the gradient

facilitates the constant removal of free inhibitor from the inner compartment, allowing the enzyme to recover over time. However, if the binding is irreversible, the enzyme cannot recover as the inhibitor remains bound to it.[221]

Risks of Irreversible Inhibitors

The development of covalently reversible inhibitors may be a desirable approach since the benefits of covalent binding remain (higher inhibition potency and residence times) while simultaneously decreasing several disadvantages that inhibitors designed to bind covalently with the target enzyme entail.[204,224] Another great advantage of inhibitors with covalent binding modes are the possibilities of targeting previously 'undruggable' targets due to a sufficiently high affinity complex formation between the irreversible inhibitor and the drug target.[225] Another approach often found for the design of TCIs is addressing a non-catalytic nucleophilic amino acid (often cysteine) that is unique to this specific enzyme with an electrophilic warhead and thus putatively leading to an enhanced selectivity for this particular enzyme over closely related off-target enzymes.[226,227]

The risks associated with covalent reactions that may take place not only with the desired target but also with off-target proteins, often undiscovered until late-stage clinical development, in many cases led to drug discovery campaigns moving away from potential candidates bearing intrinsically reactive electrophilic warheads.[189,193] These off-target interactions can lead to undesired side-effects and also toxicities, and especially idiosyncratic drug-related toxicity is a big concern, since these drug reactions occur unpredictably (**Figure 17**).[189] There is still controversy whether covalent binders actually contribute to idiosyncratic toxicity, nevertheless the use of electrophilic warheads in drug design remains a risk factor.[228] Covalent modulators with irreversible binding modes can furthermore bind to off-target proteins, and after proteolysis of the enzyme a so-called 'hapten' might develop (**Figure 17**). This small immunogenic fragment might lead to autoimmune reactions and the development of allergies.[204] To avoid these negative side effects, it is important to tune the reactivity of the warhead carefully while developing covalent inhibitors. This warhead reactivity tuning can ultimately lead to a shift from an originally irreversible covalent binding mode to a covalently reversible inhibition that maintains most advantages of covalent inhibition such as a long residence time and fast kinetics and simultaneously counteracts most risks connected to irreversible inhibition.[229–231] Despite these possible improvements of covalently reversible inhibitors compared to irreversible inhibitors, the fact that many recently approved covalent drugs, especially of those targeting kinases contain an irreversibly reacting acrylamide as warhead, demonstrates that irreversible inhibition should not be excluded.

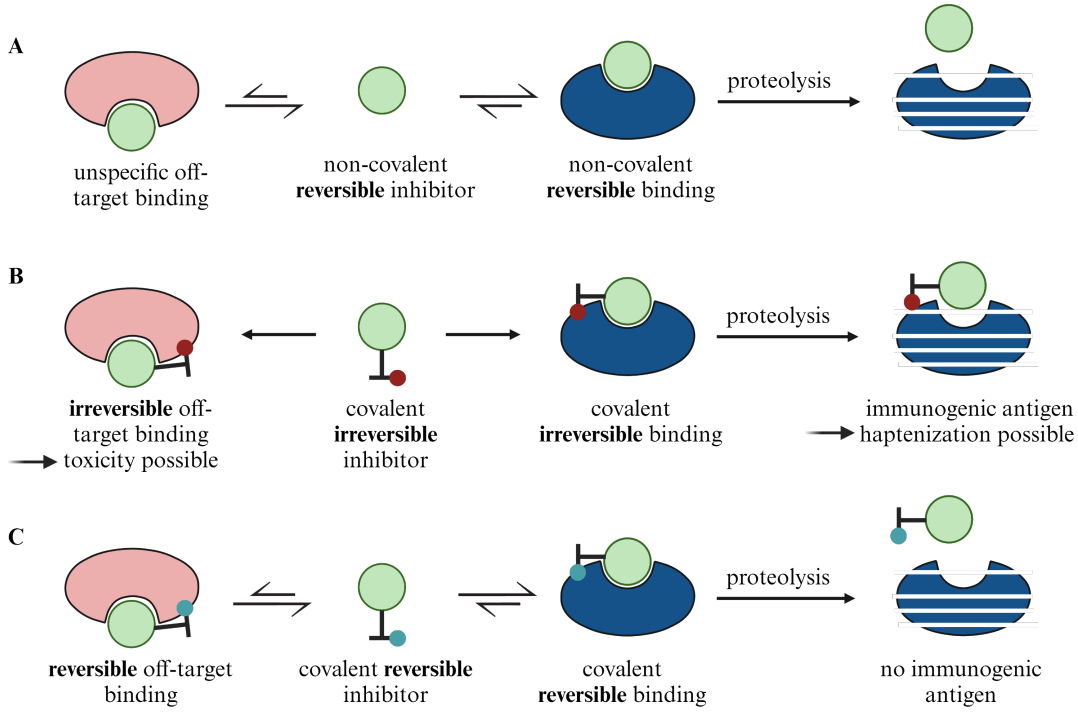

Figure 17: Mechanisms of possible inhibitor-enzyme interactions with inhibitor in green, irreversible warhead in red, reversible warhead in cyan, target enzyme in dark-blue and off-target enzyme in salmon. **A**: Non-covalent reversible inhibitor with reversible binding to the target and off-target enzymes. **B**: Covalent irreversible inhibitor with risks of toxicity and haptenization by covalent irreversible modulators. **C**: Covalent-reversible inhibitor with lowered risks of haptenization and off-target reactions.

1.4 Nanocarrier-Mediated Delivery and Reversible Linker Strategies

Despite pharmacodynamic target optimization, small molecular drugs like novel catS inhibitors may encounter translatability challenges due to their physicochemical parameters. Issues such as poor solubility and reduced bioavailability can impede their in vivo potency. Nano-sized carrier systems present opportunities to alter pharmacokinetic profiles of drugs and target their delivery, thereby preventing premature release and metabolic degradation. This enhancement boosts drug efficacy while minimizing side effects, enabling higher dosing and expanding the therapeutic window.[232] Over the last four decades, nanocarriers have been extensively studied for delivering traditional anti-cancer chemotherapeutics.[233,234] This focus has largely been driven by blood-circulating nanocarriers that passively accumulate in highly vascularized tumors through the enhanced permeability and retention (EPR) effect.[235–237] Concurrently, several studies have indicated that nano-sized drug carriers not only accumulate in lymphoid organs like the spleen but also in major first-pass organs such as the liver and lungs, where they are swiftly taken up and processed by immune cells. This phenomenon mirrors the response to classical pathogens of similar sizes, suggesting a favorable interaction between nanotechnology and the immune system.[238,239] These recent findings have sparked increased interest in nanocarriers for cancer immunotherapy.[240–242]

As mentioned in a previous chapter, the inhibition of catS by small molecule drugs in vivo is an appealing strategy for remodeling the immune TME in many different cancers towards an anti-tumor type. In this context, the delivery of catS inhibitors via nanocarriers to target-specific immune cells in the TME, particularly TAMs and myeloid-derived suppressor cells (MDSC), presents an appealing approach.

In the Q5 subproject of the collaborative research center (CRC) 1066 one goal was the development of a conjugate structure for targeted lysosomal delivery in a cancer cell model to modulate the immune TME. Oelschlaegel *et al*. have proven recently that a small molecule pan-cathepsin inhibitor (GB111-NH_2) is able to modulate metabolism and polarization of TAMs. Pharmacological inhibition of cathepsins B, L, and S using GB111-NH_2, led to a polarization shift from M2- to M1-macrophages, associated with distinct alterations in lysosomal signaling and lipid metabolism.[243]

The general composition of the planned conjugate contains a small molecule immunomodulator (catS inhibitor) with a responsive linker (optionally with a dye or fluorescent reporter) connected to a saccharide recognition unit for a targeted delivery *via* mannose receptors like the lectins CD206 and CD209 encountered for instance on the surface of DCs. A similar approach was executed successfully by Overkleeft and coworkers by designing fluorescent cathepsin inhibitor glycoconjugates which were evaluated in terms of their cell internalization and cathepsin inhibition.[244] The conjugate structure is planned to be connected to a suitable nanocarrier system *via* a responsive linker (**Figure 18A**). Alternatively, the single components of the construct can be individually immobilized on a suitable

nano-carrier, enabling the selective lysosomal release of the immunomodulator by using a responsive linker system (**Figure 18B**).

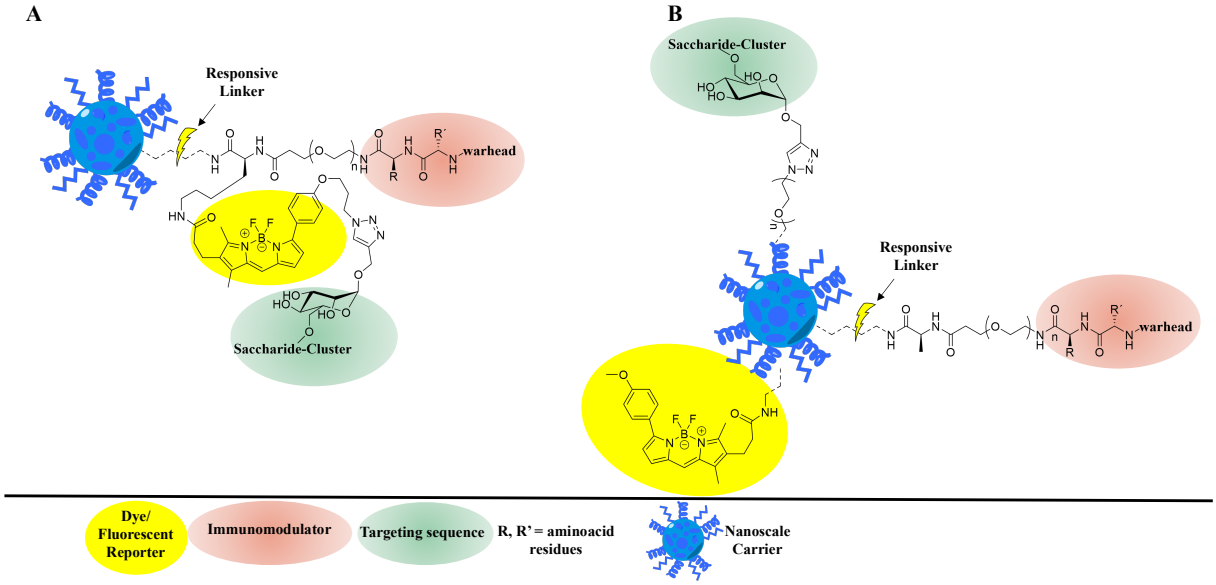

Figure 18: Schematic representation of two possible conjugate structures planned for the Q5 subproject of the CRC 1066. **A**: Single molecule approach, combining the immunomodulator with a fluorescent dye or reporter and a saccharide recognition sequence, attached via a responsive linker to a nanoscale carrier. **B**: Multiple molecules approach, immobilizing the immunomodulator via a responsive linker, while stably attaching the fluorescence reporter and the saccharide recognition sequence individually on a nanoscale carrier.

The selective release of the immunomodulator cargo in the target compartment can be achieved by using an appropriate linker chemistry, including a reversible covalent attachment of the catS inhibitor. **Figure 19** comprises a selection of pH- and redox-responsive linkers widely used for reversible attachment in tumor-targeted drug delivery approaches.[245–249] The pH-sensitive linkers include hydrazones, which are cleaved to the corresponding hydrazide and carbonyl derivative, acetals that hydrolyze to alcohols and carbonyls and Schiff bases that react to amines and a keto-moiety in acidic environments. Two examples for redox-responsive linkers are aromatic boronic acid esters that are oxidized to boronic acids, phenols and catechols and dilsulfides that can either be cleaved under reductive conditions or by rebridging with thiol-containing endogenous nucleophiles as glutathione (GSH) or peptides and proteins with nucleophilic cysteine residues.[250,251] As a first approach, the focus was laid on hydrazone-based dynamic linkers, since these are thoroughly investigated, meaning their stability under physiological conditions, as well as their cleavage under lysosomal conditions and in a TME are well-understood.[252,253] The formation of hydrazones is a reversible reaction and requires a hydrazine/hydrazide and a carbonyl-moiety that can be either a ketone or an aldehyde.

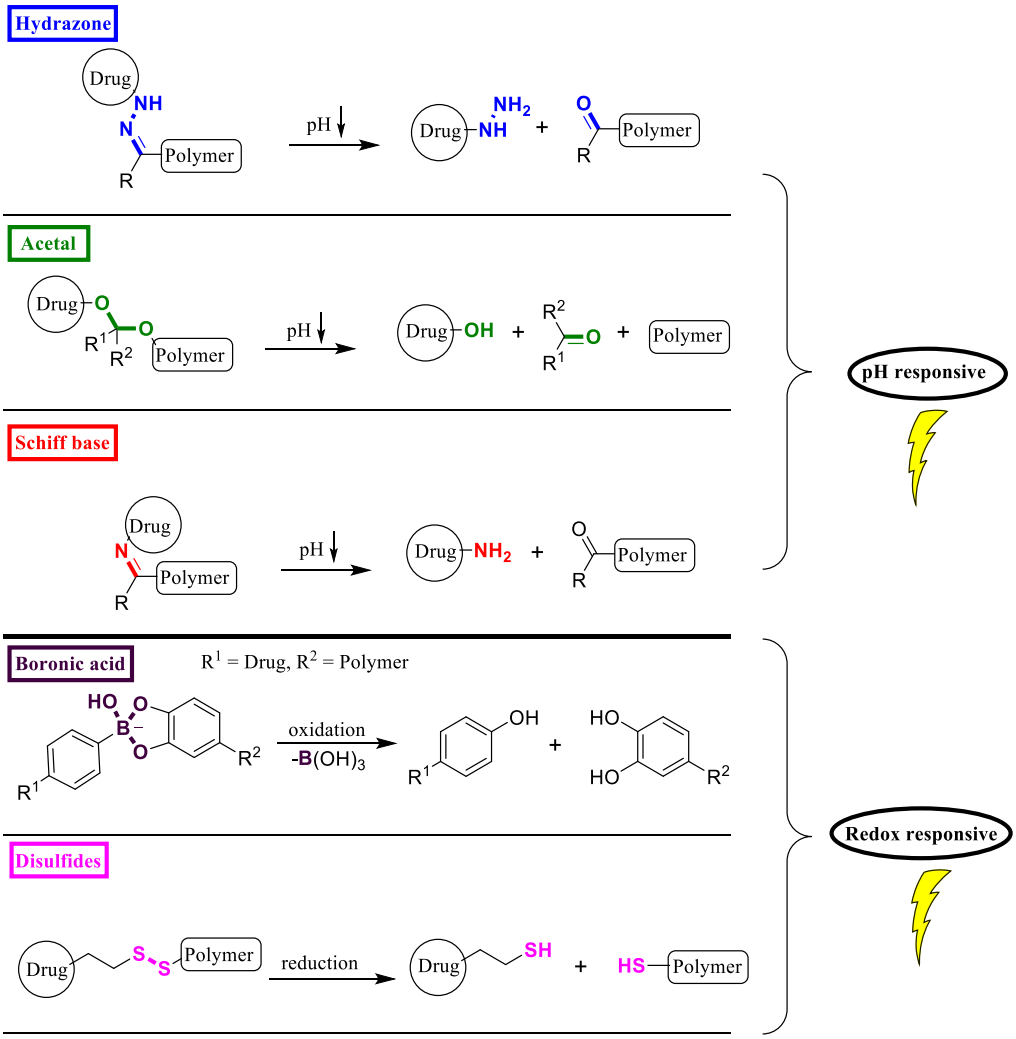

Figure 19: Overview of pH- and redox-responsive linkers and the cleavage products commonly encountered in the design of drug delivery systems.

The pH value in the endosomal and lysosomal environment is around 4–5, and hydrazones, depending on the keto- and hydrazide moieties from which they are formed have their cleavage optimum at a similar pH range. This makes hydrazones predestined to be cleavable linkers for these cellular compartments.[252]

Finally, the attachment position of the responsive linker on the catS immunomodulator has to be chosen. This can either be on the P3-position (*N*-terminus of the inhibitor since the active site of the target enzyme allows for bulkier substituents in the S3-subpocket. Alternatively, by choosing a carbonyl-based warhead as linkage position, the hydrazone can additionally protect the reactive electrophile from off-target reactions and help deliver the drug without needing to highly modify an affine and selective inhibitor and thus risking a loss in activity towards the target protease.

2 Projects

The results presented in this doctoral thesis can be divided into two projects: firstly, focusing on the design and functionalization of catS inhibitors in the framework of the CRC 1066 (subproject Q5), secondly on the interactions between protease inhibitors, containing a suitable peptidomimetic sequence in combination with various warheads, and different proteases.

2.1 Project 1: Design and Functionalization of CatS-selective Inhibitors

The first project will focus on developing and evaluating potential inhibitors for the cysteine protease cathepsin S, in the context of the CRC1066 ("*Nanodimensional polymer therapeutics for tumor therapy*") in the Q5 subproject ("*Targeting and immunomudolator structures and their coupling to theurapeutic nanosystems for oncological application*"). The focus will lie on initially developing small molecule inhibitors of catS with the option for functionalization to then immobilize them on a suitable nanocarrier system for targeted delivery.

The development of several new highly affine and selective catS inhibitors will be achieved and their inhibition types will be revealed by well-described fluorometric enzyme assays and jump dilution assays. Exchanging the nitrile warhead of established inhibitors of catS with several electron-deficient ketones and an aldehyde, is expected to create new inhibitors with fine-tuned reactivity and selectivity profiles. Further variations will be obtained by reversibly capping the warhead moiety and thus, allowing for highly reactive warheads to get possible new applications. Attaching linkers to the P3-position of catS inhibitors will enable the possibility of linking the functionalized inhibitors to nano carrier systems. The derivatization of well-investigated fluorovinylsulfones and -sulfonates known as inhibitors of similar cysteine proteases is expected to produce covalently reversible inhibitors of catS, and through SAR studies, the ideal peptidomimetic sequence in combination with either of those warheads will lead to inhibitors with high selectivities over off-target cathepsins. Molecular docking will help to understand the binding poses of these newly generated inhibitors and reveal the differences in affinities.

The following publications are part of the results obtained in this project:

(1) Natalie Fuchs[‡], **Mergim Meta**[‡], Bellinda Lantzberg, Matthias Bros, Seah Ling Kuan, Tanja Weil, Tanja Schirmeister*, "Subnanomolar Cathepsin S Inhibitors with High Selectivity: Optimizing Covalent Reversible α-Fluorovinylsulfones and α-Sulfonates as Potential Immunomodulators in Cancer", *ChemMedChem* **2023**, 18, e2023001, doi: 10.1002/cmdc.202300160.

Own contributions: Inhibitor design, inhibitor synthesis (precursor molecules **10**, **12**, **13**, **14**, **18**, **41**, **42** and final optimized inhibitor **6c**), molecular modeling and docking, SAR analysis, writing parts of the original draft, and manuscript editing.

Contribution from other authors: Inhibitor synthesis **2a–6b**, fluorometric enzyme assays, dilution assays, cytotoxicity assays, writing of the original draft, and editing of the manuscript.

(2) **Mergim Meta**‡, Collin Zimmer‡, Natalie Fuchs, Maximilian Johannes Zecher, Albin Lahu, Tanja Schirmeister*, "Structural Modifications of Covalent Cathepsin S Inhibitors: Impact on Affinity, Selectivity, and Permeability", *ACS Med. Chem. Lett.* **2024**, published ahead of print, doi: 10.1021/acsmedchemlett.4c00050.

Own contributions: Design of the study, inhibitor design, inhibitor synthesis (all except for **48**–**51**), catS, catB and catL fluorometric enzyme assays, dilution assays, hydrazone stability assays, molecular modeling and docking, writing of the original draft, and manuscript editing.

Contribution from other authors: Inhibitor synthesis (**48**–**51**), PAMPA assay, writing parts of the original draft, and manuscript editing.

2.2 Project 2: Reactivity and Selectivity of Protease Inhibitors with varying Warheads

This project will focus on the cross-reactivities of inhibitors designed for specific proteases with off-target proteases. Five selected proteases and classic peptidomimetic recognition units to address each protease individually will be used to investigate cross-target reactivities. The peptidomimetic sequences will be decorated with a set of seven different warheads to generate covalent binders. The proteases investigated in this study are two papain-like cysteine proteases (catS and rhodesain), one 3-chymotrypsin-like cysteine protease ($3CL^{pro}$), namely the SARS-Cov-2 main protease (M^{pro}), one serine protease (uPA), and a threonine protease (β5 subunit of the human 20S proteasome). The various warheads for cross reactivity assessments consist of nitriles, nitroalkenes, fluorovinylsulfones, keto-benzothiazoles, oxoenoates and β-lactams. Cross-testing of the warhead-carrying inhibitors in standard fluorometric enzyme assays against all proteases can give an insight on the impact of the peptidomimetic sequences and the warheads on affinity and selectivity. Additionally, a reactivity assay based on NMR and LC-MS investigations with model nucleophiles (thiol, thiolate, alcoholate) and model electrophiles, consisting of the same seven warheads fused to leucine will help to better categorize the reactivity of each warhead against the nucleophiles. Quantum mechanics simulations are expected to verify the experimental results and to help better explain the findings of the reactivity assay.

Due to structural similarities especially between the papain-like cysteine proteases, new lead structures for inhibiting several proteases are expected to be found, while hard-to-target active sites like those of the subunits of the 20S-proteasome are expected to hardly allow for the identification of any new potential inhibitors through this approach. Covalent and non-covalent docking approaches will help to understand the putative binding modes of highly affine ligands and the suitability of each warhead for a

covalent reaction with the different nucleophiles encountered in each active site of the different proteases. Combining several warheads with the differing peptidomimetic sequences may demonstrate limits regarding binding affinity and inhibitory potency to these kinds of combinatorial approaches while giving access to a range of off-target reactivities.

The following publication is part of the results obtained in this project:

(3) **Mergim Meta**[‡], Patrick Müller[‡], J. Laurenz Meidner[‡], Marvin Schwickert, Jessica Meyr, Kevin Schwickert, Christian Kersten, Collin Zimmer, Stefan Hammerschmidt, Ariane Frey, Albin Lahu, Sergio de la Hoz-Rodríguez, Laura Agost-Beltrán, Santiago Rodríguez, Kira Diemer, Wilhelm Neumann, Florenci V. Gonzàlez, Bernd Engels, Tanja Schirmeister. "Investigation of the Compatibility between Warheads and Peptidomimetic Sequences of Protease Inhibitors—A Comprehensive Reactivity and Selectivity Study." *Int. J. Mol. Sci.* **2023**, *24*(8), 7226, doi: 10.3390/ijms24087226.

Own contributions: Design of the study, inhibitor synthesis (**20**, **23**, **24**, **26–49**) and reactivity probes **108**, **111** and **117** with precursors (**51**, **52**, **116**), molecular modeling and docking of all inhibitors, SAR analysis, reactivity study, fluorometric enzyme assays of all inhibitors against catS, writing of the original draft, and manuscript editing.

Contributions from other authors: Inhibitor synthesis (all other inhibitors), reactivity study, fluorometric assays against all proteases except catS, quantum mechanics simulations, writing parts of the original draft, and manuscript editing.

3 List of Publications

3.1 Publications as Part of this Doctoral Thesis

3.1.1 Project 1: Design and Functionalization of CatS-selective Inhibitors

(1) Natalie Fuchs‡, **Mergim Meta**‡, Bellinda Lantzberg, Matthias Bros, Seah Ling Kuan, Tanja Weil, Tanja Schirmeister*, "Subnanomolar Cathepsin S Inhibitors with High Selectivity: Optimizing Covalent Reversible α-Fluorovinylsulfones and α-Sulfonates as Potential Immunomodulators in Cancer", *ChemMedChem* **2023**, 18, e2023001, doi: 10.1002/cmdc.202300160.

(2) **Mergim Meta**‡, Collin Zimmer‡, Natalie Fuchs, Maximilian Johannes Zecher, Albin Lahu, Tanja Schirmeister*, "Structural Modifications of Covalent Cathepsin S Inhibitors: Impact on Affinity, Selectivity, and Permeability", *ACS Med. Chem. Lett.* **2024**, published ahead of print, doi: 10.1021/acsmedchemlett.4c00050.

3.1.2 Project 2: Reactivity and Selectivity of Protease Inhibitors with varying Warheads

(3) **Mergim Meta**‡, Patrick Müller‡, J. Laurenz Meidner‡, Marvin Schwickert, Jessica Meyr, Kevin Schwickert, Christian Kersten, Collin Zimmer, Stefan Hammerschmidt, Ariane Frey, Albin Lahu, Sergio de la Hoz-Rodríguez, Laura Agost-Beltrán, Santiago Rodríguez, Kira Diemer, Wilhelm Neumann, Florenci V. Gonzàlez, Bernd Engels, Tanja Schirmeister. "Investigation of the Compatibility between Warheads and Peptidomimetic Sequences of Protease Inhibitors—A Comprehensive Reactivity and Selectivity Study." *Int. J. Mol. Sci.* **2023**, *24*(8), 7226, doi: 10.3390/ijms24087226.

3.2 Publications Beyond this Doctoral Thesis

3.2.1 Research Articles

(4) Hannah Maus, Patrick Müller, **Mergim Meta**, Sabrina N. Hoba, Stefan J. Hammerschmidt, Robert A. Zimmermann, Collin Zimmer, Natalie Fuchs, Tanja Schirmeister, Fabian Barthels "Next Generation of Fluorometric Protease Assays: 7-Nitrobenz-2-oxa-1,3-diazol-4-yl-amides (NBD-Amides) as Class-Spanning Protease Substrates." *Chem. Eur. J.* **2023***,* 29, e202301855, doi: 10.1002/chem.202301855.

(5) Natalie Fuchs, Robert A. Zimmermann, Marvin Schwickert, Annika Gunkel, Collin Zimmer, **Mergim Meta**, Kevin Schwickert, Jennifer Keiser, Cécile Haeberli, Werner Kiefer, Tanja Schirmeister. "Dual Strategy to Design New Agents Targeting *Schistosoma mansoni*: Advancing Phenotypic and SmCB1 Inhibitors for Improved Efficacy", *ACS Infect. Dis.* **2024**, *10*(5), 1664–1678, doi: 10.1021/acsinfecdis.4c00020.

3.2.2 Review Article

(6) Natalie Fuchs‡, **Mergim Meta**‡, Detlef Schuppan, Lutz Nuhn, Tanja Schirmeister. „Novel Opportunities for Cathepsin S Inhibitors in Cancer Immunotherapy by Nanocarrier-Mediated Delivery". *Cells* **2020**, 9, 2021. doi: 10.3390/cells9092021.

4 Project 1: Design and Functionalization of Cathepsin S-Selective Inhibitors

4.1 Subnanomolar Cathepsin S Inhibitors with High Selectivity: Optimizing Covalent Reversible α-Fluorovinylsulfones and α-Sulfonates as Potential Immunomodulators in Cancer

4.1.1 Context, Project Summary, and Own Contributions

The involvement of the cysteine protease catS in many tumor models and especially in tumors with an altered tumor immune environment has opened new possibilities for the use of new catS inhibitors as immune modulators in these diseases.[44–46,90] The enzyme is often overly active and overexpressed, resulting in tumor and disease progression for many patients. Recent findings suggest an improvement in the anti-tumor immune response in several cancers by either silencing or deleting the catS gene. Small molecule inhibitors designed to specifically address catS could lead to a similar outcome.[44–46]

We therefore designed peptidomimetic inhibitors starting with two (fluoro-)vinylsulfone structures. With the help of molecular docking, an SAR screening was carried out, resulting in 22 final inhibitors which were evaluated in fluorometric enzyme assays against catS and off-target cathepsins B and L. The binding modes of selected inhibitors were evaluated with jump dilution assays, and reversible, time-dependent inhibition was observed in some cases, suggesting tightly covalent reversible inhibition. The most promising inhibitor showed high selectivity (>100,000-fold) against both off-targets and a sub-nanomolar affinity (K_i = 0.08 nM; K_i^* = 0.01 nM) for the target. This highly affine and potent inhibitor with a cyclohexyl alanine in P2, homophenyl alanine in P1 and a morpholine urea in P3 combined with the reactive fluorovinylsulfonate warhead with a covalent reversible inhibition type, can act as a cornerstone for further development of catS selective inhibitors. Additionally, through molecular docking, putative binding modes of several inhibitors could be assessed and the successful incorporation of bulky residues in the P3 position displayed a tolerance of the protease, since these big side chains (e.g., boc-protected aniline or the deprotected equivalent) retained the affinity and the selectivity for the target enzyme. Finally, cell viability assays with a cancer cell line (MDA-MB-231) and dendritic cells ($CD11c^+$) revealed for selected inhibitors low cytotoxic effects at the highest concentrations applied (100 µM) which effectively is equivalent to >10,000-fold the inhibitors' K_i values. Similar structures with different linkers in this position are therefore predestined to yield highly functionalized inhibitors for the use in nanocarrier systems while retaining the high affinity towards the target enzyme. Development of inhibitor-nanocarrier constructs is therefore feasible with these inhibitors. This approach could lead to a further improvement of the inhibitors' efficacy through specific targeting to dendritic cells or other APCs.

Own contributions: Inhibitor design, inhibitor synthesis (precursor molecules **10**, **12**, **13**, **14**, **18**, **41**, **42** and final optimized inhibitor **6c**), molecular modeling and docking of all inhibitors, SAR analysis, writing parts of the original draft, and manuscript editing.

Contribution from other authors: Design of the inhibitors, inhibitor synthesis **2a–6b**, fluorometric enzyme assays, dilution assays, cytotoxicity assays, writing of the original draft, and manuscript editing.

This work has been published in ChemMedChem.

The full Supporting Information can be accessed online at doi: 10.1002/cmdc.202300160.

4.1.2 Publication

The following publication quoted within "" from page 39 to page 59 is the same as the manuscript cited on page 38.

“

Check for updates

ChemMedChem

Research Article
doi.org/10.1002/cmdc.202300160

Chemistry Europe
European Chemical Societies Publishing

www.chemmedchem.org

Subnanomolar Cathepsin S Inhibitors with High Selectivity: Optimizing Covalent Reversible α-Fluorovinylsulfones and α-Sulfonates as Potential Immunomodulators in Cancer

Natalie Fuchs[+],[a] Mergim Meta[+],[a] Bellinda Lantzberg,[b] Matthias Bros,[c] Seah Ling Kuan,[b] Tanja Weil,[b] and Tanja Schirmeister*[a]

The cysteine protease cathepsin S (CatS) is overexpressed in many tumors. It is known to be involved in tumor progression as well as antigen processing in antigen-presenting cells (APC). Recent evidence suggests that silencing CatS improves the anti-tumor immune response in several cancers. Therefore, CatS is an interesting target to modulate the immune response in these diseases. Here, we present a series of covalent-reversible CatS inhibitors based on the α-fluorovinylsulfone and -sulfonate warheads. We optimized two lead structures by molecular docking approaches, resulting in 22 final compounds which were evaluated in fluorometric enzyme assays for CatS inhibition and for selectivity towards the off-targets CatB and CatL. The most potent inhibitor in the series has subnanomolar affinity ($K_i = 0.08$ nM) and more than 100,000-fold selectivity towards cathepsins B and L. These new reversible and non-cytotoxic inhibitors could serve as interesting leads to develop new immunomodulators in cancer therapy.

Introduction

Cysteine cathepsins are ubiquitous papain-like proteases, in mammalians mainly located in the lysosome, involved in extracellular matrix degradation and intracellular protein processing.[1] They have various functions in cells and, above all, share a high structural similarity.[2] However, cathepsin S (CatS) differs from other cysteine cathepsins in its stability at neutral pH and its limited tissue distribution (mainly in antigen-presenting cells, e.g. macrophages).[3,4] CatS is known to be overexpressed in many tumors (e.g., follicular lymphoma, breast, gastric, colon, pancreatic cancer).[5–8] To date, various mechanisms how CatS is involved in tumor progression are known. For example, CatS is known to turn over extracellular matrix proteins and to drive tumor angiogenesis.[7,9] Additionally, Riese and co-workers showed that CatS regulates antigen processing and presentation in antigen-presenting cells (APC).[10–15] With this important role in immune cells, cathepsin S intervenes in the body's immune response also to tumors. It shifts MHC-II expression to MHC–I, resulting in a favored activation of CD4+ T cells (e.g., regulatory T cells) over cytotoxic CD8+ T cells.[5,6,16] Jakoš and co-workers and Wilkinson and co-workers also stated that CatS polarizes APCs from M1 to M2 phenotype that is associated with tumor progression, supporting the proliferation of myeloid-derived suppressor cells (MDSC) and tumor-associated macrophages.[9,16] This shift results in a suppressed T cell-induced immune response.[17–19] Data from murine models also indicates that CatS inhibition reduces the overall T cell immunity in healthy mice but enhances the CD8+ T cell immunity in mice with cancer.[20] Cytotoxic CD8+ T cells can attack tumor cells and thus lead to tumor volume reduction.[20] Experiments with small-interfering RNA (siRNA) targeting CatS mRNA and thus, reducing CatS expression, resulted in tumor volume and invasion reduction as well as increased apoptosis and attenuated angiogenesis.[21,22] Burden and co-workers used inhibitory CatS antibodies and observed an increased effect of chemotherapeutics plus a significant tumor growth limitation.[23,24] Furthermore, CatS overexpression occurs in follicular lymphoma including the expression of an overactive mutant (Y132D) with enhanced auto-activation.[5] Knocking down the protease leads to an improved immune response towards lymphoma cells.[6] Overall, CatS is an interesting new target to enhance anti-tumor immunogenicity and thus, stop tumor growth, especially in case of resistances to current tumor immunotherapies.[6,10,25,26] Figure 1 summarizes the mentioned effects of CatS in the tumor microenvironment (TME).

CatS is a papain-like protease expressed as an inactive zymogen.[27,28] After cleaving off the propeptide, the mature enzyme consists of 217 residues and a catalytic dyad (Cys25, His164) in the active site.[3,4,29] Despite the high structural similarity to other human cathepsins, there are various residues

[a] N. Fuchs,[+] M. Meta,[+] Prof. Dr. T. Schirmeister
Institute of Pharmaceutical and Biomedical Sciences (IPBS)
Johannes Gutenberg University Mainz
Staudingerweg 5, 55128 Mainz (Germany)
E-mail: schirmei@uni-mainz.de
[b] B. Lantzberg, Dr. S. Ling Kuan, Prof. Dr. T. Weil
Max Planck Institute for Polymer Research
Ackermannweg 10, 55128 Mainz (Germany)
[c] Dr. M. Bros
Department of Dermatology, University Medical Center Mainz
Langenbeckstr. 1, 55131 Mainz (Germany)
[+] These authors contributed equally to this work.

Supporting information for this article is available on the WWW under https://doi.org/10.1002/cmdc.202300160

ChemMedChem
Research Article
doi.org/10.1002/cmdc.202300160
Chemistry Europe
European Chemical Societies Publishing

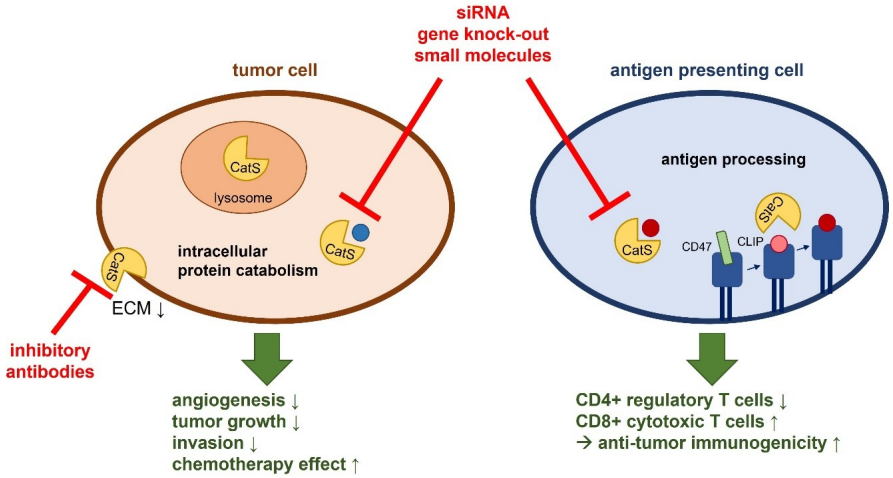

Figure 1. Cathepsin S inhibition affects tumor cells and antigen presenting cells (APC). CLIP = Class II-associated invariant chain peptide.

in the S1′ to S3 subsites that differ and can be addressed to gain selectivity.[4,29] The first selective CatS inhibitors were published in the early 2000s based on a publication by Pauly et al. that described the binding site and especially the differences towards other cysteine cathepsins.[1,29]

The S2 subsite contains a flexible Phe211 residue that can flip and open up to Phe70 from the S3 site, creating space for bulkier residues in S2. Furthermore, it allows ligand π-stacking with these Phe residues.[1,30] During the last 20 years, many cathepsin S inhibitors have been developed, including non-covalent as well as covalent ones (e.g. vinylsulfones, nitriles, aldehydes).[1,30–38] One nitrile-based inhibitor has already been tested *in vivo*. The compound led to significant reduction of tumor volume in murine models.[39] The structures of three advanced CatS inhibitors are summarized in Scheme 1.[30,40,41]

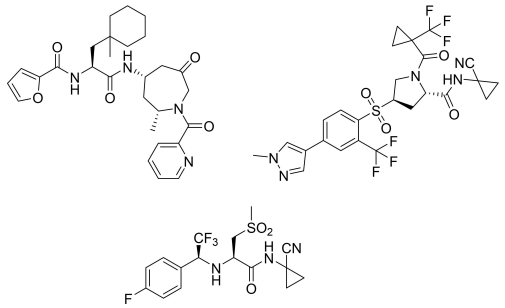

Scheme 1. Structures of three advanced published CatS inhibitors.[30,40,41]

Here, we focus on developing new selective cathepsin S inhibitors based on the structure of the well-known pan-cathepsin inhibitor K11777. This compound with an electrophilic vinylsulfone warhead is known to be a covalent irreversible cathepsin inhibitor (Figure 2).

The active site cysteine undergoes a Michael-type addition and cannot dissociate from the inhibitor after the covalent bond formation. Since irreversible inhibition has several drawbacks, e.g., off-target effects, toxicity, haptenization, we have recently developed modified K11777 derivatives by introducing a fluorine atom at the α-position of the vinylsulfone double bond.[42–44] The generated α-fluorovinylsulfone (**1 a**) undergoes a reversible Michael-type addition with thiols (Figure 2).[45] With this reversibility we maintain the benefits of covalent inhibition, e.g., longer residence times, higher potency, thus possible dosage reduction, and a lower pharmacokinetic sensitivity, without the drawbacks of irreversible inhibition mentioned above.[46–48]

Our most recent findings suggest that modifying the warhead from an α-fluorovinylsulfone (**1 a**) to an α-fluorovinylsulfonate (**1 b**) results in slowly reversible cathepsin inhibitors, further prolonging the target residence time (Figure 2).[49]

Since covalent-reversible inhibition has many benefits, we chose previously described fluorinated derivatives from Schirmeister et al. and Jung, Fuchs et al. as initial starting structures (**1 a**, **1 b**) for the development of new CatS inhibitors.[45,49] Results of molecular docking studies combined with literature-known motifs resulted in 22 new compounds (Figure 3) that were tested in fluorometric enzyme assays against cathepsins S, B, and L. We evaluated their potency and selectivity profiles in a structure-activity relationship study backed up by molecular docking results. Finally, their cytotoxicities against the breast

ChemMedChem
Research Article
doi.org/10.1002/cmdc.202300160
Chemistry Europe
European Chemical Societies Publishing

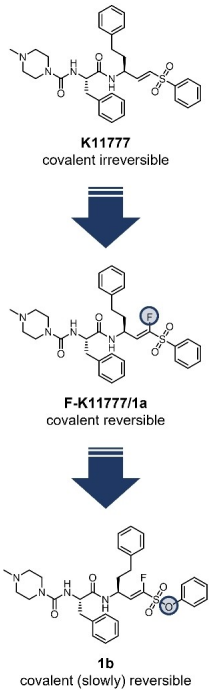

Figure 2. Reversible K11777 derivatives as lead structures for CatS inhibitor development.

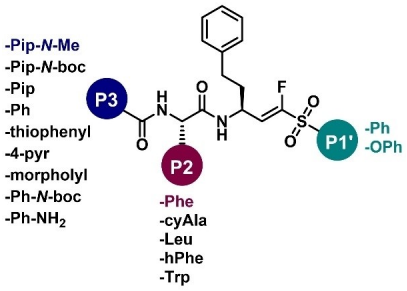

Figure 3. SAR variations for compounds **1a** (P1′ = Ph) and **1b** (P1′ = OPh). Residues of initial leads are highlighted.

cancer cell line MDA-MB-231 and murine bone marrow-derived dendritic cells were tested in cell viability assays.

Results and Discussion

Starting from lead structures **1a** and **1b**,[45,49] we prepared 22 new compounds (**2a**–**6c**, Scheme 2).

The compounds differ in their P2 and P3 positions (Scheme 2). They contain morpholine (**2c**, **3c**, **6c**), piperazine (Pip, **2b**, **3b**), *N*-boc-piperazine (Pip-*N*-boc, **2a**, **3a**), pyridine (**2d**, **3d**, **4a**–**5d**), thiophene (**2e**, **3e**) or aniline (Ph–NH_2, **6b**) in the P3 position and hPhe (**4c**, **5c**), cyAla (**4a**, **5a**, **6a**–**c**), Leu (**4b**, **5b**) and Trp (**4d**, **5d**; all with (*S*)-configured stereo center) in the P2 position. These latter residues were previously described to improve the binding affinity in CatS inhibitors.[34] For the covalently reacting warhead functionality, we prepared α-fluorovinylsulfones and the corresponding α-fluorovinylsulfonates occupying the P1 position.

Chemistry

The synthesis route allowed many combinations of the two warhead variations with various dipeptides, resulting in the final inhibitors **1a**–**6c**.

Warhead preparation

To prepare the warhead, we first synthesized fluorinated phosphonates **11** and **12** (Scheme 3) as previously published.[49] To synthesize aldehyde **14**, we prepared the Weinreb amide **13**

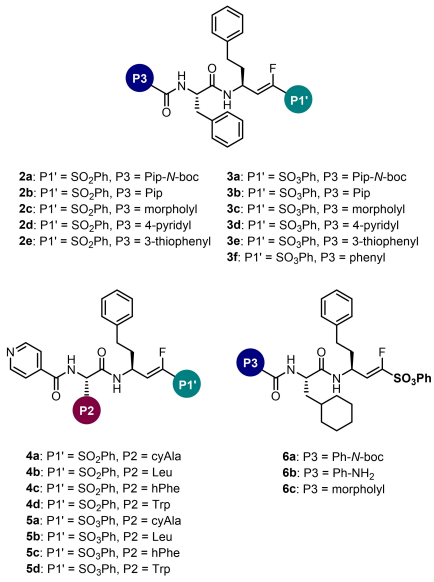

2a: P1′ = SO_2Ph, P3 = Pip-*N*-boc
2b: P1′ = SO_2Ph, P3 = Pip
2c: P1′ = SO_2Ph, P3 = morpholyl
2d: P1′ = SO_2Ph, P3 = 4-pyridyl
2e: P1′ = SO_2Ph, P3 = 3-thiophenyl

3a: P1′ = SO_3Ph, P3 = Pip-*N*-boc
3b: P1′ = SO_3Ph, P3 = Pip
3c: P1′ = SO_3Ph, P3 = morpholyl
3d: P1′ = SO_3Ph, P3 = 4-pyridyl
3e: P1′ = SO_3Ph, P3 = 3-thiophenyl
3f: P1′ = SO_3Ph, P3 = phenyl

4a: P1′ = SO_2Ph, P2 = cyAla
4b: P1′ = SO_2Ph, P2 = Leu
4c: P1′ = SO_2Ph, P2 = hPhe
4d: P1′ = SO_2Ph, P2 = Trp
5a: P1′ = SO_3Ph, P2 = cyAla
5b: P1′ = SO_3Ph, P2 = Leu
5c: P1′ = SO_3Ph, P2 = hPhe
5d: P1′ = SO_3Ph, P2 = Trp

6a: P3 = Ph-*N*-boc
6b: P3 = Ph-NH_2
6c: P3 = morpholyl

Scheme 2. Optimized cathepsin S inhibitors with variations in P1′, P2 and P3.

ChemMedChem
Research Article
doi.org/10.1002/cmdc.202300160
Chemistry Europe
European Chemical Societies Publishing

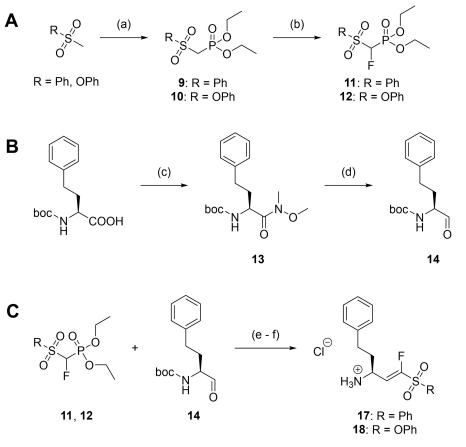

Scheme 3. (**A**) Phosphonate preparation (**9**–**12**). (a) KHMDS/*n*-BuLi, DECP; THF; −78/0 °C; 3 h; 43–82 %. (b) LHMDS, Selectfluor; THF/DMF; −78 °C–0 °C; 4 h; 45–46 %. (**B**) Aldehyde preparation (**13**–**14**). (c) *N,O*-dimethyl hydroxylamine, HOBt, TBTU, DIPEA; DCM; 0 °C – rt; 12 h; 100 %. (d) $LiAlH_4$; diethyl ether; 0 °C; 2 h; 99 %. (**C**) HWE olefination (**15**–**16**) and boc deprotection (**17**–**18**). (e) LHMDS; THF; −78 °C; 4 h; 46–59 %. (f) 4 M HCl; dioxane; rt; 2 h; 88–95 %.

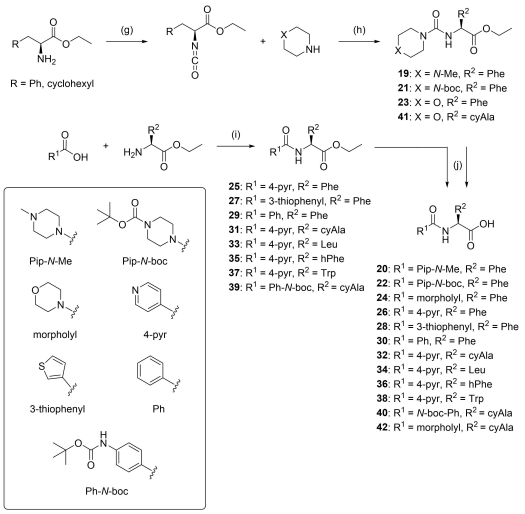

Scheme 4. Synthesis of dipeptides **20**–**42**. (g) Triphosgene, $NaHCO_3$; DCM/toluene; 0 °C; 3 h; 64 %. (h) DIPEA; THF; 0 °C – rt; 12–24 h; 84–100 %. (i) HOBt, TBTU, DIPEA; DCM; 0 °C – rt; 12–24 h; 67–100 %. (j) LiOH×1 H_2O; THF/H2O; rt; 12–24 h; 44–100 %.

of boc-homophenylalanine which was subsequently reduced to **14** using $LiAlH_4$ (Scheme 2). Aldehyde **14** and phosphonates **11** or **12** then reacted in a Horner-Wadsworth-Emmons olefination, providing fluorovinylsulfone **15** and fluorovinylsulfonate **16**. Boc-deprotection with HCl in dioxane resulted in **17**/**18** (Scheme 3).

Dipeptide synthesis

For ester-protected dipeptides **19**, **21**, **23** and **41**, we prepared isocyanates which then reacted with piperazine derivatives or morpholine. We synthesized the other ester-protected dipeptides using standard amide coupling reactions. The cleavage of the ester moieties by hydrolysis under basic conditions gave access to the final dipeptides **20**–**42** (Scheme 4).

Amide couplings

Warheads **17** or **18** were coupled with dipeptides **20**–**42** in standard amide coupling reactions (Scheme 5). The resulting inhibitors **1a**–**6c** were purified by HPLC (>95 % purity in all cases). For some compounds (**4c**, **6a**, **6b**) the formation of diastereomers could not be avoided, but the (*E*)-configurations of the isolated, purified and tested inhibitors were confirmed in all cases using the coupling constants in the NMR.

Fluorometric enzyme assays

The synthesized compounds' inhibitory activities against CatS and the off-targets CatB and CatL were tested using well-known fluorometric enzyme assays (Table 1).[50] The inhibitors were initially screened at different concentrations (20 μM, 1 μM) followed by IC_{50}/K_i value determination if >50 % inhibition at 20 μM. For more information regarding assay procedures and calculations of inhibition constants see 'Fluorometric enzyme assay' in the Experimental Section.

We started by varying the P3 position of lead compounds **1a** and **1b** (Figure 3) and prepared two compound sets, namely the corresponding fluorovinylsulfones/-sulfonates (**2a**–**6c**), and evaluated their inhibitory activities and selectivities (Table 1). We generally observed all α-fluorovinylsulfonates (**3a**–**3f** & **5a**–**5c**) to be more potent cathepsin S inhibitors than the corresponding α-fluorovinylsulfones (**2a**–**2e** & **4a**–**4d**) which already improves their selectivity towards CatB and CatL (Table 1).

We noted a good inhibition for compound **2c** (K_i = 40 nM), but a low selectivity (only 9.3-fold vs. CatB and 4.5-fold vs. CatL). The corresponding fluorovinylsulfonate **3c** has a 40-fold increased inhibitory activity (K_i = 0.9 nM), also resulting in higher selectivity towards other cathepsins (1,333-fold vs. CatB, 333-fold vs. CatL).

Next, we altered the P2 position while maintaining a 4-pyridyl residue in P3, an effective strategy to achieve the most potent and selective P2 residues. The 4-pyr moiety was among

ChemMedChem
Research Article
doi.org/10.1002/cmdc.202300160
Chemistry Europe
European Chemical Societies Publishing

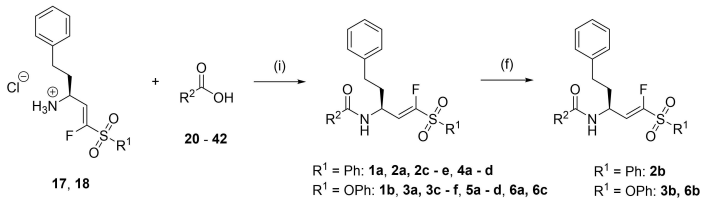

Scheme 5. Amide coupling reactions of warheads and dipeptides resulting in the final inhibitors **1a**–**6c**. (i) HOBt, TBTU or HATU, DIPEA; DCM or DCM/DMF; 0 °C – rt; 12–24 h; 11–65 %. (f) 4 M HCl; dioxane; rt; 2 h; 74–96 %.

Table 1. Enzyme assay results for compounds **2a**–**6c** compared with **1a** and **1b**.

Compd	P1′	P2	P3	Ki CatS [μM]	Ki CatB [μM]	SI CatB/CatS	Ki CatL [μM]	SI CatL/CatS
1a	Ph	Phe	Pip-*N*-Me	1.2 ± 0.28	0.47[a]	0.39	0.023[a]	0.02
1b	OPh	Phe	Pip-*N*-Me	0.010 ± 0.002[c]	0.26 ± 0.038	26	0.024 ± 0.003	2.4
2a	Ph	Phe	Pip-*N*-boc	0.14 ± 0.056	> 12	> 86	> 10	> 71
2b	Ph	Phe	Pip	1.3 ± 0.37	0.66 ± 0.084	0.51	0.79 ± 0.21	0.61
2c	Ph	Phe	morpholyl	0.040 ± 0.004	0.37 ± 0.096	9.3	0.18 ± 0.043	4.5
2d	Ph	Phe	4-pyridyl	0.10 ± 0.012	3.1[a]	31	0.11[a]	1.1
2e	Ph	Phe	3-thiophenyl	0.057 ± 0.008	1.1 ± 0.38	19	0.56 ± 0.097	9.8
3a	OPh	Phe	Pip-*N*-boc	0.0085 ± 0.0045[c]	> 12	> 1,400	> 10	> 1,100
3b	OPh	Phe	Pip	0.0057 ± 0.0023[c]	0.84 ± 0.20	147	0.087 ± 0.010	15
3c	OPh	Phe	morpholyl	0.0009 ± 0.0005[c]	1.2 ± 0.20	1,333	0.30 ± 0.014	333
3d	OPh	Phe	4-pyridyl	0.0008 ± 0.0004[c]	1.7[b]	85	0.26[b]	13
3e	OPh	Phe	3-thiophenyl	0.011 ± 0.0039[c]	4.0 ± 0.98	363	0.97 ± 0.059	88
3f	OPh	Phe	Ph	0.0073 ± 0.0018[c]	> 12	> 1,600	0.19 ± 0.16	26
4a	Ph	cyAla	4-pyridyl	0.0059 ± 0.0008	> 15	> 2,500	> 10	> 1,700
4b	Ph	Leu	4-pyridyl	0.11 ± 0.011	> 12	> 110	0.56 ± 0.11	5.1
4c	Ph	hPhe	4-pyridyl	0.17 ± 0.0033	> 15	> 88	> 10	> 59
4d	Ph	Trp	4-pyridyl	0.32 ± 0.043	> 12	> 38	2.3 ± 0.61	7.2
5a	OPh	cyAla	4-pyridyl	0.0079 ± 0.0038[c]	> 15	> 1,900	> 10	> 1,300
5b	OPh	Leu	4-pyridyl	0.035 ± 0.012[c]	> 12	> 340	> 10	> 290
5c	OPh	hPhe	4-pyridyl	0.24 ± 0.11[c]	> 12	> 50	> 10	> 42
5d	OPh	Trp	4-pyridyl	0.018 ± 0.0023[c]	1.7 ± 0.17	94	0.66 ± 0.076	37
6a	OPh	cyAla	Ph-*N*-boc	0.0059 ± 0.0018[c]	> 12	> 2,000	> 10	> 1,700
6b	OPh	cyAla	Ph-NH_2	0.0090 ± 0.0017[c]	> 12	> 1,330	> 10	> 1,100
6c	OPh	cyAla	morpholyl	0.00009 ± 0.00002[c]	> 12	> 150,000	> 10	> 125,000

[a] See Schirmeister et al.[45] [b] See Jung, Fuchs, et al.[49] [c] Time-dependent inhibition.

the top two residues in P3 regarding potency and selectivity with a better synthetic accessibility than morpholyl.[35]

Here, we also prepared corresponding α-fluorovinylsulfones/-sulfonates (**4a**–**5d**) and determined their inhibitory activities and selectivity profiles (Table 1). The cyAla residue in P2 seems to be the most favorable, with K_i values in the low nanomolar range (5.9–7.9 nM) for both warheads (**4a**, **5a**, see Table 1). The resulting selectivity towards CatB and CatL is > 1,000-fold for both compounds and enzymes. Leucin in P2 combined with an α-fluorovinylsulfonate (**5b**) also shows good CatS inhibition (K_i = 35 nM) and high selectivity, but lacks selectivity compared to **5a** with cyAla in P2. Homophenylalanine and tryptophane are not suitable as they lack affinity and selectivity compared to the most favorable compounds.

Based on the results from these first optimizations, we prepared three additional compounds (**6a**–**6c**) with cyAla in P2 and modifications in P3. For future attachments of our inhibitors onto nanodelivery systems via various linkers, we chose to introduce an amino-substituted phenyl ring in the P3 position (**6b**). We also tested the *N*-boc protected intermediate **6a**. Since we had found the morpholyl substituted compounds **2c**, **3c** to be very potent, with K_i values of 0.9 nM (**3c**) and 40 nM (**2c**) respectively, we prepared a final inhibitor combining the favorable cyAla residue in P2 with the morpholyl moiety in P3 (**6c**). The results shown in Table 1 reveal that all three moieties are suitable for the P3 position with K_i values in the low nanomolar or even subnanomolar range and high selectivities towards cathepsins B and L. However, it should be noted that combining suitable residues in P2, P3 and the most potent warhead is essential to achieve a highly active and selective inhibitor. Compound **6c** (morpholyl in P3, cyAla in P2, F-vinylsulfonate warhead) with a K_i value around 90 pM and more than 100,000-fold selectivity towards the other two cathepsins is the most potent and selective inhibitor of the series.

To verify the extraordinarily high inhibition potency of **6c**, we also used an alternative substrate (*Z*-Phe-Arg-AMC) and

ChemMedChem
Research Article
doi.org/10.1002/cmdc.202300160
Chemistry Europe
European Chemical Societies Publishing

repeated the inhibition experiments, resulting in a similar K_i (120 pM, see Figure 5 and Fluorometric enzyme assay).

Generally, the progress curves for α-fluorovinylsulfones are linear, indicating that the inhibition is not time-dependent (Figure 4). For the α-fluorovinylsulfonates, we observed time-dependent inhibition (Figure 5) with biphasic binding behavior as we have reported previously for α-fluorovinylsulfonate inhibitors of the cysteine protease rhodesain.[49] Thus, we also determined further inhibition constants, such as k_3, k_4 and K_i* (dissociation constant of final covalent complex) using the slow-binding equation for these compounds [**1b**, **3a–f**, **5a–6c**, Table 2, and Equation (1), which depicts enzyme-inhibitor complex formation and the relevant constants].[51]

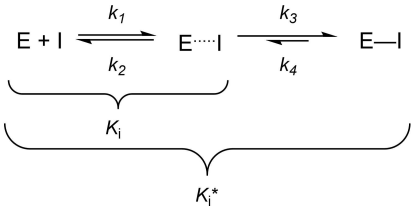

(1)

We found the rate constant of the dissociation of the final complex (k_4) to be significantly lower than the association rate constant (k_3) for all time-dependent compounds (Table 2), suggesting tight-binding behavior. The dissociation constants of the final covalent complexes (K_i*) are in the low nanomolar

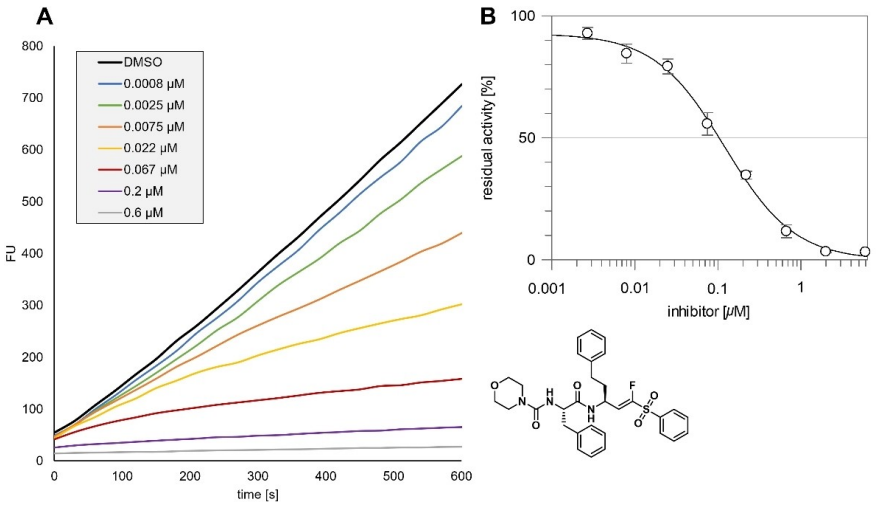

Figure 4. Assay results for **2c** (bottom right). (**A**) Fluorescence-time plot for **2c** vs. CatS with different inhibitor concentrations [µM] showing linear progress curves. (**B**) Residual enzyme activity [%] vs. inhibitor concentration [µM] for IC_{50} calculation. K_i value was calculated using the Cheng-Prusoff equation.[51]

Table 2. Inhibition data and kinetic constants for time-dependent CatS inhibitors.[a]

Compd	P2	P3	Ki [µM]	k3 [s-1]	k4 [s-1]	Ki* [µM]
1b	Phe	Pip-*N*-Me	0.010 ± 0.002	0.0015	0.0002	0.0012
3a	Phe	Pip-*N*-boc	0.0085 ± 0.0045	0.0024	0.0004	0.0012
3b	Phe	Pip	0.0057 ± 0.0023	0.0020	0.0004	0.0010
3c	Phe	Morpholyl	0.0009 ± 0.0005	0.0021	0.0003	0.00011
3d	Phe	4-pyridyl	0.0008 ± 0.0004	0.0012	0.0004	0.00020
3e	Phe	3-thiophenyl	0.011 ± 0.0039	0.0016	0.0002	0.0012
3f	Phe	Ph	0.0073 ± 0.0018	0.0018	0.0003	0.0010
5a	cyAla	4-pyridyl	0.0079 ± 0.0038	0.0015	0.0003	0.0013
5b	Leu	4-pyridyl	0.035 ± 0.012	0.0016	0.0003	0.0055
5c	hPhe	4-pyridyl	0.24 ± 0.11	0.0017	0.0002	0.025
5d	Trp	4-pyridyl	0.018 ± 0.0023	0.0022	0.0002	0.0015
6a	cyAla	Ph-*N*-boc	0.0059 ± 0.0018	0.0019	0.0002	0.00056
6b	cyAla	Ph-NH_2	0.0090 ± 0.0017	0.0007	0.0001	0.00038
6c	cyAla	morpholyl	0.00009 ± 0.00002	0.0017	0.0002	0.00001

[a] k_3, k_4 and K_i* calculated with the slow-binding equation.[52]

ChemMedChem
Research Article
doi.org/10.1002/cmdc.202300160
Chemistry Europe
European Chemical Societies Publishing

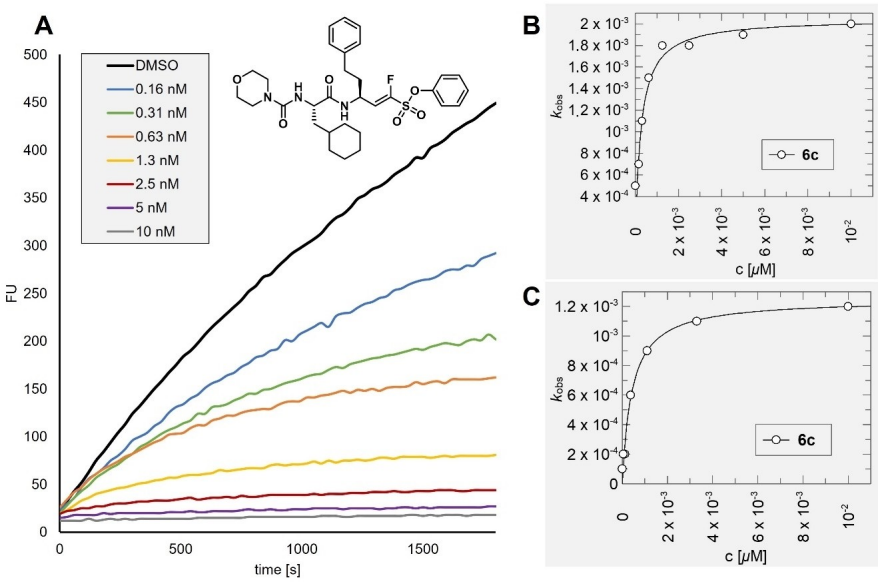

Figure 5. Assay results for **6c** (bottom right). (**A**) Fluorescence-time plot for **6c** vs. CatS with different inhibitor concentrations [nM] showing a biphasic behavior, thus a time-dependent inhibition mode. Substrate: *Z*-Val-Val-Arg-AMC. (**B**) k_{obs} [s^{-1}] vs. inhibitor concentration [μM] plots resulting from assays with substrate *Z*-Val-Val-Arg-AMC for K_i calculation using the slow-binding equation.[52] (**C**) k_{obs} [s^{-1}] vs. Inhibitor concentration [μM] plots resulting from assays with substrate *Z*-Phe-Arg-AMC for K_i calculation using the slow-binding equation.[52]

to subnanomolar range proving the very tight binding of the inhibitors.

Dilution assay

With dilution assays, we proved that the inhibitors are reversible as expected from our previous experiences with such compounds.[49] For the experiments, two compounds (F-vinylsulfonate **3c**, F-vinylsulfone **4a**) were incubated with cathepsin S, followed by 100-fold dilution with substrate-containing assay buffer. In case of reversible inhibition, the enzyme activity should recover. Furthermore, we used the pan-cathepsin inhibitor K11777 as an irreversible control.[53]

Figure 6 shows that enzyme activity can be recovered for F-vinylsulfones and -sulfonates, suggesting reversible inhibition as anticipated.

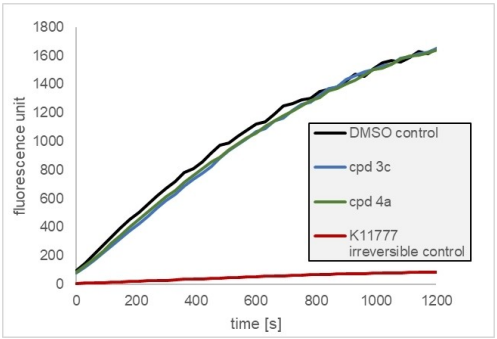

Figure 6. Dilution assays. DMSO as control (black) and **K11777** as irreversible control (red). Incubation of CatS with compounds **3c** (F-vinylsulfonate, blue) and **4a** (F-vinylsulfone, green) followed by 100-fold dilution results in an enzyme activity recovery.

SAR discussion

Comparing the K_i values of the lead compounds F-vinylsulfone **1a** (K_i = 1.2 μM) and F-vinylsulfonate **1b** (K_i = 0.010 μM) with P3 substituted inhibitors **2a**–**2e** and **3a**–**3f** shows significantly enhanced affinity towards the target enzyme CatS in all cases except for piperidyl substituted vinylsulfone **2b** (K_i = 1.3 μM) and 3-thiophenyl substituted vinylsulfonate **3e** (K_i = 0.011 μM). The non-covalent docking results show scores in the same range or even higher compared to the leads **1a** & **1b**. For compound **3f** the predicted score for the stability of the covalent complex is even higher compared to the lead compounds (see Table B, Supporting Information). Additionally,

ChemMedChem
Research Article
doi.org/10.1002/cmdc.202300160
Chemistry Europe
European Chemical Societies Publishing

the selectivities for CatS increased significantly towards CatB for all P3 modified compounds (**2a**–**3f**) by up to 220-fold for inhibitor **2a** vs **1a**. The selectivity towards CatL also improved in all cases (**2a**–**3f**) from 0.02-fold for **1a** to >71-fold for **2a** (vinylsulfones) and from 2.4-fold for **1b** to >1,100-fold for **3a** (vinylsulfonates). Overall, the vinylsulfonate warhead resulted in more potent inhibitors as exemplified for compounds **2b** vs **3b**. Superposition of the covalent docking poses of both compounds revealed that the phenylalanine substituent of **3b** leads to a different orientation of the phenyl ring inside the S2 subpocket of the active site, where additional face to edge and face to face π-stacking interactions with Phe211 and Phe70 could be possible, possibly leading to tighter binding of **3b** compared to **2b** (Figure 7).

Replacing phenylalanine in P2 with four different amino acids while maintaining the 4-pyridyl substituent in P3 lead to the result that the cyAla-residue is best suited to address the S2 pocket of the enzyme with both warheads. This is highlighted by the increase in potency for the vinylsulfone-based inhibitor **4a** (K_i = 0.006 μM) compared to **2d** (K_i = 0.10 μM) and a better selectivity towards both off-targets (>2,500-fold vs CatB and >1,700-fold vs CatL). For the vinylsulfonate-based inhibitor series, the same exchange resulted in a potency drop of about 10-fold (**3d** vs **5a**) but a big jump in selectivity (>1,900-fold vs CatL and >1300-fold vs CatL) for inhibitor **5a**. This might be due to the sp^3-hybridization of the carbon atoms of the cyAla substituent, which better fills the S2 subpocket of CatS and presumably generates new non-polar interactions with the subpocket atoms compared to the sp^2-hybridized planar phenyl ring (Figure 8). The S2 pockets of both off-target cathepsins lack the depth for accepting bulky residues. Additionally, a water molecule present in the S2 pocket, could putatively be expelled by the hydrophobic cyAla residue and thus lead to a change in entropy and thereby have an impact on the binding free energy.

Combining the cyAla motif in P2 with morpholine in P3 and the vinylsulfonate warhead yielded the most potent inhibitor **6c**, with a K_i-value in the picomolar range and excellent selectivities over CatB (>150,000) and CatL (>125,000). Superposition of the non-covalent docking pose of **6c** with the covalent enzyme-inhibitor complex shows that all polar interactions between the non-covalently bond inhibitor and the enzyme should still be intact after the covalent bond formation (Figure 9). Compound **6c** also has one of the highest scores for the stability of the covalent enzyme inhibitor complex (Affinity △G, MOE-score = −6.0 kcal/mol) as well as the second highest HYDE-score of all inhibitors with −50 kJ/mol (Table B, Supporting Information).

The incorporation of an amine functionality in the P3 site for compound **6b** (K_i = 9 nM) and its boc-protected intermediate **6a** (K_i = 6 nM) did not deteriorate the affinity or the selectivity for the target enzyme (Table 1). Therefore, **6b** can be used in future studies with nanodelivery systems.

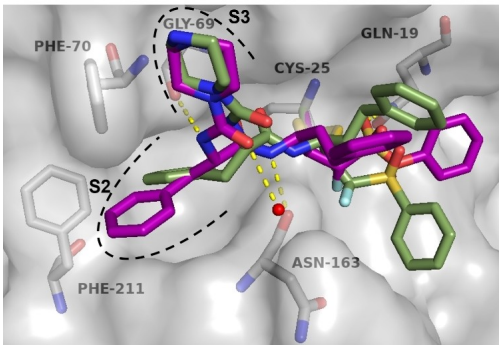

Figure 7. Superposition of the covalent docking poses of **2b** (smudge green carbon atoms) and **3b** (purple carbon atoms) inside the active site of CatS (pdb: 1NPZ). Polar interactions between **3b** and the enzyme are depicted as yellow dashed lines.

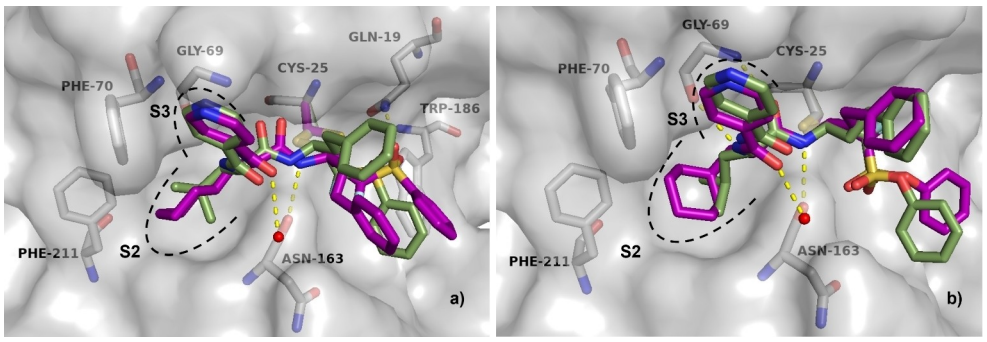

Figure 8. Predicted binding modes and non-covalent interactions (yellow dashed lines) of different inhibitors inside the CatS binding pocket (pdb: 1NPZ). (**A**) Superposition of the covalent docking poses of **4a** (purple carbon-atoms) & **4b** (smudge green carbon atoms). (**B**) Superposition of the covalent docking poses of **5a** (purple carbon-atoms) & **5b** (smudge green carbon atoms).

ChemMedChem
Research Article
doi.org/10.1002/cmdc.202300160
Chemistry Europe
European Chemical Societies Publishing

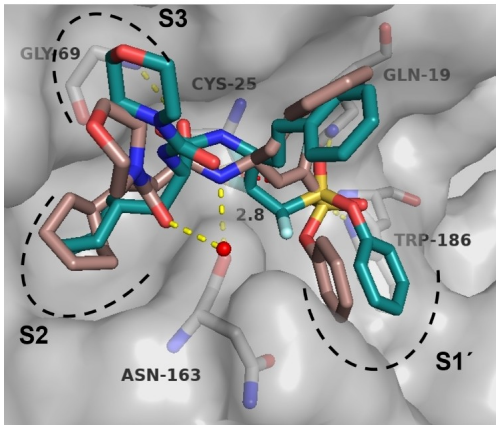

Figure 9. Superposition of the non-covalent docking pose of **6c** (darksalmon carbon atoms) and the covalent docking pose of **6c** (teal carbon atoms) inside the active site of CatS (pdb: 1NPZ). Polar interactions between the non-covalent pose of **6c** and the enzyme are depicted as yellow dashed lines. The distance between the electrophilic C-atom of **6c** and Cys25 is shown as red dashed line with the measured distance in Å.

Cell viability

Selected compounds were tested in a CellTiter-Glo Luminescent Cell Viability assay to assess their cytotoxicity. We used MDA-MB-231 cells which are breast cancer cells that compensate the inhibition of CatS and other cathepsins. Therefore, only unspecific cytotoxic effects, that are not related to CatS inhibition, are detected.[54] We did not observe significant cytotoxicity (Figure 10) after 24 h treatment at concentrations >1,000-fold higher (20 μM) than the compounds' K_i values in the low nanomolar range. Only compounds **5a** and **6b** exhibited low cytotoxic effects at the highest concentration applied (100 μM), which was >10,000-fold the compounds' K_i values. In conclusion, the exemplarily selected compounds do not affect cell viability of MDA-MB-231 cells at their biologically active concentrations.

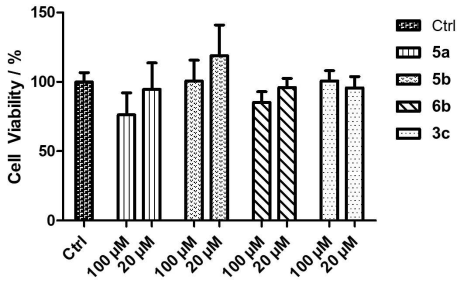

Figure 10. Cell viability of compounds **5a**, **5b**, **6b** and **3c**-treated MDA-MB-231 cells determined by CellTiter-Glo Luminescent Cell Viability Assay. Cells were treated for 24 h with each compound at two different concentrations, 100 μM or 20 μM, respectively. Significant cytotoxic effect was observed for MDA-MB-231 cells treated with **5a** and **6b** at 100 μM. All experiments were performed in quadruplicates and data are shown as mean ± SD from three independent experiments.

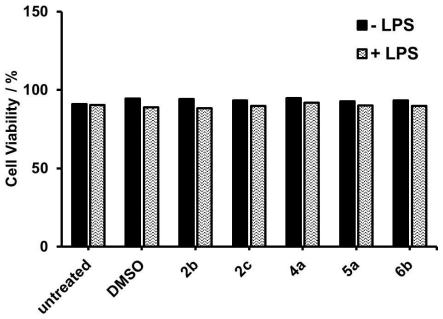

Figure 11. Cell viability of compounds **2b**, **2c**, **4a**, **5a**, and **6b**-treated murine CD11c$^+$ DC. Cells were treated for 24 h with each compound at 1 μM concentration. No significant cytotoxic effects were observed.

In addition, the cytotoxic effect of several compounds was also tested on single cell level using murine DC. The various compounds (1 μM) were applied alone or followed by administration of the DC activator lipopolysaccharide (100 ng/mL) required to achieve robust T cell stimulatory activity. Neither compound exerted major cytotoxic activity on CD11c$^+$ DC at concentrations about 1,000-fold higher than their K_i values as assessed using membrane impermeable fixable viability dye, which binds to amines of cytoplasmic proteins of dead cells with a porous cell membrane (Figure 11).

Conclusions

Here, we have demonstrated that α-fluorovinylsulfones and -sulfonates are potent covalent-reversible cathepsin S inhibitors. Both warheads are well suitable for the target enzyme, with the α-fluorovinylsulfonates being more effective. Starting from the K11777 scaffold, we replaced residues in the P2 and P3 positions, resulting in high affinity compounds, some of them being highly selective against off-target cathepsins. In the P3 position, we observed a morpholyl (**3c**) or 4-pyridyl (**3d**) residue to be most suitable with K_i values in the subnanomolar range and moderate selectivity. In the P2 position, we found that cyAla (**4a**, **5a**) increased the selectivity immensely with K_i values in the low nanomolar range for the on-target CatS. Combining the best-performing residues of P2 and P3 to form a morpholyl-cyAla-hPhe-F-vinylsulfonate-Ph motif (**6c**) proved to be most effective with subnanomolar affinity (K_i = 0.09 nM, K_i^* = 0.01 nM) and exceptional selectivity towards cathepsins B and L (>150,000/125,000-fold). The time-dependent inhibition enables slow-tight binding, thus prolonging target residence times.

ChemMedChem
Research Article
doi.org/10.1002/cmdc.202300160
Chemistry Europe
European Chemical Societies Publishing

Therefore, compound **6c** will be an excellent candidate for further optimizations regarding new small molecule immunomodulators in cancer therapy, where already resistances to existing immunotherapies are known.[26] Cell viability experiments using a non-CatS sensitive cancer cell line and murine derived dendritic cells both did not show cytotoxic effects for all tested inhibitors at relevant concentrations (>1,000-fold K_i). The next steps include immunoassays with macrophages or dendritic cells to evaluate the potential of our CatS inhibitors, e.g., for immune cell polarization. This could involve markers like MHC-I and MHC-II expression as well as functional assays for T cell activation.

Moreover, development of inhibitor-nanocarrier constructs is possible with these compounds. By attaching cathepsin S inhibitors to nanocarriers, their efficacy could be further enhanced through specific targeting, e.g., to dendritic cells or other APC.[25] Compound **6b** with a free amino moiety (K_i = 9 nM, SI > 1,000) allows the attachment of various functionalities, such as linkers or nanodelivery systems.

Experimental Section

General

All reagents and solvents were purchased from Sigma-Aldrich, Alfa Aesar, Acros, TCI, BLD Pharmatech, Carbolution or Carl Roth in analytical or HPLC grade quality. Chemicals were used without further purification, whereas solvents were distilled and desiccated by standard methods if necessary. ^{1}H and ^{13}C spectra were recorded on a Bruker Fourier 300 device using DMSO-d_6 or $CDCl_3$ as solvents. Chemical shifts δ are given in parts per million (ppm) using residual proton peaks of the solvent as internal standard (^{1}H/^{13}C: DMSO 2.50/39.52 ppm; $CHCl_3$ 7.26/77.16 ppm). The compound purity was determined via HPLC-MS at λ = 254 nm using an Agilent 1100 series HPLC with an Agilent Poroshell 120 EC-C_{18} column (150×2.10 mm, 4 µm) coupled with an Agilent 1100 series LC/MSD Trap with electron spray ionization (ESI) in positive mode. All compounds tested in enzymatic assays are ≥95% pure by HPLC analysis. The mobile phase consisted of a variable mixture of ACN and H_2O with 0.01% formic acid. For purification we used a Varian PrepStar system (model 218) with a MZ-Aqua Perfect C_{18} column (250×20 mm, 7 µm) by MZ-Analysentechnik. Column chromatography was performed with silica gel (0.040–0.063 mm) and all reactions were monitored by thin-layer chromatography using Macherey-Nagel Alugram Xtra SIL G/UV254 silica gel 60 plates for detection at λ = 254 nm. Melting points were determined in open capillaries with a Schorpp Device Technology MPM-H3 instrument. Optical rotation $[\alpha]_D^{22}$ was measured on a Krss P3000 polarimeter (c = 10 mg/mL in MeOH) at 22 °C.

Syntheses

General procedures

Procedure A (HWE olefination)

The respective phosphonate (1.0 eq) was dissolved in dry THF and cooled to −78 °C. Then, 1 M KHMDS or LHMDS in THF (1.3 eq) was added dropwise and stirred for 30 min, followed by addition of boc-L-homophenylalaninal (**14**, 1.1 eq). The mixture was stirred for 3–5 h at −78 °C and stopped by adding water. The solvent was evaporated under reduced pressure and the residue was extracted with EA (3×), washed with water (2×), sat. aq. $NaHCO_3$ (2×), and brine (2×), then dried over Na_2SO_4. Purification by column chromatography.

Procedure B (amide couplings)

The carboxylic acid (1.2 eq) was dissolved in DCM or a mixture of DCM/DMF, and cooled to 0 °C. Then, HOBt (1.2 eq), TBTU (1.2 eq), and DIPEA (3.5 eq) were added, and the mixture was stirred for 20 min until all components dissolved. The respective amine (1.0 eq) was added, and the mixture was stirred for an additional 12–24 h, then stopped by adding water. The mixture was extracted with DCM (2×) and the combined organic extracts were washed with water (2×), sat. aq. $NaHCO_3$ (2×), and brine (2×). After drying the crude product over Na_2SO_4, it was purified by column chromatography.

Procedure C (boc deprotection)

HCl (4 M) in dioxane was added dropwise to the boc-protected amine (1.0 eq) until all components dissolve. The mixture was stirred for 2–12 h and the product was precipitated with diethyl ether and lyophilized afterwards.

Procedure D (alkaline hydrolysis)

The ester (1.0 eq) was dissolved in THF. LiOH monohydrate (4.0 eq) was dissolved in water and added to the reaction dropwise. The mixture was stirred for 12–24 h, then the solvent was removed under reduced pressure. The pH of the aqueous phase was adjusted with $KHSO_4$ to 5, giving the products as solids that were further lyophilized.

Starting material preparation

Ethyl (S)-2-isocyanato-3-phenylpropanoate (7)

Phenylalanine ethyl ester (1.0 eq, 10 mmol, 2.2 g) was dissolved in DCM and an sat. aq. $NaHCO_3$ solution and cooled to 0 °C. Triphosgene (0.33 eq, 3.3 mmol, 0.99 g) was added and the mixture was stirred for 1 h. The mixture was extracted with DCM (2×) and the combined organic extracts were washed with sat. aq. $NaHCO_3$ (2×), and brine (2×), then dried over Na_2SO_4 and concentrated under reduced pressure, resulting in the crude product that was used without further purification (1.4 g, 6.4 mmol, 64%). ^{1}H NMR (300 MHz, $CDCl_3$) δ[ppm] = 7.35–7.03 (m, 5H), 4.73–4.51 (m, 1H), 4.30–4.07 (m, 2H), 3.16–2.91 (m, 2H), 1.32–1.09 (m, 3H). ^{13}C NMR (75 MHz, $CDCl_3$) δ[ppm] = 170.7, 135.7, 129.5, 128.7, 127.5, 62.7, 58.7, 40.1, 14.2. $[\alpha]_D^{22} = -9°$.

Ethyl (*S*)-2-amino-3-cyclohexylpropanoate (8)

(*S*)-2-Amino-3-cyclohexylpropanoic acid (1.0 eq, 10 mmol, 1.7 g) was dissolved in EtOH and $SOCl_2$ (1.1 eq, 11 mmol, 0.8 mL) was added dropwise. The mixture was stirred under reflux for 12 h and the reaction was stopped with sat. aq. $NaHCO_3$. The solvent was evaporated under reduced pressure and the residue was extracted with EA, giving the crude product that was used without further purification (1.4 g, 7.0 mmol, 68%). ^{1}H NMR (300 MHz, $CDCl_3$) δ[ppm] = 4.20–4.01 (m, 2H), 4.00–3.83 (m, 2H, NH_2), 3.75 (tt, J = 9.3, 7.0 Hz, 1H), 1.90 (t, J = 7.0 Hz, 2H), 1.65–1.31 (m, 11H), 1.24 (t, J =

ChemMedChem
Research Article
doi.org/10.1002/cmdc.202300160
Chemistry Europe
European Chemical Societies Publishing

8.0 Hz, 3H). ^{13}C NMR (75 MHz, $CDCl_3$) δ[ppm] = 173.1, 60.5, 54.7, 36.9, 33.4, 33.0, 26.2, 25.5, 13.9. $[\alpha]_D^{22} = -25°$.

Phosphonate preparation

Diethyl ((phenylsulfonyl)methyl)phosphonate (9)

Phenyl methylsulfone (1.0 eq, 15 mmol, 2.2 g) was dissolved in dry THF and cooled to 0 °C. After dropwise addition of 2.5 M *n*-BuLi in hexanes (2.5 eq, 37.5 mmol, 15 mL), the mixture was stirred for 30 min. Then, DECP (1.1 eq, 16.5 mmol, 2.71 mL) was added and the mixture was stirred for 3 h. The reaction was stopped with acetic acid, and the solvent was evaporated under reduced pressure. The residue was extracted with EA (3×) and the combined extracts were washed with water (2×), and brine (2×), then dried over Na_2SO_4. The crude product was purified using column chromatography (CH:EA 1:3 – 100% EA), resulting in a yellow oil (3.6 g, 12.3 mmol, 82%). ^{1}H NMR (300 MHz, DMSO-d_6) δ[ppm] = 8.00–7.90 (m, 2H), 7.79–7.54 (m, 3H), 4.44 (d, J = 17.0 Hz, 2H), 4.06–3.88 (m, 4H), 1.21–1.04 (m, 6H). ^{13}C NMR (75 MHz, DMSO-d_6) δ[ppm] = 140.5, 133.8, 129.0, 127.8, 62.3, 52.3, 50.6, 16.0.

Phenyl (diethoxyphosphoryl)methanesulfonate (10)

Phenyl methanesulfonate (1.0 eq, 67 mmol, 11.54 g) was dissolved in dry THF and cooled to −78 °C. Then, 1 M KHMDS (1.3 eq, 88 mmol, 88 mL) was added dropwise and the mixture was stirred for 30 min. Afterwards, DECP (1.1 eq, 74 mmol, 12.2 mL) was added and the mixture was stirred for 3 h and stopped by adding sat. aq. NH_4Cl. The solvent was evaporated under reduced pressure and the residue was extracted with EA (3×). The combined extracts were washed with water (2×), and brine (2×), then dried over Na_2SO_4. The crude product was purified by column chromatography (CH:EA 1:2 – 100% EA), resulting in a colorless oil (9.0 g, 29 mmol, 43%). ^{1}H NMR (300 MHz, DMSO-d_6) δ[ppm] = 7.55–7.44 (m, 2H), 7.42–7.31 (m, 3H), 4.63 (d, J = 17.4 Hz, 2H), 4.24–4.05 (m, 4H), 1.25 (t, J = 7.0 Hz, 6H). ^{13}C NMR (75 MHz, DMSO-d_6) δ[ppm] = 148.9, 130.2, 127.5, 122.3, 62.9, 47.7, 45.9, 16.1.

Diethyl (fluoro(phenylsulfonyl)methyl)phosphonate (11)

9 (1.0 eq, 18 mmol, 5.4 g) was dissolved in dry THF and cooled to −78 °C. Then, 1 M LHMDS in THF (1.3 eq, 24 mmol, 24 mL) was added dropwise and the mixture was stirred for 30 min. Afterwards, *Selectfluor* (1.5 eq, 27 mmol, 9.6 g) was dissolved in DMF and added to the mixture. It was stirred for 4 h at 0 °C and stopped by adding sat. aq. NH_4Cl. The solvent was evaporated under reduced pressure and the residue was extracted with DCM (3×). The combined extracts were washed with water (2×), sat. aq. $NaHCO_3$ (2×), and brine (2×), then dried over Na_2SO_4. The crude product was purified by column chromatography (CH:EA 2:1–1:2), resulting in a colorless solid (2.5 g, 8.0 mmol, 45%). ^{1}H NMR (300 MHz, DMSO-d_6) δ[ppm] = 8.00–7.92 (m, 2H), 7.88–7.76 (m, 1H), 7.77–7.65 (m, 2H), 6.62 (dd, J = 42.8, 6.8 Hz, 1H), 4.27–4.02 (m, 4H), 1.30–1.16 (m, 6H). ^{13}C NMR (75 MHz, DMSO-d_6) δ[ppm] = 136.2, 135.2, 129.5, 129.3, 64.3, 64.1, 16.1. MP = 67–69 °C.

Phenyl (diethoxyphosphoryl)fluoromethanesulfonate (12)

10 (1.0 eq, 28 mmol, 8.9 g) was dissolved in dry THF and cooled to −78 °C. Then, 1 M LHMDS in THF (1.3 eq, 37 mmol, 37 mL) was added dropwise and the mixture was stirred for 30 min. Afterwards, *Selectfluor* (1.5 eq, 42.5 mmol, 15.0 g) was dissolved in DMF and added to the mixture. It was allowed to warm to 0 °C, stirred for 4 h, and stopped by adding sat. aq. NH_4Cl. The solvent was evaporated under reduced pressure and the residue was extracted with DCM (3×). The combined extracts were washed with water (2×), sat. aq. $NaHCO_3$ (2×), and brine (2×), then dried over Na_2SO_4. The crude product was purified by column chromatography (CH:EA 2:1–1:2), resulting in a colorless oil (4.4 g, 13.3 mmol, 46%). ^{1}H NMR (300 MHz, $CDCl_3$) δ[ppm] = 7.40–7.19 (m, 2H), 7.22–7.02 (m, 3H), 5.66 (dd, J = 45.2, 7.2 Hz, 1H), 4.37–4.18 (m, 1H), 4.18–4.02 (m, 4H), 1.41–1.14 (m, 6H). ^{13}C NMR (75 MHz, $CDCl_3$) δ[ppm] = 129.6, 127.8, 124.8, 122.0, 119.9, 64.5, 15.9.

Aldehyde preparation

tert-Butyl (*S*)-(1-(methoxy(methyl)amino)-1-oxo-4-phenylbutan-2-yl) carbamate (13)

Boc-L-homophenylalanine (1.2 eq, 18 mmol, 5.0 g) was dissolved in DCM and cooled to 0 °C. Then, HOBt (1.2 eq, 18 mmol, 2.4 g), TBTU (1.2 eq, 18 mmol, 5.8 g), and DIPEA (3.5 eq, 52.5 mmol, 9.2 mL) were added and the mixture was stirred for 20 min until all components were dissolved. *N,O*-Dimethyl hydroxylamine (1.0 eq, 15 mmol, 1.5 g) was added and the mixture was stirred for an additional 12–24 h, then stopped by adding water. The mixture was extracted with DCM (2×) and the combined organic extracts were washed with water (2×), sat. aq. $NaHCO_3$ (2×), and brine (2×). After drying the crude product over Na_2SO_4, it was purified by column chromatography (CH:EA 2:1–1:4), giving the product as a colorless oil (4.8 g, 15 mmol, 100%). ^{1}H NMR (300 MHz, DMSO-d_6) δ[ppm] = 6.77–6.65 (m, 2H), 6.66–6.51 (m, 3H), 3.82–3.65 (m, 1H), 2.99 (s, 3H), 2.76 (s, 3H), 2.22–2.03 (m, 1H), 2.01–1.87 (m, 2H), 1.23 (q, J = 7.0, 6.4 Hz, 2H), 0.91–0.78 (m, 9H). ^{13}C NMR (75 MHz, DMSO-d_6) δ[ppm] = 155.6, 141.1, 128.4, 128.2, 125.8, 77.9, 60.9, 50.09, 40.4, 40.1, 39.8, 39.5, 39.2, 39.0, 38.7, 32.3, 31.6, 28.2, 26.3. $[\alpha]_D^{22} = -40°$.

tert-Butyl (*S*)-(1-oxo-4-phenylbutan-2-yl)carbamate (14)

13 (1.0 eq, 15 mmol, 5.2 g) was dissolved in dry diethyl ether and cooled to 0 °C. $LiAlH_4$ (1.3 eq, 19.5 mmol, 0.74 g) was added in portions and the mixture was stirred for 2 h. Afterwards, the reaction was stopped with 0.33 M $KHSO_4$ and the mixture was extracted with diethyl ether (2×). The combined extracts were washed with water (2×), 1 M HCl (2×), sat. aq. $NaHCO_3$ (2×), and brine (2×). The product was dried over Na_2SO_4, resulting in a colorless oil that solidified upon standing (3.9 g, 14.7 mmol, 99%). ^{1}H NMR (300 MHz, $CDCl_3$) δ[ppm] = 9.55 (s, 1H), 7.46–7.00 (m, 5H), 5.07 (s, 1H), 4.37–4.09 (m, 1H), 2.71 (t, J = 7.5 Hz, 2H), 2.37–2.01 (m, 2H), 1.56–1.28 (m, 9H). ^{13}C NMR (75 MHz, $CDCl_3$) δ[ppm] = 199.7, 128.8, 128.6, 126.5, 77.6, 77.2, 76.7, 66.0, 31.6, 31.1, 28.4, 15.4. $[\alpha]_D^{22} = -28°$.

Warhead preparation

tert-Butyl (*S,E*)-(1-fluoro-5-phenyl-1-(phenylsulfonyl)pent-1-en-3-yl)carbamate (15)

15 was prepared according to procedure A using 1 M LHMDS (2.6 mmol, 2.6 mL), phosphonate **11** (2.0 mmol, 0.60 g), and aldehyde 14 (2.2 mmol, 0.58 g). Purification by column chromatography (CH:EA 6:1–4:1) resulted in a colorless oil (0.50 g, 1.2 mmol, 59%). ^{1}H NMR (300 MHz, $CDCl_3$) δ[ppm] = 8.10 (s, 2H), 7.77–7.51 (m, 3H), 7.40–7.19 (m, 5H), 5.85 (dd, $J_{H\text{-}F}$ = 21.3 Hz, $J_{H\text{-}H}$ = 10.1 Hz, 1H), 5.38–5.22 (m, 1H), 4.81–4.68 (m, 1H), 2.80 (ddd, J = 16.9, 10.2, 6.0 Hz, 2H), 2.13–1.80 (m, 2H), 1.47 (s, 9H). ^{13}C NMR (75 MHz, $CDCl_3$)

ChemMedChem | Research Article doi.org/10.1002/cmdc.202300160 | Chemistry Europe European Chemical Societies Publishing

δ[ppm] = 149.8 (d, $J_{C\text{-}F}$ = 299 Hz), 140.8, 137.6, 134.5, 129.4, 128.9, 128.6, 128.4, 126.2, 121.0 (d, $J_{C\text{-}F}$ = 4.2 Hz), 77.0, 46.1 (d, $J_{C\text{-}F}$ = 2.2 Hz), 32.0, 31.0, 28.3. $[\alpha]_D^{22} = -10°$.

Phenyl (*S,E*)-3-((*tert*-butoxycarbonyl)amino)-1-fluoro-5-phenylpent-1-ene-1-sulfonate (16)

16 was prepared according to procedure A using phosphonate **12** (4.0 mmol, 1.3 g). Purification by column chromatography (CH : EA 5 : 1–3 : 1) resulted in a colorless oil (0.80 g, 1.8 mmol, 46 %). ^{1}H NMR (300 MHz, $CDCl_3$) δ[ppm] = 7.46–7.32 (m, 2H), 7.32–7.15 (m, 6H), 7.10 (d, J = 7.0 Hz, 2H), 5.91 (dd, $J_{H\text{-}F}$ = 31.3 Hz, $J_{H\text{-}H}$ = 8.6 Hz, 1H), 4.68–4.27 (m, 2H), 2.66–2.43 (m, 2H), 1.97–1.66 (m, 2H), 1.43 (s, 9H). ^{13}C NMR (75 MHz, $CDCl_3$) δ[ppm] = 154.8, 150.8, 148.9 (d, $J_{C\text{-}F}$ = 296 Hz), 140.2, 130.2, 128.8, 128.4, 128.0, 126.5, 122.4 (d, $J_{C\text{-}F}$ = 4.1 Hz), 122.3, 80.4, 46.3 (d, $J_{C\text{-}F}$ = 2.1 Hz), 35.9, 31.9, 28.4. $[\alpha]_D^{22} = -15°$.

(S,E)-1-Fluoro-5-phenyl-1-(phenylsulfonyl)pent-1-en-3-aminium chloride (17)

17 was prepared according to procedure C using **15** (1.2 mmol, 0.50 g), resulting in a colorless solid (0.39 g, 1.1 mmol, 95 %). ^{1}H NMR (300 MHz, DMSO-d_6) δ[ppm] = 8.71 (s, 3H), 8.02 (dd, J = 7.3, 1.7 Hz, 2H), 7.97–7.82 (m, 1H), 7.76 (dd, J = 8.4, 7.0 Hz, 2H), 7.28–7.10 (m, 3H), 7.11–7.02 (m, 2H), 6.55 (dd, $J_{H\text{-}F}$ = 32.6 Hz, $J_{H\text{-}H}$ = 9.8 Hz, 1H), 4.07–3.94 (m, 1H), 2.57–2.39 (m, 2H), 2.26–1.95 (m, 2H). ^{13}C NMR (75 MHz, DMSO-d_6) δ[ppm] = 154.6 (d, $J_{C\text{-}F}$ = 298 Hz), 140.3, 136.4, 136.1, 130.7, 130.2, 129.0, 128.9, 128.6, 126.7, 115.0 (d, $J_{C\text{-}F}$ = 3.5 Hz), 45.5 (d, $J_{C\text{-}F}$ = 2.6 Hz), 33.9 (d, $J_{C\text{-}F}$ = 1.3 Hz), 31.0. $[\alpha]_D^{22} = -15°$. MP = 130–132 °C.

Phenyl (S,E)-3-amino-1-fluoro-5-phenylpent-1-ene-1-sulfonate hydrochloride (18)

18 was prepared according to procedure C using **16** (1.7 mmol, 0.73 g), resulting in a colorless solid (0.55 g, 1.5 mmol, 88 %). ^{1}H NMR (300 MHz, DMSO-d_6) δ[ppm] = 8.77 (s, 3H), 7.59–7.50 (m, 2H), 7.49–7.39 (m, 3H), 7.36 (t, J = 7.2 Hz, 2H), 7.28–7.21 (m, 1H), 7.21–7.11 (m, 2H), 6.45 (dd, $J_{H\text{-}F}$ = 32 Hz, $J_{H\text{-}H}$ = 9.7 Hz, 1H), 4.15 (td, J = 9.2, 5.3 Hz, 1H), 2.52–2.36 (m, 2H), 2.22–2.03 (m, 1H), 2.02–1.85 (m, 1H). ^{13}C NMR (75 MHz, DMSO-d_6) δ[ppm] = 149.7 (d, $J_{C\text{-}F}$ = 300 Hz), 149.0, 140.4, 130.9, 129.3, 129.2, 128.9, 126.4, 122.3, 118.6 (d, $J_{C\text{-}F}$ = 3.2 Hz), 45.5 (d, $J_{C\text{-}F}$ = 2.2 Hz), 40.5, 33.6, 30.5. $[\alpha]_D^{22} = -13°$. MP = 141–143 °C.

Dipeptide preparation

Ethyl (4-methylpiperazine-1-carbonyl)-l-phenylalaninate (19)

Compound **7** (1.0 eq, 8.5 mmol, 1.9 g) was dissolved in THF and cooled to 0 °C. Then, *N*-methyl piperazine (1.1 eq, 9.3 mmol, 1.0 mL) was added dropwise. After 12 h, THF was removed under reduced pressure and the residue was extracted with EA (3×). The combined organic extracts were washed with water (2×), sat. aq. $NaHCO_3$ (2×), and brine (2×). The organic layer was dried with Na_2SO_4 and evaporated. Purification by column chromatography (DCM : MeOH 19 : 1) resulted in a colorless solid (2.4 g, 7.4 mmol, 87 %). ^{1}H NMR (300 MHz, DMSO-d_6) δ[ppm] = 7.35–7.09 (m, 5H), 6.79 (d, J = 7.9 Hz, 1H, NH), 4.23 (ddd, J = 8.9, 7.8, 6.5 Hz, 1H), 4.01 (qd, J = 7.1, 1.7 Hz, 2H), 3.24 (q, J = 4.5 Hz, 4H), 3.04–2.83 (m, 2H), 2.20–2.15 (m, 4H), 2.13 (s, 3H), 1.09 (t, J = 7.1 Hz, 3H). ^{13}C NMR (75 MHz, DMSO-d_6) δ[ppm] = 173.0, 157.2, 138.0, 129.3, 128.3, 126.5, 60.3, 55.7, 54.4, 45.8, 43.5, 36.8, 14.1. $[\alpha]_D^{22} = -18°$. MP = 97–99 °C.

(4-Methylpiperazine-1-carbonyl)-L-phenylalanine (20)

20 was prepared according to procedure D using **19** (7.4 mmol, 2.4 g), resulting in a colorless solid (1.8 g, 6.3 mmol, 85 %). ^{1}H NMR (300 MHz, DMSO-d_6) δ[ppm] = 7.33–7.05 (m, 5H), 6.68 (d, J = 7.9 Hz, 1H), 4.28 –4.09 (m, 1H), 3.50–3.16 (m, 4H), 2.98 (m, 2H), 2.46–2.30 (m, 4H), 2.25 (s, 3H). ^{13}C NMR (75 MHz, DMSO-d_6) δ[ppm] = 174.6, 157.1, 139.0, 129.4, 128.0, 126.1, 56.0, 53.1, 44.8, 42.7, 39.5, 36.9. $[\alpha]_D^{22} = -17°$. MP = 121–123 °C.

tert-Butyl (*S*)-4-((1-ethoxy-1-oxo-3-phenylpropan-2-yl)carbamoyl) piperazine-1-carboxylate (21)

1-Boc piperazine (1.1 eq, 1.3 mmol, 0.24 g) was dissolved in THF. Compound **7** (1.0 eq, 1.2 mmol, 0.27 g) was added dropwise, and the mixture was stirred for 18 h at room temperature. Then, the solvent was evaporated, and the residue was extracted with EA (3×). The combined organic extracts were washed with water (2×), sat. aq. $NaHCO_3$ (2×), and brine. The crude product was dried with Na_2SO_4, and the solvent was evaporated under reduced pressure. Purification by column chromatography (DCM : MeOH 49 : 1) gave the product as a colorless oil (0.41 g, 1.0 mmol, 84 %). ^{1}H NMR (300 MHz, $CDCl_3$) δ[ppm] = 7.33–7.18 (m, 3H), 7.11 (dd, J = 7.7, 1.8 Hz, 2H), 4.89 (d, J = 7.5 Hz, 1H, NH), 4.76 (q, J = 6.1 Hz, 1H), 4.17 (q, J = 7.1 Hz, 2H), 3.48–3.23 (m, 8H), 3.09 (dd, J = 13.1, 5.8 Hz), 1.85 (s, 1H), 1.46 (s, 9H), 1.24 (td, J = 7.1, 1.0 Hz, 3H). ^{13}C NMR (75 MHz, $CDCl_3$) δ[ppm] = 172.7, 156.6, 154.7, 136.3, 129.5, 128.6, 127.2, 80.3, 61.6, 54.5, 53.6, 43.6, 38.5, 28.5, 14.3. $[\alpha]_D^{22} = -24°$.

(4-(*tert*-Butoxycarbonyl)piperazine-1-carbonyl)-l-phenylalanine (22)

22 was prepared according to procedure D using **21** (0.94 mmol, 0.38 g), resulting in a colorless solid (0.27 g, 0.71 mmol, 76 %). ^{1}H NMR (300 MHz, $CDCl_3$) δ[ppm] = 8.79 (s, 1H, OH), 7.33–7.22 (m, 3H), 7.20–7.14 (m, 2H), 5.07 (d, J = 7.1 Hz, 1H, NH), 4.65 (q, J = 6.4 Hz, 1H), 3.42–3.21 (m, 8H), 3.21–3.04 (m, 2H), 1.45 (s, 9H). ^{13}C NMR (75 MHz, $CDCl_3$) δ[ppm] = 174.7, 157.5, 154.8, 136.4, 129.5, 128.8, 127.3, 80.6, 55.0, 43.7, 37.4, 28.5. $[\alpha]_D^{22} = -23°$. MP = 82–84 °C.

Ethyl (morpholine-4-carbonyl)-L-phenylalaninate (23)

Compound **7** (1.0 eq, 4.5 mmol, 1.0 g) was dissolved in THF and cooled to 0 °C. Then, DIPEA (2.5 eq, 11 mmol, 2.0 mL) and morpholine (1.4 eq, 6.4 mmol, 0.55 mL) were added dropwise. After 12 h, THF was removed under reduced pressure and the residue was extracted with EA (3×). The combined organic extracts were washed with water (2×), sat. aq. $NaHCO_3$ (2×), and brine (2×). The organic layer was dried with Na_2SO_4 and evaporated, giving a colorless oil (1.3 g, 4.5 mmol, 100 %). ^{1}H NMR (300 MHz, $CDCl_3$) δ[ppm] = 7.38–7.16 (m, 5H), 7.12 (d, J = 11.7 Hz, 1H, NH), 4.69 (dt, J = 11.7, 7.0 Hz, 1H), 4.27–3.98 (m, 2H), 3.64 (td, J = 7.1, 1.3 Hz, 4H), 3.38 (dt, J = 10.6, 7.1 Hz, 4H), 2.97 (ddt, J = 7.0, 2.6, 0.9 Hz, 2H), 1.22 (t, J = 8.0 Hz, 3H). ^{13}C NMR (75 MHz, $CDCl_3$) δ[ppm] = 172.1, 157.3, 136.8, 129.2, 128.6, 127.2, 66.0, 61.7, 55.2, 46.7, 37.6, 14.1. $[\alpha]_D^{22} = -19°$.

(Morpholine-4-carbonyl)-L-phenylalanine (24)

24 was prepared according to procedure D using **23** (4.5 mmol, 1.3 g), resulting in a colorless oil (0.71 g, 2.7 mmol, 59 %). ^{1}H NMR

ChemMedChem
Research Article
doi.org/10.1002/cmdc.202300160
Chemistry Europe
European Chemical Societies Publishing

(300 MHz, $CDCl_3$) δ[ppm] = 7.77 (d, J = 11.9 Hz, 1H), 7.31–7.11 (m, 5H), 4.48 (dt, J = 11.9, 7.0 Hz, 1H), 3.64 (td, J = 7.1, 1.7 Hz, 4H), 3.30 (dt, J = 8.8, 7.1 Hz, 4H), 3.03 (dq, J = 7.0, 1.0 Hz, 2H). ^{13}C NMR (75 MHz, $CDCl_3$) δ[ppm] = 174.8, 157.6, 137.0, 130.1, 128.7, 126.9, 66.0, 56.2, 46.5, 37.5. $[\alpha]_D^{22} = -12°$.

(S)-Ethyl-2-(isonicotinamido)-3-phenylpropanoate (25)

25 was prepared according to procedure B using L-phenylalanine ethyl ester hydrochloride (14 mmol, 3.0 g) and isonicotinic acid (15 mmol, 1.9 g). Purification by column chromatography (CH:EA 1:4) gave a colorless oil (3.3 g, 12 mmol, 84%). ^{1}H NMR (300 MHz, DMSO-d_6) δ[ppm] = 9.18 (d, J = 7.9 Hz, 1H, NH), 8.76–8.68 (m, 2H), 7.72–7.64 (m, 2H), 7.33–7.15 (m, 5H), 4.69 (ddd, J = 10.1, 7.8, 5.2 Hz, 1H), 3.65 (s, 3H), 3.20 (dd, J = 13.7, 5.3 Hz, 1H), 3.08 (dd, J = 13.7, 10.2 Hz, 1H). ^{13}C NMR (75 MHz, DMSO-d_6) δ[ppm] = 171.8, 164.9, 150.3, 140.5, 137.5, 129.1, 128.3, 126.6, 121.3, 54.3, 52.1, 36.2. $[\alpha]_D^{22} = -37°$.

(S)-2-(Isonicotinamido)-3-phenylpropanoic acid (26)

26 was prepared according to procedure D using **25** (7.8 mmol, 2.2 g), resulting in a colorless solid (1.4 g, 5.0 mmol, 65%). ^{1}H NMR (300 MHz, DMSO-d_6) δ[ppm] = 12.87 (s, 1H, OH), 9.04 (d, J = 8.2 Hz, 1H, NH), 8.76–8.66 (m, 2H), 7.74–7.62 (m, 2H), 7.36–7.22 (m, 4H), 7.22–7.13 (m, 1H), 4.64 (ddd, J = 10.7, 8.1, 4.4 Hz, 1H), 3.22 (dd, J = 13.8, 4.5 Hz, 1H), 3.05 (dd, J = 13.8, 10.7 Hz, 1H). ^{13}C NMR (75 MHz, DMSO-d_6) δ[ppm] = 172.8, 164.8, 150.3, 140.8, 138.0, 129.1, 128.3, 126.5, 121.3, 54.3, 36.2. $[\alpha]_D^{22} = -35°$. MP = 166–168 °C.

Ethyl (thiophene-3-carbonyl)-L-phenylalaninate (27)

27 was prepared according to procedure B using L-phenylalanine ethyl ester hydrochloride (20 mmol, 4.5 g) and thiophene-3-carboxylic acid (20 mmol, 1.9 g), resulting in a colorless oil (5.5 g, 19 mmol, 95%). ^{1}H NMR (300 MHz, $CDCl_3$) δ[ppm] = 8.06 (d, J = 11.9 Hz, 1H, NH), 7.98 (dd, J = 2.7, 1.6 Hz, 1H), 7.73–7.49 (m, 2H), 7.34–7.07 (m, 5H), 4.85 (dt, J = 11.9, 7.0 Hz, 1H), 4.31–3.95 (m, 2H), 3.16–2.89 (m, 2H), 1.34–1.11 (m, 3H). ^{13}C NMR (75 MHz, $CDCl_3$) δ[ppm] = 171.8, 162.9, 136.8, 134.4, 130.2, 129.9, 129.2, 128.6, 127.2, 125.9, 61.6, 53.9, 37.7, 14.1. $[\alpha]_D^{22} = -25°$.

(Thiophene-3-carbonyl)-L-phenylalanine (28)

28 was prepared according to procedure D using **27** (15 mmol, 4.4 g), resulting in a colorless solid (4.0 g, 15 mmol, 100%). ^{1}H NMR (300 MHz, $CDCl_3$) δ[ppm] = 9.60 (s, 1H, OH), 8.22 (d, J = 12.1 Hz, 1H, NH), 7.95 (dd, J = 2.8, 1.6 Hz, 1H), 7.76 (dd, J = 7.5, 1.5 Hz, 1H), 7.60 (dd, J = 7.4, 2.8 Hz, 1H), 7.38–7.16 (m, 5H), 4.66 (dt, J = 12.1, 7.0 Hz, 1H), 3.35–3.04 (m, 2H). ^{13}C NMR (75 MHz, $CDCl_3$) δ[ppm] = 173.8, 163.0, 137.4, 134.6, 130.5, 130.1, 130.0, 128.7, 127.0, 125.4, 54.9, 37.5. $[\alpha]_D^{22} = -20°$. MP = 95–97 °C.

Ethyl benzoyl-L-phenylalaninate (29)

29 was prepared according to procedure B using L-phenylalanine ethyl ester hydrochloride (22 mmol, 5.0 g) and benzoic acid (26 mmol, 3.2 g), resulting in a colorless solid (5.2 g, 18 mmol, 80%). ^{1}H NMR (300 MHz, $CDCl_3$) δ[ppm] = 8.04 (d, J = 11.9 Hz, 1H, NH), 7.80–7.70 (m, 2H), 7.65–7.49 (m, 1H), 7.41–7.33 (m, 2H), 7.31–7.14 (m, 5H), 4.88 (dt, J = 11.9, 7.0 Hz, 1H), 4.32–3.93 (m, 2H), 3.17–2.90 (m, 2H), 1.26 (t, J = 8.0 Hz, 3H). ^{13}C NMR (75 MHz, $CDCl_3$) δ[ppm] = 171.8, 167.1, 136.8, 133.8, 131.8, 129.3, 128.9, 128.6, 127.4, 127.2, 61.5, 54.2, 37.80, 14.3. $[\alpha]_D^{22} = -28°$. MP = 115–117 °C.

Benzoyl-L-phenylalanine (30)

30 was prepared according to procedure D using **29** (6.4 mmol, 1.9 g), resulting in a colorless solid (1.6 g, 5.8 mmol, 91%). ^{1}H NMR (300 MHz, $CDCl_3$) δ[ppm] = 9.55 (s, 1H, OH), 8.29 (d, J = 11.9 Hz, 1H, NH), 7.83–7.60 (m, 3H), 7.51–7.42 (m, 1H), 7.38–7.35 (m, 3H), 7.34–7.15 (m, 7H), 4.67 (dt, J = 12.1, 7.0 Hz, 1H), 3.31–3.07 (m, 3H). ^{13}C NMR (75 MHz, $CDCl_3$) δ[ppm] = 174.8, 167.0, 137.4, 134.2, 131.7, 130.1, 128.7, 128.7, 127.4, 126.9, 54.8, 37.5. $[\alpha]_D^{22} = -20°$. MP = 148–150 °C.

Ethyl (S)-3-cyclohexyl-2-(isonicotinamido)propanoate (31)

31 was prepared according to procedure B using **8** (6.5 mmol, 1.3 g) and isonicotinic acid (7.8 mmol, 0.96 g). Purification by column chromatography (CH:EA 1:1 – 100% EA) resulted in a colorless oil (1.8 g, 5.9 mmol, 93%). ^{1}H NMR (300 MHz, $CDCl_3$) δ[ppm] = 8.71–8.53 (m, 2H), 7.65–7.46 (m, 2H), 7.05 (d, J = 8.2 Hz, 1H, NH), 4.77 (ddd, J = 9.0, 8.1, 5.4 Hz, 1H), 4.24–4.08 (m, 2H), 1.96 (s, 2H), 1.82–1.49 (m, 10H), 1.46–1.27 (m, 1H), 1.27–1.11 (m, 3H). ^{13}C NMR (75 MHz, $CDCl_3$) δ[ppm] = 174.2, 165.3, 150.5, 141.1, 121.1, 61.4, 51.8, 34.4, 33.5, 32.7, 26.4, 26.2, 26.1, 14.2. $[\alpha]_D^{22} = -29°$.

(S)-3-Cyclohexyl-2-(isonicotinamido)propanoic acid (32)

32 was prepared according to procedure D using **31** (5.9 mmol, 1.8 g), resulting in a colorless solid (0.80 g, 2.9 mmol, 49%). ^{1}H NMR (300 MHz, DMSO-d_6) δ[ppm] = 8.89 (d, J = 7.9 Hz, 1H, *NH*), 8.78–8.57 (m, 2H), 7.97–7.61 (m, 2H), 4.47 (ddd, J = 10.4, 7.8, 4.7 Hz, 1H), 1.82–1.49 (m, 6H), 1.51–1.25 (m, 1H), 1.25–0.98 (m, 3H), 1.00–0.77 (m, 3H). ^{13}C NMR (75 MHz, DMSO-d_6) δ[ppm] = 173.9, 165.0, 150.3, 140.9, 121.4, 50.3, 37.9, 33.8, 33.2, 31.5, 26.0, 25.7, 25.6. $[\alpha]_D^{22} = -35°$. MP = 115–117 °C.

Ethyl isonicotinoyl-L-leucinate (33)

33 was prepared according to procedure B using L-leucin ethyl ester hydrochloride (6.0 mmol, 1.2 g) and isonicotinic acid (7.2 mmol, 0.9 g), resulting in a yellow oil (1.6 g, 6.0 mmol, 100%). ^{1}H NMR (300 MHz, DMSO-d_6) δ[ppm] = 8.84 (d, J = 7.7 Hz, 1H), 8.65–8.49 (m, 2H), 7.69–7.51 (m, 2H), 4.45–4.17 (m, 1H), 3.93 (q, J = 7.2 Hz, 2H), 1.69–1.37 (m, 2H), 1.21 (dt, J = 11.8, 6.8 Hz, 1H), 1.00 (t, J = 7.1 Hz, 3H), 0.81–0.56 (m, 6H). ^{13}C NMR (75 MHz, DMSO-d_6) δ[ppm] = 172.6, 165.6, 150.7, 141.2, 121.8, 61.0, 51.6, 39.6, 24.9, 23.2, 21.6, 14.5. $[\alpha]_D^{22} = -28°$.

Isonicotinoyl-L-leucine (34)

34 was prepared according to procedure D using **33** (6.0 mmol, 1.6 g), resulting in a yellow solid (1.3 g, 5.4 mmol, 90%). ^{1}H NMR (300 MHz, DMSO-d_6) δ[ppm] = 9.43 (d, J = 7.7 Hz, 1H, *NH*), 9.08–8.77 (m, 2H), 8.32–8.10 (m, 2H), 4.43 (ddd, J = 11.1, 7.7, 4.2 Hz, 1H), 1.99–1.72 (m, 1H), 1.72–1.43 (m, 2H), 1.00–0.66 (m, 6H). ^{13}C NMR (75 MHz, DMSO-d_6) δ[ppm] = 173.8, 164.1, 146.2, 145.6, 124.2, 39.9, 51.8, 25.0, 23.4, 21.6. $[\alpha]_D^{22} = -14°$. MP = 122–124 °C.

Ethyl (S)-2-(isonicotinamido)-4-phenylbutanoate (35)

35 was prepared according to procedure B using L-homophenylalanine ethyl ester hydrochloride (6.0 mmol, 1.5 g) and isonicotinic acid (7.2 mmol, 0.89 g), resulting in a yellow solid (1.2 g, 3.8 mmol, 67%). ^{1}H NMR (300 MHz, DMSO-d_6) δ[ppm] = 8.99–8.81 (m, 1H, *NH*), 8.66–8.47 (m, 2H), 7.62 (dt, J = 4.5, 1.8 Hz, 2H), 7.17–6.89 (m, 5H), 4.20 (qd, J = 7.4, 1.7 Hz, 1H), 4.00–3.85 (m, 2H), 2.61–2.50 (m, 2H),

ChemMedChem | Research Article doi.org/10.1002/cmdc.202300160 | Chemistry Europe European Chemical Societies Publishing

1.98–1.84 (m, 2H), 0.99 (td, J=7.1, 1.7 Hz, 3H). ^{13}C NMR (75 MHz, DMSO-d_6) δ[ppm]=172.2, 165.8, 150.7, 141.3, 141.2, 128.9, 128.8, 126.5, 121.9, 61.1, 52.8, 32.7, 32.1, 14.5. $[\alpha]_D^{22}=-30°$. MP=101–103 °C.

(S)-2-(Isonicotinamido)-4-phenylbutanoic acid (36)

36 was prepared according to procedure D using **35** (3.8 mmol, 1.2 g), resulting in a yellow solid (0.6 g, 2.1 mmol, 56%). ^{1}H NMR (300 MHz, DMSO-d_6) δ[ppm]=12.72 (s, 1H, *OH*), 9.01 (d, J=7.7 Hz, 1H, *NH*), 8.75 (q, J=2.2 Hz, 2H), 7.81 (q, J=2.3 Hz, 2H), 7.46–7.03 (m, 5H), 4.34 (q, J=7.6, 7.1 Hz, 1H), 2.92–2.51 (m, 2H), 2.23–1.94 (m, 2H). ^{13}C NMR (75 MHz, DMSO-d_6) δ[ppm]=173.8, 165.7, 150.7, 141.4, 128.9, 128.8, 126.4, 121.9, 52.7, 32.7, 32.2. $[\alpha]_D^{22}=-31°$. MP=133–135 °C.

Ethyl isonicotinoyl-L-tryptophanate (37)

37 was prepared according to procedure B using L-tryptophane ethyl ester hydrochloride (6.0 mmol, 1.6 g) and isonicotinic acid (7.2 mmol, 0.89 g), resulting in a yellow oil (2.0 g, 6.0 mmol, 100%). ^{1}H NMR (300 MHz, $CDCl_3$) δ[ppm]=8.70–8.60 (m, 2H), 8.54 (s, 1H, *NH*), 7.55–7.49 (m, 1H), 7.49–7.42 (m, 2H), 7.35 (dt, J=8.2, 1.0 Hz, 1H), 7.22–7.02 (m, 2H), 7.00 (d, J=2.4 Hz, 1H), 6.82 (d, J=7.7 Hz, 1H), 5.10 (dt, J=7.7, 5.3 Hz, 1H), 4.19 (qd, J=7.2, 4.2 Hz, 2H), 3.54–3.35 (m, 2H), 1.26 (t, J=7.1 Hz, 3H). ^{13}C NMR (75 MHz, $CDCl_3$) δ[ppm]=171.7, 165.1, 150.5, 141.2, 136.3, 127.8, 123.0, 122.5, 121.1, 119.9, 118.6, 111.6, 109.8, 61.9, 53.9, 27.6, 14.2. $[\alpha]_D^{22}=-14°$.

Isonicotinoyl-L-tryptophan (38)

38 was prepared according to procedure D using **37** (6.0 mmol, 2.0 g), resulting in an orange solid (0.81 g, 2.6 mmol, 44%). ^{1}H NMR (300 MHz, DMSO-d_6) δ[ppm]=10.93 (d, J=2.4 Hz, 1H, *OH*), 9.00 (d, J=7.9 Hz, 1H, *NH*), 8.82–8.54 (m, 2H), 7.78–7.69 (m, 2H), 7.59 (d, J=7.8 Hz, 1H), 7.32 (d, J=8.0 Hz, 1H), 7.22 (d, J=2.3 Hz, 1H), 7.10–6.91 (m, 2H), 4.66 (ddd, J=9.5, 7.8, 4.5 Hz, 1H), 3.45–3.12 (m, 2H). ^{13}C NMR (75 MHz, DMSO-d_6) δ[ppm]=173.3, 164.8, 150.2, 141.0, 136.1, 127.2, 123.7, 121.4, 120.9, 118.3, 118.2, 111.5, 110.4, 54.2, 26.7. $[\alpha]_D^{22}=-10°$. MP=150–152 °C.

Ethyl (*S*)-2-(4-((*tert*-butoxycarbonyl)amino)benzamido)-3-cyclohexylpropanoate (39)

39 was prepared according to procedure B using *N*-boc-4-amino benzoic acid (7.5 mmol, 1.5 g), resulting in a colorless solid (3.1 g, 7.5 mmol, 100%). ^{1}H NMR (300 MHz, $CDCl_3$) δ[ppm]=7.97–7.85 (m, 1H), 7.62–7.38 (m, 4H), 6.38 (d, J=8.2 Hz, 1H), 4.61 (td, J=8.5, 5.6 Hz, 1H), 3.99 (qd, J=7.1, 1.9 Hz, 2H), 2.58 (s, 1H), 1.66–1.52 (m, 2H), 1.33–0.89 (m, 18H), 0.92–0.49 (m, 3H). ^{13}C NMR (75 MHz, $CDCl_3$) δ[ppm]=173.5, 166.7, 152.6, 142.0, 132.3, 128.3, 128.1, 117.8, 81.0, 61.4, 50.7, 34.4, 33.5, 32.8, 28.4, 28.3, 26.4, 26.2, 26.1, 14.2. $[\alpha]_D^{22}=-12°$. MP=87–89 °C.

(S)-2-(4-((tert-Butoxycarbonyl)amino)benzamido)-3-cyclohexylpropanoic acid (40)

40 was prepared according to procedure D using **39** (7.5 mmol, 3.1 g), resulting in a colorless solid (2.7 g, 6.9 mmol, 92%). ^{1}H NMR (300 MHz, DMSO-d_6) δ[ppm]=9.47 (d, J=32.7 Hz, 1H), 8.18 (d, J=7.9 Hz, 1H), 7.78–7.49 (m, 2H), 7.46–7.19 (m, 2H), 4.45–4.11 (m, 1H), 3.54–3.07 (m, 2H), 2.37–2.08 (m, 1H), 1.64–1.29 (m, 10H), 1.40–1.21 (m, 9 H). ^{13}C NMR (75 MHz, DMSO) δ[ppm]=174.9, 167.5, 153.0, 144.2, 130.8, 124.5, 117.7, 117.5, 80.1, 50.6, 34.3, 33.7, 31.9, 28.5, 28.5, 26.5, 25.6. $[\alpha]_D^{22}=-11°$. MP=104–106 °C.

(4-Morpholine-1-carbonyl)-L-cyclohexylalanine methylester (41)

L-Cyclohexylalanine methylester hydrochloride (1.0 eq, 2.48 mmol, 0.55 g) was dissolved in DCM and a sat. aq. $NaHCO_3$ (40 mL) solution and cooled to 0 °C. Triphosgene (0.33 eq, 0.83 mmol, 0.25 g) was added and the mixture was stirred for 30 min. The mixture was extracted with DCM (2×40 mL) and the combined organic extracts were washed with sat. aq. $NaHCO_3$ (2×30 mL), and brine (2×30 mL), then dried over Na_2SO_4 and concentrated under reduced pressure, resulting in a crude product that was dissolved in THF (30 mL) and cooled to 0 °C. Morpholine (1.0 eq, 2.5 mmol, 0.22 g) was added and the mixture stirred for 1 h. The solvent was removed under reduced pressure. Water and ethyl acetate were added to the crude residue, which was then extracted with ethyl acetate (3×25 mL), washed with brine (2×20 mL), dried over Na_2SO_4, and concentrated under reduced pressure to yield a colorless oil (0.75 g, 2.5 mmol, 98%). ^{1}H NMR (300 MHz, $CDCl_3$) δ[ppm]=4.96–4.83 (m, 1H), 4.58–4.40 (m, 1H), 4.09 (q, J=7.1 Hz, 1H), 3.70 (s, 3H), 3.69–3.61 (m, 4H), 3.41–3.28 (m, 4H), 2.01 (s, 1H), 1.76 (d, J=12.8 Hz, 1H), 1.70–1.55 (m, 6H), 1.53–1.43 (m, 1H), 1.38–1.28 (m, 1H), 1.28–1.10 (m, 4H), 1.02–0.75 (m, 2H). ^{13}C NMR (75 MHz, $CDCl_3$) δ[ppm]=175.1, 157.4, 66.5, 52.3, 51.6, 44.1, 40.4, 34.2, 33.6, 32.7, 26.4, 26.2, 26.1, 21.1, 14.3. $[\alpha]_D^{22}=+16°$. MP=105–106 °C.

(4-Morpholine-1-carbonyl)-L-cyclohexylalanine (42)

42 was prepared according to procedure D using **41** (1.0 eq, 0.7 g, 2.4 mmol), resulting in a colorless solid (0.65 g, 2.3 mmol, 97%).^{1}H NMR (300 MHz, $CDCl_3$) δ[ppm]=9.37 (s, 1H), 5.27–5.07 (m, 1H), 4.41 (s, 1H), 3.75–3.55 (m, 4H), 3.46–3.28 (m, 4H), 1.83–1.47 (m, 6H), 1.44–1.30 (m, 1H), 1.26–1.04 (m, 4H), 1.04–0.79 (m, 2H). ^{13}C NMR (75 MHz, $CDCl_3$) δ[ppm]=176.9, 158.1, 66.5, 51.9, 44.2, 39.6, 34.3, 33.6, 32.6, 26.6, 26.2, 26.1. 176.9, 158.1, 66.5, 51.9, 44.2, 39.6, 34.3, 33.6, 32.6, 26.5, 26.2, 26.1. $[\alpha]_D^{22}=+20°$. MP=96–97 °C.

Inhibitor preparation

N-((*S*)-1-(((*S,E*)-1-Fluoro-5-phenyl-1-(phenylsulfonyl)pent-1-en-3-yl)amino)-1-oxo-3-phenylpropan-2-yl)-4-methylpiperazine-1-carboxamide (1 a)

1 a was published previously and provided in form of a colorless solid. For experimental data, see Schirmeister et al.[45]

Phenyl (*S,E*)-1-fluoro-3-((*S*)-2- (4-methylpiperazine-1-carboxamido)-3-phenylpropanamido)-5-phenylpent-1-ene-1-sulfonate (1 b)

1 b was published previously and provided in form of a colorless solid. For experimental date see Jung, Fuchs et al.[49]

tert-Butyl 4-(((*S*)-1-(((*S,E*)-1-fluoro-5-phenyl-1-(phenylsulfonyl)pent-1-en-3-yl)amino)-1-oxo-3-phenylpropan-2-yl)carbamoyl)piperazine-1-carboxylate (2 a)

2 a was prepared as published previously[46] according to procedure B using **17** (0.70 mmol, 0.25 g) and **22** (0.84 mmol, 0.30 g). Purification via HPLC resulted in a colorless solid (0.15 g, 0.22 mmol,

ChemMedChem
Research Article
doi.org/10.1002/cmdc.202300160
Chemistry Europe
European Chemical Societies Publishing

32%). ^{1}H NMR (300 MHz, DMSO-d_6) δ[ppm] = 8.24 (d, J = 7.7 Hz, 1H), 7.98–7.90 (m, 2H), 7.89–7.77 (m, 1H), 7.79–7.67 (m, 2H), 7.31–7.12 (m, 8H), 7.13–7.05 (m, 2H), 6.66 (d, J = 8.2 Hz, 1H), 6.26 (dd, $J_{H\text{-}F}$ = 33.9 Hz, $J_{H\text{-}H}$ = 8.9 Hz, 1H), 4.51 (t, J = 7.8 Hz, 1H), 4.28 (td, J = 8.8, 5.6 Hz, 1H), 3.23 (dd, J = 9.5, 5.4 Hz, 8H), 2.99–2.70 (m, 2H), 1.99–1.64 (m, 2H), 1.39 (s, 9H). ^{13}C NMR (75 MHz, DMSO-d_6) δ[ppm] = 172.4, 157.4, 154.3, 141.3, 138.8, 137.1, 135.7, 130.6, 129.7, 128.8, 128.7, 128.6, 128.4, 126.6, 126.4, 119.8, 79.5, 56.4, 44.2, 43.8, 37.8, 35.5, 31.5, 28.5. $[\alpha]_D^{22} = -16°$. MP = 87–89 °C. ESI-MS: [M + H$^+$] calc. 679.2, found 679.1. Purity: 99%.

4-(((*S*)-1-(((*S,E*)-1-Fluoro-5-phenyl-1-(phenylsulfonyl)pent-1-en-3-yl)amino)-1-oxo-3-phenylpropan-2-yl)carbamoyl)piperazin-1-ium chloride (2b)

2b was published previously and provided in form of a colorless solid. For experimental date see Jung, Fuchs et al.[49]

N-((*S*)-1-(((*S,E*)-1-Fluoro-5-phenyl-1-(phenylsulfonyl)pent-1-en-3-yl)amino)-1-oxo-3-phenylpropan-2-yl) morpholine-4-carboxamide (2c)

2c was prepared according to procedure B using **17** (0.70 mmol, 0.25 g) and **24** (0.84 mmol, 0.23 g). Purification via HPLC resulted in a colorless solid (0.15 g, 0.26 mmol, 37%). ^{1}H NMR (300 MHz, DMSO-d_6) δ[ppm] = 8.25 (d, J = 7.7 Hz, 1H), 8.00–7.90 (m, 2H), 7.89–7.79 (m, 1H), 7.78–7.66 (m, 2H), 7.30–7.13 (m, 8H), 7.15–7.05 (m, 2H), 6.62 (d, J = 8.1 Hz, 1H), 6.26 (dd, $J_{H\text{-}F}$ = 33.9 Hz, $J_{H\text{-}H}$ = 8.9 Hz, 1H), 4.61–4.42 (m, 1H), 4.36–4.16 (m, 1H), 3.57–3.39 (m, 4H), 3.29–3.13 (m, 4H), 2.98–2.72 (m, 2H), 2.58–2.38 (m, J = 2.8, 2.4 Hz, 2H), 1.99–1.64 (m, 2H). ^{13}C NMR (75 MHz, DMSO-d_6) δ[ppm] = 172.8, 158.1, 155.8, 141.7, 139.2, 137.5, 136.0, 130.9, 130.1, 129.1, 129.0, 128.8, 127.0, 126.8, 120.1, 66.7, 56.8, 44.8, 44.6, 41.2, 38.1, 35.8, 31.8. $[\alpha]_D^{22} = -10°$. MP = 95–97 °C. ESI-MS: [M + H$^+$] calc. 580.2, found 580.0. Purity: 100%.

N-((*S*)-1-(((*S,E*)-1-Fluoro-5-phenyl-1-(phenylsulfonyl)pent-1-en-3-yl)amino)-1-oxo-3-phenylpropan-2-yl)isonicotinamide (2d)

2d was published previously and provided in form of a colorless solid. For experimental date see Jung, Fuchs et al.[49]

N-((*S*)-1-(((*S,E*)-1-Fluoro-5-phenyl-1-(phenylsulfonyl)pent-1-en-3-yl)amino)-1-oxo-3-phenylpropan-2-yl)thiophene-3-carbrboxamide (2e)

2e was prepared according to procedure B using **17** (0.70 mmol, 0.25 g) and **28** (0.84 mmol, 0.23 g). Purification via HPLC resulted in a colorless solid (0.090 g, 0.16 mmol, 22%). ^{1}H NMR (300 MHz, DMSO-d_6) δ[ppm] = 8.51–8.37 (m, 2H), 8.17 (ddd, J = 6.5, 3.0, 1.3 Hz, 1H), 7.99–7.85 (m, 2H), 7.87–7.76 (m, 1H), 7.77–7.60 (m, 2H), 7.59–7.44 (m, 2H), 7.36–7.00 (m, 10H), 6.32 (ddd, $J_{H\text{-}F}$ = 33.7 Hz, 24.5 Hz, $J_{H\text{-}H}$ = 9.0 Hz, 1H), 4.77–4.36 (m, 2H), 3.14–2.82 (m, 2H), 2.45–2.31 (m, 2H), 2.01–1.64 (m, 2H). ^{13}C NMR (75 MHz, DMSO-d_6) δ[ppm] = 171.5, 162.4, 141.2, 138.5, 137.7, 137.0, 135.7, 130.6, 130.5, 129.6, 128.7, 128.6, 128.6, 127.5, 127.0, 126.8, 126.4, 119.6, 55.2, 44.4, 37.8, 31.5. $[\alpha]_D^{22} = -21°$. MP = 136–138 °C. ESI-MS: [M + H$^+$] calc. 577.2, found 577.2. Purity: 100%.

tert-Butyl 4-(((S)-1-(((*S,E*)-1-fluoro-1-(phenoxysulfonyl)-5-phenylpent-1-en-3-yl)amino)-1-oxo-3-phenylpropan-2-yl)carbamoyl)piperazine-1-carboxylate (3a)

3a was prepared according to procedure B using **18** (0.67 mmol, 0.25 g) and **22** (0.81 mmol, 0.29 g). Purification via HPLC resulted in a colorless solid (0.18 g, 0.26 mmol, 43%). ^{1}H NMR (300 MHz, DMSO-d_6) δ[ppm] = 8.17 (d, J = 7.6 Hz, 1H, *NH*), 7.54–7.44 (m, 2H), 7.43–7.35 (m, 1H), 7.34–7.10 (m, 12H), 6.68 (d, J = 8.2 Hz, 1H, *NH*), 6.03 (dd, $J_{H\text{-}F}$ = 33.3 Hz, $J_{H\text{-}H}$ = 9.0 Hz, 1H), 4.56 (q, J = 7.8 Hz, 1H), 4.28 (td, J = 8.8, 5.9 Hz, 1H), 3.28–3.08 (m, 8H), 2.99–2.70 (m, 2H), 2.51–2.37 (m, 2H), 1.90–1.65 (m, 2H), 1.39 (s, 9H). ^{13}C NMR (75 MHz, DMSO-d_6) δ[ppm] = 172.6, 157.5, 154.3, 149.2, 141.2, 138.7, 130.9, 129.7, 128.8, 128.7, 128.4, 126.6, 126.4, 124.0, 122.5, 79.5, 56.4, 44.3, 43.8, 37.8, 34.9, 31.3, 28.5. $[\alpha]_D^{22} = -18°$. MP = 107–109 °C. ESI-MS: [M + H$^+$] calc. 639.2, found 639.1. Purity: 99%.

4-(((*S*)-1-(((*S,E*)-1-Fluoro-1-(phenoxysulfonyl)-5-phenylpent-1-en-3-yl)amino)-1-oxo-3-phenylpropan-2-yl)carbamoyl)piperperazin-1-ium chloride (3b)

3b was prepared according to procedure C using **3a** (0.23 mmol, 0.16 g). Purification via HPLC resulted in a colorless solid (0.14 g, 0.22 mmol, 96%). ^{1}H NMR (300 MHz, DMSO-d_6) δ[ppm] = 9.29 (s, 2H), 8.40 (d, J = 7.4 Hz, 1H), 7.53–7.43 (m, 2H), 7.42–7.35 (m, 1H), 7.34–7.12 (m, 12H), 7.06–6.96 (m, 1H), 6.03 (dd, $J_{H\text{-}F}$ = 33.3 Hz, $J_{H\text{-}H}$ = 9.0 Hz, 1H), 4.65–4.46 (m, 1H), 4.37–4.17 (m, 1H), 3.62–3.44 (m, 4H), 3.12–2.76 (m, 4H), 2.50–2.35 (m, 2H), 1.91–1.63 (m, 2H). ^{13}C NMR (75 MHz, DMSO-d_6) δ[ppm] = 172.5, 157.2, 149.2, 145.4, 141.3, 138.7, 130.9, 129.7, 128.8, 128.7, 128.5, 126.7, 126.4, 124.0, 122.4, 56.7, 44.5, 42.9, 41.1, 37.9, 34.9, 31.4. $[\alpha]_D^{22} = -16°$. MP = 125–127 °C. ESI-MS: [M + H$^+$] calc. 595.2, found 595.1. Purity: 98%.

Phenyl (*S,E*)-1-fluoro-3-((*S*)-2-(morpholine-4-carboxamido)-3-phenylpropanamido)-5-phenylpent-1-ene-1-sulfonate (3c)

3c was prepared according to procedure B using **18** (0.40 mmol, 0.15 g) and **24** (0.48 mmol, 0.13 g). Purification via HPLC resulted in a colorless solid (0.14 g, 0.24 mmol, 59%). ^{1}H NMR (300 MHz, DMSO-d_6) δ[ppm] = 8.18 (d, J = 7.6 Hz, 1H, *NH*), 7.54–7.43 (m, 3H), 7.43–7.35 (m, 2H), 7.36–7.10 (m, 10H), 6.64 (d, J = 8.2 Hz, 1H, *NH*), 6.03 (dd, $J_{H\text{-}F}$ = 33.3 Hz, $J_{H\text{-}H}$ = 9.0 Hz, 1H), 4.58 (p, J = 7.7 Hz, 1H), 4.29 (td, J = 8.7, 5.9 Hz, 1H), 3.54–3.40 (m, 4H), 3.31–3.13 (m, 4H), 2.97–2.76 (m, 2H), 2.55–2.38 (m, 2H), 1.88–1.65 (m, 2H). ^{13}C NMR (75 MHz, DMSO-d_6) δ[ppm] = 172.6, 157.7, 149.3, 149.2, 145.4, 141.2, 138.7, 130.9, 129.7, 128.8, 128.7, 128.4, 126.6, 126.4, 124.0, 122.5, 122.4, 66.3, 56.4, 44.4, 40.8, 37.8, 34.9, 31.3. $[\alpha]_D^{22} = -12°$. ESI-MS: [M + H$^+$] calc. 596.2, found 596.1. Purity: 97%.

Phenyl (*S,E*)-1-fluoro-3-((*S*)-2-(isonicotinamido)-3-phenylpropanamido)-5-phenylpent-1-ene-1-sulfonate (3d)

3d was published previously and provided in form of a colorless solid. For experimental date see Jung, Fuchs et al.[49]

Phenyl (*S,E*)-1-fluoro-5-phenyl-3-((*S*)-3-phenyl-2-(thiophene-3-carboxamido)propanamido)pent-1-ene-1-sulfonate (3e)

3e was prepared according to procedure B using **18** (0.40 mmol, 0.15 g) and **28** (0.48 mmol, 0.13 g). Purification via HPLC resulted in a colorless solid (0.14 g, 0.24 mmol, 59%). ^{1}H NMR (300 MHz, DMSO-d_6) δ[ppm] = 8.53–8.39 (m, 2H), 8.34 (d, J = 7.6 Hz, 1H), 8.19 (ddd, J = 11.6, 2.9, 1.3 Hz, 1H), 7.61–7.43 (m, 2H), 7.45–7.34 (m, 1H),

ChemMedChem
Research Article
doi.org/10.1002/cmdc.202300160
Chemistry Europe
European Chemical Societies Publishing

7.35–7.17 (m, 10H), 7.19–7.10 (m, 3H), 6.10 (dd, $J_{H\text{-}F}$ = 33.3 Hz, $J_{H\text{-}H}$ = 9.1 Hz, 1H), 4.81–4.46 (m, 2H), 3.13–2.86 (m, 2H), 2.47–2.32 (m, 2H), 1.99–1.60 (m, 2H). ^{13}C NMR (75 MHz, DMSO-d_6) δ[ppm] = 171.7, 171.6, 162.4, 162.2, 149.1, 141.2, 141.2, 138.4, 137.7, 130.9, 130.8, 129.6, 129.6, 128.8, 128.7, 128.6, 128.5, 127.5, 127.1, 126.8, 126.4, 123.9, 122.5, 55.0, 40.8, 39.2, 38.1, 26.8. $[\alpha]_D^{22} = -20°$. MP = 119–121 °C. ESI-MS: [M + H$^+$] calc. 593.2, found 593.2. Purity: 99 %.

Phenyl (*S,E*)-3-((*S*)-2-benzamido-3-phenylpropanamido)-1-fluoro-5-phenylpent-1-ene-1-sulfonate (3 f)

3 f was prepared according to procedure B using **18** (0.40 mmol, 0.15 g) and **30** (0.48 mmol, 0.13 g). Purification via HPLC resulted in a colorless solid (0.025 g, 0.043 mmol, 11 %). ^{1}H NMR (300 MHz, DMSO-d_6) δ[ppm] = 8.68–8.57 (m, 1H, *NH*), 8.47–8.29 (m, 1H, *NH*), 7.90–7.76 (m, 2H), 7.60–7.04 (m, 20H), 6.25 (dd, $J_{H\text{-}F}$ = 15.4 Hz, $J_{H\text{-}H}$ = 9.2 Hz, 1H), 5.00–4.75 (m, 1H), 4.78–4.47 (m, 1H), 3.16–2.93 (m, 2H), 2.61–2.36 (m, 2H), 1.94–1.67 (m, 2H). ^{13}C NMR (75 MHz, DMSO-d_6) δ[ppm] = 171.7, 166.7, 149.2, 141.2, 138.5, 134.4, 134.3, 132.1, 131.8, 130.9, 130.8, 130.8, 129.6, 129.6, 128.8, 128.8, 128.7, 128.7, 128.6, 127.9, 127.9, 127.8, 126.8, 126.4, 123.9, 122.5, 55.4, 45.1, 39.2, 31.7, 31.4. $[\alpha]_D^{22} = -15°$. MP = 150–152 °C. ESI-MS: [M + H$^+$] calc. 587.2, found 587.0. Purity: 96 %.

N-((*S*)-3-Cyclohexyl-1-(((*S,E*)-1-fluoro-5-phenyl-1-(phenylsulfonyl)pent-1-en-3-yl)amino)-1-oxopropan-2-yl)isonicotinamide (4 a)

4 a was prepared according to procedure B using **17** (0.32 mmol, 0.11 g) and **32** (0.39 mmol, 0.11 g), resulting in a colorless solid (0.052 g, 0.090 mmol, 28 %) after purification via HPLC. ^{1}H NMR (300 MHz, DMSO-d_6) δ[ppm] = 8.85–8.66 (m, 2H), 8.42 (d, J = 7.8 Hz, 1H), 7.96–7.87 (m, 2H), 7.85–7.76 (m, 3H), 7.73–7.61 (m, 2H), 7.35–7.04 (m, 5H), 6.35 (dd, $J_{H\text{-}F}$ = 33.2 Hz, $J_{H\text{-}H}$ = 8.9 Hz, 1H), 4.52 (dt, J = 15.1, 7.9 Hz, 2H), 2.97–2.83 (m, 2H), 1.98–1.77 (m, 2H), 1.77–1.49 (m, 8H), 1.43–1.20 (m, 3H), 1.12 (d, J = 7.9 Hz, 2H). ^{13}C NMR (75 MHz, DMSO-d_6) δ[ppm] = 172.1, 165.3, 150.6, 141.4, 141.3, 137.0, 135.6, 130.5, 128.7, 128.6, 126.4, 122.0, 52.0, 40.8, 34.2, 33.5, 31.6, 26.5, 26.2, 26.1. $[\alpha]_D^{22} = -15°$. MP = 108–110 °C. ESI-MS: [M + H$^+$] calc. 578.2, found 578.2. Purity: 95 %.

N-((*S*)-1-(((*S,E*)-1-Fluoro-5-phenyl-1-(phenylsulfonyl)pent-1-en-3-yl)amino)-4-methyl-1-oxopentan-2-yl)isonicotinamide (4 b)

4 b was prepared according to procedure B using **17** (0.32 mmol, 0.11 g) and **34** (0.39 mmol, 0.090 g), resulting in a colorless solid (0.045 g, 0.083 mmol, 26 %) after purification via HPLC. ^{1}H NMR (300 MHz, DMSO-d_6) δ[ppm] = 8.80–8.58 (m, 2H), 8.06–7.81 (m, 2H), 7.87–7.66 (m, 3H), 7.69–7.47 (m, 3H), 7.33–7.20 (m, 3H), 7.24–7.07 (m, 1H), 6.12 (d, J = 10.4 Hz, 1H), 5.86 (dd, $J_{H\text{-}F}$ = 32.5 Hz, $J_{H\text{-}H}$ = 8.1 Hz, 1H), 4.70–4.54 (m, 1H), 4.43–4.11 (m, 1H), 2.84–2.40 (m, 2H), 2.17–1.76 (m, 2H), 1.73–1.48 (m, 2H), 1.53–1.32 (m, 1H), 1.05–0.64 (m, 6H). ^{13}C NMR (75 MHz, DMSO-d_6) δ[ppm] = 173.0, 166.9, 150.6, 142.4, 141.9, 140.8, 140.4, 137.9, 133.5, 129.4, 128.5, 127.8, 126.1, 122.0, 121.8, 121.1, 53.0, 47.1, 40.8, 35.9, 32.6, 24.6, 22.3. $[\alpha]_D^{22} = -13°$. MP = 90–92 °C. ESI-MS: [M + H$^+$] calc. 538.2, found 538.0. Purity: 99 %.

N-((*S*)-1-(((*S,E*)-1-Fluoro-5-phenyl-1-(phenylsulfonyl)pent-1-en-3-yl)amino)-1-oxo-4-phenylbutan-2-yl)isonicotinamide (4 c)

4 c was prepared according to procedure B using **17** (0.28 mmol, 0.10 g) and **36** (0.34 mmol, 0.10 g), resulting in a diastereomeric mixture which was separated via HPLC to yield the pure compound with (*E*)-configuration as a colorless solid (0.043 g, 0.073 mmol, 26 %). ^{1}H NMR (300 MHz,DMSO-d_6) δ[ppm] = 8.96–8.50 (m, 2H), 8.40 (d, J = 7.9 Hz, 1H), 7.96–7.41 (m, 6H), 7.41–6.69 (m, 11H), 6.39 (dd, $J_{H\text{-}F}$ = 34.0 Hz, $J_{H\text{-}H}$ = 8.9 Hz, 1H), 4.69–4.12 (m, 2H), 3.59–3.07 (m, 2H), 2.77–2.50 (m, 2H), 2.14–1.70 (m, 2H). ^{13}C NMR (75 MHz, DMSO-d_6) δ[ppm] = 171.9, 166.0, 151.1, 142.1, 136.1, 131.0, 129.2, 126.8, 122.5, 120.0, 106.9, 70.3, 44.8, 34.0, 32.8, 30.1. $[\alpha]_D^{22} = -19°$. MP = 85–87 °C. ESI-MS: [M + H$^+$] calc. 586.2, found 586.2. Purity: 95 %.

N-((*S*)-1-(((*S,E*)-1-Fluoro-5-phenyl-1-(phenylsulfonyl)pent-1-en-3-yl)amino)-3-(1H-indol-3-yl)-1-oxopropan-2-yl)isonicotinamide (4 d)

4 d was prepared according to procedure B using **17** (0.28 mmol, 0.10 g) and **38** (0.34 mmol, 0.11 g), resulting in a colorless solid (0.054 g, 0.088 mmol, 31 %) after purification via HPLC. ^{1}H NMR (300 MHz, $CDCl_3$) δ[ppm] = 10.73 (t, J = 3.4 Hz, 1H), 8.89–8.73 (m, 1H), 8.73–8.55 (m, 2H), 8.51–8.32 (m, 1H), 8.01–7.47 (m, 8H), 7.32–6.80 (m, 9H), 6.31 (ddd, $J_{H\text{-}F}$ = 33.8 Hz, $J_{H\text{-}F}$ = 8.9, 4.7 Hz, 1H), 4.73–4.56 (m, 1H), 4.50 (q, J = 8.1 Hz, 1H), 3.22–2.99 (m, 2H), 2.85–2.38 (m, 2H), 2.05–1.52 (m, 2H). ^{13}C NMR (75 MHz, $CDCl_3$) δ[ppm] = 172.0, 168.6, 150.9, 141.6, 139.4, 138.6, 137.3, 133.6, 129.6, 128.4, 128.2, 127.6, 126.0, 123.9, 123.0, 122.8, 121.6, 121.2, 119.1, 118.8, 117.8, 116.8, 113.1, 110.1, 54.7, 47.0, 37.4, 32.4, 28.4. $[\alpha]_D^{22} = -21°$. MP = 101–103 °C. ESI-MS: [M + H$^+$] calc. 611.2, found 611.2. Purity: 96 %.

Phenyl (*S,E*)-3-((S)-3-cyclohexyl-2-(isonicotinamido) propanamido)-1-fluoro-5-phenylpent-1-ene-1-sulfonate (5 a)

5 a was prepared according to procedure B using **18** (0.27 mmol, 0.10 g) and **32** (0.32 mmol, 0.088 g), resulting in a colorless solid (0.038 g, 0.064 mmol, 24 %) after purification via HPLC. ^{1}H NMR (300 MHz, DMSO-d_6) δ[ppm] = 8.89–8.71 (m, 2H), 8.44 (m, 1H), 7.96–7.87 (m, 2H), 7.87–7.79 (m, 3H), 7.77–7.66 (m, 2H), 7.41–7.09 (m, 5H), 6.40 (dd, $J_{H\text{-}F}$ = 33.1 Hz, $J_{H\text{-}H}$ = 9.0 Hz, 1H), 4.58 (dt, J = 15.2, 7.9 Hz, 2H), 2.99–2.88 (m, 2H), 2.00–1.80 (m, 2H), 1.78–1.48 (m, 8H), 1.48–1.25 (m, 3H), 1.16 (d, J = 7.9 Hz, 2H). ^{13}C NMR (75 MHz, DMSO-d_6) δ[ppm] = 172.2, 165.5, 150.9, 141.5, 141.4, 137.2, 135.9, 130.6, 128.9, 128.8, 126.7, 122.5, 52.4, 41.2, 34.6, 33.9, 32.0, 26.6, 26.3, 26.0. $[\alpha]_D^{22} = -12°$. MP = 123–125 °C. ESI-MS: [M + H$^+$] calc. 594.2, found 594.2. Purity: 99 %.

Phenyl (*S,E*)-1-fluoro-3-((*S*)-2-(isonicotinamido)-4-methylpentanamido)-5-phenylpent-1-ene-1-sulfonate (5 b)

5 b was prepared according to procedure B using **18** (0.25 mmol, 0.093 g) and **34** (0.30 mmol, 0.071 g), resulting in a colorless solid (0.031 g, 0.056 mmol, 22 %) after purification via HPLC. ^{1}H NMR (300 MHz, $CDCl_3$) δ[ppm] = 8.81 (d, J = 8.4 Hz, 1H), 8.73 (s, 2H), 8.36 (dd, J = 14.8, 8.0 Hz, 1H), 7.80 (d, J = 7.5 Hz, 2H), 7.54–7.36 (m, 2H), 7.35–7.08 (m, 7H), 7.01 (d, J = 7.5 Hz, 1H), 6.15 (dd, $J_{H\text{-}F}$ = 32.4 Hz, $J_{H\text{-}H}$ = 8.8 Hz, 1H), 4.89 (s, 1H), 4.69–4.31 (m, 1H), 1.67 (s, 2H), 1.10–0.58 (m, 11H). ^{13}C NMR (75 MHz, $CDCl_3$) δ[ppm] = 173.0, 166.9, 150.6, 147.8, 147.7, 141.9, 140.8, 136.8, 134.8, 131.2, 131.1, 129.3, 128.5, 126.8, 126.1, 122.4, 121.1, 53.0, 47.1, 40.8, 35.9, 32.6, 24.6, 22.3. $[\alpha]_D^{22} = -20°$. MP = 76–78 °C. ESI-MS: [M + H$^+$] calc. 554.2, found 554.0. Purity: 99 %.

Phenyl (*S,E*)-1-fluoro-3-((*S*)-2-(isonicotinamido)-4-phenylbutanamido)-5-phenylpent-1-ene-1-sulfonate (5 c)

5 c was prepared according to procedure B using **18** (0.40 mmol, 0.15 g) and **36** (0.48 mmol, 0.18 g), resulting in a colorless solid

ChemMedChem
Research Article
doi.org/10.1002/cmdc.202300160
Chemistry Europe
European Chemical Societies Publishing

(0.060 g, 0.10 mmol, 25%) after purification via HPLC. ^{1}H NMR (300 MHz, $CDCl_3$) δ[ppm] = 9.02 (dd, J = 7.6, 5.4 Hz, 1H), 8.88 (t, J = 5.3 Hz, 2H), 8.53 (d, J = 7.9 Hz, 1H), 8.09–7.82 (m, 5H), 7.86–7.66 (m, 2H), 7.51–7.09 (m, 10H), 6.51 (ddd, $J_{H\text{-}F}$ = 33.9 Hz, $J_{H\text{-}F}$ = 8.9, 5.1 Hz, 1H), 4.83–4.34 (m, 2H), 2.86–2.68 (m, 4H), 2.33–1.81 (m, 4H). ^{13}C NMR (75 MHz, $CDCl_3$) δ[ppm] = 172.2, 166.3, 151.6, 142.2, 136.5, 131.4, 129.5, 127.0, 122.9, 120.4, 107.3, 70.4, 44.9, 34.3, 32.8, 30.3. $[\alpha]_D^{22} = -15°$. MP = 96–98 °C. ESI-MS: [M + H$^+$] calc. 602.2, found 602.2. Purity: 99%.

Phenyl (*S,E*)-3-((*S*)-3-(1H-indol-3-yl)-2-(isonicotinamido) propanamido)-1-fluoro-5-phenylpent-1-ene-1-sulfonate (5 d)

5 d was prepared according to procedure B using **18** (0.54 mmol, 0.20 g) and **38** (0.65 mmol, 0.20 g), resulting in a colorless solid (0.071 g, 0.11 mmol, 20%) after purification via HPLC. ^{1}H NMR (300 MHz, $CDCl_3$) δ[ppm] = 10.68–10.33 (m, 1H), 8.75–8.52 (m, 1H), 8.50–8.35 (m, 2H), 8.22 (d, J = 8.5 Hz, 1H), 7.79–7.51 (m, 4H), 7.52–7.36 (m, 5H), 7.09–6.67 (m, 9H), 6.12 (dd, $J_{H\text{-}F}$ = 33.9 Hz, $J_{H\text{-}H}$ = 8.9 Hz, 1H), 4.60–4.14 (m, 2H), 3.00–2.80 (m, 2H), 2.67–2.39 (m, 2H), 1.80–1.39 (m, 2H). ^{13}C NMR (75 MHz, $CDCl_3$) δ[ppm] = 172.0, 168.6, 150.9, 149.4, 141.6, 138.6, 137.3, 133.0, 132.9, 129.8, 128.4, 127.6, 127.3, 126.0, 123.9, 122.1, 121.6, 121.2, 119.1, 117.8, 117.0, 115.0, 113.1, 110.1, 54.7, 47.1, 47.0, 37.4, 32.4, 28.4. $[\alpha]_D^{22} = -22°$. MP = 114–116 °C. ESI-MS: [M + H$^+$] calc. 627.2, found 627.1. Purity: 96%.

Phenyl (*S,E*)-3-((*S*)-2-(4-((*tert*-butoxycarbonyl)amino) benzamido)-3-cyclohexylpropanamido)-1-fluoro-5-phenylpent-1-ene-1-sulfonate (6 a)

6 a was prepared according to procedure B using **18** (0.54 mmol, 0.20 g) and **40** (0.65 mmol, 0.25 g), resulting in a diastereomeric mixture which was separated via HPLC to yield the pure compound with (*E*)-configuration as a colorless solid (0.25 g, 0.35 mmol, 65%) after purification via HPLC. ^{1}H NMR (300 MHz, DMSO-d_6) δ[ppm] = 9.60 (d, J = 2.6 Hz, 1H), 8.40–8.10 (m, 2H), 7.94–7.70 (m, 2H), 7.61–7.34 (m, 4H), 7.35–7.05 (m, 6H), 7.00 (d, J = 7.2 Hz, 2H), 6.15 (dd, $J_{H\text{-}F}$ = 33.2 Hz, $J_{H\text{-}H}$ = 9.0 Hz, 1H), 4.95–4.81 (m, 1H), 4.66–4.38 (m, 1H), 2.61–2.32 (m, 2H), 1.85–1.52 (m, 8H), 1.48 (s, 9H), 1.28–1.02 (m, 3H), 1.04–0.73 (m, 2H). ^{13}C NMR (75 MHz, DMSO-d_6) δ[ppm] = 166.3, 153.1, 142.9, 141.2, 130.9, 128.9, 128.8, 128.7, 127.8, 122.4, 117.5, 79.9, 34.3, 32.4, 31.5, 28.5, 26.5, 26.1. $[\alpha]_D^{22} = -15°$. MP = 118–120 °C. ESI-MS: [M + Na$^+$] calc. 730.2, found 730.2. Purity: 97%.

4-(((*S*)-3-Cyclohexyl-1-(((*S,E*)-1-fluoro-1-(phenoxysulfonyl)-5-phenylpent-1-en-3-yl)amino)-1-oxopropan-2-yl)carbamoyl) benzenaminium chloride (6 b)

6 b was prepared according to procedure C using **6 a** (0.35 mmol, 0.25 g). Purification via HPLC resulted in a diastereomeric mixture which was separated via HPLC to yield the pure compound with (*E*)-configuration as a colorless solid (0.17 g, 0.26 mmol, 74%). ^{1}H NMR (300 MHz, DMSO-d_6) δ[ppm] = 8.56–8.19 (m, 4H), 8.06–7.72 (m, 2H), 7.61–7.07 (m, 10H), 7.07–6.90 (m, 2H), 6.45 (dd, J = 21.8, 10.0 Hz, 1H), 6.14 (dd, $J_{H\text{-}F}$ = 33.3 Hz, $J_{H\text{-}H}$ = 9.1 Hz, 1H), 5.06–4.72 (m, 1H), 4.66–4.35 (m, 1H), 2.63–2.34 (m, 2H), 2.34–2.09 (m, 2H), 1.98–1.43 (m, 6H), 1.45–0.99 (m, 3H), 1.04–0.73 (m, 2H). ^{13}C NMR (75 MHz, DMSO-d_6) δ[ppm] = 172.7, 166.0, 149.2, 141.2, 130.9, 129.6, 128.8, 128.7, 126.4, 122.4, 120.1, 66.8, 34.3, 33.59, 32.4, 31.5, 26.5, 26.2, 26.1. $[\alpha]_D^{22} = -9°$. MP = 130–132 °C. ESI-MS: [M + H$^+$] calc. 607.3, found 607.2. Purity: 95%.

Phenyl (*S,E*)-3-((*S*)-3-cyclohexyl-2-(morpholine-4-carboxamido)propanamido)-1-fluoro-5-phenylpent-1-ene-1-sulfonate (6 c)

6 c was prepared according to procedure B using **18** (0.08 mmol, 0.030 g) and **42** (0.08 mmol, 23 mg), resulting in a colorless solid (5.5 mg, 0.009 mmol, 9%) after purification via HPLC. ^{1}H NMR (600 MHz, DMSO-d_6) δ[ppm] = 8.32 (s, 1H), 8.15 (d, J = 7.7 Hz, 1H), 7.52–7.37 (m, 3H), 7.33–7.11 (m, 5H), 6.51 (d, J = 7.9 Hz, 1H), 6.11 (dd, J = 33.3, 9.0 Hz, 1H), 4.61–4.52 (m, 1H), 4.17–4.08 (m, 1H), 3.60–3.46 (m, 4H), 3.33–3.22 (m, 4H), 1.88–1.71 (m, 2H), 1.71–1.55 (m, 4H), 1.53–1.36 (m, 3H), 1.30–1.21 (m, 2H), 1.19–1.06 (m, 4H), 0.95–0.75 (m, 3H). ^{13}C NMR (151 MHz, DMSO-d_6) δ[ppm] = 173.2, 157.5, 148.7, 147.8, 145.9, 140.9, 130.5, 126.0, 123.6, 122.0, 79.2, 66.0, 52.0, 44.1, 43.78, 34.5, 33.7, 33.2, 32.0, 30.9, 26.1, 25.8, 25.7. $[\alpha]_D^{22} = -2°$. MP = 116–117 °C. ESI-MS: [M + Na$^+$] calc. 601.3, found 601.2. Purity: 95%.

Molecular docking

Since the inhibitors were designed to react covalently with cysteine-25 of CatS, two different docking approaches were followed. First, a conventional non-covalent docking was performed, to estimate affinity and geometry of the pre-organized enzyme-inhibitor complex, secondly a covalent docking was used to determine the final covalent enzyme-inhibitor complex. In both docking setups a crystallographic reference ligand was used for validation via redocking (Table A, Supporting Information). Molecular docking experiments were performed using the following crystal structure freely available in the protein data bank (PDB):[55] Cathepsin S covalently bound to *N*-2-(morpholin-4-ylcarbonyl)-*N*-[(3*S*)-1-phenyl-5-(phenylsulfonyl)pentan-3-yl]-l-leucinamide (C1P), PDB entry 1NPZ.[29] For both docking approaches, chain A of the dimer of 1NPZ was extracted via PyMOL 2.5.2.[56] All ligands were energetically minimized prior docking with Molecular operating environment (MOE Version 2020.09)[57] using the MMF94x force field.[58] For visual presentation of the top binding poses, PyMOL 2.5.2 was used.[56]

Docking approach A: non-covalent docking with LeadIT

The non-covalent docking was performed with LeadIT 2.3.2.[59] The receptors were prepared in MOE with the protonate3D functionality and the covalent bond between the co-crystallized ligand and the corresponding protease was untethered via the Builder tool in MOE. For the receptor the binding site was defined as a 6.5 Å shell around the bound reference ligand. Water molecules that form at least three hydrogen bonds with the receptor and ligand were kept as part of the binding site. The docking was performed under default settings using the enthalpy-entropy hybrid approach with 2,000 solutions per iteration and fragmentation. Only the top pose of the initial docking was kept and re-scored using the HYDE scoring function.[60] For the docking, pharmacophore constraints needed to be included to obtain reasonable binding modes. The nitrogen atoms of the peptide backbone were therefore defined as H-bond donors with a 1 Å sphere radius.

Docking approach B: covalent docking with MOE

Covalent docking was performed with MOE. The receptor was prepared using the 3D protonation tool inside MOE. For the covalent reaction of the different warheads, the already existing template reactions were used. Initial 30 poses from the triangle match placement with London △G scoring were re-scored using the Affinity △G scoring function and induced fit refinement

ChemMedChem
Research Article
doi.org/10.1002/cmdc.202300160
Chemistry Europe
European Chemical Societies Publishing

implemented in MOE. 10 Poses were kept and visually inspected for binding geometry the interactions matching between the docked inhibitor pose and co-crystallized ligand with the enzyme. The poses best matching inspected interaction patterns are further discussed.

Fluorometric enzyme assay

Cathepsin S

Assay procedure

The assay was modified after Brömme et al.[50] The fluorescence increase upon cleavage of the fluorogenic substrate *Z*-Val-Val-Arg-AMC by Cathepsin S (CatS) was monitored by a Tecan Spark fluorimeter (δ excitation: 365 nm, δ emission: 460 nm; Tecan Group, Switzerland). CatS (recombinant from *E. coli*, SigmaAldrich, Germany) was incubated with enzyme buffer (35 mM potassium phosphate, 35 mM sodium acetate, 2 mM DTT, 2 mM EDTA, pH 6.5) at room temperature for 20–30 min. Assay buffer (50 mM KH_2PO_4, 50 mM K_2HPO_4, 2.5 mM DTT, 2.5 mM EDTA, pH 6.5) was mixed with 1–5 nM CatS in enzyme buffer, followed by inhibitor in DMSO or DMSO (negative control), and 10 μM substrate *Z*-Val-Val-Arg-AMC (Bachem, Switzerland). Black, flat-bottom 96-well microtiter plates (Greiner Bio-One, Germany) were used. Inhibitor screening concentrations started at 20 μM, followed by 1 μM, 200 nM, and 50 nM.

K_M determination

The assay was performed as described above using different concentrations of *Z*-Val-Val-Arg-AMC (3.125 μM, 6.25 μM, 12.5 μM, 25 μM, 50 μM) and Z-Phe-Arg-AMC (0.41 μM, 1.2 μM, 3.7 μM, 11 μM, 33 μM, 60 μM, 100 μM). GraFit (version 5.0.13, 2006, Erithracus Software Ltd., UK)[61] was used for data analysis and non-linear regression. The K_M value was calculated as described by Michaelis-Menten [Equation (2), K_M = 34 μM for Z-Val-Val-Arg-AMC; K_M = 35 μM for Z-Phe-Arg-AMC]:

$$v_0 = \frac{v_{max} \cdot [S]}{K_M + [S]} \quad (2)$$

in which v_0 = initial velocity; v_{max} = maximal velocity; [S] = substrate concentration.

The graphs are shown in the Supporting Information.

IC_{50} and K_i calculations

GraFit (version 5.0.13, 2006, Erithracus Software Ltd., UK) was used for data analysis and non-linear regression.[61]

For compounds without a time-dependent mode of inhibition (fluorinated vinylsulfones as inhibitors of CatS, CatB, CatL; fluorinated vinylsulfonates as inhibitors of CatB, CatL), the residual enzyme activity in % was plotted against the inhibitor concentration in μM. Then, IC_{50} values were obtained by non-linear regression [Equation (3)]:

$$v_i = \frac{v_0}{1 + (\frac{[I]}{IC_{50}})^S} \quad (3)$$

in which v_0 = enzyme activity without inhibitor; v_i = enzyme activity in presence of inhibitor; [I] = inhibitor concentration; S = slope factor.

K_i values were calculated by using the Cheng-Prusoff equation to correct the IC_{50} values to zero substrate concentration [Equation (4)]:[51]

$$K_i = \frac{IC_{50} \text{ or } K_i^{app}}{1 + \frac{[S]}{K_M}} \quad (4)$$

in which CatS: [S] = 10 μM, K_M = 34 μM. CatB: [S] = 100 μM, K_M = 150 μM. CatL: [S] = 6.25 μM, K_M = 6.5 μM.

For compounds with a time-dependent mode of inhibition (fluorinated vinylsulfonates as inhibitors of CatS), the K_i values were calculated as published previously for slow, tight binders [Equation (5)].[49]

$$E + I \underset{k_2}{\overset{k_1}{\rightleftharpoons}} E^{\cdots}I \underset{k_4}{\overset{k_3}{\rightleftharpoons}} E{-}I \quad (5)$$

in which E = enzyme; I = inhibitor, k = reaction constant; E…I = non-covalent enzyme-inhibitor complex; E–I = covalent enzyme-inhibitor complex.

The initial (v_i) and steady-state (v_s) velocities in inhibitor presence and the pseudo-first order rate constants k_{obs} were determined for different inhibitor concentrations. The progress curves were fitted to the slow-binding equation [Equation (6)]:[52]

$$[P] = v_s \cdot t + \frac{v_i - v_s}{k_{obs}} \cdot [1 - \exp(-k_{obs} \cdot t)] + off \quad (6)$$

in which v_s = steady-state velocity, v_i = initial velocity, off = offset.

Then, the k_{obs} values were plotted against the inhibitor concentrations [I] with the following Equation (7):

$$k_{obs} = k_4 + \left(\frac{k_3 \cdot [I]}{K_i^{app} + [I]}\right) \quad (7)$$

in which K_i^{app} determination using k_{obs}.

The resulting dissociation constant of the initial enzyme-inhibitor complex K_i^{app} was then corrected to zero substrate concentration using the Cheng-Prusoff relationship (Equation 4), giving the K_i value.[51]

Dilution assay

Dilution assays were performed for selected compounds as published previously.[49] CatS (0.5 μM) in enzyme buffer (90 μL) was incubated for with inhibitors (10 μL in DMSO) for 30 min in concentrations corresponding to tenfold the IC_{50} value obtained from the fluorometric enzyme assay ensuring complete inhibition. These mixtures (2 μL) were diluted 100-fold in assay buffer (198 μL) containing 5 μL substrate (400 μM) to give a final substrate concentration of 10 μM. Recovery of enzyme activity was measured immediately by fluorescence readout. CatS with DMSO and no inhibitor added was used as a reference while the irreversible inhibitor K11777 was used as an irreversible control.[53]

ChemMedChem
Research Article
doi.org/10.1002/cmdc.202300160
Chemistry Europe
European Chemical Societies Publishing

Selectivity towards CatL and CatB[45,49]

Cathepsin B (CatB, SigmaAldrich, Germany) and cathepsin L (CatL, Sigma-Aldrich, Germany) were incubated in enzyme buffer (50 mM Tris-HCl, 5 mM EDTA, 200 mM NaCl, 2 mM DTT, pH 6.5) at room temperature for 20–30 min. Assay buffer (50 mM Tris-HCl, 5 mM EDTA, 200 mM NaCl, 0.005% Brij35, pH 6.5) was mixed with CatB or CatL in enzyme buffer, then inhibitor in DMSO or DMSO (negative control) was added, followed by 100 μM (CatB) or 6.25 μM (CatL) substrate *Z*-Phe-Arg-AMC (Bachem, Switzerland). The enzyme activity was monitored by a Tecan Spark (Tecan Group, Switzerland) fluorescence reader using black Greiner flat-bottom 96-well microtiter plates (Greiner Bio-One GmbH, Germany). Inhibitor screening concentrations started at 20 μM, followed by 1 μM, and 200 nM if the percentual inhibition exceeded 50% for the previous inhibitor concentration. IC_{50} values were determined for inhibitors with >50% inhibition at 20 μM.

Cytotoxicity

Cell culture

The human cell line MDA-MB-231 from adenocarcinomic breast tissue was cultured at 37 °C and 5% CO_2 in Dulbeccos Modified Eagles Medium (DMEM, 4.5 g/L D-glucose, L-glutamine; Gibco by ThermoFisher Scientific, Germany), supplemented with 10% FBS (SigmaAldrich, Germany) and 1% Penicillin/Streptomycin (Invitrogen, Germany). Cells were cultured in a T75 culture flask and passaged two to three times per week using TrypLE™ Express (Gibco by ThermoFisher Scientific, Germany).

Murine bone marrow derived from C7BL/6 mice was seeded (2× 10 cells/mL) in untreated 12 well plates (Gibco by ThermoFisher Scientific, Germany) using Iscoves Modified Dulbecco's Medium, supplement with 5% FBS, 2 mM L-glutamine, 100 IU/mL penicillin, 100 μg/mL streptomycin and 50 μM β-mercaptoethanol (all components from Sigma-Aldrich, Germany) and 10 ng/mL GM-CSF (MILTENYI BIOTEC, Germany). Media was replenished on days 3 and 6 of culture.

Cell viability assay

MDA-MB-231 cells were seeded at a density of 2,500 cells/well in a white half area 96-well plate (Greiner Bio-One, Germany) and incubated at 37 °C. 24 h after seeding, the medium was removed and cells were treated with 50 μL of either 100 μM or 20 μM solution of compounds **5a**, **5b**, **6b** and **3c** in fresh culture medium (0.1% DMSO) or culture medium (0.1% DMSO) only. For each condition, quadruplicates were performed. Cells were incubated for 24 h. After the treatment, CellTiter-Glo® Assay solution (50 μL) was added to each well, and the plate was placed on an orbital shaker for 2 minutes and subsequently incubated 10 minutes at room temperature. Luminescence readout was performed with a Promega GloMax®-Multi Detection System using the manufacturer's protocol.

DC cytotoxicity

On day 7 of DC culture, compounds (1 μM) and lipopolysaccharide (100 ng/mL) was applied as indicated. On the following day, samples were harvested, washed with buffer (PBS, 2% FBS, 2 mM EDTA) and preincubated with Fc receptor blocking rat-anti-mouse antibody (clone 2.4G2; ThermoFisher Scientific, Germany) to prevent unspecific antibody binding. Then, samples were incubated with phycoerythrin-labeled rat-anti-mouse CD11c antibody (clone N418; ThermoFisher Scientific, Germany) to delineate $CD11c^+$ DC, washed with PBS and incubated with allophycocyanin-eFluor780 tandem conjugate labeled fixable viability dye to detect dead cells within the $CD11c^+$ DC fraction. Fluorescence intensities were measured using an Attune NxT Flow Cytometer and were analyzed using Attune NxT software (both from ThermoFisher Scientific, Germany).

Abbreviations

ACN, acetonitrile; AMC, 7-amino-4-methylcoumarin; APC, antigen-presenting cell; boc, tert-butyl carbamoyl; CatB, cathepsin B; CatL, cathepsin L; CatS, cathepsin S; CH, cyclohexane; compd, compound; cyAla, cyclohexylalanine; DC, dendritic cell; DCM, dichloromethane; DECP, diethyl chlorophosphate; DIPEA, *N,N*-diisopropylethylamine; DMF, dimethylformamide; EA, ethyl acetate; HOBt, 1-hydroxybenzotriazole; hPhe, homophenylalanine; HWE, Horner-Wadsworth-Emmons; KHMDS, potassium bis(trimethylsilyl)amide; LHMDS, lithium bis(trimethylsilyl)amide; Me, methyl; Pip, piperazine; SAR, structure-activity relationship; SI, selectivity index; TBTU, 2-(1*H*-benzotriazole-1-yl)-1,1,3,3-tetramethylaminium tetrafluoroborate; THF, tetrahydrofuran, Z/Cbz; benzyloxycarbonyl.

Supporting Information

The supporting information includes molecular docking score tables, enzyme assay plots, and characterization data (LC–MS, NMR) and is available free of charge.

Acknowledgements

We acknowledge Ann-Katrin Fuchs, Albin Lahu, and Anna Riede (all at Johannes Gutenberg University Mainz) for their support in this project, as well as all other co-workers in the Q5 subproject of the CRC1066 (JGU Mainz, MPIP Mainz). Financial support by the Deutsche Forschungsgemeinschaft (DFG) in the framework of the CRC 1066 (Nanodimensional Polymeric Therapeutics for Tumor Therapy), project Q5 (Targeting and Immunomodulator Structures and their Coupling to Therapeutic Nanosystems for Oncological Application) is gratefully acknowledged. Open Access funding enabled and organized by Projekt DEAL.

Conflict of Interests

The authors declare no conflicts of interest.

Data Availability Statement

The data that support the findings of this study are available in the supplementary material of this article.

ChemMedChem
Research Article
doi.org/10.1002/cmdc.202300160
Chemistry Europe
European Chemical Societies Publishing

Keywords: cathepsins · inhibitors · molecular docking · structure-activity relationship · tumor microenvironment

[1] V. Leroy, S. Thurairatnam, *Exp. Opin. Therap. Patents* **2005**, *14*, 301–311.
[2] H.-H. Otto, T. Schirmeister, *Chem. Rev.* **1997**, *97*, 133–171.
[3] H. Kirschke, B. Wiederanders, D. Brömme, A. Rinne, *Cathepsin S from Bovine Spleen. Biochem. J.* **1989**, *264*, 467–473.
[4] G. P. Shi, A. C. Webb, K. E. Foster, J. H. M. Knoll, C. A. Lemere, J. S. Munger, H. A. Chapman, *J. Biol. Chem.* **1994**, *269*, 11530–11536.
[5] D. Bararia, J. A. Hildebrand, S. Stolz, S. Haebe, S. Alig, C. P. Trevisani, F. Osorio-Barrios, M. D. Bartoschek, M. Mentz, A. Pastore, E. Gaitzsch, M. Heide, V. Jurinovic, K. Rautter, J. Gunawardana, M. B. Sabdia, M. Szczepanowski, J. Richter, W. Klapper, A. Louissaint, C. Ludwig, S. Bultmann, H. Leonhardt, S. Eustermann, K. P. Hopfner, W. Hiddemann, M. von Bergwelt-Baildon, C. Steidl, R. Kridel, J. W. D. Tobin, M. K. Gandhi, D. M. Weinstock, M. Schmidt-Supprian, M. B. Sárosi, M. Rudelius, V. Passerini, J. Mautner, O. Weigert, *Cell Rep.* **2020**, *31*, 107522.
[6] E. Dheilly, E. Battistello, N. Katanayeva, S. Sungalee, J. Michaux, G. Duns, S. Wehrle, J. Sordet-Dessimoz, M. Mina, J. Racle, P. Farinha, G. Coukos, D. Gfeller, A. Mottok, R. Kridel, B. E. Correia, C. Steidl, M. Bassani-Sternberg, G. Ciriello, V. Zoete, E. Oricchio, *Cancer Cell* **2020**, *37*, 674–689.e12.
[7] S. H. McDowell, S. A. Gallaher, R. E. Burden, C. J. Scott, *Biochim. Biophys. Acta Mol. Cell Res.* **2020**, *1867*, 118781.
[8] A. C. Da Costa, F. Santa-Cruz, L. A. R. Mattos, M. A. R. Aquino, C. R. Martins, Á. A. B. Ferraz, J. L. Figueiredo, *Mol. Clin. Oncol.* **2020**, *12*, 99–103.
[9] R. D. A. Wilkinson, A. Young, R. E. Burden, R. Williams, C. J. Scott, *Mol. Cancer* **2016**, *15*, 1–11.
[10] R. J. Riese, R. N. Mitchell, J. A. Villadangos, G. P. Shi, J. T. Palmer, E. R. Karp, G. T. De Sanctis, H. L. Ploegh, H. A. Chapman, *J. Clin. Invest.* **1998**, *101*, 2351–2363.
[11] J. A. Villadangos, R. J. Riese, C. Peters, H. A. Chapman, H. L. Ploegh, *J. Exp. Med.* **1997**, *186*, 549–560.
[12] R. J. Riese, P. R. Wolf, D. Brömme, L. R. Natkin, J. A. Villadangos, H. L. Ploegh, H. A. Chapman, *Immunity* **1996**, *4*, 357–366.
[13] S. Guo-Ping, J. A. Villadangos, G. Dranoff, C. Small, G. Lijuan, K. J. Haley, R. Riese, H. L. Ploegh, H. A. Chapman, *Immunity* **1999**, *10*, 197–206.
[14] C. Beers, A. Burich, M. J. Kleijmeer, J. M. Griffith, P. Wong, A. Y. Rudensky, *J. Immunol.* **2005**, *174*, 1205–1212.
[15] L. C. Hsing, A. Y. Rudensky, *Immunol. Rev.* **2005**, *207*, 229–241.
[16] T. Jakoš, A. Pišlar, A. Jewett, J. Kos, *Front. Immunol.* **2019**, *10*, 2037.
[17] B. Farhood, M. Najafi, K. Mortezaee, *J. Cell. Physiol.* **2019**, *234*, 8509–8521.
[18] V. Quaranta, M. C. Schmid, *Cells* **2019**, *8*, 747.
[19] C. Fu, A. Jiang, *Front. Immunol.* **2018**, *9*, 3059.
[20] X. Yan, C. Wu, T. Chen, M. M. Santos, C. L. Liu, C. Yang, L. Zhang, J. Ren, S. Liao, H. Guo, G. K. Sukhova, G. P. Shi, *Mol. Immunol.* **2017**, *82*, 66–74.
[21] W. L. Liu, D. Liu, K. Cheng, Y. J. Liu, S. Xing, P. D. Chi, X. H. Liu, N. Xue, Y. Z. Lai, L. Guo, G. Zhang, *Oncotarget* **2016**, *7*, 28124.
[22] Y. Yixuan, L. S. Kiat, C. L. Yee, L. Huiyin, C. Yunhao, C. P. Kuan, A. Hassan, W. T. Ting, S. T. Manuel, Y. K. Guan, L. Y. Pin, *J. Proteome Res.* **2010**, *9*, 4767–4778.
[23] R. E. Burden, J. A. Gormley, D. Kuehn, C. Ward, H. F. Kwok, M. Gazdoiu, A. McClurg, T. J. Jaquin, J. A. Johnston, C. J. Scott, S. A. Olwill, *Biochimie* **2012**, *94*, 487–493.
[24] R. E. Burden, J. A. Gormley, T. J. Jaquin, D. M. Small, D. J. Quinn, S. M. Hegarty, C. Ward, B. Walker, J. A. Johnston, S. A. Olwill, C. J. Scott, *Clin. Cancer Res.* **2009**, *15*, 6042–6051.
[25] N. Fuchs, M. Meta, D. Schuppan, L. Nuhn, T. Schirmeister, *Cells* **2020**, *9*, 2021.
[26] R. Bai, N. Chen, L. Li, N. Du, L. Bai, Z. Lv, H. Tian, J. Cui, *Front. Oncol.* **2020**, *10*, 1290.
[27] J. R. Somoza, H. Zhan, K. K. Bowman, L. Yu, K. D. Mortara, J. T. Palmer, J. M. Clark, M. E. McGrath, *Biochemistry* **2000**, *39*, 12543–12551.
[28] G. Kopitar, M. Dolinar, B. Štrukelj, J. Pungerčar, V. Turk, *Eur. J. Biochem.* **1996**, *236*, 558–562.
[29] T. A. Pauly, T. Sulea, M. Ammirati, J. Sivaraman, D. E. Danley, M. C. Griffor, A. V. Kamath, I. K. Wang, E. R. Laird, A. P. Seddon, R. Ménard, M. Cygler, V. L. Rath, *Biochemistry* **2003**, *42*, 3203–3213.
[30] J. Y. Gauthier, W. C. Black, I. Courchesne, W. Cromlish, S. Desmarais, R. Houle, S. Lamontagne, C. S. Li, F. Massé, D. J. McKay, M. Ouellet, J. Robichaud, J. F. Truchon, V. L. Truong, Q. Wang, M. D. Percival, *Bioorg. Med. Chem. Lett.* **2007**, *17*, 4929–4933.
[31] D. C. Tully, H. Liu, A. K. Chatterjee, P. B. Alper, R. Epple, J. A. Williams, M. J. Roberts, D. H. Woodmansee, B. T. Masick, C. Tumanut, J. Li, G. Spraggon, M. Hornsby, J. Chang, T. Tuntland, T. Hollenbeck, P. Gordon, J. L. Harris, D. S. Karanewsky, *Bioorg. Med. Chem. Lett.* **2006**, *16*, 5112–5117.
[32] J. Cai, J. Robinson, S. Belshaw, K. Everett, X. Fradera, M. Van Zeeland, L. Van Berkom, P. Van Rijnsbergen, L. Popplestone, M. Baugh, M. Dempster, J. Bruin, W. Hamilton, E. Kinghorn, P. Westwood, J. Kerr, Z. Rankovic, W. Arbuckle, D. J. Bennett, P. S. Jones, C. Long, I. Martin, J. C. M. Uitdehaag, T. Meulemans, *Bioorg. Med. Chem. Lett.* **2010**, *20*, 6890–6894.
[33] P. K. Jadhav, M. A. Schiffler, K. Gavardinas, E. J. Kim, D. P. Matthews, M. A. Staszak, D. S. Coffey, B. W. Shaw, K. C. Cassidy, R. A. Brier, Y. Zhang, R. M. Christie, W. F. Matter, K. Qing, J. D. Durbin, Y. Wang, G. G. Deng, *ACS Med. Chem. Lett.* **2014**, *5*, 1138–1142.
[34] S. Ahmad, M. I. Siddiqi, *J. Mol. Model.* **2017**, *23*, 92.
[35] Y. D. Ward, D. S. Thomson, L. L. Frye, C. L. Cywin, T. Morwick, M. J. Emmanuel, R. Zindell, D. McNeil, Y. Bekkali, M. Giradot, M. Hrapchak, M. DeTuri, K. Crane, D. White, S. Pav, Y. Wang, M. H. Hao, C. A. Grygon, M. E. Labadia, D. M. Freeman, W. Davidson, J. L. Hopkins, M. L. Brown, D. M. Spero, *J. Med. Chem.* **2002**, *45*, 5471–5482.
[36] A. Lee-Dutra, D. K. Wiener, S. Sun, *Exp. Opin. Therap. Patents* **2011**, *21*, 311–337.
[37] J. J. M. Wiener, S. Sun, R. L. Thurmond, *Curr. Top. Med. Chem.* **2010**, *10*, 717–732.
[38] H. Hilpert, H. Mauser, R. Humm, L. Anselm, H. Kuehne, G. Hartmann, S. Gruener, D. W. Banner, J. Benz, B. Gsell, A. Kuglstatter, M. Stihle, R. Thoma, R. A. Sanchez, H. Iding, B. Wirz, W. Haap, *J. Med. Chem.* **2013**, *56*, 9789–9801.
[39] R. D. A. Wilkinson, A. Young, R. E. Burden, R. Williams, C. J. Scott, *Mol. Cancer* **2016**, *15*, 1–11.
[40] J. K. Kerns, H. Nie, W. Bondinell, K. L. Widdowson, D. S. Yamashita, A. Rahman, P. L. Podolin, D. C. Carpenter, Q. Jin, B. Riflade, X. Dong, N. Nevins, P. M. Keller, L. Mitchell, T. Tomaszek, *Bioorg. Med. Chem. Lett.* **2011**, *21*, 4409–4415.
[41] H. A. Katsuhisa Kitano, S. Hamaguchi, *(12) Patent Application Publication (10) Pub. No.: US 2010/0292345 A1 Patent Application Publication*, **2010**.
[42] R. A. Bauer, *Drug Discovery Today* **2015**, *20*, 1061–1073.
[43] A. S. Kalgutkar, D. K. Dalvie, *Expert Opin. Drug Discovery* **2012**, *7*, 561–581.
[44] C. Lammert, S. Einarsson, C. Saha, A. Niklasson, E. Bjornsson, N. Chalasani, *Hepatology* **2008**, *47*, 2003–2009.
[45] T. Schirmeister, J. Kesselring, S. Jung, T. H. Schneider, A. Weickert, J. Becker, W. Lee, D. Bamberger, P. R. Wich, U. Distler, S. Tenzer, P. Johé, U. A. Hellmich, B. Engels, *J. Am. Chem. Soc.* **2016**, *138*, 8332–8335.
[46] C. U. Lee, T. N. Grossmann, *Angew. Chem. Int. Ed.* **2012**, *51*, 8699–8700.
[47] R. A. Copeland, D. L. Pompliano, T. D. Meek, *Nat. Rev. Drug Discovery* **2006**, *5*, 730–739.
[48] J. M. Bradshaw, J. M. McFarland, V. O. Paavilainen, A. Bisconte, D. Tam, V. T. Phan, S. Romanov, D. Finkle, J. Shu, V. Patel, T. Ton, X. Li, D. G. Loughhead, P. A. Nunn, D. E. Karr, M. E. Gerritsen, J. O. Funk, T. D. Owens, E. Verner, K. A. Brameld, R. J. Hill, D. M. Goldstein, J. Taunton, *Nat. Chem. Biol.* **2015**, *11*, 525–531.
[49] S. Jung, N. Fuchs, P. Johe, A. Wagner, E. Diehl, T. Yuliani, C. Zimmer, F. Barthels, R. A. Zimmermann, P. Klein, W. Waigel, J. Meyr, T. Opatz, S. Tenzer, U. Distler, H. J. Räder, C. Kersten, B. Engels, U. A. Hellmich, J. Klein, T. Schirmeister, *J. Med. Chem.* **2021**, *64*, 12322–12358.
[50] D. Brömme, *Curr. Protoc. Protein Sci.* **2000**, *21*, 21.2.1–21.2.14.
[51] C. Yung-Chi, W. H. Prusoff, *Biochem. Pharmacol.* **1973**, *22*, 3099–3108.
[52] D. L. Purich, *Enzyme Kinetics, Catalysis and Control, A Reference of Theory and Best-Practice Methods*, Elsevier, **2010**.
[53] I. D. Kerr, J. H. Lee, C. J. Farady, R. Marion, M. Rickert, M. Sajid, K. C. Pandey, C. R. Caffrey, J. Legac, E. Hansell, J. H. Mckerrow, C. S. Craik, P. J. Rosenthal, L. S. Brinen, *J. Biol. Chem.* **2009**, *284*, 25697–25703.
[54] C. L. Wilder, C. Walton, V. Watson, F. A. A. Stewart, J. Johnson, S. R. Peyton, C. K. Payne, V. Odero-Marah, M. O. Platt, *Int. J. Biochem. Cell Biol.* **2016**, *79*, 199–208.

ChemMedChem
Research Article
doi.org/10.1002/cmdc.202300160
Chemistry Europe
European Chemical Societies Publishing

[55] H. M. Berman, J. Westbrook, Z. Feng, G. Gilliland, T. N. Bhat, H. Weissig, I. N. Shindyalov, P. E. Bourne, *Nucleic Acids Res.* **2000**, *28*, 235–242.
[56] L. Schrödinger, W. DeLano, The PyMOL Molecular Graphics System. Schrödinger, LLC. **2020**. http://www.pymol.org/pymol.
[57] Molecular Operating Environment (MOE). Chemical Computing Group ULC: 1010 Sherbrooke St. West, Suite #910, Montreal, QC, Canada, H3 A 2R7 **2020**.
[58] T. A. Halgren, *J. Comput. Chem.* **1999**, *20*, 720–729.
[59] LeadIT. BioSolveIT GmbH: Sankt Augustin, Germany **2017**. www.biosolveit.de/LeadIT.
[60] I. Reulecke, G. Lange, J. Albrecht, R. Klein, M. Rarey, *ChemMedChem* **2008**, *3*, 885–897.
[61] GraFit. Erithracus Software Ltd.: UK **2006**.

Manuscript received: March 21, 2023
Revised manuscript received: May 18, 2023
Accepted manuscript online: May 24, 2023
Version of record online: June 1, 2023

”

4.2 Structural Modifications of Covalent Cathepsin S Inhibitors: Impact on Affinity, Selectivity, and Permeability

4.2.1 Context, Project Summary, and Own Contributions

Several small molecule inhibitors have been targeting the active site cysteine (cys-25) of catS reported to date, many of them inhibiting the enzyme either reversibly or irreversibly. As of today, none of the developed clinical candidates have been approved by the FDA and most of the inhibitors were designed for the use in autoimmune diseases.[46,54,109,114,135] However, since the approval of the first cysteine protease inhibitor nirmatrelvir in 2021, there is a resurgence of covalent modulators for cysteine proteases.[128] Of the several covalent catS inhibitors developed in recent years, most of them bear a covalently reversible reacting nitrile as electrophile next to the P1 position. Warheads with similar reaction mechanisms and inhibition types are aldehydes and ketones. While most inhibitors with an aldehyde as warhead are almost exclusively used as affinity-based probes or experimental substances, due to their high inherent reactivity towards several nucleophiles and nucleophilic residues in enzymes, there have been SAR campaigns focusing on developing functionalized derivatives of these highly reactive inhibitors to make them more viable as potential drugs.[139,140] For inhibitors bearing ketones as warheads, the electrophilicity and the resulting inhibition type can be finely modulated by adding either electron withdrawing or electron donating groups conjugated to the ketone moiety or by adding larger substituents, that can attribute to additional non-covalent interactions with the binding pocket, thus enhancing the affinity. Additionally, the design of quiescent affinity labeling warheads like the acyloxymethyl ketone can lead to inhibitors with two inhibition modes.[141,143,254,255]

In this study, 17 nitrile inhibitors, five ketone-based, and one aldehyde inhibitor of catS were synthesized and tested against the target and off-target cathepsins in fluorometric enzyme assays. Different side chains among the nitrile-based inhibitors yielded compounds with comparable affinity to the starting inhibitors and revealed affinity limitations. Some inhibitors displayed improved selectivities against off-targets cathepsins B and L and high membrane permeabilities. Introducing an aldehyde warhead led to a sub-nanomolar inhibitor with favorable selectivities, a slowly covalent-reversible inhibition mechanism, and a high permeability. Using the aldehyde and one ketone inhibitor, two warhead-masking hydrazone derivatives were synthesized that showed susceptibility to cleavage under acidic conditions and led to a up to 56-fold drop in affinity, demonstrating the successful masking of the highly reactive warheads. Certain derivatives showed time-dependent and reversible inhibition behaviors, impacting membrane permeability, and suggesting potential candidates for in vivo studies. Correlation analyses provided insights into structural factors influencing membrane transport, and guiding future modifications.

Own contributions: Design of the study, inhibitor synthesis (all except for **48**–**51**), catS, catB and catL fluorometric enzyme assays, dilution assays, hydrazone stability assays, molecular modeling and docking, writing of the original draft, and manuscript editing.

Contribution from other authors: Inhibitor synthesis (**48**–**51**), PAMPA assay, and writing parts of the original draft and manuscript editing.

This work has been published ahead of print in ACS Medicinal Chemistry Letters.

The appended Supporting Information represents an abridged version. The full Supporting Information can be accessed online at doi: 10.1021/acsmedchemlett.4c00050.

4.2.2 Publication

The following publication quoted within “” from page 62 to page 69 is the same as the manuscript cited on page 61.

“

ACS Medicinal Chemistry Letters

pubs.acs.org/acsmedchemlett Letter

Structural Modifications of Covalent Cathepsin S Inhibitors: Impact on Affinity, Selectivity, and Permeability

Published as part of ACS Medicinal Chemistry Letters virtual special issue “Exploring Covalent Modulators in Drug Discovery and Chemical Biology”.

Mergim Meta,[‡] Collin Zimmer,[‡] Natalie Fuchs, Maximilian Johannes Zecher, Albin Lahu, and Tanja Schirmeister*

Cite This: https://doi.org/10.1021/acsmedchemlett.4c00050 Read Online

ACCESS | Metrics & More | Article Recommendations | Supporting Information

ABSTRACT: Cathepsin S (catS) is a member of the cysteine protease family with limited tissue distribution, which is predominantly found in antigen-presenting cells. Due to overexpression and overactivity of catS in numerous cancers, inhibition of catS is supposed to improve the antitumor response. Here, we explore the potential of small-molecule catS inhibitors emphasizing their in vitro pharmacodynamics and pharmacokinetics. Membrane permeability of selected inhibitors was measured with a Parallel Artificial Membrane Permeation Assay and correlated to calculated physicochemical parameters and inhibition data. The binding kinetics and inhibition types of potent and selective new inhibitors with unexplored warheads were investigated. Our unique approach involves reversible masking of these potent warheads, allowing for further customization without compromising affinity or selectivity. The most promising inhibitors in this study include covalent aldehyde and ketone derivatives reversibly masked as hydrazones as potential candidates for therapeutic interventions targeting catalytic enzymes and modulating the immune response in cancer.

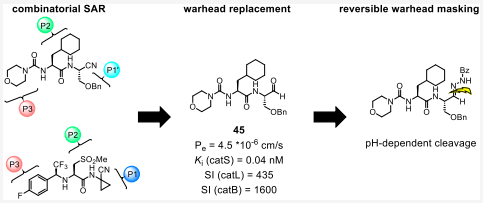

KEYWORDS: *Cathepsin S, covalent inhibition, structure−activity relation, membrane permeability, reversible warheads*

Cysteine cathepsins are essential enzymes of the papain-like family of proteases with several physiological functions, such as extracellular matrix degradation and processing of damaged proteins in the endolysosomal pathway.[1] Cathepsin S (catS) takes a special role, since this protease is stable and catalytically active at neutral pH, and it has a limited tissue distribution (mainly in antigen-presenting cells, e.g. dendritic cells).[2] CatS has emerged as a potential target for several pathological conditions such as Sjögren's syndrome, psoriasis, and many types of cancer.[3,4] It is overexpressed and overactive in several tumors such as follicular lymphoma, breast cancer, or astrocytoma, and many mechanisms that explain how catS is involved in tumor progression are known.[5,6] CatS is also found extracellularly and is known to degrade extracellular matrix proteins and to drive angiogenesis.[7] It is a major regulator of antigen processing and presentation via the MHC-II pathway in antigen-presenting cells (APCs).[8,9] In a follicular lymphoma model, the overexpression and overactivation of the enzyme led to the shift from the MHC-II to the MHC-I pathway, thus inducing a favored activation of regulatory CD4$^+$ T cells over cytotoxic CD8$^+$ T cells, which ultimately led to a suppression of the antitumor immune response.[5,6,10] One possible strategy to tackle this immune-suppressive milieu of the tumor microenvironment (TME) is the use of small-molecule catS inhibitors, since catS is involved in the polarization of APCs from the M1 phenotype to the M2 phenotype.[3,5,6] The use of inhibitory antibodies, siRNA, and knockout experiments has already shown that the antitumor immune response could be enhanced through the inhibition of catS, by shifting the ratio of CD8$^+$ T cells to CD4$^+$ T cells toward the cytotoxic CD8$^+$ T cells.[5,6] Furthermore, inhibition of several cathepsins with a pan-cathepsin inhibitor led to polarization of tumor-associated macrophages and a shift from M2 macrophages to M1 macrophages, ultimately leading to an increase of pro-inflammatory mediators.[11] To date, several small-molecule inhibitors have been reported, many of them targeting the active site cysteine (Cys-25) in an either reversible or irreversible covalent manner.[12,13] As of today, none of the developed clinical candidates have been approved by the FDA

Received: January 30, 2024
Revised: May 24, 2024
Accepted: May 30, 2024

and most of the developed inhibitors were designed for use in autoimmune diseases.[14] There has been an emergency approval for the first nitrile-based cysteine protease-targeting inhibitor nirmatrelvir in combination with the CYP-450 inhibitor ritonavir for the short-term treatment of COVID-19 infections in 2021. This clinical setting is different from the requirements of chronic catS inhibitor administration in autoimmune and oncological diseases. Clinical development of catS inhibitors has not led to approvals so far; nevertheless, the search for covalent modulators of cysteine proteases is on the rise.[15] Figure 1 shows

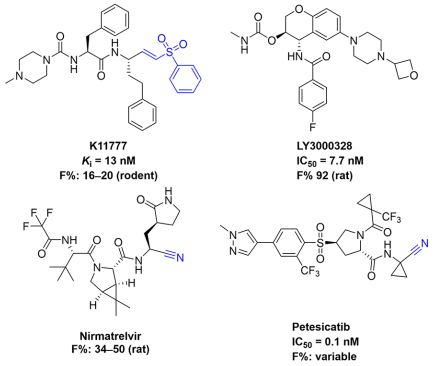

Figure 1. Structures, inhibition data against catS, and bioavailabilities (F%) of developed cathepsin S inhibitors and nirmatrelvir. Warheads are highlighted in blue.[17−19]

the structures of nirmatrelvir and three developed catS inhibitors, consisting of the irreversible pan-cathepsin inhibitor K11777, the noncovalent inhibitor LY3000328, and the covalent-reversible nitrile inhibitor petesicatib.[1,12,16,17]

In this study, we further explored peptidomimetic small-molecule inhibitors starting from nitriles with a focus on their pharmacodynamics (affinity and binding kinetics) and pharmacokinetics (membrane permeability). Additionally, through the exchange of the nitrile warhead with α-substituted ketones or an aldehyde, a set of newly generated inhibitors was synthesized and tested for their affinity and selectivity toward catS (Figure 2). One goal was the development of inhibitors with masked warheads, which can be further decorated with advanced reversible linker systems in the future. So far, in many cases, the developed small-molecule inhibitors have been derivatized with bulky linkers, leading to a dramatic structural change, which can lead to a loss in affinity or selectivity toward the target enzyme.[20] With our approach, highly potent and reactive warheads such as aldehyde or electron-deficient ketones can be masked reversibly as hydrazones, lowering the rate of off-target reactions while retaining the high affinities toward the target protease after controlled release. Two selected inhibitors (an aldehyde and a ketone) were therefore transformed to hydrazones for reversible warhead capping. Subsequently, the ability to release the free inhibitor in an acidic environment was inspected.

We aimed for a combinatorial approach with two catS selective inhibitors as starting points. Through merging and further derivatizing the P1, P2, and P3 substituents, which all have an impact on binding affinity, with aromatic and nonaromatic substituents that have proven to increase affinities toward the target enzyme, we aimed to gain insight into the

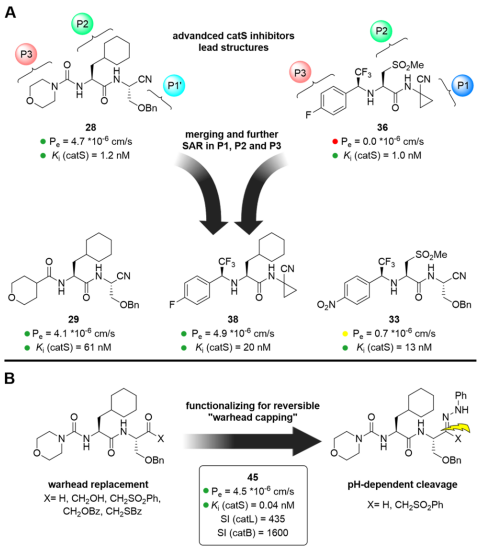

Figure 2. Aim and scope of the present study: (A) combinatorial SAR study through merging of two potent catS inhibitors and further substitutions, and (B) subsequent warhead replacement and reversible capping of the warhead. Created with BioRender.com.

selectivity profiles and membrane permeability of newly generated compounds.[12,13] Therefore, we prepared nitrile-based inhibitors with five different P3 residues frequently encountered in catS inhibitor design: three attached to the peptide as aryl-amides (pyridine-, 2*H*-tetrahydropyran-, and morpholine-4-carboxamide) and two attached as aryl-trifluoroethylamines (TFE) as amide isosters (4-fluoro- and 4-nitrophenyl-TFE). The amide isosters are used with in vivo application in mind, since they offer increased metabolic stability.[12] In P2, we chose L-cyclohexyl alanine (Cha) and a methylated and oxidized cysteine, since these residues in P2 led to the most potent and selective inhibitors in previous studies.[12,13,21] To gain information regarding whether a residue addressing the S1 subpocket or a substituent designed for occupying the S1′ site would be more beneficial, we prepared our inhibitors with three different P1 amino acids containing the nitrile warhead, namely, *O*-benzyl-L-serine (OBnSer), L-homophenylalanine (hPhe), and 1-aminocyclopropane-1-carboxylic acid (Acc). Although some of the synthesized inhibitors were already tested against catS in the past, we present them here again with novel data on off-target affinities, as well as membrane permeability.[12,13] Replacement of the nitrile warhead of one of the starting structures with electron-deficient ketones and an aldehyde led to new catS inhibitors from which two could be capped as hydrazones. In the future, this strategy opens the possibility of reversibly attaching the potential immunomodulators on different carrier systems. The pH-dependent release of the free inhibitor from hydrazone was explored for two selected inhibitors via HPLC/MS.

The detailed synthesis procedure of all final inhibitors with Schemes S1−S3 can be accessed in the Supporting Information (SI).

https://doi.org/10.1021/acsmedchemlett.4c00050
ACS Med. Chem. Lett. XXXX, XXX, XXX−XXX

Table 1A. Inhibition Data for Nitrile-Based Inhibitors 22−41[a]

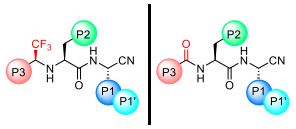

				K_i [nM]		
compound	P3	P2	P1/P1′	catS[b]	catB	catL
	Trifluoroethyl Amines					
34	4-Nitro-phenyl-	SO_2Me	hPhe	3.6 ± 1.8	36 ± 1	>10 000
33	4-Nitro-phenyl-	SO_2Me	*O*BnSer	13 ± 2	82 ± 8[b]	>10 000
37	4-Nitro-phenyl-	SO_2Me	Acc	7.8 ± 0.7	>12 000	>10 000
22	4-Fluoro-phenyl-	SO_2Me	*O*BnSer	2.4 ± 0.2	157[b]	1951[b]
36[c]	4-Fluoro-phenyl-	SO_2Me	Acc	1.0 ± 0.1	1670[b]	7106[b]
25	4-Fluoro-phenyl-	Cha	hPhe	146 ± 15	>12 000	>10 000
26	4-Fluoro-phenyl-	Cha	*O*BnSer	11 ± 3	>12 000	>10 000
38	4-Fluoro-phenyl-	Cha	Acc	20 ± 1	>12 000	1498[b]
	Carboxamides					
27[c]	Morpholine-4-	Cha	hPhe	5.7 ± 0.5	7847[b]	2536[b]
28[c]	Morpholine-4-	Cha	*O*BnSer	1.2 ± 0.1	1054[b]	543[b]
39[c]	Morpholine-4-	Cha	Acc	1.5 ± 0.1	>12 000	385[b]
30	Tetrahydropyran-4-	Cha	hPhe	382 ± 10	>12 000	6335
29	Tetrahydropyran-4-	Cha	*O*BnSer	61 ± 7	>12 000	5036
40	Tetrahydropyran-4-	Cha	Acc	117 ± 8	>12 000	1675
32	Pyridine-4-	Cha	hPhe	13 ± 1	1667[b]	1463[b]
31[c]	Pyridine-4-	Cha	*O*BnSer	11 ± 1	1906[b]	1024[b]
41	Pyridine-4	Cha	Acc	13 ± 1	>12 000	716[b]

[a]Data are shown as mean ± SD of at least duplicate experiments. [b]K_i values were obtained from K_i^{app} values, using the Cheng−Prusoff equation. [c]Inhibition data against catS for these compounds have already been published elsewhere and were reproduced in this study.[12,13]

Table 1B. Inhibition Data for Aldehyde- (45), Ketone-Based Inhibitors (44−51), and Hydrazones (46 and 47)[a]

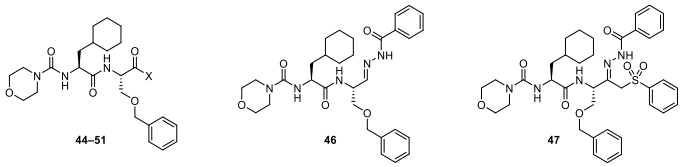

		K_i/K_i^* [nM]	k_{inact} (s^{-1})/k_{2nd} (M^{-1} s^{-1})	K_i[b] [nM]	
Cpd	X	catS		catB	catL
45	H	0.039 ± 0.005/0.016 ± 0.001[c]	–	64 ± 6	17 ± 2
44	CH_2SO_2Ph	331 ± 40/43 ± 13[c]	–	>510	>600
46[e]	–	2.2 ± 0.2	–	142 ± 9	21 ± 1
47[e]	–	989 ± 150	–	>12 000	>2500
50	CH_2OBz	25 ± 2[b]	–	>2550	>600
49	CH_2SBz	165 ± 18[b]	–	>10 000	>3000
51	CH_2OH	67 ± 3[b]	–	>2550	>600
48	CH_2Cl	0.5 ± 0.1[b]	0.0023 ± 0.0002/4.3 × 10^6 ± 1.2 × 10^6	n.d.[f]	n.d.[f]
52	vinylsulfone[g]	3.0 ± 0.6[d]	0.020 ± 0.001/7.2 × 10^6 ± 2.4 × 10^5	n.d.[f]	n.d.[f]

[a]Data are shown as mean ± SD of at least duplicate experiments. [b]K_i values were obtained from K_i^{app} values using the Cheng−Prusoff equation. [c]K_i and K_i^* values were obtained from K_i^{app} and $K_i^{*\,app}$. [d]k_{inact} and k_{2nd} were determined from plotting k_{obs} values against inhibitor concentration, as described previously.[22] [e]Inhibitory activity of **46** stems mainly from unmasked **45**, whereas, for hydrazone **47**, the inhibition of liberated **44** is of minor impact, estimated from reported affinities of carbonyl species **44** and **45**, and expected liberated amount by cleavage assays (Figure S7). [f]n.d. = not determined. [g]Data taken from ref 22.

All synthesized inhibitors were tested against catS and off-target cathepsins L and B (catL, catB) in fluorometric enzyme assays and their inhibition constants (K_i for all, K_i^* for slowly reversible, k_{inact} and k_{2nd} for irreversible binders) determined.[21,22] Finally, the membrane permeability of selected inhibitors was measured with a Parallel Artificial Membrane

https://doi.org/10.1021/acsmedchemlett.4c00050
ACS Med. Chem. Lett. XXXX, XXX, XXX−XXX

Permeation Assay (PAMPA) and correlated with the inhibition data and with calculated physicochemical parameters (log *P*; topological polar surface area, TPSA). For a more-detailed description on the assay procedure, see the methods section in the SI. The results for the nitrile-based inhibitors are summarized in Table 1A; the results for the inhibitors with other warheads are listed in Table 1B.

The exchange of the different side chains between the nitrile-based inhibitors produced eight new inhibitors with affinities in the low double-digit nanomolar range or even lower, similar to the starting compounds **28** and **36**, with K_i values of 1.2 nM and 1.0 nM, respectively (Table 1A).[22,23] It was also observed that the tetrahydropyran derivatives and inhibitor **25** showed significantly higher K_i values, compared to those of **28** and **36**. Overall, the selectivity against the off-targets catB and catL remained in the same range, e.g., compound **37** retained a good selectivity of >1500 over catB, compared to 1670 for starting inhibitor **36**, and even higher selectivity compared to the other starting inhibitor **28** (1054 over catB; see the SI). Compound **34** reached a higher selectivity over catL, compared to the second starting molecule **28** (>2778 over catL vs 453 for compound **28** vs catL, as given in the SI) (see Table 1A).

Exchanging the nitrile warhead of starting compound **28** with an aldehyde (**45**) led to a subnanomolar inhibitor with good selectivities over catB (≥1600; see the SI) and catL (≥435; see the SI), respectively. Further variations of the aldehyde included several α-substituted ketones which are known to react covalent-reversibly (through their ketone moiety) or depending on the quality of the leaving group in the α-position, irreversibly with papain-like cysteine proteases.[24] Visually inspecting the progress curves of the aldehyde (**45**) and the chloromethylketone (**48**) indicated time-dependent inhibition for both inhibitors. Since aldehydes react covalent-reversibly, compound **45** was evaluated as a slow-reversible binder of catS, while the chloromethylketone warhead of **48** is an irreversible inactivator of cysteine-proteases.[25] For the determination of K_i and K_i^* of **45**, we followed a procedure well described for slow-reversible tight binders (see Figure S1).[26,27] The plotting of the initial velocity v_i against the inhibitor concentration leads to K_i^{app} and a similar plotting of the steady-state velocity (v_s) against the inhibitor concentration gives access to $K_i^{*\,app}$, which can then be transformed to the corresponding K_i and $K_i^{*\,app}$ values with the Cheng−Prusoff equation.[26]

For the chloromethylketone (**48**) plotting k_{obs} values against the inhibitor concentration as described previously for irreversible inhibitors, revealed a subnanomolar inhibition constant and a second-order rate of $4.3 \times 10^6 \pm 1.2 \times 10^6$ $M^{-1}\,s^{-1}$, which confirms the high reactivity of this inhibitor class.

To our surprise, **50** did not show time-dependent inhibition in the time scale of the assay. The acyloxymethylketone warhead is known to eventually react irreversibly by substitution of the phenyl carboxylate leaving group.[24] The analogous thio derivative **49** also did not show time-dependent inhibition, leading us to the assumption that, for both inhibitors, a very slow irreversible step follows the reversible enzyme−inhibitor complex formation as described by Brady et al.[29] We were able to determine K_i values for the non-time-dependent first step of the inhibition process (Table 1B). Hydroxymethylketone inhibitor **51** did not exhibit time-dependent inhibition, as expected for this type of warhead; therefore, the K_i value was calculated.[25] Finally, inhibitor **44** with a new type of warhead (α-sulfonylphenyl methylketone) clearly showed time-dependent inhibition. To differ between reversible and irreversible binding, dilution assays (Figure 3) were performed for selected inhibitors with new warheads against catS (**44** and **49**−**52**; see Table 1B).

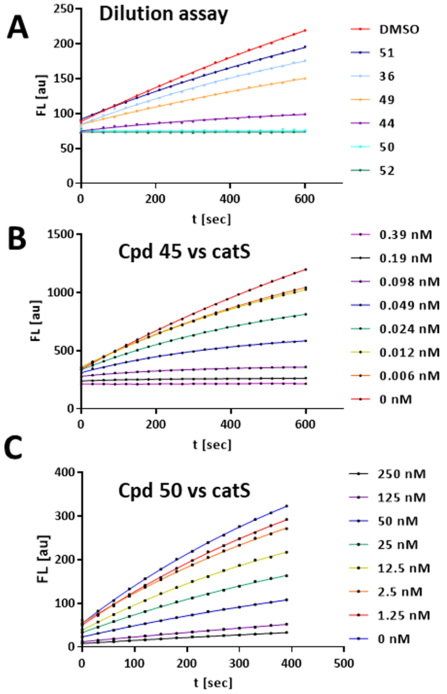

Figure 3. (A) Dilution assay of DMSO control (red), compounds **51** (dark blue), **36** (reversible nitrile, blue), **49** (orange), **44** (purple), **50** (cyan), and irreversible control **52** (vinylsulfone, green). Inhibitors were incubated at 20-fold K_i or $K_i^{*\,app}$ concentrations followed by 100-fold dilution, resulting in enzyme recovery in cases of DMSO and compounds **51**, **36**, **49** (linear progress curves), and **44** (time-dependent progress curve). Progress curves of (B) inhibitor **45**, catS and (C) inhibitor **50**, catS, showing the time-dependent inhibition by cpd **45** and non-time-dependent inhibition by cpd **50**.

K_i and $K_i^{*\,app}$ values for the slow-reversible inhibitor **44** were then calculated as described for **45** (Table 1B).[22]

The results of the dilution assays confirmed the irreversible binding behavior of acyloxymethyl ketone **50** (cyan, Figure 3A) since the enzyme activity did not recover, similar to the irreversible vinylsulfone control inhibitor **52** (green). Comparing the progress curves of the dilution assays of nitrile inhibitor **36** (blue) with the hydroxymethylketone **51** (dark blue) confirmed the reversibility of both warheads, which is well-described in the literature, since the hydroxymethylketone inhibitor **51** has no adequate leaving group.[7,30] Interestingly, inhibitors **49** (orange) and **44** (purple) seem to show a reversible binding behavior, since, for both, a recovery of the enzyme activity was observed. In the case of **44**, the progress curve is time-dependent, which indicates slow, reversible binding. Inspecting the noncovalent docking poses of **44** and **50** inside the active site of catS indicated that the electrophilic carbon atoms of **44** and **50** are in similarly close proximity to the

https://doi.org/10.1021/acsmedchemlett.4c00050
ACS Med. Chem. Lett. XXXX, XXX, XXX−XXX

nucleophilic thiol of Cys-25 (distance: 2.9 and 3.4 Å for **44**; 2.7 and 3.8 Å for **50**; see Figure 4). Interestingly, inhibitor **50** has

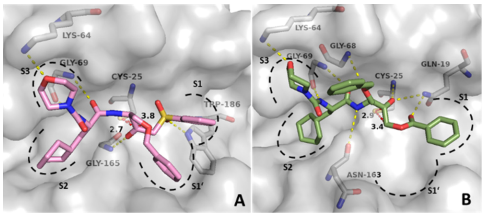

Figure 4. Noncovalent docking poses of **44** ((A) pink C atoms) and (**50** (B), green C atoms) inside the active site of catS (pdb entry: 1MS6). Polar interactions between the inhibitors and active site amino acids are depicted as yellow dashed lines. The distance between the sulfur atom of Cys-25 and the electrophilic C atoms of **44** and **50** is depicted as a red dashed line and the distance is given in Å.

more polar interactions with the binding pocket, compared to **44** (Figure 4), which could help to understand the lower K_i of **50**, in comparison to **44**.

The inhibitory potency of **46** is mainly attributed to traces of cleaved aldehyde **45**, whereas that for **47** (≤5% free **44** under assay conditions) is mainly attributed to the noncleaved hydrazone. The hydrazone derivative **47** showed a 3-fold drop in affinity toward catS, compared to unmasked **44**, and **46** even had a 56-fold drop in affinity, compared to free aldehyde **45**, proving the successful masking of both inhibitors. To investigate the liberation, both hydrazones were incubated in an acidic (pH 4 as artificial lysosomal conditions) and neutral (pH 7.4) environment (see the SI for a detailed description of the methodology). After incubating the respective inhibitor for 24 h at 37 °C, the amount of free aldehyde **45** and ketone **44** was higher at the lower pH value, compared to physiological conditions, indicating a higher cleavage rate under acidic conditions, especially for **46** (80% free inhibitor after 24 h at pH 4). The cleavage of **47** was slower (13% free inhibitor after 24 h at pH 4), indicating a lower hydrolysis rate. These findings highlight the reversible nature of the capped warheads especially under acidic conditions, as they appear in many tumors (Figures S7−S15).[6]

For the clinical candidates presented in Figure 1, oral bioavailability was shown during the drug development process.[31−35] However, some catS inhibitors in the literature suffer from poor experimental permeability (<0.5 × 10^{-6} cm/s).[36] To underline the utility of the newly synthesized compounds in in cellulo and in vivo contexts, their ability to cross membranes was assessed. For this determination, the well-established high-throughput PAMPA approach was used, and detection/quantification was performed by HPLC/MS.[37] By observing a compound's time-dependent permeation of an artificial membrane derived from phospholipids in *n*-dodecane, a good estimation of its passive permeability can be made.[38,39] To rationalize this for future derivatization campaigns, a correlation with the log *P* and TPSA of the compounds is depicted in Figure 5 (all compounds are calculated to be predominantly uncharged in physiologic media).[40] The correlation between physicochemical parameters such as log *P*, PAMPA permeability, and human intestinal absorption can be employed in the context of biopharmaceutics class determination.[41]

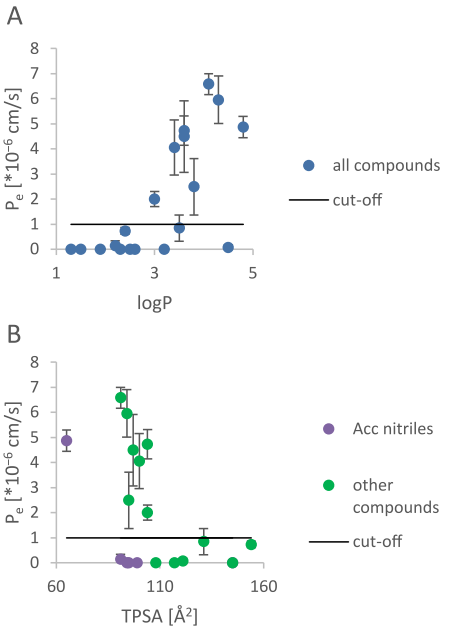

Figure 5. (A) Correlation of log *P* and permeability (P_e) for 19 compounds. (B) Correlation of TPSA and permeability (P_e), divided into two subsets (6 Acc nitriles and 13 others). "Cut-off" depicts the effective permeability value, above which compounds were considered relevantly permeable (P_e > 1 × 10^{-6} cm/s).

For most Acc-containing nitrile inhibitors, very low permeabilities (oftentimes with no permeation detected) were observed. This is also reflected in their low log *P* values of 1.3−2.5. Another highly hydrophilic structure hindering permeation appears to be the methylsulfonyl alanine as the P2 moiety, which can be inferred from the comparison of **36**, **22**, and **38**. While the exchange of P1 to *O*BnSer (**36** → **22**) increases the log *P* value by 1 and does not promote a real improvement in permeability in this case, the exchange of P2 to cyclohexyl alanine (**36** → **38**) increases the log *P* value by ca. 3, resulting in a compound with acceptable permeability. Therefore, **38** is the only compound with Acc in P1 that shows detectable permeation, while no compound with methylsulfonyl alanine as P2 showed appreciable permeation. Note that the combination of the lipophilic fluoro-aryl TFE and Cha moieties in P3 and P2, respectively, can result in unfavorable physicochemical properties due to high lipophilicity if a larger hydrophobic P1 amino acid is used (i.e., **25**, **26**). Excessive lipophilicity is the reason why four inhibitors (**25**, **26**, **49**, and **50**, log *P* ≥ 4.8) could not be assessed with this method, due to a combination of low aqueous solubility and their structurally inherent low detectability (weak ionizability and/or spectrophotometric properties). In contrast, well-balanced lipophilicities can be described for six inhibitors (**27**−**32**) with log *P* values of 3.0−4.3 that, therefore, show appreciable permeabilities ((2−7) × 10^{-6} cm/s). In this subgroup, the hPhe-containing inhibitor always has slightly better permeability than the *O*BnSer-containing analogue. Additionally, a difference in the impact of the P3 residue can

https://doi.org/10.1021/acsmedchemlett.4c00050
ACS Med. Chem. Lett. XXXX, XXX, XXX−XXX

Table 2. Permeability (P_e) as Determined by PAMPA ($n \geq 4$), and Calculated Physicochemical Parameters log*P* and TPSA for the Listed Compounds Clustered by Structural Features[a]

Cpd	P_e [$\times 10^{-6}$ cm/s]	log *P*	TPSA [Å^2]	Cpd	P_e [$\times 10^{-6}$ cm/s]	log *P*	TPSA [Å^2]
	Nitriles, Acc P1				**Nitriles, Other**		
36	0.0 ± 0.0	1.5	99	**27**	6.0 ± 1.0	4.3	94
37	0.0 ± 0.0	1.3	145	**28**	4.7 ± 0.6	3.6	104
38	4.9 ± 0.4	4.8	65	**29**	4.1 ± 1.1	3.4	100
39	0.0 ± 0.0	2.5	94	**30**	6.6 ± 0.4	4.1	91
40	0.1 ± 0.2	2.2	91	**31**	2.0 ± 0.3	3.0	104
41	0.0 ± 0.0	1.9	95	**32**	2.5 ± 1.1	3.8	95
	Nitriles, Methylsulfonyl Alanine P2				**Aldehyde, Ketones, Hydrazone**		
22	0.0 ± 0.0	2.6	108	**45**	4.5 ± 1.4	3.6	97
33	0.7 ± 0.1	2.4	154	**44**[b]	0.8 ± 0.5	3.5	131
34	0.0 ± 0.0	3.2	145	**51**	0.0 ± 0.0	2.3	117
				46	0.1 ± 0.1	4.5	121

[a]log*P* and TPSA were calculated using the Molinformation molecular properties calculator (https://www.molinspiration.com/).[28] [b]Instability detected (see Figures S3−S6 for stability investigations); only peaks with the expected concomitant *m*/*z* signal were used for quantification.

be observed in which the permeability trends are tetrahydropyran = morpholine > pyridine. Another observation is that the exchange of the warhead between nitrile and aldehyde (**28** → **45**) does not strongly influence the permeability, which is also reflected by identical log *P* values, indicating the possible transfer of the structure-related trends to the respective aldehydes. As depicted in Figure 5A, the trend for the presented compound set (Table 2) is that, in most cases, a log *P* value of >3 is required for good permeation and in the log *P* range of 3−5, a loose proportionality between log *P* and P_e is seen. This underlines the necessity of detailed structure−permeability relationship studies to predict the influence of distinct structural modifications, in addition to the facile calculation of log *P*.

The correlation between the permeability and TPSA also shows interesting relations. The best permeability is observed for compounds with TPSAs of 91−104 Å^2. If the threshold is exceeded (TPSA values of 108−154 Å^2), it results in a drastic decrease in permeation due to increased hydrophilicity. The most impactful moiety in this context seems to be the P3 nitrobenzene (e.g., in **33**, **34**, and **37**) and, after that, the P2 methylsulfonyl alanine. The compounds with TPSA values of >110 Å^2 are assumed to not have the ability to be effectively immersed in an apolar membrane and are therefore not transported through it. However, there are other compounds with seemingly adequate TPSA values (91−99 Å^2) that still have low permeability, namely most Acc nitriles. This can be attributed to the fact that the TPSA is an absolute measure. If the relatively smaller total surface area of the P1 Acc nitriles is considered, it becomes obvious that much of their surface area is polar, in contrast to the other compounds with comparable TPSA values that carry the much larger OBnSer or hPhe in P1. **38** seems to be the exception to the detrimental Acc effect, which indicates that it can be balanced out by the introduction of very lipophilic moieties, as reasoned above. The mentioned distinction of Acc nitriles from other nitriles in the set is also visible in Figure 5B. Each depicted subset has its own cutoff for permeability, which is lower for Acc nitriles (<90 Å^2) than for the other compounds (<110 Å^2).

While **47** could not be assessed for permeability due to solubility limitations, the hydrazone **46** has low permeability ($0.1 \pm 0.1 \times 10^{-6}$ cm/s), probably due to the high TPSA, despite its adequate log *P* value. This is important, because it underlines the utility of the warhead modification. It not only limits its strong electrophilicity but also hinders its cell permeation until it arrives in an environment as acidic as the TME, where the more-permeable and more-reactive warhead is liberated.

In summary, we successfully synthesized 17 nitrile inhibitors as well as five ketone-based inhibitors and one aldehyde inhibitor of catS and tested them on this interesting target and on off-target cathepsins in fluorometric enzyme assays. The exchange of different side chains among nitrile-based inhibitors produced some inhibitors with affinities that were comparable to that of the starting compounds and elucidated some clear affinity limitations. The starting compounds **28** and **36** already exhibited excellent K_i values, laying the background for the subsequent modifications. Two of the newly produced inhibitors even showed improved selectivities against off-target cathepsins B and L over the starting molecules. Introducing an aldehyde warhead in place of the nitrile led to a subnanomolar inhibitor with favorable selectivities.

The aldehyde and ketone derivatives showed time-dependent inhibition and suggested slow-reversible binding for certain compounds. Acyloxymethylketone **50** exhibited irreversible behavior in the dilution assay, while hydroxymethylketone **51** and surprisingly **49** displayed reversible characteristics. The introduction of a new warhead, α-sulfonylphenyl methylketone (**44**), demonstrated time-dependent reversible inhibition. Furthermore, warhead-masking hydrazone derivatives **46** and **47** were synthesized and examined, revealing their susceptibility to cleavage under acidic conditions. The clear difference in liberation kinetics (for **46**: 50% liberated after 24 h at pH 7.4 vs 50% liberated after 2 h at pH 4) are promising for delivery systems with targeted release in the acidic TME (e.g., attachment of the aldehyde to nanoparticles as a hydrazone) where pH values below 7 are commonly encountered.[42] The reversible attachment to nano carriers via the hydrazone moiety is expected to render the low membrane permeability of the hydrazones irrelevant by overriding the pharmacokinetic properties.

The assessment of membrane permeability highlighted some nitriles (esp. **30**) and the aldehyde (**45**) as promising novel candidates for in vivo studies while underlining challenges for inhibitors with strong hydrophilic groups. Correlation analyses between log *P*, TPSA, and permeability provided insights into the structural factors influencing transport across membranes and gave indications for future structural modification campaigns guided by calculated physicochemical properties.

https://doi.org/10.1021/acsmedchemlett.4c00050
ACS Med. Chem. Lett. XXXX, XXX, XXX−XXX

To conclude, this comprehensive investigation provides valuable insights into the design and behavior of catS inhibitors, paving the way for further optimization and development of potential therapeutic candidates.

■ ASSOCIATED CONTENT

Supporting Information

The Supporting Information is available free of charge at https://pubs.acs.org/doi/10.1021/acsmedchemlett.4c00050.

Full experimental details on synthesis, materials and methods, additional figures on kinetic evaluations, stability analysis, molecular docking score tables, and characterization data (PDF)

■ AUTHOR INFORMATION

Corresponding Author

Tanja Schirmeister − *Institute of Pharmaceutical and Biomedical Sciences, Johannes Gutenberg University Mainz, 55128 Mainz, Germany*; Email: schirmei@uni-mainz.de

Authors

Mergim Meta − *Institute of Pharmaceutical and Biomedical Sciences, Johannes Gutenberg University Mainz, 55128 Mainz, Germany*; orcid.org/0000-0003-3601-9523

Collin Zimmer − *Institute of Pharmaceutical and Biomedical Sciences, Johannes Gutenberg University Mainz, 55128 Mainz, Germany*

Natalie Fuchs − *Institute of Pharmaceutical and Biomedical Sciences, Johannes Gutenberg University Mainz, 55128 Mainz, Germany*; orcid.org/0000-0001-6404-676X

Maximilian Johannes Zecher − *Institute of Pharmaceutical and Biomedical Sciences, Johannes Gutenberg University Mainz, 55128 Mainz, Germany*

Albin Lahu − *Institute of Pharmaceutical and Biomedical Sciences, Johannes Gutenberg University Mainz, 55128 Mainz, Germany*

Complete contact information is available at: https://pubs.acs.org/10.1021/acsmedchemlett.4c00050

Author Contributions

‡Mergim Meta and Collin Zimmer contributed equally. All authors have given approval to the final version of the manuscript.

Funding

Financial support by the DFG (Deutsche Forschungsgemeinschaft) in the framework of the CRC 1066 (Nanodimensional Polymeric Therapeutics for Tumor Therapy), project Q5 (Targeting and Immunomodulator Structures and their Coupling to Therapeutic Nanosystems for Oncological Application) is gratefully acknowledged.

Notes

The authors declare no competing financial interest.

■ ACKNOWLEDGMENTS

We would kindly like to acknowledge the support of Michael Klein for creating figures with BioRender during this project.

■ ABBREVIATIONS

Acc, 1-aminocyclopropylcarboxylic acid; AMC, 7-amino-4-methylcoumarin; catB, human cathepsin B; catL, human cathepsin L; catS, human cathepsin S; Cha, cyclohexylalanine; cpd, compound; DMP, Dess−Martin periodinane; DTT, dithiothreitol; eq, equivalent; hPhe, homophenylalanine; PAMPA, parallel artificial membrane permeation assay; *O*BnSer, *O*-benzyl-L-serine; TFE, trifluoroethylamine; TME, tumor microenvironment; TPSA, topological polar surface area

■ REFERENCES

(1) Otto, H.-H.; Schirmeister, T. Cysteine Proteases and Their Inhibitors. *Chem. Rev.* **1997**, *97* (1), 133−172.

(2) Shi, G. P.; Webb, A. C.; Foster, K. E.; Knoll, J. H. M.; Lemere, C. A.; Munger, J. S.; Chapman, H. A. Human Cathepsin S: Chromosomal Localization, Gene Structure, and Tissue Distribution. *J. Biol. Chem.* **1994**, *269* (15), 11530−11536.

(3) Fuchs, N.; Meta, M.; Schuppan, D.; Nuhn, L.; Schirmeister, T. Novel Opportunities for Cathepsin S Inhibitors in Cancer Immunotherapy by Nanocarrier-Mediated Delivery. *Cells* **2020**, *9*, 2021 (NLM (Medline), Sept. 2, 2020).

(4) Edman, M. C.; Janga, S. R.; Meng, Z.; Bechtold, M.; Chen, A. F.; Kim, C.; Naman, L.; Sarma, A.; Teekappanavar, N.; Kim, A. Y.; Madrigal, S.; Singh, S.; Ortiz, E.; Christianakis, S.; Arkfeld, D. G.; Mack, W. J.; Heur, M.; Stohl, W.; Hamm-Alvarez, S. F. Increased Cathepsin S Activity Associated with Decreased Protease Inhibitory Capacity Contributes to Altered Tear Proteins in Sjögren's Syndrome Patients. *Sci. Rep.* **2018**, *8* (1), 11044.

(5) Bararia, D.; Hildebrand, J. A.; Stolz, S.; Haebe, S.; Alig, S.; Trevisani, C. P.; Osorio-Barrios, F.; Bartoschek, M. D.; Mentz, M.; Pastore, A.; Gaitzsch, E.; Heide, M.; Jurinovic, V.; Rautter, K.; Gunawardana, J.; Sabdia, M. B.; Szczepanowski, M.; Richter, J.; Klapper, W.; Louissaint, A.; Ludwig, C.; Bultmann, S.; Leonhardt, H.; Eustermann, S.; Hopfner, K. P.; Hiddemann, W.; von Bergwelt-Baildon, M.; Steidl, C.; Kridel, R.; Tobin, J. W. D.; Gandhi, M. K.; Weinstock, D. M.; Schmidt-Supprian, M.; Sárosi, M. B.; Rudelius, M.; Passerini, V.; Mautner, J.; Weigert, O. Cathepsin S Alterations Induce a Tumor-Promoting Immune Microenvironment in Follicular Lymphoma. *Cell Rep.* **2020**, *31* (5), 107522.

(6) Dheilly, E.; Battistello, E.; Katanayeva, N.; Sungalee, S.; Michaux, J.; Duns, G.; Wehrle, S.; Sordet-Dessimoz, J.; Mina, M.; Racle, J.; et al. Cathepsin S Regulates Antigen Processing and T Cell Activity in Non-Hodgkin Lymphoma. *Cancer Cell* **2020**, *37* (5), 674−689.e12.

(7) Wilkinson, R. D. A.; Young, A.; Burden, R. E.; Williams, R.; Scott, C. J. A Bioavailable Cathepsin S Nitrile Inhibitor Abrogates Tumor Development. *Mol. Cancer* **2016**, *15* (1), 29.

(8) Villadangos, J. A.; Riese, R. J.; Peters, C.; Chapman, H. A.; Ploegh, H. L. Degradation of Mouse Invariant Chain: Roles of Cathepsins S and D and the Influence of Major Histocompatibility Complex Polymorphism. *J. Exp. Med.* **1997**, *186* (4), 549−560.

(9) Beers, C.; Burich, A.; Kleijmeer, M. J.; Griffith, J. M.; Wong, P.; Rudensky, A. Y. Cathepsin S Controls MHC Class II-Mediated Antigen Presentation by Epithelial Cells In Vivo. *J. Immunol.* **2005**, *174* (3), 1205−1212.

(10) Jakoš, T.; Pišlar, A.; Jewett, A.; Kos, J. Cysteine Cathepsins in Tumor-Associated Immune Cells. *Front. Immunol.* **2019**, *10*, 2037.

(11) Oelschlaegel, D.; Sadan, T. W.; Salpeter, S.; Krug, S.; Blum, G.; Schmitz, W.; Schulze, A.; Michl, P. Cathepsin Inhibition Modulates Metabolism and Polarization of Tumor-Associated Macrophages. *Cancers (Basel)* **2020**, *12* (9), 2579.

(12) Gauthier, J. Y.; Black, W. C.; Courchesne, I.; Cromlish, W.; Desmarais, S.; Houle, R.; Lamontagne, S.; Li, C. S.; Massé, F.; McKay, D. J.; Ouellet, M.; Robichaud, J.; Truchon, J. F.; Truong, V. L.; Wang, Q.; Percival, M. D. The Identification of Potent, Selective, and Bioavailable Cathepsin S Inhibitors. *Bioorg. Med. Chem. Lett.* **2007**, *17* (17), 4929−4933.

(13) Ward, Y. D.; Thomson, D. S.; Frye, L. L.; Cywin, C. L.; Morwick, T.; Emmanuel, M. J.; Zindell, R.; McNeil, D.; Bekkali, Y.; Giradot, M.; et al. Design and Synthesis of Dipeptide Nitriles as Reversible and Potent Cathepsin S Inhibitors. *J. Med. Chem.* **2002**, *45* (25), 5471−5482.

(14) Biasizzo, M.; Javoršek, U.; Vidak, E.; Zarić, M.; Turk, B. Cysteine Cathepsins: A Long and Winding Road towards Clinics. *Mol. Aspects Med.* **2022**, *88*, 101150.
(15) Owen, D. R.; Allerton, C. M. N.; Anderson, A. S.; Aschenbrenner, L.; Avery, M.; Berritt, S.; Boras, B.; Cardin, R. D.; Carlo, A.; Coffman, K. J.; et al. An Oral SARS-CoV-2 M pro Inhibitor Clinical Candidate for the Treatment of COVID-19. *Science* **2021**, *374* (6575), 1586−1593.
(16) Jadhav, P. K.; Schiffler, M. A.; Gavardinas, K.; Kim, E. J.; Matthews, D. P.; Staszak, M. A.; Coffey, D. S.; Shaw, B. W.; Cassidy, K. C.; Brier, R. A.; Zhang, Y.; Christie, R. M.; Matter, W. F.; Qing, K.; Durbin, J. D.; Wang, Y.; Deng, G. G. Discovery of Cathepsin S Inhibitor LY3000328 for the Treatment of Abdominal Aortic Aneurysm. *ACS Med. Chem. Lett.* **2014**, *5* (10), 1138−1142.
(17) Eng, H.; Dantonio, A. L.; Kadar, E. P.; Obach, R. S.; Di, L.; Lin, J.; Patel, N. C.; Boras, B.; Walker, G. S.; Novak, J. J.; Kimoto, E.; Singh, R. S. P.; Kalgutkar, A. S. Disposition of Nirmatrelvir, an Orally Bioavailable Inhibitor of SARS-CoV-2 3C-Like Protease, across Animals and Humans. *Drug Metab. Dispos.* **2022**, *50* (5), 576−590.
(18) Abdulla, M.-H.; Lim, K.-C.; Sajid, M.; McKerrow, J. H.; Caffrey, C. R. Schistosomiasis Mansoni: Novel Chemotherapy Using a Cysteine Protease Inhibitor. *PLoS Med.* **2007**, *4* (1), e14.
(19) Jadhav, P. K.; Schiffler, M. A.; Gavardinas, K.; Kim, E. J.; Matthews, D. P.; Staszak, M. A.; Coffey, D. S.; Shaw, B. W.; Cassidy, K. C.; Brier, R. A.; Zhang, Y.; Christie, R. M.; Matter, W. F.; Qing, K.; Durbin, J. D.; Wang, Y.; Deng, G. G. Discovery of Cathepsin S Inhibitor LY3000328 for the Treatment of Abdominal Aortic Aneurysm. *ACS Med. Chem. Lett.* **2014**, *5* (10), 1138−1142.
(20) Mikhaylov, G.; Klimpel, D.; Schaschke, N.; Mikac, U.; Vizovisek, M.; Fonovic, M.; Turk, V.; Turk, B.; Vasiljeva, O. Selective Targeting of Tumor and Stromal Cells By a Nanocarrier System Displaying Lipidated Cathepsin B Inhibitor. *Angew. Chem., Int. Ed.* **2014**, *53* (38), 10077−10081.
(21) Fuchs, N.; Meta, M.; Lantzberg, B.; Bros, M.; Ling Kuan, S.; Weil, T.; Schirmeister, T. Subnanomolar Cathepsin S Inhibitors with High Selectivity: Optimizing Covalent Reversible α-Fluorovinylsulfones and α-Sulfonates as Potential Immunomodulators in Cancer. *ChemMedChem.* **2023**, *18* (15), e202300160.
(22) Müller, P.; Meta, M.; Meidner, J. L.; Schwickert, M.; Meyr, J.; Schwickert, K.; Kersten, C.; Zimmer, C.; Hammerschmidt, S. J.; Frey, A.; Lahu, A.; de la Hoz-Rodríguez, S.; Agost-Beltrán, L.; Rodríguez, S.; Diemer, K.; Neumann, W.; Gonzàlez, F. V.; Engels, B.; Schirmeister, T. Investigation of the Compatibility between Warheads and Peptidomimetic Sequences of Protease Inhibitors—A Comprehensive Reactivity and Selectivity Study. *Int. J. Mol. Sci.* **2023**, *24* (8), 7226.
(23) Maus, H.; Müller, P.; Meta, M.; Hoba, S. N.; Hammerschmidt, S. J.; Zimmermann, R. A.; Zimmer, C.; Fuchs, N.; Schirmeister, T.; Barthels, F. Next Generation of Fluorometric Protease Assays: 7-Nitrobenz-2-oxa-1,3-diazol-4-yl amides (NBD Amides) as Class Spanning Protease Substrates. *Chem.—Eur. J.* **2023**, *29* (50), e202301855.
(24) Krantz, A.; Copp, L. J.; Coles, P. J.; Smith, R. A.; Heard, S. B. Peptidyl (Acyloxy)Methyl Ketones and the Quiescent Affinity Label Concept: The Departing Group as a Variable Structural Element in the Design of Inactivators of Cysteine Proteinases. *Biochemistry* **1991**, *30*, 4678−4687.
(25) Hoffman, R. L.; Kania, R. S.; Brothers, M. A.; Davies, J. F.; Ferre, R. A.; Gajiwala, K. S.; He, M.; Hogan, R. J.; Kozminski, K.; Li, L. Y.; Lockner, J. W.; Lou, J.; Marra, M. T.; Mitchell, L. J.; Murray, B. W.; Nieman, J. A.; Noell, S.; Planken, S. P.; Rowe, T.; Ryan, K.; Smith, G. J.; Solowiej, J. E.; Steppan, C. M.; Taggart, B. Discovery of Ketone-Based Covalent Inhibitors of Coronavirus 3CL Proteases for the Potential Therapeutic Treatment of COVID-19. *J. Med. Chem.* **2020**, *63* (21), 12725−12747.
(26) Klein, P.; Barthels, F.; Johe, P.; Wagner, A.; Tenzer, S.; Distler, U.; Le, T. A.; Schmid, P.; Engel, V.; Engels, B.; Hellmich, U. A.; Opatz, T.; Schirmeister, T. Naphthoquinones as Covalent Reversible Inhibitors of Cysteine Proteases—Studies on Inhibition Mechanism and Kinetics. *Molecules* **2020**, *25* (9), 2064.
(27) Mons, E.; Roet, S.; Kim, R. Q.; Mulder, M. P. C. A Comprehensive Guide for Assessing Covalent Inhibition in Enzymatic Assays Illustrated with Kinetic Simulations. *Curr. Protoc.* **2022**, *2* (6), e419.
(28) *Molinspiration Cheminformatics Free Web Services*; Molinspiration, Slovensky Grob, Slovak Republic; available via the Internet at: https://www.molinspiration.com.
(29) Brady, K. A Catalytic Mechanism for Caspase-1 and for Bimodal Inhibition of Caspase-1 by Activated Aspartic Ketones. *Bioorg. Med. Chem.* **1999**, *7* (4), 621−631.
(30) Bai, B.; Belovodskiy, A.; Hena, M.; Kandadai, A. S.; Joyce, M. A.; Saffran, H. A.; Shields, J. A.; Khan, M. B.; Arutyunova, E.; Lu, J.; Bajwa, S. K.; Hockman, D.; Fischer, C.; Lamer, T.; Vuong, W.; Van Belkum, M. J.; Gu, Z.; Lin, F.; Du, Y.; Xu, J.; Rahim, M.; Young, H. S.; Vederas, J. C.; Tyrrell, D. L.; Lemieux, M. J.; Nieman, J. A. Peptidomimetic α-Acyloxymethylketone Warheads with Six-Membered Lactam P1 Glutamine Mimic: SARS-CoV-2 3CL Protease Inhibition, Coronavirus Antiviral Activity, and in Vitro Biological Stability. *J. Med. Chem.* **2022**, *65* (4), 2905−2925.
(31) Barr, S. C.; Warner, K. L.; Kornreic, B. G.; Piscitelli, J.; Wolfe, A.; Benet, L.; McKerrow, J. H. A Cysteine Protease Inhibitor Protects Dogs from Cardiac Damage during Infection by Trypanosoma Cruzi. *Antimicrob. Agents Chemother.* **2005**, *49* (12), 5160−5161.
(32) Engel, J. C.; Doyle, P. S.; Hsieh, I.; Mckerrow, J. H. Cysteine Protease Inhibitors Cure an Experimental Trypanosoma cruzi Infection. *J. Exp. Med.* **1998**, *188*, 725−734.
(33) Kratochwil, N. A.; Stillhart, C.; Diack, C.; Nagel, S.; Al Kotbi, N.; Frey, N. Population Pharmacokinetic Analysis of RO5459072, a Low Water-Soluble Drug Exhibiting Complex Food-Drug Interactions. *Br. J. Clin. Pharmacol.* **2021**, *87* (9), 3550−3560.
(34) Payne, C. D.; Deeg, M. A.; Chan, M.; Tan, L. H.; LaBell, E. S.; Shen, T.; DeBrota, D. J. Pharmacokinetics and Pharmacodynamics of the Cathepsin S Inhibitor, LY3000328, in Healthy Subjects. *Br. J. Clin. Pharmacol.* **2014**, *78* (6), 1334−1342.
(35) Olson, J. Antimalarial Effects in Mice of Orally Administered Peptidyl Cysteine Protease Inhibitors. *Bioorg. Med. Chem.* **1999**, *7* (4), 633−638.
(36) Schade, M.; Merla, B.; Lesch, B.; Wagener, M.; Timmermanns, S.; Pletinckx, K.; Hertrampf, T. Highly Selective Sub-Nanomolar Cathepsin S Inhibitors by Merging Fragment Binders with Nitrile Inhibitors. *J. Med. Chem.* **2020**, *63* (20), 11801−11808.
(37) Kansy, M.; Senner, F.; Gubernator, K. Communications to the Editor Physicochemical High Throughput Screening: Parallel Artificial Membrane Permeation Assay in the Description of Passive Absorption Processes. *J. Med. Chem.* **1998**, *41* (7), 1007−1010.
(38) Zhu, C.; Jiang, L.; Chen, T.-M.; Hwang, K.-K. A Comparative Study of Artificial Membrane Permeability Assay for High Throughput Profiling of Drug Absorption Potential. *Eur. J. Med. Chem.* **2002**, *37*, 399−407.
(39) Kerns, E. H.; Di, L.; Petusky, S.; Farris, M.; Ley, R.; Jupp, P. Combined Application of Parallel Artificial Membrane Permeability Assay and Caco-2 Permeability Assays in Drug Discovery. *J. Pharm. Sci.* **2004**, *93* (6), 1440−1453.
(40) Chemaxon. *Playground v1.6.1*. Available via the Internet at: https://playground.calculators.cxn.io/ (accessed Jan. 28, 2024).
(41) Box, K.; Comer, J. Using Measured pK_a, Log P and Solubility to Investigate Supersaturation and Predict BCS Class. *Curr. Drug Metab.* **2008**, *9* (9), 869−878.
(42) Justus, C. R.; Dong, L.; Yang, L. V. Acidic Tumor Microenvironment and pH-Sensing G Protein-Coupled Receptors. *Front. Physiol.* **2013**, *4*, 354.

https://doi.org/10.1021/acsmedchemlett.4c00050
ACS Med. Chem. Lett. XXXX, XXX, XXX−XXX

”

Supporting information

Structural Modifications of Covalent Cathepsin S Inhibitors: Impact on Affinity, Selectivity, and Permeability

Mergim Meta[‡,1], Collin Zimmer[‡,1], Natalie Fuchs[1], Maximilian Johannes Zecher[1], Albin Lahu[1] and Tanja Schirmeister[1]*.

[‡]*Both authors contributed equally*

[1] *Institute of Pharmaceutical and Biomedical Sciences, Johannes Gutenberg University Mainz, Staudingerweg 5, 55128 Mainz, Germany.*

**Corresponding author: Prof. Dr. Tanja Schirmeister, schirmei@uni-mainz.de.*

Content

Synthesis Schemes 2
Fluorometric Enzyme Assays 6
Dilution Assay 8
Permeability (PAMPA) 9
Molecular Docking 10
Stability Analyses for Compound 44 12
Hydrazone Cleavage 15
General Synthesis Methods 20
NMR-Spectra and chromatograms of final inhibitors 43
References 93

Synthesis Schemes

The P2-P3 residues of the nitrile inhibitors were prepared by three different paths depending on the desired P2-P3 bridge: amide, urea or TFE (**Scheme 1**). For preparing amides, the corresponding P3 acid was coupled with methyl ester hydrochlorides of the P2 amino acid via HATU coupling. Preparing the urea bond between P2 and P3 was achieved through the isocyanate intermediate with triphosgene which was converted under basic conditions to the urea with the methyl ester hydrochloride of the P2 amino acid. Finally, the inhibitors containing TFE as bridge between P2 and P3 were prepared following a reductive amination protocol.[1] To obtain the final dipeptides with free carboxy terminus, the methyl esters were cleaved under basic conditions.

Scheme S1. Synthesis of compounds **5**–**19**: Reagents and conditions: (a) Boc_2O, NEt_3, CH_2Cl_2, rt, overnight, 97 %; (b) (1) K_2CO_3, MeI, 0 °C→rt overnight, (2) HCl (4.0 M in dioxane), 4 h, rt, 87 %; (c) (1) MeOK, MeOH, –78 °C, (2) $NaBH_4$, DME, 0 °C, (3) $ZnCl_2$, Et_2O, 2 h, –40 °C, 39–69 %. (d) Oxone®, MeOH/H_2O, 0 °C→rt, 95 %; (e) HATU, 2,4,6-collidine, DCM/DMF, overnight, 53–98 %; (f) LiOH, H_2O/THF, 16 h, rt, 77–98 %; (g) triphosgene, $NaHCO_3$, DCM, 3 h, 0 °C, 98 %.

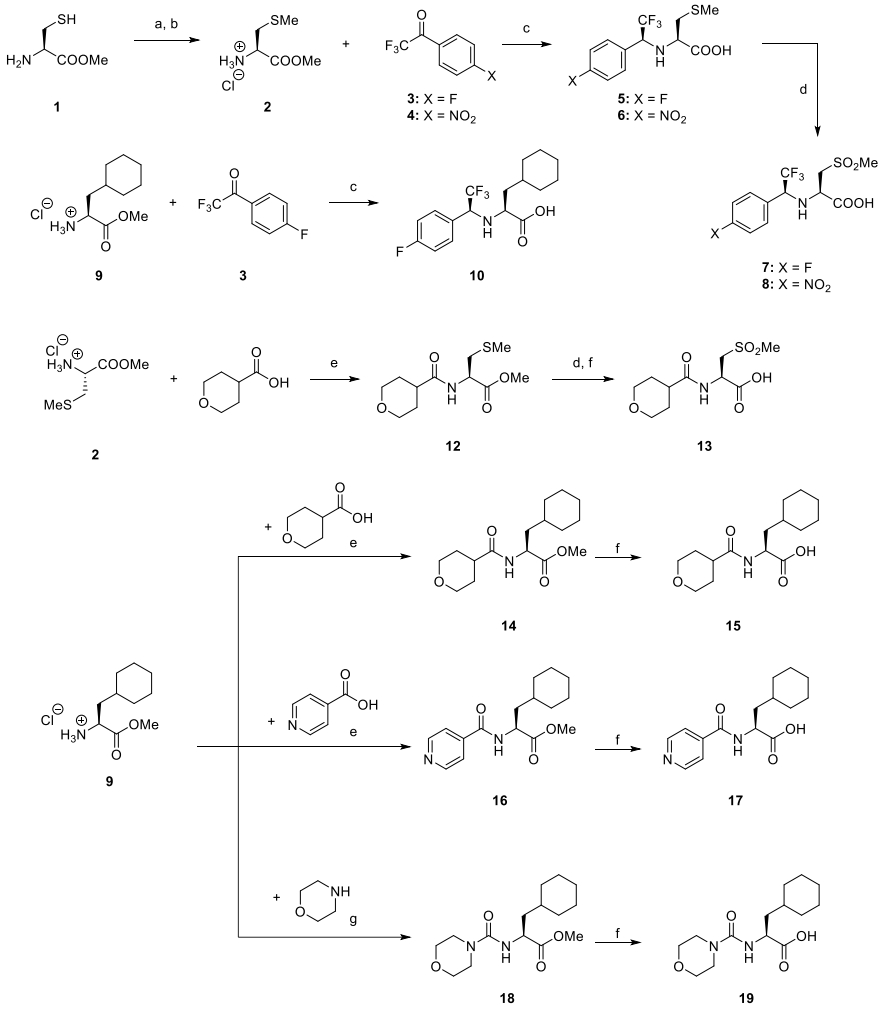

For introducing the nitrile warhead, one of two possible pathways was chosen. If possible, the P1 amino acid was converted to the corresponding amino acid amide which was subsequently coupled with the P2-P3-intermediate and in the final step dehydrated using cyanuric chloride. In most cases, the dehydration did not yield the desired nitrile, therefore the P1´ amino nitriles were prepared via Strecker synthesis of 3-phenylpropionaldehyde and benzyloxyacetaldehyde to yield the hPhe- and *O*BnSer-nitriles, respectively, as described previously (**Scheme 2**).[2] The crude P1´ nitriles were then coupled with the respective P2-P3 residue under standard HATU coupling conditions. Inhibitors containing the Acc nitrile in P1

were prepared via coupling with the commercially available 1-cyanocyclopropylamine hydrochloride.

Scheme S2. Synthesis of final nitrile inhibitors **22**–**41**: Reagents and conditions: (a) (1) TBTU, NEt_3, NH_4OH; (2) TFA/DCM, 2 h, 86–88 %; (b) HATU, 2,4,6-collidine, DCM/DMF, overnight, 79–96 %; (c) cyanuric chloride, DMF, 0 °C, 16 h, 34 %.

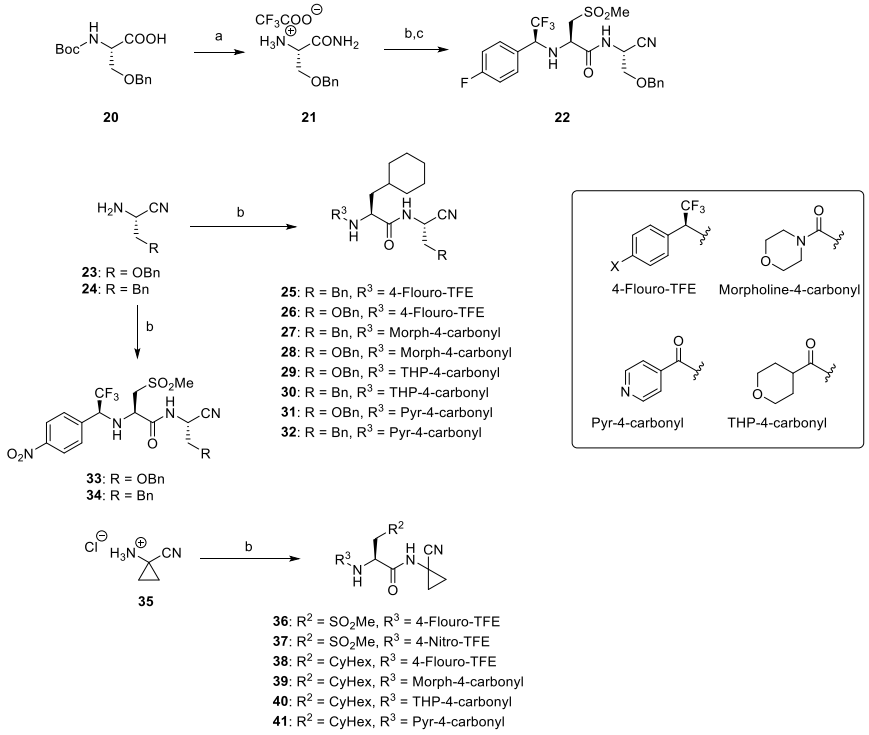

For the synthesis of inhibitor **45**, boc-protected methyl *O*-benzyl-L-serinate (**42**) was coupled with **19** after deprotection of the boc group and subsequently reduced to the corresponding alcohol. Finally, oxidation of the alcohol with Dess-Martin periodinane (DMP) led to inhibitor **45**. The ketone-based inhibitors were prepared starting from the chloromethylketone **48** which was synthesized according to literature.[3] Acylthiomethylketone **49**, acyloxymethylketone **50** and hydroxymethylketone **51** were prepared under mildly basic conditions via nucleophilic substitutions (**Scheme 3**).[4,5] Hydrazone derivatives **46** and **47** were synthesized by converting the corresponding ketone or aldehyde inhibitor with benzohydrazide in a condensation reaction (**Scheme 3**).

Scheme S3. Synthesis of aldehyde- and ketone-based inhibitors and hydrazones. Reagents and conditions: (a) HCl (4.0 M in dioxane), rt, 4 h, 80 %; (b) HATU, 2,4,6-collidine, DCM/DMF, overnight, 76 %; (c) (d) DMP, DCM, rt, 12 h, 70 %; (e) (1) $MeSO_2Ph$, *n*-BuLi, THF, –78 °C → rt, 3 h, 72 %; (2) HCl (4.0 M in dioxane), 4 h, 99 %; (f) benzohydrazide, MeOH, 16 h, rt, 47–78 %; (g) thiobenzoic acid, K_2CO_3, THF, 16 h, rt, 45 %; (h) CsF, benzoic acid, DMF, 64 °C, 4 h, 10 %; (i) $NaHCO_3$, H_2O, DMF, 2 h, 40 °C, 14 %.

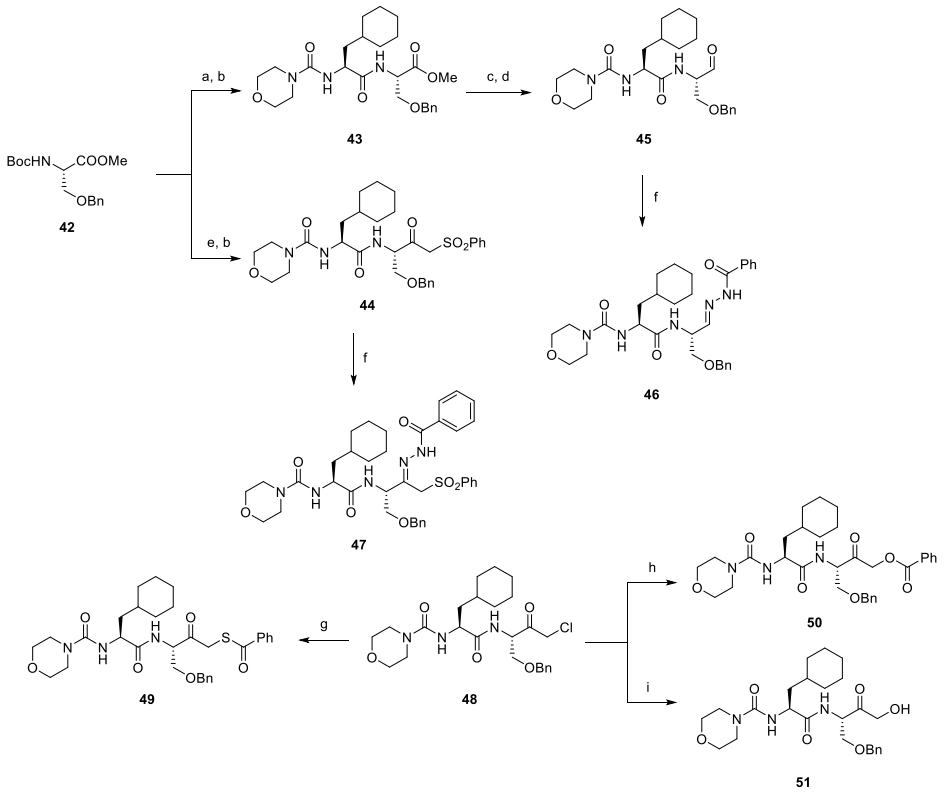

Fluorometric Enzyme Assays

CatS

The fluorescence increase upon cleavage of the fluorogenic substrate Z-Val-Val-Arg-AMC by cathepsin S (catS) was monitored by a TECAN SPARK fluorimeter (δ excitation: 365 nm, δ emission: 460 nm; TECAN GROUP, Switzerland). CatS (recombinant from *E. coli*, SIGMA-ALDRICH, Germany) was incubated with enzyme buffer (35 mM potassium phosphate, 35 mM sodium acetate, 2 mM DTT, 2 mM EDTA, pH 6.5) at room temperature for 45 min. Assay buffer (50 mM KH_2PO_4, 50 mM K_2HPO_4, 2.5 mM DTT, 2.5 mM EDTA, pH 6.5) was mixed with catS (final concentration 15 nM) in enzyme buffer, followed by inhibitor dissolved in DMSO or DMSO (negative control), and substrate (10 µM) Z-Val-Val-Arg-AMC (BACHEM, Switzerland). Black, flat-bottom 96-well microtiter plates (GREINER BIO-ONE, Germany) were used. Inhibitor screening concentrations started at 20 µM, followed by further concentrations until IC_{50}-determination was possible.

K_i^{app}, K_i, K_i^* calculations.

GRAFIT (version 5.0.13, 2006, ERITHRACUS SOFTWARE LTD., UK) was used for data analysis and non-linear regression.[6]

K_i^{app}, k_{obs}, k_{inact} and k_{2nd} calculations

GraphPad Prism version 9.5.1 for Windows, GraphPad Software, Boston, Massachusetts USA, www.graphpad.com, was used for data analysis and non-linear regression.[7]

For compounds showing a time-independent mode of inhibition (nitriles & ketones except **44**, **45** and **48**) the residual enzyme activity in % was plotted against the inhibitor concentration in nM. Then, K_i^{app} values were obtained by non-linear regression according to Equation 1. as

$$\frac{v_i}{v_0} = \frac{range}{1+(\frac{[I]}{IC_{50}})^S} + background \qquad (1)$$

Equation 1. v_0 = enzyme activity without inhibitor; v_i = enzyme activity in presence of inhibitor; [I] = inhibitor concentration; s = slope factor.

In case of **44** & **45**, K_i^{app} and K_i^{*app} values were obtained by a method described by Klein *et* al.[8] K_i and K_i^* values were calculated by using the Cheng-Prusoff equation to correct the K_i^{app} or K_i^{*app} values to zero substrate concentration (Equation 2):[9]

$$K_i \; or \; K_i^* = \frac{K_i^{app} or \; K_i^{*app}}{1+\frac{[S]}{K_M}} \qquad (2)$$

Equation 2. CatS: [S] = 10 μM, K_M = 34 μM. CatB: [S] = 100 μM, K_M = 150 μM. CatL: [S] = 6.25 μM, K_M = 6.5 μM.[10,11]

For the irreversible, time-dependent chloromethylketone **48**, the K_i value was calculated as published previously for irreversible binders.[2,12] The pseudo-first order rate constants k_{obs} were determined for different inhibitor concentrations as described previously. The progress curves were then fitted to the exponential Equation 3:[2]

$$F = [P]^{\propto}(1 - e^{-k_{obs} \cdot t}) + \text{offset} \qquad (3)$$

Equation 3. *F* = fluorescence intensity, [P] = product concentration, offset = background fluorescence.

The k_{obs} values were then plotted against the inhibitor concentrations [*I*] with the hyperbolic **Equation 4**:

$$k_{\mathrm{obs}} = \frac{k_{\mathrm{inact}}[I]}{K_{\mathrm{i}}^{\mathrm{app}} + [I]} \quad (4)$$

The resulting dissociation constant of the initial enzyme-inhibitor complex K_i^{app} was then corrected to zero substrate concentration using the Cheng-Prusoff relationship (Equation 2), giving the K_I value.[13]

The second-order rate constant of inhibition k_{2nd} were calculated from **Equation 5**.[14]

$$k_{2\mathrm{nd}} = \frac{k_{\mathrm{inact}}}{K_{\mathrm{i}}} \quad (5)$$

Figure S1 comprises dose-response curves of **44** and **45** at initial (first 90 s) and steady-state velocities (last 90 s).

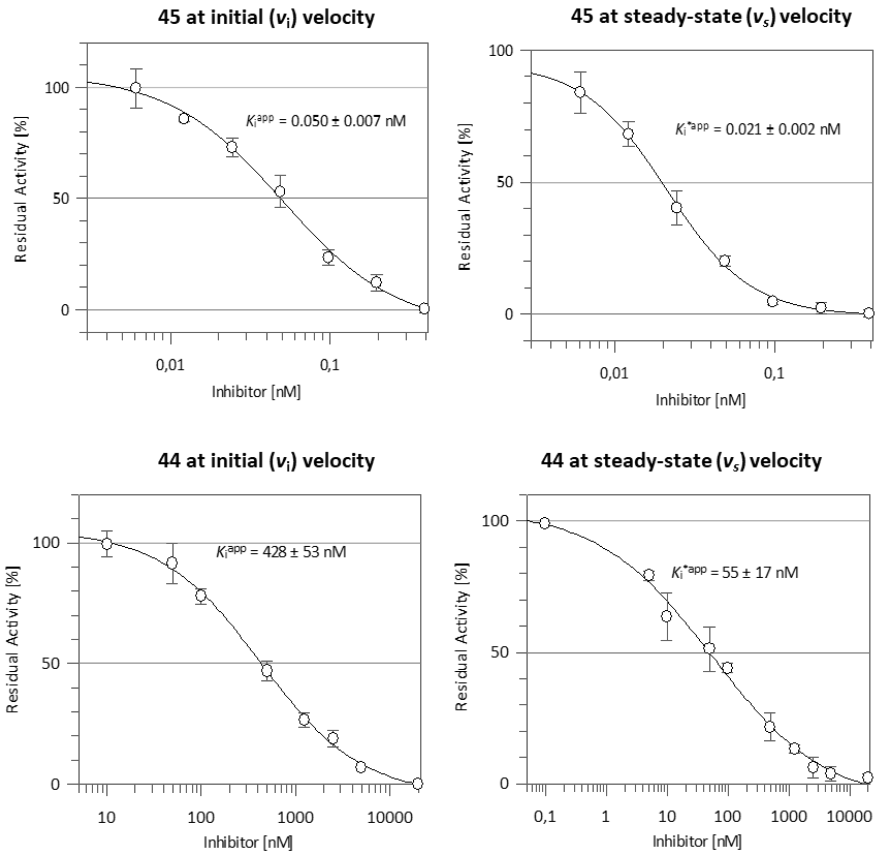

Figure S1: dose-response curves of **44** and **45** at initial and steady-state velocities.

Dilution Assay

Dilution assays were performed for selected compounds as published previously.[15] CatS (180 nM) was incubated with inhibitors (2 μL in DMSO) for 60 min in concentrations ranging from ten- to twentyfold the K_i value obtained from the fluorometric enzyme assay ensuring complete inhibition of the enzyme. These mixtures (2 μL) were diluted 100-fold in assay buffer (198 μL) containing 5 μL substrate (400 μM) to give a final substrate concentration of 10 μM. Recovery of enzyme activity was measured immediately by fluorescence readout. DMSO instead of inhibitor solution was used as a reference while the irreversible vinylsulfone-(VS) inhibitor **52** was used as an irreversible control.[2]

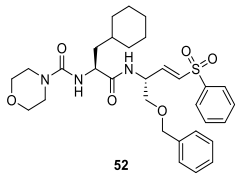

52

Figure S2: Structure of irreversible VS-inhibitor **52**.

Selectivity towards human cathepsin off-targets[16]

Cathepsin B (catB, SIGMA-ALDRICH, Darmstadt, Germany) and cathepsin L (catL, SIGMA-ALDRICH, Darmstadt, Germany) were incubated in enzyme buffer (50 mM Tris-HCl, 5 mM EDTA, 200 mM NaCl, 2 mM DTT, pH 6.5) at room temperature for 20 – 30 min. Assay buffer (50 mM Tris-HCl, 5 mM EDTA, 200 mM NaCl, 0.005 % Brij35, pH 6.5) was mixed with cathepsin B or L in enzyme buffer, then inhibitor in DMSO or DMSO (negative control) was added, followed by 100 μM (catB) or 6.25 μM (catL) substrate *Z*-Phe-Arg-AMC (BACHEM, Switzerland). Measurements were performed on a TECAN SPARK (δ excitation: 365 nm, δ emission: 460 nm; TECAN GROUP, Männedorf, Switzerland) plate reader on black GREINER BIO-ONE CHIMNEY 96 well microtiter plates (GREINER BIO-ONE GMBH, Frickenhausen, Germany). Inhibitor screening concentrations started at 20 μM, followed by 1 μM, 200 nM, and 50 nM. K_i values were determined for inhibitors with >50% inhibition at 20 μM.

Molecular Docking

Two different docking approaches were followed, since the inhibitors were designed to react covalently with the active site cysteine-25 of cathepsin S. First, a conventional non-covalent docking was performed, to estimate affinity and geometry of the pre-organized enzyme-inhibitor complex, secondly a covalent docking was used to determine the final covalent enzyme-inhibitor complex.

In both docking setups a crystallographic reference ligand (BLN) was used for validation *via* redocking (**Table S2**).

Molecular docking experiments were performed using the following crystal structures freely available in the protein data bank (PDB):[21] cathepsin S covalently bound to morpholine-4-carboxylic acid [1s-(2-benzyloxy-1r-cyano-ethylcarbamoyl)-3-methyl-butyl]amide (PDB entry 1MS6).[22] All ligands were energetically minimized before docking with Molecular operating environment (MOE 2020.09)[23] using the MMF94x force field.[24]

Docking approach 1: non-covalent docking with LeadIT

The non-covalent docking was performed with LeadIT-2.3.2.[25] The receptor was prepared in MOE with the protonate3D functionality and the covalent bonds between the co-crystallized ligands and the corresponding protease were untethered *via* the Builder tool in MOE. The binding site was defined as a 6.5 Å shell around the bound reference ligand. Water molecules that form at least three hydrogen bonds with the receptor and ligand were kept as part of the binding site. The docking was performed under default settings using the enthalpy-entropy hybrid approach with 2000 solutions *per* iteration and fragmentation. Only the top pose of the initial docking was kept and re-scored using the HYDE scoring function.[26]

Docking approach 2: covalent docking with MOE

Covalent docking was performed with MOE (version 2020.09). The receptors were prepared using the 3D protonation tool inside MOE. For the covalent reaction of the different warheads, the already existing template reactions were used or customized using the combinatorial library tool of MOE. Initial 30 poses from the triangle match placement with London ΔG scoring were re-scored using the Affinity ΔG scoring function and induced fit refinement implemented in MOE. 10 Poses were kept and visually inspected for binding geometry the interactions matching between the docked inhibitor pose and co-crystallized ligand with the enzyme. The poses best matching inspected interaction patterns are further discussed.

Table S1: Redocking of reference ligand BLN.

Enzyme (pdb entry)	Reference ligand ID	Redocking FlexX (RMSD/ Å)	FlexX score (kJ/mol)
Cathepsin S (1MS6)	BLN	0.94	–18.0

Table S2: Results of molecular docking analysis for cathepsin S (pdb-ID: 1MS6).

Cpd	Distance (electrophilic C-Cys25-S) / Å	FlexX score (kJ/mol)	Hyde score (kJ/ mol)	Covalent docking score (Affinity ΔG, MOE/ kcal/mol)
44	2.7, 3.8*	–29.9	–7	–5.8
45	2.8	–26.6	–49	–3.9
49	3.1, 2.8*	–24.9	–20	–4.4
50	2.9, 3.4*	–28.2	–29	–5.9
51	2.6	–26.5	–36	–4.8

*These inhibitors contain two possible electrophilic carbon atoms.

Hydrazone Cleavage

The hydrazone inhibitor **46** or **47** (200 µM) was dissolved in a lysosomal mixture solution containing NaOAc (20 mM), EDTA (2 mM) and glutathione (GSH, 2.5 mM) at pH 4 and pH 7.4 and was incubated for 24 h at 37 °C. An aliquot of this mixture (10 µL) was taken after 0 h, 2 h, 4 h, with acetonitrile (40 µL) and subsequently injected into an LC-MS-System. The base peak chromatograms (BPC) of free inhibitor and hydrazone capped inhibitor was then measured (**Figures S7–S15**) and the increase in free inhibitor at the lower pH over time registered. No reaction with GSH was observed during the timespan of monitoring the hydrazone cleavage.

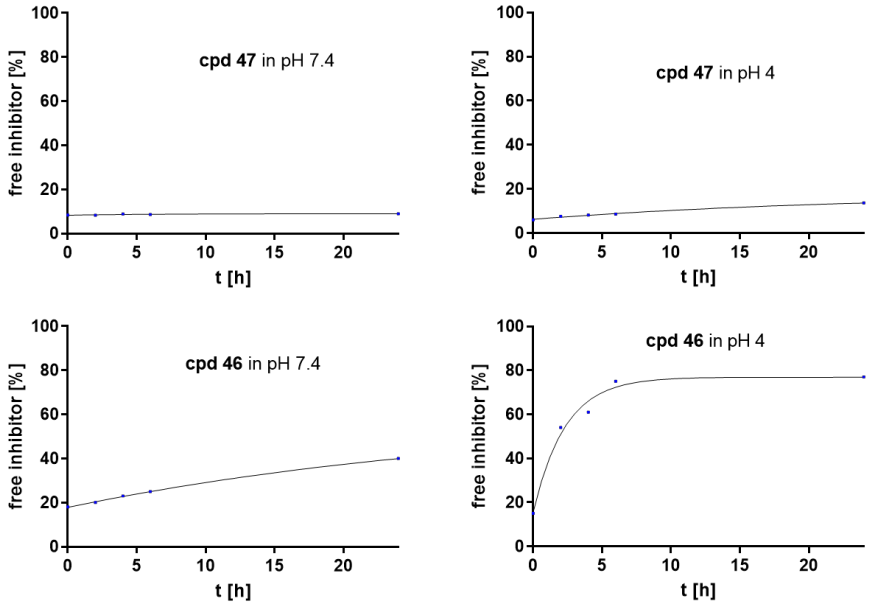

Figure S7: Percentage of free inhibitors **45** and **44** after cleavage of hydrazones **46** and **47** in lysosomal mixture solution of pH 4 and pH 7 from 0 h to 24 h.

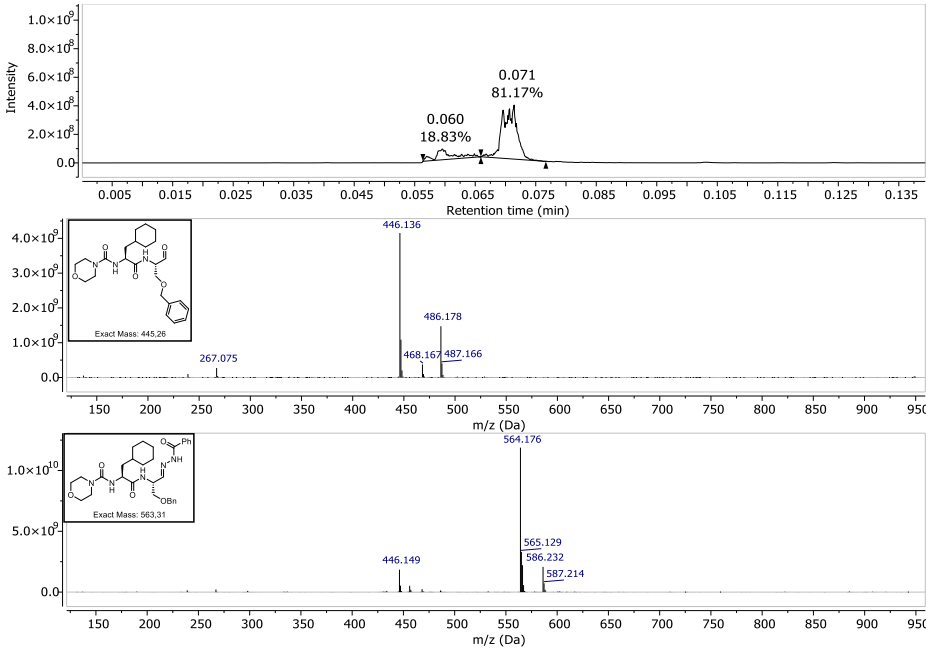

Figure S8. Base peak-chromatogram and the identified m/z (Da) of free inhibitor **45** and hydrazone **46** after 0 h incubation at pH 7.4.

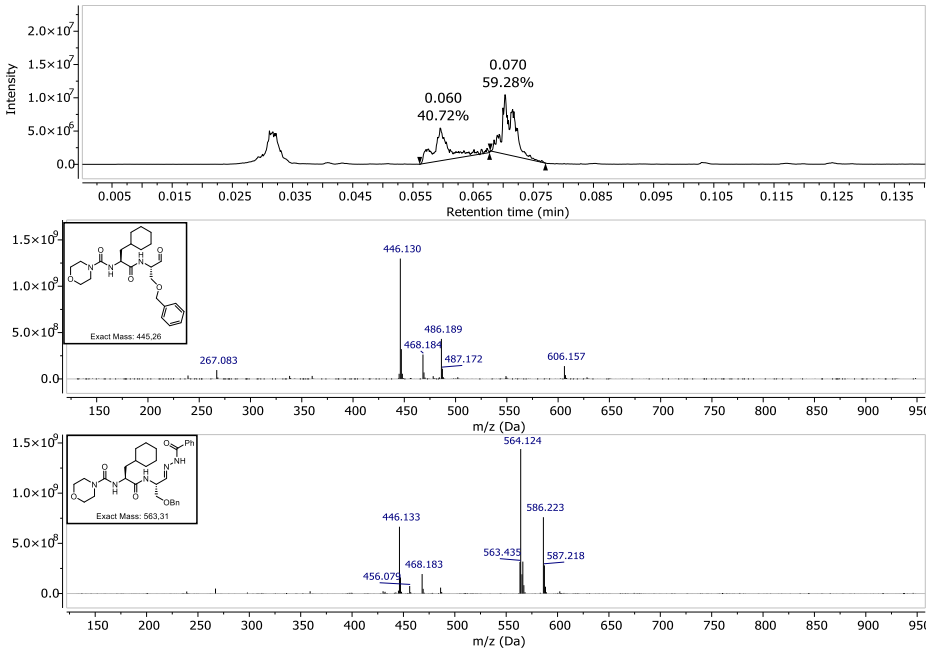

Figure S9. Base peak-chromatogram and the identified m/z (Da) of free inhibitor **45** and hydrazone **46** after 24 h incubation at pH 7.4.

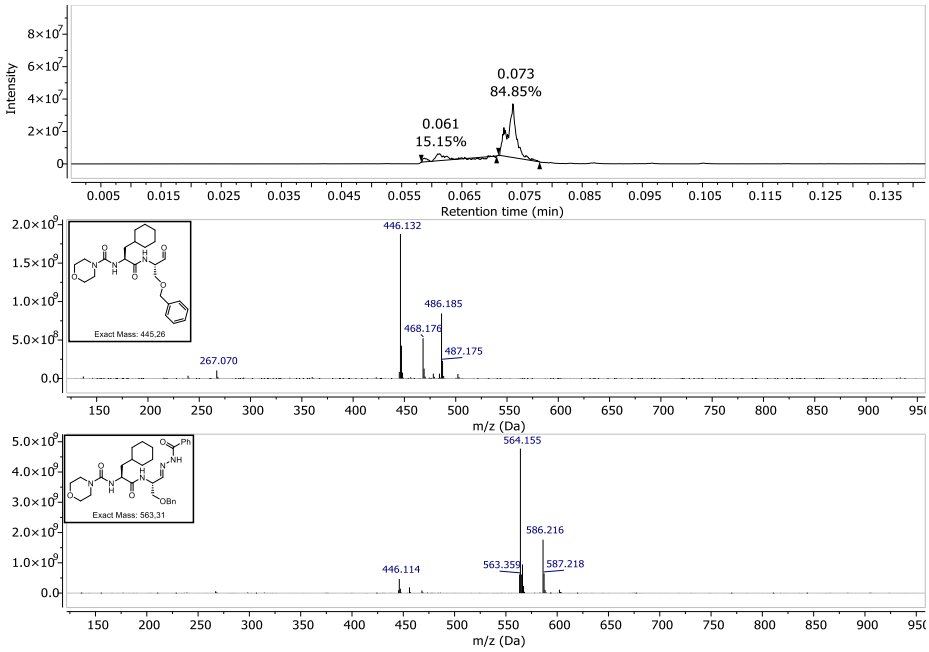

Figure S10. Base peak-chromatogram and the identified m/z (Da) of free inhibitor **45** and hydrazone **46** after 0 h incubation at pH 4.

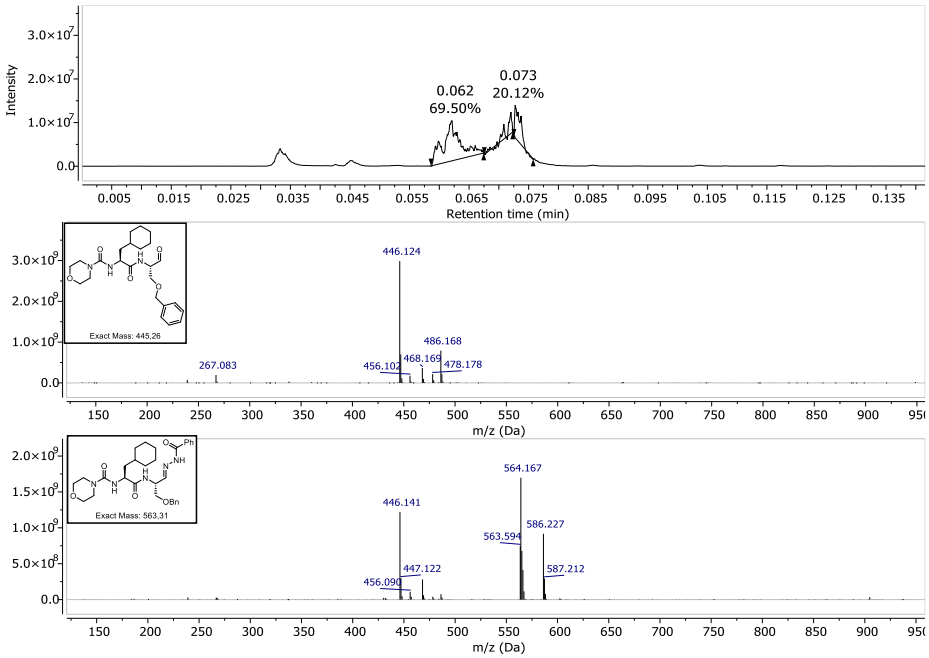

Figure S11. Base peak-chromatogram and the identified m/z (Da) of free inhibitor **45** and hydrazone **46** after 24 h incubation at pH 4.

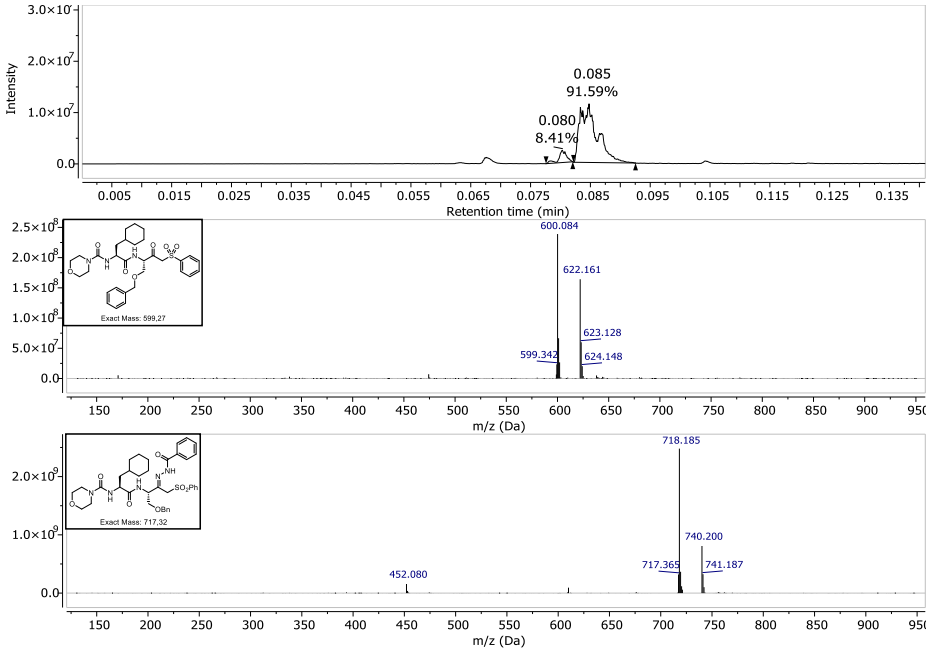

Figure S12. Base peak-chromatogram and the identified m/z (Da) of free inhibitor **44** and hydrazone **47** after 0 h incubation at pH 7.4.

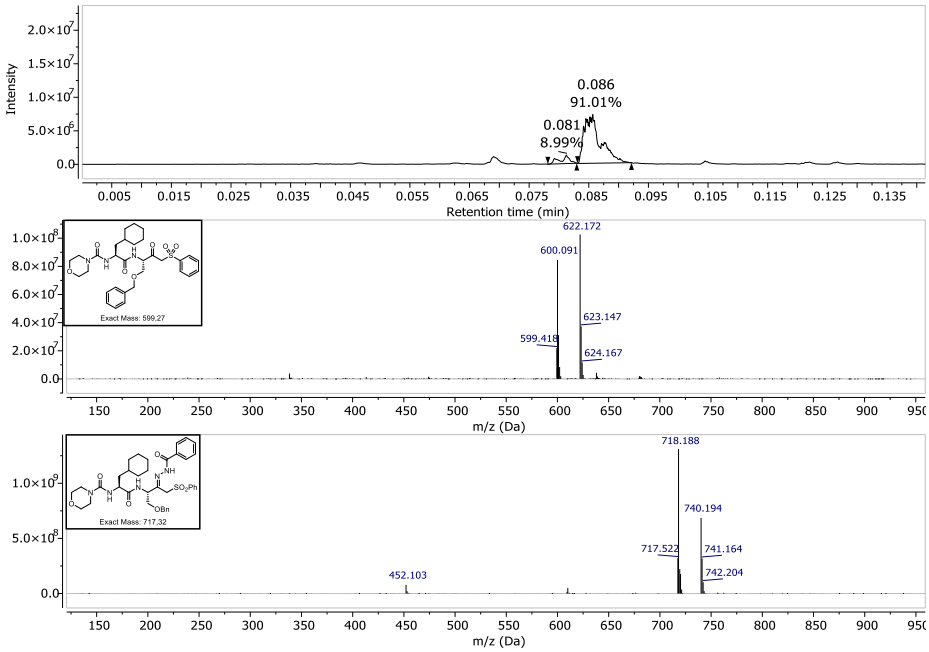

Figure S13. Base peak-chromatogram and the identified m/z (Da) of free inhibitor **44** and hydrazone **47** after 24 h incubation at pH 4.

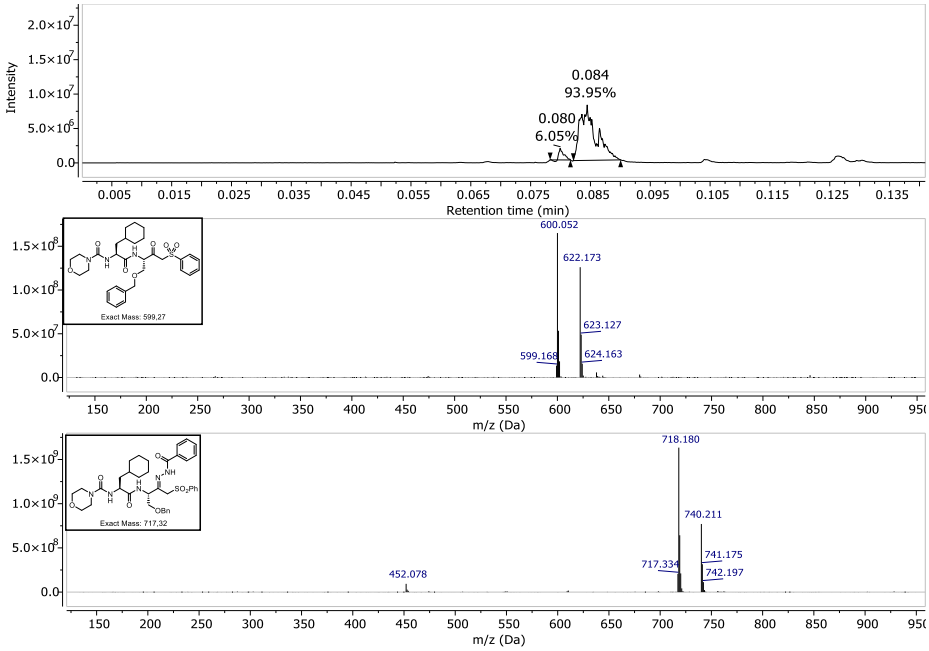

Figure S14. Base peak-chromatogram and the identified m/z (Da) of free inhibitor **44** and hydrazone **47** after 0 h incubation at pH 7.4.

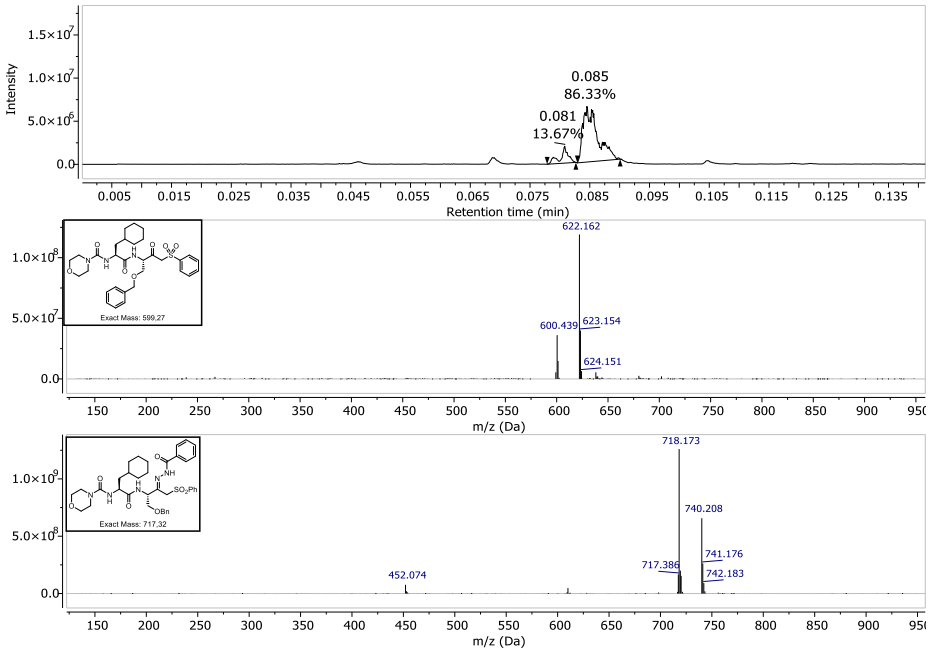

Figure S15. Base peak-chromatogram and the identified m/z (Da) of free inhibitor **44** and hydrazone **47** after 24 h incubation at pH 4.

General Synthesis Methods

All reagents and solvents were purchased commercially and used as provided by the supplier without further purification. Solvents for synthesis, extraction, and chromatography were of analytical grade. Moisture-sensitive reactions were carried out under argon atmosphere, and anhydrous solvents were used as provided by the commercial supplier. No unexpected or unusually high safety hazards were encountered.

Reaction progress was monitored by thin-layer chromatography using Alugram Xtra F254 silica plates from *Macherey-Nagel* and/or HPLC-MS. An Agilent 1100 series HPLC system and an Agilent Poroshell 120 EC-C18, 150 x 2.10 mm, 4 μm column coupled to an Agilent 1100 series LC/MSD Trap with electron spray ionization (ESI), was used. The identities and purities of compounds were determined by the same HPLC-MS system with a gradient of acetonitrile and water (+0.1 % formic acid). Signals were detected at 210/254 nm with quantitation by AUC and masses were determined in positive ionization mode (ESI). HPLC purification was performed with the Agilent 1290 II Infinity Preparative LC System using an InfinityLab Pursuit XRs C18, 30 x 250 mm, 5 µm, preparative LC column. Flash chromatography was performed with silica gel (0.040 – 0.063 mm) from *Macherey-Nagel*. If possible, optical rotations $[\alpha]_D^{22}$ were measured using a P3000 polarimeter from *Krüss* at 22 °C and are reported in ml·dm^{-1}·g^{-1} with the concentration *c* being g/100 ml. Melting points (uncorrected) were measured with an MPM-H3 using semi-open capillaries. NMR spectra were recorded as stated individually on Bruker Fourier 300 MHz and Bruker Avance III 600 MHz. Chemical shifts are indicated in parts per million (ppm), with the solvent resonance ($CDCl_3$, DMSO-d_6 or CD_3OD from *Deutero GmbH*) as internal standard. The purity of all compounds tested in biological assays was ≥95 % as determined by HPLC-MS.

General procedures

A Boc deprotection

The Boc-protected amino acid or dipeptide (1.0 eq) was dissolved in 2 mL 1,4-dioxane and 3 mL of a 4.0 M HCl-solution in 1,4-dioxane was added dropwise. The mixture was stirred at room temperature (rt) until completion of the deprotection could be observed via TLC monitoring. The solvent was then removed under reduced pressure and the deprotected target compound could be obtained and was used in the next step without further purification and characterization.

B Ester cleavage with LiOH

The ester (1.0 eq) was dissolved in THF (20 mL) and mixed with a solution of LiOH (3.0 eq) in water (20 mL). The resulting mixture was stirred for 18 h at room temperature. After the reaction was complete as indicated by TLC, the solvent was evaporated under reduced pressure and to the resulting crude product hydrochloric acid (1.0 M) was added until pH = 3 was reached. The mixture was then extracted with EtOAc (3x 20 mL) and after phase separation, the combined organic layers were dried over anhydrous Na_2SO_4. The solvent was evaporated under reduced pressure yielding the target carboxylic acid as a colorless oil or a colorless solid.

C: Peptide coupling with HATU

The carboxylic acid (1.0 eq) was dissolved in a mixture of DCM/DMF (9:1) at 0 °C. Under stirring HATU (1.2 eq) was added in portions. Afterwards 2,4,6- collidine (3.0 eq) was added and stirred for an additional 10 min at 0 °C. The amine (1.0 eq) was added in portions or dropwise diluted in DCM and the reaction mixture was allowed to reach room temperature and stirred overnight. H_2O (30 mL) was added, and the organic phase separated. The aqueous phase was extracted with EtOAc (3x 20 mL). The combined organic extracts were washed with brine (40 mL) and dried over anhydrous $NaSO_4$. The solvent was evaporated under reduced pressure to give a crude product that was purified using either column chromatography or via preparative HPLC.

2, (*S*)-Methyl-L-cysteine methyl ester hydrochloride

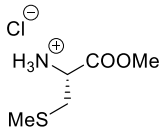

1. L-Cysteine methyl ester hydrochloride **1** (5.0 g, 29.1 mmol, 1.0 eq) was dissolved in DCM (20 mL) at rt. NEt_3 (4.0 mL, 29.1 mmol, 1.0 eq) was added dropwise, and after 10 min Boc_2O (6.4 g, 29.1 mmol, 1.0 eq) was added in portions. After completion of the reaction, indicated by TLC monitoring, water (30 mL) was added and after separating the phases, the organic solvent was evaporated under reduced pressure yielding the boc-protected intermediate which was used without further purification.

2. The boc-protected intermediate (2.0 g, 8.5 mmol, 1.0 eq) was dissolved in DMF (50 mL) at 0 °C and subsequently MeI (1.2 g, 8.5 mmol, 1.0 eq) and K_2CO_3 (1.2 g, 8.5 mmol, 1.0 eq) were added. The mixture was allowed to reach rt and stirred overnight. After completion, indicated by TLC, water (50 mL) and EtOAc (50 mL) were added, and the aqueous phase extracted with EtOAc (3x 50 mL). After washing the organic phase with brine (25 mL) and water (25 mL) the solvent was evaporated and the residue dissolved in HCl (10 mL, 4 M in dioxane). After stirring for 2 h, the solvent was evaporated yielding the title compound as a colorless oil. (1.4 g, 7.4 mmol, 87 %). ^{1}H-NMR (300 MHz, $CDCl_3$): δ/ppm = 8.67 (s, 3H), 3.95 (t, *J* = 5.7 Hz, 1H), 3.51 (s, 3H), 2.88 (d, *J* = 5.7 Hz, 2H), 1.86 (s, 3H). ^{13}C-NMR (75 MHz, $CDCl_3$): δ/ppm = 169.4, 53.8, 51.9, 33.4, 27.6, 14.8. $[\alpha]_D^{25}$ = +5 (*c* 1.00, DMF). MS (ESI) *m/z* XX could not be detected by mass spectrometry.

5, (*S*)-Methyl-*N*-((*S*)-2,2,2-trifluoro-1-(4-fluorophenyl) ethyl)-L-cysteine

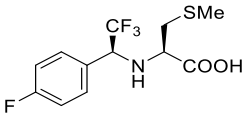

1 (*S*)-Methyl-L-cysteine methyl ester hydrochloride **3** (580 mg; 3.12 mmol; 1.0 eq) was dissolved in MeOH (10 mL) at –78 °C. (4-Fluoro)-trifluoroacetophenone (600 mg; 3.12 mmol; 1.0 eq) and potassium methanolate (438 mg; 6.24 mmol; 2.0 eq) were added and the mixture was stirred overnight at rt.

2. In another flask, $NaBH_4$ (472 mg; 12.48 mmol; 4.0 eq) was dissolved in ethylenglycoldimethylether (10 mL) and $ZnCl_2$ (15 mL; 2 M; in Et_2O) was added at 0 °C. The mixture was stirred overnight at rt. On the next day, mixture 1 was cooled to –40 °C and diluted with acetonitrile (ACN, 15 mL). Over a period of 20 min mixture 2 was slowly added to mixture 1 and the resulting mixture stirred for an additional 2.5 h at –40 °C. After quenching with acetone (40 mL) the mixture was warmed to rt and poured into an ice-water mixture. The pH was adjusted to 4 using HCl (1 M) and afterwards the phases were separated, and the aqueous phase extracted with EtOAc (3x 25 mL). The organic phase was dried over Na_2SO_4 and

the solvent was evaporated. The resulting residue was purified on silica gel via column chromatography (^{c}Hex/EtOAc/AcOH = 3:1:0.1), resulting in a colorless oil (665 mg, 2.13 mmol, 69 %). ^{1}H-NMR (300 MHz, $CDCl_3$): δ/ppm = 7.43–7.34 (m, 2H), 7.14–7.02 (m, 2H), 4.26 (q, *J* = 7.1 Hz, 1H), 3.67 (t, *J* = 5.6 Hz, 1H), 2.91 (d, *J* = 5.6 Hz, 2H), 2.15 (s, 3H).^{13}C-NMR (75 MHz, $CDCl_3$): δ/ppm = 177.5, 165.0, 161.7, 130.4, 129.6, 116.0, 63.1, 62.7, 62.3, 61.9, 58.5, 56.9, 36.9, 16.4. $[\alpha]_D^{25}$ = +5 (*c* 1.00, $CHCl_3$). MS (ESI) *m/z* calculated for $[C_{12}H_{14}F_4NO_2S]^+$ ($[M+H]^+$): 312.1, found: 312.2.

7, Methylsulfonyl-((*S*)-2,2,2-trifluoro-1-(4-fluorophenyl) ethyl)-D-alanine

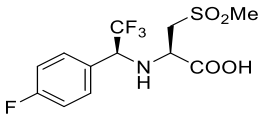

(*S*)-Methyl-*N*-((*S*)-2,2,2-trifluoro-1-(4-fluorophenyl) ethyl)-L-cysteine, **5** (1.2 g, 3.8 mmol, 1.0 eq) was dissolved in MeOH (10 mL) and oxone® (3.5 g, 11.3 mmol, 3.0 eq) was dissolved in water (10 mL) and both solutions were mixed at 0 °C. After stirring for 1.5 h at rt, MeOH was evaporated and to the aqueous phase, brine (10 mL) and EtOAc (15 mL) were added. After extraction with EtOAc (3x 25 mL) the organic extracts were combined and dried over Na_2SO_4. The solvents were evaporated, and the title compound was obtained as a colorless oil (727 mg, 2.0 mmol, 95 %). ^{1}H-NMR (300 MHz, $CDCl_3$): δ/ppm = 7.52 – 7.31 (m, 2H), 7.19 – 6.96 (m, 2H), 4.51 – 4.11 (m, 1H), 3.95 – 3.74 (m, 1H), 3.65 – 3.25 (m, 2H), 3.14 (s, 3H).^{13}C-NMR (75 MHz, $CDCl_3$): δ/ppm = 173.9, 165.0, 161.7, 130.4, 129.1, 116.0, 62.8, 56.9, 55.7, 43.8. $[\alpha]_D^{25}$ = +10 (*c* 1.00, $CHCl_3$) MS (ESI) *m/z* calculated for $[C_{12}H_{13}F_4NO_4SNa]^+$ ($[M+Na]^+$): 366.0, found: 366.0.

6, (*S*)-Methyl-*N*-((*S*)-2,2,2-trifluoro-1-(4-nitro-phenyl) ethyl)-L-cysteine

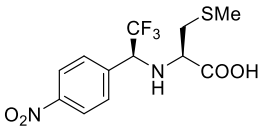

6 was synthesized with the same method as **5** but with methyl 2,2,2-trifluoro-1-(4-nitrophenyl) ethan-1-one (1.2 g, 5.6 mmol, 1.0 eq) and *S*-methyl-L-cysteine methyl ester hydrochloride **2** (1.1 g; 5.6 mmol; 1.0 eq) as starting materials. After purification on silica gel via column chromatography (^{c}Hex/EtOAc/AcOH = 3:1:0.1), a pale yellowish oil was obtained (774 mg, 2.2 mmol, 39 %). ^{1}H-NMR (300 MHz, $CDCl_3$): δ/ppm = 8.27 – 8.21 (m, 2H), 7.65 – 7.59 (m, 2H), 4.45 (m, 1H), 3.71 (t, J = 5.6 Hz, 1H), 2.92 (dd, J = 5.6, 1.6 Hz, 2H), 2.15 (s, 3H). ^{13}C-NMR (75 MHz, $CDCl_3$): δ/ppm = 177.6, 148.6, 141.0, 129.7, 124.1, 62.6 (q, J = 29.6 Hz), 58.7, 57.2, 37.1, 16.4. $[\alpha]_D^{25}$ = +15 (*c* 1.00, MeOH). MS (ESI) *m/z* calculated for $[C_{12}H_{14}F_3N_2O_4S]^+$ ($[M+H]^+$): 339.1, found: 339.0.

8, Methylsulfonyl-((*S*)-2,2,2-trifluoro-1-(4-nitrophenyl) ethyl)-D-alanine

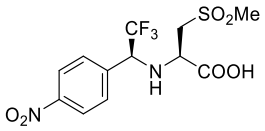

(*S*)-Methyl-*N*-((*S*)-2,2,2-trifluoro-1-(4-nitro-phenyl) ethyl)-L-cystein, **6** (1.1 g, 3.1 mmol, 1.0 eq) was dissolved in MeOH (10 mL) and oxone® (2.9 g, 9.3 mmol, 3.0 eq) was dissolved in water (10 mL) and added at 0 °C. After stirring for 1.5 h at rt, MeOH was evaporated and to the aqueous residue brine (10 mL) and EtOAc (15 mL) were added. After extraction with EtOAc (3x 25 mL) the organic extracts were combined and dried over Na_2SO_4. The solvents were evaporated, and the title compound was obtained as a colorless solid (1.1 g, 3.1 mmol, 99 %). ^{1}H-NMR (300 MHz, $CDCl_3$): δ/ppm = 8.42 – 8.37 (m, 1H), 8.34 – 8.18 (m, 2H), 7.82 (m, 2H), 4.11 (q, *J* = 7.1 Hz, 1H), 3.92 (t, *J* = 7.1, 4.1 Hz, 1H), 3.15 (s, 3H), 3.05 (d, *J* = 7.3 Hz, 2H). ^{13}C-NMR (75 MHz, $CDCl_3$): δ/ppm = 173.9, 148.6, 138.9, 131.3, 124.2, 124.0, 60.8, 57.1, 43.7, 42.9, 21.0, 14.1. $[\alpha]_D^{25}$ = +65 (*c* 1.00, MeOH). Mp. 96–97 °C. MS (ESI) *m/z* calculated for $[C_{12}H_{14}F_3N_2O_6S]^+$ ($[M+H]^+$): 371.0, found: 371.0.

10, (*S*)-3-Cyclohexyl-2-(((*S*)-2,2,2-trifluoro-1-(4-fluorophenyl)ethyl)amino)propanoic acid

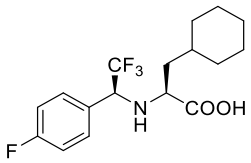

10 was synthesized with the same method as **5** but with (4-fluoro)-trifluoroacetophenone **3** (1.7 g; 9.0 mmol; 1.0 eq) and L-cyclohexylalanine methyl ester hydrochloride **9** (2.0 g; 9.0 mmol; 1.0 eq) as starting materials. After purification on silica gel via column chromatography (^{c}Hex/EtOAc/AcOH = 3:1:0.1), the title compound was obtained as a colorless solid (3.0 g, 8.7 mmol, 96 %). ^{1}H-NMR (300 MHz, CD_3OD) δ 7.50 – 7.35 (m, 2H), 7.24 – 6.96 (m, 2H), 4.36 – 4.13 (m, 1H), 3.47 – 3.38 (m, 1H), 1.83 – 1.34 (m, 8H), 1.32 – 1.07 (m, 3H), 0.98 – 0.78 (m, 2H). ^{13}C-NMR (75 MHz, CD_3OD): δ/ppm = 178.4, 166.0, 162.7, 132.5, 131.7, 128.9, 116.3, 63.21 – 61.56 (m), 59.3, 56.5, 42.2, 35.3, 34.8, 33.8, 27.6. $[\alpha]_D^{25}$ = –9 (*c* 1.00, MeOH). Mp. 93–94 °C. MS (ESI) *m/z* calculated for $[C_{17}H_{22}F_4NO_2]^+$ ($[M+H]^+$): 348.2, found: 348.1.

12, Methyl (*S*)-methyl-*N*-(tetrahydro-2*H*-pyran-4-carbonyl)-L-cysteinate

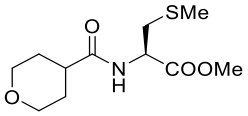

12 was synthesized according to general procedure C with **2** (0.5 g, 2.7 mmol, 1.0 eq) and tetrahydro-2*H*-pyran-4-carboxylic acid (0.39 g, 2.7 mmol, 1.0 eq) yielding the title compound as a colorless resin (0.55 g, 2.1 mmol, 78 %) after purification on silica gel (^{c}Hex/EtOAc= 1:2). ^{1}H-NMR (300 MHz, CD_3OD): δ/ppm = 4.68 (dd, *J* = 8.5, 5.1 Hz, 1H), 4.13 – 3.93 (m, 2H), 3.79 (s, 3H), 3.60 – 3.40 (m, 1H), 3.03 (dd, *J* = 13.9, 5.1 Hz, 1H), 2.87 (dd, *J* = 13.9, 8.6 Hz, 1H), 2.70 – 2.54 (m, 1H), 2.17 (s, 3H), 1.94 – 1.69 (m, 5H). ^{13}C-NMR (75 MHz, CD_3OD): δ/ppm = 177.4, 172.8, 68.2, 52.9, 42.6, 36.4, 30.2, 15.7. $[\alpha]_D^{25}$ = –18 (*c* 1.00, MeOH). MS (ESI) *m/z* calculated for $[C_{11}H_{20}NO_4S^+]$ ($[M+H]^+$): 262.1, found: 262.0.

13, Methylsulfonyl-(tetrahydro-2*H*-pyran-4-carbonyl)-D-alanine

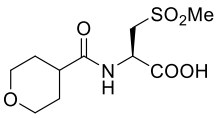

1. Methyl (*S*)-methyl-*N*-(tetrahydro-2*H*-pyran-4-carbonyl)-L-cysteinate **12** (340 mg, 1.3 mmol, 1.0 eq) was dissolved in MeOH (20 mL) and cooled to 0 °C. Oxone® (1.2 g, 3.9 mmol, 3.0 eq) dissolved in water (20 mL) was added and the mixture was stirred for 1.5 h at rt. MeOH was evaporated and the aqueous residue diluted with brine (pH 1). After extraction with EtOAc (3x 25 mL) the organic extracts were combined and dried over Na_2SO_4. The solvents were evaporated, yielding a colorless resin (293 mg, 1.0 mmol, 77 %) that was used in the next step without further purification.

2. The methyl ester of the crude oil (260 mg, 0.87 mmol, 1.0 eq) was cleaved according to general procedure B, yielding a colorless sticky oil (220 mg, 0.8 mmol, 91 %). ^{1}H-NMR (300 MHz, DMSO-d_6): δ/ppm = 4.67 – 4.47 (m, 1H), 3.88 – 3.71 (m, 2H), 3.71 – 3.39 (m, 2H), 3.34 – 3.17 (m, 2H), 2.98 (s, 3H), 2.46 – 2.19 (m, 2H), 1.70 – 1.23 (m, 4H).^{13}C-NMR (75 MHz, DMSO-d_6): δ/ppm = 174.4, 171.1, 79.1, 66.5, 54.7, 47.8, 45.9, 41.8, 28.8, 25.5. $[\alpha]_D^{25}$ = –4 (*c* 1.00, MeOH). MS (ESI) *m/z* calculated for $[C_{10}H_{18}NO_6S^+]$ ($[M+H]^+$): 280.1, found: 280.1.

14, Methyl (*S*)-3-cyclohexyl-2-(tetrahydro-2*H*-pyran-4-carboxamido) propanoate

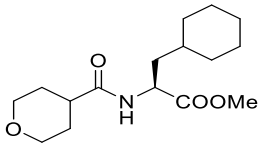

14 was synthesized according to general procedure C by coupling **9** (2.0 g, 9.0 mmol, 1.0 eq) and tetrahydro-2*H*-pyran-4-carboxylic acid (1.2 g, 9.0 mmol, 1.0 eq) yielding the title compound as a colorless oil (2.6 g, 8.7 mmol, 96 %) that was used in the next step without further purification or characterization.

15, Methyl (*S*)-3-cyclohexyl-2-(tetrahydro-2*H*-pyran-4-carboxamido) propanoate

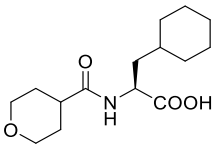

15 was synthesized according to general procedure B by cleaving the methyl ester of **14** (2.6 g, 8.7 mmol, 1.0 eq) yielding the title compound as a colorless solid (1.9 g, 6.9 mmol, 77 %). ^{1}H-NMR (300 MHz, DMSO-d_6): δ/ppm = 7.97 (d, *J* = 8.1 Hz, 1H), 4.34 – 4.14 (m, 1H), 3.92 – 3.70 (m, 2H), 3.36 – 3.12 (m, 2H), 2.47 – 2.38 (m, 1H), 1.71 – 1.42 (m, 10H), 1.35 – 0.66 (m, 6H). ^{13}C-NMR (75 MHz, DMSO-d_6): δ/ppm = 174.4, 174.0, 66.4, 49.2, 33.7, 33.2, 31.5, 29.1, 28.8, 26.0, 25.8, 25.7. $[\alpha]_D^{25}$ = 24 (*c* 1.00, MeOH). MS (ESI) *m/z* calculated for $[C_{15}H_{26}NO_4]^+$ ($[M+H]^+$): 284.2, found: 284.1.

16, Methyl (*S*)-3-cyclohexyl-2-(isonicotinamido) propanoate

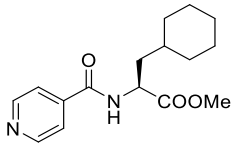

16 was synthesized according to general procedure C by coupling L-cyclohexylalanine methyl ester hydrochloride **9** (0.9 g, 4.1 mmol, 1.0 eq) and isonicotinic acid (0.5 g, 4.1 mmol, 1.0 eq) yielding the title compound as a colorless oil (1.2 g, 4.0 mmol, 98 %) after purification on silica gel (^{c}Hex/EtOAc= 1:3). ^{1}H-NMR (300 MHz, DMSO-d_6): δ/ppm = 9.04 (d, *J* = 7.6 Hz, 1H), 8.84 – 8.58 (m, 2H), 7.87 – 7.66 (m, 2H), 4.59 – 4.43 (m, 1H), 3.64 (s, 3H), 1.82 – 1.52 (m, 7H), 1.43 – 1.27 (m, 1H), 1.23 – 0.74 (m, 5H). ^{13}C-NMR (75 MHz, DMSO-d_6): δ/ppm = 172.9, 165.3, 150.4, 140.8, 121.5, 52.1, 50.5, 37.8, 33.8, 33.2, 31.6, 26.1, 25.8, 25.6. $[\alpha]_D^{25}$ = –20 (*c* 1.00, MeOH). MS (ESI) *m/z* calculated for $[C_{16}H_{23}N_2O_3]^+$ ($[M+H]^+$): 291.2, found: 291.1.

17, (*S*)-3-cyclohexyl-2-(isonicotinamido) propanoic acid

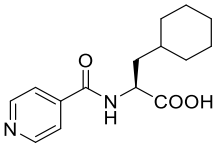

17 was synthesized according to general procedure B by cleaving the methyl ester of **16** (1.2 g, 4.0 mmol, 1.0 eq) yielding the title compound as a colorless solid (0.97 g, 3.5 mmol, 88 %). ^{1}H-NMR (300 MHz, DMSO-d_6): δ/ppm = 8.97 (d, *J* = 7.8 Hz, 1H), 8.83 – 8.65 (m, 2H), 7.96 – 7.72 (m, 2H), 4.58 – 4.41 (m, 1H), 1.81 – 1.51 (m, 6H), 1.47 – 1.29 (m, 1H), 1.26 – 0.77 (m, 5H). ^{13}C-NMR (75 MHz, DMSO-d_6): δ/ppm = 173.9, 164.7, 149.4, 141.9, 121.9, 50.4, 37.9, 33.8, 33.2, 31.5, 26.1, 25.8, 25.6. $[\alpha]_D^{25}$ = –14 (*c* 1.00, MeOH). MS (ESI) *m/z* calculated for $[C_{15}H_{21}N_2O_3]^+$ ($[M+H]^+$): 277.2, found: 277.1.

18, 4-Morpholine-1-carbonyl-L-cyclohexyl alanine-methyl ester

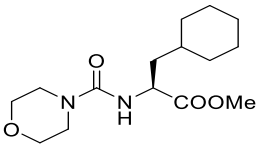

9 (0.55 g, 2.48 mmol, 1.0 eq) was dissolved in DCM (20 mL) and saturated $NaHCO_3$ solution (40 mL) and cooled to 0°C. Triphosgene (0.25 g, 0.83 mmol, 0.33 eq) was added and the mixture was stirred for 30 min. The mixture was extracted with DCM (2x 40 mL) and the combined organic layers were washed with saturated $NaHCO_3$ solution (2x 30 mL), and brine (2x 30 mL), then dried over anhydrous Na_2SO_4 and concentrated under reduced pressure, resulting in a crude product that was dissolved in THF (30 mL) and cooled to 0 °C. Morpholine (1.0 eq, 2.48 mmol, 0.22 g) was added and the mixture stirred for one hour. The solvent was removed under reduced pressure. Water (30 ml) was added to the crude residue, which was then extracted with EtOAc (3x 20 mL). The combined organic layers were washed with brine (2x 20 mL), dried over anhydrous Na_2SO_4, and concentrated under reduced pressure to yield a colorless oil (0.75 g, 2.46 mmol, 98 %). ^{1}H-NMR (300 MHz, $CDCl_3$): δ/ppm = 4.94 – 4.83 (m, 1H), 4.56 – 4.45 (m, 1H), 3.71 (s, 3H), 3.70 – 3.64 (m, 4H), 3.41 – 3.33 (m, 4H), 1.77 – 1.59 (m, 6H), 1.53 – 1.42 (m, 1H), 1.41 – 1.31 (m, 1H), 1.24 – 1.11 (m, 3H), 0.99 – 0.84 (m, 2H). ^{13}C-NMR (75 MHz, $CDCl_3$): δ/ppm = 175.1, 157.4, 66.5, 52.3, 51.6, 44.1, 40.4, 34.2, 33.6, 32.7, 26.4, 26.2, 26.1, 21.1, 14.3. $[\alpha]_D^{22}$ = –9 (*c* 1.00, $CHCl_3$). MS (ESI) *m/z* calculated for $[C_{15}H_{26}N_2O_4Na]^+$ ($[M+Na]^+$): 321.18, found: 321.18.

19, 4-Morpholin-1-carbonyl-L-cyclohexyl alanine

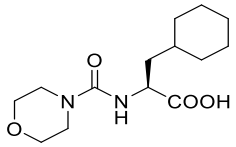

19 was prepared according to procedure B using **18** (1.0 eq, 0.7 g, 2.35 mmol), resulting in a colorless solid (0.65 g, 2.29 mmol, 97 %).^{1}H-NMR (300 MHz, $CDCl_3$): δ/ppm = 9.37 (s, 1H), 5.27 – 5.07 (m, 1H), 4.41 (s, 1H), 3.75 – 3.55 (m, 4H), 3.46 – 3.28 (m, 4H), 1.83 – 1.47 (m, 6H), 1.44 – 1.30 (m, 1H), 1.26 – 1.04 (m, 4H), 1.04 – 0.79 (m, 2H). ^{13}C-NMR (75 MHz, $CDCl_3$): δ/ppm = 176.9, 158.1, 66.5, 51.9, 44.2, 39.6, 34.3, 33.6, 32.6, 26.6, 26.2, 26.1. 176.9, 158.1, 66.5, 51.9, 44.2, 39.6, 34.3, 33.6, 32.6, 26.5, 26.2, 26.1. Mp: 96–97 °C. $[\alpha]_D^{22}$ = –22 (*c* 1.00, $CHCl_3$). MS (ESI) *m/z* calculated for $[C_{14}H_{24}N_2O_4Na]^+$ ($[M+Na]^+$): 307.2, found: 307.2.

21, (*S*)-1-amino-3-(benzyloxy)-1-oxopropan-2-amino 2,2,2-trifluoroacetate

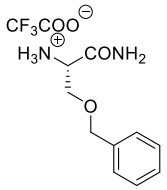

Boc-*O*-benzyl-L-serine **20** (3.0 g, 10.2 mmol, 1.0 eq) was dissolved in DMF (20 mL) and cooled to 0 °C. Hydroxybenzotriazole-monohydrate (HOBt·H_2O, 1.9 g, 12.2 mmol, 1.2 eq) and 1-ethyl-3-(3-dimethylaminopropyl) carbodiimide-hydrochloride (EDC·HCl, 2.1 g, 11.2 mmol, 1.1 eq) were added and after stirring for 20 min NH_4OH (5 mL) was added and the mixture was stirred for an additional 16 h at rt. After adding DCM (50 mL) a white precipitate formed which was filtered und the filtrate was washed with brine (15 mL) and sat. $NaHCO_3$ (15 mL). The organic extracts were dried over anhydrous Na_2SO_4, and concentrated under reduced pressure to yield a colorless solid (2.1 g, 7.2 mmol, 71 %) that was subsequently dissolved in a mixture of trifluoroacetic acid (TFA, 10 mL) and DCM (10 mL) and stirred for 30 min at rt. After completion of the reaction, the solvents were evaporated, yielding a colorless sticky resin (2.2 g, 7.1 mmol, 99 %). ^{1}H-NMR (300 MHz, D_2O): δ/ppm = 7.57 – 7.08 (m, 5H), 4.72 – 4.48 (m, 2H), 4.28 – 4.14 (m, 1H), 4.00 – 3.79 (m, 2H). ^{13}C-NMR (75 MHz, D_2O): δ/ppm = 169.6, 162.5, 136.7, 128.7, 128.4, 128.3 114.4, 73.1, 67.3, 52.9. $[\alpha]_D^{25}$ = –16 (*c* 1.00, MeOH). MS (ESI) *m/z* calculated for $[C_{10}H_{15}N_2O_2]^+$ ($[M+H]^+$): 195.1, found: 195.0.

22, (*R*)-*N*-((*R*)-2-(benzyloxy)-1-cyanoethyl)-3-(methylsulfonyl)-2-(((*S*)-2,2,2-trifluoro-1-(4-fluorophenyl) ethyl) amino) propenamide

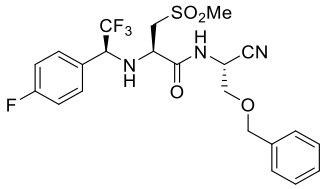

21 was coupled with **7** according to general procedure C, yielding the peptide-amide as a crude (110 mg, 0.21 mmol, 1.0 eq) which was dissolved in in DMF (10 mL) and mixed with cyanuric chloride (39 mg, 0.21 mmol, 1.0 eq) at 0 °C. The mixture was stirred at rt overnight until full consumption of the starting material. After adding EtOAc (25 mL) and water (25 mL) and separating the phases, the aqueous phase was extracted with EtOAc (3x 25 mL) and the combined organic extracts washed with brine (1x 20 mL) and water (2x 20 mL) and dried over anhydrous Na_2SO_4 and concentrated under reduced pressure. The crude product was purified via preparative HPLC yielding **22** as a colorless solid (36 mg, 0.07 mmol, 34 %). ^{1}H-NMR (300 MHz, $CDCl_3$): δ/ppm = 8.56 (d, *J* = 8.1 Hz, 1H), 7.34 – 7.16 (m, 7H), 6.98 – 6.85 (m, 2H), 4.79 – 4.66 (m, 1H), 4.55 – 4.43 (m, 2H), 4.16 (q, *J* = 7.3 Hz, 1H), 3.81 – 3.72 (m, 1H), 3.52 – 3.29 (m, 1H), 3.28 – 3.05 (m, 3H), 2.99 (s, 3H). ^{13}C-NMR (75 MHz, $CDCl_3$): δ/ppm = 170.6, 164.8, 161.5, 136.8, 10.6, 130.5, 128.6, 128.2, 127.9, 116.8, 116.0, 115.7, 73.5, 68.5, 63.1, 62.7, 56.8, 56.1, 43.4, 40.8, 40.5, 40.3, 39.9, 39.7, 39.4. Mp: 98–99 °C. $[\alpha]_D^{22}$ = –11 (*c* 1.00, $CHCl_3$). MS (ESI) *m/z* calculated for $[C_{22}H_{23}F_4N_3O_4SNa]^+$ ([M+Na]$^+$): 524.1, found: 524.1, Purity: 99 %.

25, (*S*)-*N*-((*S*)-1-cyano-3-phenylpropyl)-3-cyclohexyl-2-(((*S*)-2,2,2-trifluoro-1-(4-fluorophenyl) ethyl) amino) propanamide

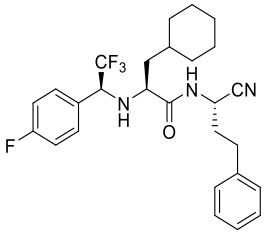

25 was synthesized according to general procedure C by coupling **10** (100 mg, 0.29 mmol, 1.0 eq) and aminonitrile **24** (46 mg, 0.29 mmol, 1.0 eq) yielding the title compound as a colorless solid (36 mg, 0.07 mmol, 26 %) after purification via HPLC. ^{1}H-NMR (300 MHz, $CDCl_3$): δ/ppm = 7.41 – 6.82 (m, 9H), 5.00 – 4.53 (m, 1H), 4.15 – 3.75 (m, 1H), 3.48 – 2.99 (m, 1H), 2.92 – 2.57 (m, 2H), 2.23 – 1.78 (m, 2H), 1.77 – 0.81 (m, 13H). ^{13}C-NMR (75 MHz, $CDCl_3$): δ/ppm = 173.8, 139.3, 130.2, 129.0, 128.4, 126.9, 118.2, 116.2, 62.8, 59.3, 58.9, 58.3, 57.8, 41.4, 39.9, 34.8, 34.4, 33.9, 32.7, 31.8, 31.6, 26.3, 26.1, 25.9. Mp: 103–104 °C. $[\alpha]_D^{22}$ = –36 (*c* 1.00, $CHCl_3$). MS (ESI) *m/z* calculated for $[C_{27}H_{32}F_4N_3O]^+$ ([M+H]$^+$): 490.2, found: 490.1, Purity: 99 %.

26, (*S*)-*N*-((*R*)-2-(benzyloxy)-1-cyanoethyl)-3-cyclohexyl-2-(((S)-2,2,2-trifluoro-1-(4-fluorophenyl) ethyl) amino) propanamide

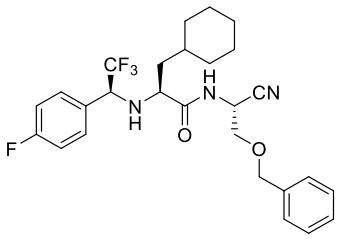

26 was synthesized according to general procedure C by coupling **10** (150 mg, 0.43 mmol, 1.0 eq) and aminonitrile **23** (76 mg, 0.43 mmol, 1.0 eq) yielding the title compound as a colorless solid (48 mg, 0.09 mmol, 22 %) after purification via HPLC. ^{1}H-NMR (300 MHz, $CDCl_3$): δ/ppm = 7.66 (d, *J* = 8.7 Hz, 1H), 7.29 – 7.18 (m, 7H), 7.04 – 6.91 (m, 2H), 4.96 – 4.88 (m, 1H), 4.79 (dt, *J* = 8.9, 3.8 Hz, 1H), 4.61 – 4.51 (m, 1H), 4.51 – 4.41 (m, 2H), 3.99 (q, *J* = 7.1 Hz, 1H), 3.80 (q, *J* = 7.6 Hz, 1H), 3.71 – 3.63 (m, 1H), 3.61 – 3.49 (m, 1H), 1.68 – 1.38 (m, 2H), 1.30 – 1.19 (m, 1H), 1.11 – 0.70 (m, 8H). ^{13}C-NMR (75 MHz, $CDCl_3$): δ/ppm = 173.9, 165.0, 161.7, 136.7, 130.5, 128.9, 128.8, 128.4, 128.0, 117.0, 116.4, 73.7, 68.6, 58.7, 57.7, 41.3, 40.4, 34.3, 33.9, 32.7, 31.7, 29.8, 27.0, 26.4, 26.3. Mp: 143–144 °C. $[\alpha]_D^{22}$ = –29 (*c* 1.00, $CHCl_3$). MS (ESI) *m/z* calculated for $[C_{27}H_{32}F_4N_3O_2]^+$ ($[M+H]^+$): 506.2, found: 506.2, Purity: 97 %.

27, *N*-((*S*)-1-(((*S*)-1-cyano-3-phenylpropyl) amino)-3-cyclohexyl-1-oxopropan-2-yl) morpholine-4-carboxamide

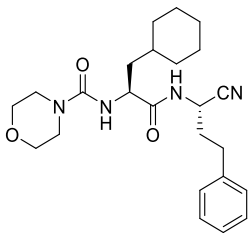

27 was synthesized according to general procedure C by coupling **19** (50 mg, 0.18 mmol, 1.0 eq) and aminonitrile **24** (30 mg, 0.18 mmol, 1.0 eq) yielding the title compound as a colorless solid (66 mg, 0.15 mmol, 88%) after purification via HPLC. ^{1}H-NMR (300 MHz, $CDCl_3$): δ/ppm = 8.71 – 8.40 (m, 1H), 7.43 – 7.01 (m, 5H), 6.08 – 5.81 (m, 1H), 4.74 – 4.55 (m, 1H), 4.52 – 4.30 (m, 1H), 3.72 – 3.48 (m, 4H), 3.44 – 3.20 (m, 4H), 2.89 – 2.60 (m, 2H), 2.20 – 1.98 (m, 2H), 1.77 – 0.74 (m, 13H). ^{13}C-NMR (75 MHz, $CDCl_3$): δ/ppm = 174.6, 157.8, 139.5, 128.8, 128.4, 126.7, 118.6, 66.5, 52.6, 44.2, 40.0, 34.2, 33.6, 32.8, 31.6, 26.3. Mp: 133–134 °C. $[\alpha]_D^{22}$ = –12 (*c* 1.00, $CHCl_3$). MS (ESI) *m/z* calculated for $[C_{24}H_{35}N_4O_3]^+$ ($[M+H]^+$): 427.3, found: 427.2, Purity: 99 %.

28, *N*-((*S*)-1-((*R*-2-(Benzyloxy)-1-cyanoethyl) amino)-3-cyclohexyl-1-oxopropan-2-yl) morpholine-4-carboxamide-L-cyclohexylalanine-methylester-hydrochloride

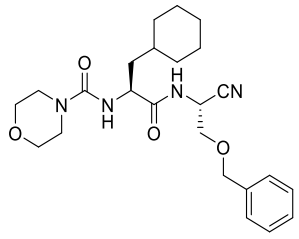

Coupling of the aminonitrile **23** (31 mg, 0.18 mmol, 1.0 eq) with **19** (50 mg, 0.18 mmol, 1.0 eq) according to general procedure C followed by preparative HPLC purification yielded **28** as a colorless solid (20 mg, 0.05 mmol, 26 %). ^{1}H-NMR (300 MHz, $CDCl_3$): δ/ppm = 7.34 – 7.20 (m, 5H), 5.00 – 4.83 (m, 1H), 4.49 (d, *J* = 4.1 Hz, 2H), 4.39 (d, *J* = 7.2 Hz, 1H), 3.71 – 3.44 (m, 4H), 3.34 – 3.15 (m, 4H), 1.73 – 1.38 (m, 8H), 1.33 – 1.02 (m, 6H), 0.96 – 0.70 (m, 3H).^{13}C-NMR (75 MHz, $CDCl_3$): δ/ppm = 173.8, 157.5, 136.9, 128.7, 128.3, 127.9, 117.3, 73.7, 68.9, 66.4, 52.3, 44.2, 40.9, 40.1, 34.3, 33.6, 32.9, 26.4, 26.3, 26.2. Mp: 140–141 °C. $[\alpha]_D^{22}$ = –20 (*c* 1.00, $CHCl_3$). MS (ESI) *m/z* calculated for $[C_{24}H_{34}N_4O_4Na]^+$ ($[M+Na]^+$): 465.3, found: 465.2. Purity: 98 %.

29, *N*-((*S*)-1-(((*R*)-2-(benzyloxy)-1-cyanoethyl) amino)-3-cyclohexyl-1-oxopropan-2-yl) tetrahydro-2*H*-pyran-4-carboxamide

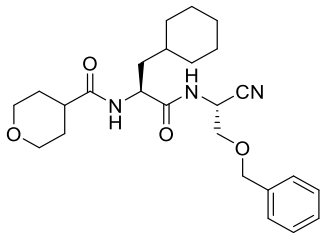

29 was synthesized according to general procedure C by coupling **15** (50 mg, 0.18 mmol, 1.0 eq) and aminonitrile **23** (31 mg, 0.18 mmol, 1.0 eq) yielding the title compound as a colorless sticky resin (35 mg, 0.08 mmol, 45 %). ^{1}H-NMR (300 MHz, $CDCl_3$): δ/ppm = 7.35–7.16 (m, 5H); 4.91 (s, 1H); 4.53 (s, 2H); 3.90 (d, *J* = 8.6 Hz, 2H); 3.59 (q, *J* = 10.0 Hz, 2H); 3.31 (q, *J* = 9.8 Hz, 2H); 2.36–2.30 (m, 1H); 1.82–1.42 (m, 12H); 1.16–0.93 (m, 5H); 0.89–0.78 (m, 3H). ^{13}C-NMR (75 MHz, $CDCl_3$): δ/ppm = 174.9, 172.4, 136.8, 128.8, 128.4, 128.0, 117.1, 73.8, 68.8, 67.2, 67.1, 50.7, 42.0, 40.9, 39.6, 34.3, 33.7, 32.9, 29.4, 29.0, 26.4, 26.3, 26.2. Mp: 126–127 °C. $[\alpha]_D^{22}$ = –44 (*c* 1.00, $CHCl_3$). MS (ESI) *m/z* calculated for $[C_{25}H_{36}N_3O_4]^+$ ($[M+H]^+$): 442.3, found: 442.2, Purity: 99 %.

30, *N*-((*S*)-1-(((*S*)-1-cyano-3-phenylpropyl) amino)-3-cyclohexyl-1-oxopropan-2-yl) tetrahydro-2*H*-pyran-4-carboxamide

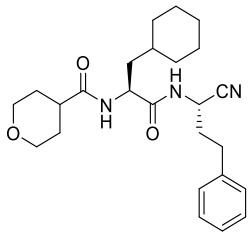

30 was synthesized according to general procedure C by coupling **15** (50 mg, 0.18 mmol, 1.0 eq) and crude aminonitrile **24** (30 mg, 0.18 mmol, 1.0 eq) yielding the title compound as a colorless solid (13 mg, 0.03 mmol, 17 %). ^{1}H-NMR (600 MHz, $CDCl_3$): δ/ppm = 7.36 – 7.27 (m, 3H), 7.25 – 7.13 (m, 4H), 6.48 (s, 1H), 4.71 – 4.64 (m, 1H), 4.61 – 4.51 (m, 1H), 4.04 – 3.94 (m, 2H), 3.44 – 3.34 (m, 2H), 2.83 – 2.71 (m, 2H), 2.48 – 2.38 (m, 1H), 2.19 – 2.07 (m, 2H), 1.84 – 1.51 (m, 10H), 1.32 – 1.06 (m, 4H), 0.98 – 0.80 (m, 2H). ^{13}C-NMR (150 MHz, $CDCl_3$): δ/ppm = 175.6, 172.4, 139.2, 128.9, 128.5, 126.8, 118.3, 67.2, 50.8, 42.0, 34.3, 33.6, 32.8, 31.6, 29.4, 28.9, 26.3, 26.2, 26.1. Mp: 94–95 °C. $[\alpha]_D^{22}$ = –21 (*c* 1.00, $CHCl_3$). MS (ESI) *m/z* calculated for $[C_{25}H_{35}N_3O_3Na]^+$ ($[M+Na]^+$): 448.3, found: 448.2, Purity: 99 %.

31, *N*-((*S*)-1-(((*R*)-2-(benzyloxy)-1-cyanoethyl) amino)-3-cyclohexyl-1-oxopropan-2-yl) isonicotinamide

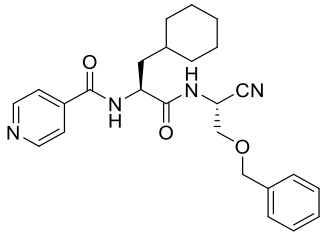

31 was synthesized according to general procedure C by coupling **17** (42 mg, 0.15 mmol, 1.0 eq) and **23** (27 mg, 0.15 mmol, 1.0 eq) yielding the title compound as a colorless solid (8 mg, 0.02 mmol, 13 %). ^{1}H-NMR (600 MHz, DMSO-d_6): δ/ppm = 9.11 – 9.02 (m, 2H), 8.86 – 8.79 (m, 2H), 8.05 – 7.90 (m, 2H), 7.42 – 7.15 (m, 5H), 5.19 – 4.93 (m, 1H), 4.71 – 4.49 (m, 3H), 3.78 – 3.59 (m, 2H), 1.81 – 1.44 (m, 7H), 1.40 – 1.24 (m, 1H), 1.18 – 1.02 (m, 3H), 0.97 – 0.74 (m, 2H). ^{13}C-NMR (150 MHz, DMSO-d_6): δ/ppm = 172.4, 164.5, 148.5, 142.7, 137.7, 128.4, 127.8, 122.6, 122.5, 118.3, 72.3, 68.4, 68.2, 51.2, 40.5, 33.7, 33.3, 31.7, 26.1, 25.8, 25.6. Mp: 64–65 °C. MS (ESI) *m/z* calculated for $[C_{25}H_{31}N_4O_3]^+$ ($[M+H]^+$): 435.2, found: 435.1, Purity: 96 %.

32, *N*-((*S*)-1-(((*S*)-1-cyano-3-phenylpropyl) amino)-3-cyclohexyl-1-oxopropan-2-yl) isonicotinamide

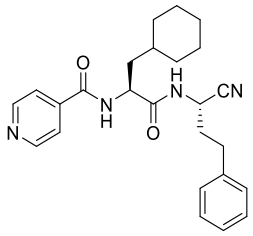

32 was synthesized according to general procedure C by coupling **17** (42 mg, 0.3 mmol, 1.0 eq) and crude aminonitrile **24** (24 mg, 0.15 mmol, 1.0 eq) yielding the title compound as a pale-yellow solid (18 mg, 0.04 mmol, 28 %) after purification via HPLC. ^{1}H-NMR (300 MHz, $CDCl_3$): δ/ppm = 8.82 (s, 2H), 8.19 – 7.58 (m, 3H), 7.39 – 6.99 (m, 5H), 4.88 – 4.49 (m, 2H), 2.89 – 2.62 (m, 2H), 2.28 – 2.07 (m, 2H), 1.77 – 1.55 (m, 6H), 1.40 – 1.04 (m, 4H), 1.00 – 0.76 (m, 2H). ^{13}C-NMR (75 MHz, $CDCl_3$): δ/ppm = 172.6, 172.2, 165.3, 148.9, 139.1, 128.9, 128.5, 126.9, 122.2, 118.3, 52.1, 40.5, 39.4, 34.3, 33.5, 32.8, 31.6, 26.3, 26.1. Mp: 139–140 °C. $[\alpha]_D^{22}$ = 10 (*c* 1.00, $CHCl_3$). MS (ESI) *m/z* calculated for $[C_{25}H_{31}N_4O_2]^+$ ($[M+H]^+$): 419.2, found: 419.1, Purity: 99 %.

33, (*R*)-*N*-((*R*)-2-(benzyloxy)-1-cyanoethyl)-3-(methylsulfonyl)-2-(((*S*)-2,2,2-trifluoro-1-(4-nitrophenyl) ethyl) amino) propanamide

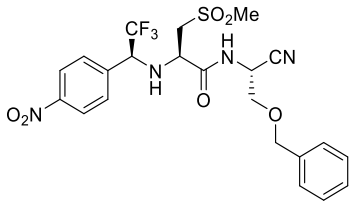

33 was synthesized according to general procedure C by coupling **8** (40 mg, 0.11 mmol, 1.0 eq) and **23** (19 mg, 0.11 mmol, 1.0 eq) yielding the title compound as a colorless solid (48 mg, 0.09 mmol, 82 %) after purification via HPLC. ^{1}H-NMR (300 MHz, $CDCl_3$): δ/ppm = 8.25 – 8.08 (m, 2H), 7.60 – 7.46 (m, 2H), 7.42 – 7.29 (m, 7H), 4.83 (s, 1H), 4.74 – 4.39 (m, 4H), 3.86 – 3.68 (m, 2H), 3.45 – 3.22 (m, 2H), 3.04 (s, 3H). ^{13}C-NMR (75 MHz, $CDCl_3$): δ/ppm = 170.2, 148.9, 139.5, 136.6, 130.1, 129.0, 128.9, 128.1, 124.3, 116.7, 73.9, 68.3, 63.1, 56.6, 55.9, 55.4, 43.3, 41.1. Mp: 105–106 °C. $[\alpha]_D^{22}$ = –22 (*c* 1.00, $CHCl_3$). MS (ESI) *m/z* calculated for $[C_{22}H_{24}F_3N_4O_6S]^+$ ($[M+H]^+$): 529.1, found: 529.0, Purity: 99 %.

34, (*R*)-*N*-((*S*)-1-cyano-3-phenylpropyl)-3-(methylsulfonyl)-2-(((*S*)-2,2,2-trifluoro-1-(4-nitrophenyl) ethyl) amino) propanamide

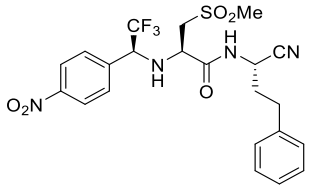

34 was synthesized according to general procedure C by coupling **8** (40 mg, 0.11 mmol, 1.0 eq) and **24** (18 mg, 0.11 mmol, 1.0 eq) yielding the title compound as a colorless solid (12 mg, 0.023 mmol, 21 %) after purification via HPLC. ^{1}H-NMR (300 MHz, CD_3OD): δ/ppm = 8.27 (t, *J* = 8.3 Hz, 2H), 7.60 (t, *J* = 9.3 Hz, 2H), 7.44 – 7.06 (m, 5H), 4.84 – 4.60 (m, 1H), 4.50 – 4.18 (m, 1H), 3.78 – 3.64 (m, 1H), 3.48 – 3.15 (m, 2H), 3.08 (s, 2H), 2.94 – 2.86 (m, 1H), 2.82 – 2.67 (m, 2H), 2.28 – 1.94 (m, 4H). ^{13}C-NMR (75 MHz, CD_3OD): δ/ppm = 169.6, 148.9, 139.0, 130.0, 129.1, 128.5, 128.4, 127.1, 124.4, 117.8, 56.2, 43.3, 42.8, 40.7, 34.2, 31.6. Mp: 93–94 °C. $[\alpha]_D^{22}$ = –6 (*c* 1.00, $CHCl_3$). MS (ESI) *m/z* calculated for $[C_{22}H_{24}F_3N_4O_5S]^+$ ($[M+H]^+$): 513.1, found: 513.1, Purity: 99 %.

36, (*R*)-*N*-(1-cyanocyclopropyl)-3-(methylsulfonyl)-2-(((*S*)-2,2,2-trifluoro-1-(4-fluorophenyl) ethyl) amino) propanamide

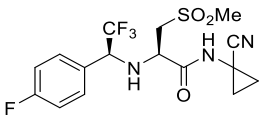

36 was synthesized according to general procedure C by coupling 1-aminocyclopropan-carboxylic acid **35** (237 mg; 2.0 mmol; 1.1 eq) and **7** (618 mg, 1.8 mmol, 1.0 eq) yielding the title compound as a colorless solid (685 g, 1.78 mmol, 98 %) after purification on silica gel ($CHCl_3$/MeOH = 50:1). ^{1}H-NMR (300 MHz, DMSO-d_6): δ/ppm = 9.03 (s, 1H), 7.45 (dd, *J* = 8.6, 5.5 Hz, 2H), 7.23 (t, *J* = 8.9 Hz, 2H), 4.36 (p, *J* = 7.8 Hz, 1H), 3.69 (td, *J* = 10.0, 9.5, 3.6 Hz, 1H), 3.58–3.41 (m, 2H), 3.11 (s, 3H), 1.50–1.25 (m, 2H), 1.09–0.96 (m, 1H), 0.84–0.67 (m, 1H). ^{13}C-NMR (75 MHz, DMSO-d_6): δ/ppm = 171.7, 164.0, 160.8, 130.6, 130.5, 120.3, 115.6, 115.3, 61.3, 60.9, 56.6, 56.2, 43.1, 19.6, 15.4. Mp: 203–204 °C. $[\alpha]_D^{22}$ = 16 (*c* 1.00, MeOH). MS (ESI) *m/z* calculated for $[C_{16}H_{18}F_4N_3O_3S]^+$ ($[M+H]^+$): 408.1, found: 408.1, Purity: 95 %.

37, (*R*)-*N*-(1-cyanocyclopropyl)-3-(methylsulfonyl)-2-(((*S*)-2,2,2-trifluoro-1-(4-nitrophenyl) ethyl) amino) propanamide

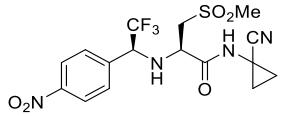

37 was synthesized according to general procedure C by coupling 1-aminocyclopropan-carboxylic acid **35** (237 mg; 2.0 mmol; 1.1 eq) and **8** (618 mg, 1.8 mmol, 1.0 eq) yielding the title compound as a colorless solid (685 g, 1.78 mmol, 98 %) after purification on silica gel ($CHCl_3$/MeOH = 50:1). ^{1}H-NMR (300 MHz, DMSO-d_6): δ/ppm = 9.09 – 8.78 (m, 1H), 8.36 – 8.09 (m, 2H), 7.91 – 7.55 (m, 2H), 4.70 – 4.48 (m, 1H), 3.86 – 3.42 (m, 2H), 3.11 (s, 3H), 1.64 – 0.65 (m, 6H). ^{13}C-NMR (75 MHz, DMSO-d_6): δ/ppm = 171.6, 147.9, 141.5, 129.9, 123.6, 120.2, 79.2, 56.8, 56.2, 43.1, 19.5, 15.6, 15.4. Mp: 200–201 °C. $[\alpha]_D^{22}$ = 55 (*c* 1.00, $CHCl_3$). MS (ESI) *m/z* calculated for $[C_{16}H_{17}F_3N_4O_5SNa]^+$ ($[M+Na]^+$): 457.1, found: 457.1, Purity: 96 %.

38, (*S*)-*N*-(1-cyanocyclopropyl)-3-cyclohexyl-2-(((*S*)-2,2,2-trifluoro-1-(4-fluorophenyl) ethyl) amino) propanamide

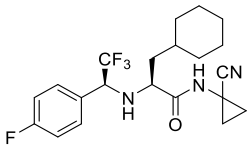

38 was synthesized according to general procedure C by coupling 1-aminocyclopropan-carboxylic acid **35** (248 mg; 2.1 mmol; 1.1 eq) and **10** (700 mg, 1.9 mmol, 1.0 eq) yielding the title compound as colorless solid (249 mg, 0.57 mmol, 30 %) after purification on silica gel ($CHCl_3$/MeOH = 100:1). ^{1}H-NMR (300 MHz, $CDCl_3$): δ/ppm = 7.50 – 7.28 (m, 2H), 7.18 – 6.97 (m, 2H), 4.25 – 3.67 (m, 1H), 3.46 – 2.92 (m, 1H), 2.43 – 2.15 (m, 1H), 1.88 – 0.79 (m, 17H). ^{13}C-NMR (75 MHz, $CDCl_3$): δ/ppm = 174.7, 164.0, 165.1, 161.8, 130.5, 130.1, 119.8, 116.5, 63.5, 59.2, 58.3, 41.1, 34.3, 33.8, 32.8, 31.8, 26.2, 20.1, 16.6. Mp: 118–119 °C. $[\alpha]_D^{22}$ = 23 (*c* 1.00, $CHCl_3$). MS (ESI) *m/z* calculated for $[C_{21}H_{26}F_4N_3O]^+$ ($[M+H]^+$): 412.2, found: 412.2, Purity: 97 %.

39, (*S*)-*N*-(1-((1-cyanocyclopropyl) amino)-3-cyclohexyl-1-oxopropan-2-yl) morpholine-4-carboxamide

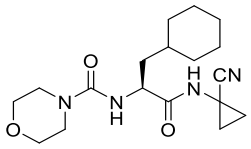

39 was synthesized according to general procedure C by coupling 1-aminocyclopropan-carboxylic acid **35** (33 mg; 0.28 mmol; 1.0 eq) and **19** (80 mg, 0.28 mmol, 1.0 eq) yielding the title compound as colorless solid (97 mg, 0.27 mmol, 96 %) after purification via HPLC. ^{1}H-NMR

(300 MHz, $CDCl_3$): δ/ppm = 8.54 (s, 1H), 6.16 – 5.86 (m, 1H), 4.38 – 4.16 (m, 1H), 3.77 – 3.57 (m, 4H), 3.47 – 3.24 (m, 4H), 1.76 – 1.54 (m, 6H), 1.53 – 1.38 (m, 3H), 1.36 – 1.07 (m, 6H), 1.00 – 0.75 (m, 2H). ^{13}C-NMR (75 MHz, $CDCl_3$): δ/ppm = 176.2, 157.9, 120.3, 66.6, 52.5, 44.2, 39.4, 38.7, 34.3, 33.6, 32.7, 26.2, 20.5, 16.8, 16.2. Mp: 193–194 °C. $[\alpha]_D^{22}$ = 19 (*c* 1.00, MeOH). MS (ESI) *m/z* calculated for $[C_{18}H_{29}N_4O_3]^+$ ($[M+H]^+$): 349.2, found: 349.2, Purity: 98 %.

40, (*S*)-*N*-(1-((1-cyanocyclopropyl) amino)-3-cyclohexyl-1-oxopropan-2-yl) tetrahydro-2*H*-pyran-4-carboxamide

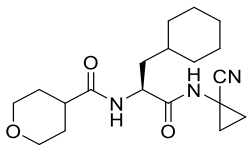

40 was synthesized according to general procedure C by coupling 1-aminocyclopropan-carboxylic acid **35** (50 mg; 0.42 mmol; 1.0 eq) and **15** (120 mg, 0.42 mmol, 1.0 eq) yielding the title compound as colorless solid (123 g, 0.35 mmol, 84 %) after purification via HPLC. ($CHCl_3$/MeOH = 50:1). ^{1}H-NMR (300 MHz, $CDCl_3$): δ/ppm = 7.96 (s, 1H), 6.63 (s, 1H), 4.51 (s, 1H), 4.16 – 3.75 (m, 2H), 3.51 – 3.31 (m, 2H), 3.06 (m, 1H), 2.45 (s, 1H), 1.89 – 1.40 (m, 12H), 1.30 – 1.04 (m, 6H), 1.00 – 0.73 (m, 2H). ^{13}C-NMR (75 MHz, $CDCl_3$): δ/ppm = 175.5, 173.7, 119.9, 67.2, 50.6, 42.1, 39.3, 34.4, 33.6, 32.9, 29.5, 29.1, 26.4, 20.6, 16.9, 16.6. Mp: 122–123 °C. $[\alpha]_D^{22}$ = 16 (*c* 1.00, MeOH). MS (ESI) *m/z* calculated for $[C_{19}H_{30}N_3O_3]^+$ ($[M+H]^+$): 348.2, found: 348.1, Purity: 95 %.

41, (*S*)-*N*-(1-((1-cyanocyclopropyl) amino)-3-cyclohexyl-1-oxopropan-2-yl) isonicotinamide

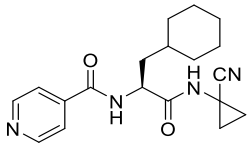

41 was synthesized according to general procedure C by coupling 1-aminocyclopropan-carboxylic acid **35** (64 mg; 0.54 mmol; 1.0 eq) and **17** (150 mg, 0.54 mmol, 1.0 eq) yielding the title compound as pale yellow solid (685 g, 1.78 mmol, 98 %) after purification via HPLC. ^{1}H-NMR (300 MHz, $CDCl_3$): δ/ppm = 8.79 – 8.61 (m, 2H), 7.89 – 7.60 (m, 2H), 7.70 (s, 2H), 4.70 (q, *J* = 8.3 Hz, 1H), 1.82 – 1.43 (m, 9H), 1.37 – 0.99 (m, 6H), 0.99 – 0.70 (m, 2H). ^{13}C-NMR (75 MHz, $CDCl_3$): δ/ppm = 174.6, 165.8, 149.9, 140.9, 128.6, 127.8, 121.7, 120.0, 51.9, 42.1, 41.5, 39.0, 34.3, 33.5, 32.6, 26.3, 26.0, 20.7, 16.7, 16.4. Mp: 95–96 °C. $[\alpha]_D^{22}$ = 11 (*c* 1.00, MeOH). MS (ESI) *m/z* calculated for $[C_{19}H_{25}N_4O_2]^+$ ($[M+H]^+$): 341.2, found: 341.2, Purity: 99 %.

43, Methyl *O*-benzyl-*N*-((*S*)-3-cyclohexyl-2-(morpholine-4-carboxamido) propanoyl)-L-serinate

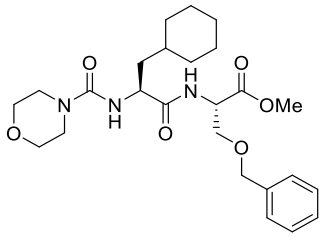

Deprotection of **42** (217 mg, 0.7 mmol, 1.0 eq) was performed following general procedure A. The deprotected amino acid was then coupled with **19** (200 mg, 0.7 mmol, 1.0 eq) following general procedure C. After purification via column chromatography (CH/EtOAc 1:3), **43** could be obtained as a colorless oil (253 mg, 0.53 mmol, 76 %). ^{1}H-NMR (300 MHz, $CDCl_3$): δ/ppm = 7.36 – 7.19 (m, 5H), 4.69 (dt, *J* = 8.2, 3.4 Hz, 1H), 4.58 – 4.37 (m, 3H), 3.86 (dd, *J* = 9.6, 3.4 Hz, 1H), 3.71 (s, 3H), 3.68 – 3.52 (m, 5H), 3.41 – 3.24 (m, 4H), 1.86 – 1.58 (m, 6H), 1.57 – 1.31 (m, 3H), 1.29 – 0.80 (m, 6H). ^{13}C-NMR (75 MHz, $CDCl_3$): δ/ppm = 173.7, 170.5, 157.5, 137.6, 128.5, 127.9, 127.7, 73.4, 69.6, 66.5, 52.8, 52.6, 52.4, 44.2, 40.6, 34.2, 33.7, 32.9, 26.5, 26.3, 26.2. $[\alpha]_D^{22}$ = 13 (*c* 1.00, $CHCl_3$). MS (ESI) *m/z* calculated for $[C_{25}H_{37}N_3O_6Na]^+$ ($[M+Na]^+$): 498.3, found: 498.2.

45, *N*-((*S*)-1-(((*S*)-1-(benzyloxy)-3-oxopropan-2-yl) amino)-3-cyclohexyl-1-oxopropan-2-yl) morpholine-4-carboxamide

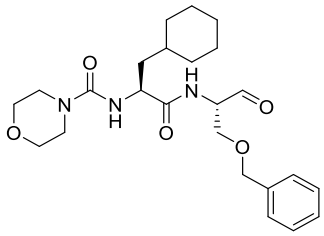

(1) To a solution of **43** (132 mg, 0.28 mmol, 1.0 eq) in THF (15 mL) at 0 °C, $NaBH_4$ (42 mg, 1.11 mmol, 4.0 eq) and MeOH (1.2 mL) were added. The mixture was stirred for 16 h at rt and upon completion, diluted with saturated NH_4Cl solution (30 mL). After extraction with EtOAc (3x 25 mL) the combined organic layers were washed with saturated NH_4Cl solution (20 mL) and brine (20 mL), dried over anhydrous Na_2SO_4 and concentrated under reduced pressure to yield the C-terminal hydroxy-peptide as a colorless solid (114 mg, 0.25 mmol, 91 %), which was used subsequently in the next step.

(2) To a solution of the C-terminal hydroxy-peptide (45 mg, 0.1 mmol, 1.0 eq) in DCM (10 mL) dess-martin-periodinane (51 mg, 0.12 mmol, 1.2 eq) was added and the mixture was stirred at rt for 12 h. After completion, indicated by TLC, the mixture was filtrated, washed a saturated $Na_2S_2O_3$ solution (15 mL), a saturated $NaHCO_3$ solution (15 mL) and brine (20 mL). The mixture

was dried over anhydrous Na_2SO_4, concentrated under reduced pressure, and subsequently purified via column chromatography ($CHCl_3$/MeOH 30:1), to yield **47** as a colorless solid (31 mg, 0.07 mmol, 70 %). ^{1}H-NMR (300 MHz, $CDCl_3$): δ/ppm = 9.56 (s, 1H), 7.43 – 7.17 (m, 5H), 5.15 – 4.96 (m, 1H), 4.76 – 4.34 (m, 3H), 4.25 (s, 1H), 3.99 (dd, *J* = 9.7, 3.6 Hz, 1H), 3.75 – 3.53 (m, 4H), 3.48 – 3.20 (m, 4H), 1.84 – 1.47 (m, 6H), 1.40 – 0.77 (m, 8H). ^{13}C-NMR (75 MHz, $CDCl_3$): δ/ppm = 198.3, 174.1, 157.5, 137.3, 128.6 127.8, 127.7, 73.7, 67.5, 66.5, 59.0,52.4, 44.2, 40.6, 34.3, 33.7, 32.9, 26.5, 26.3. Mp: 85–86 °C. $[\alpha]_D^{22}$ = 20 (*c* 1.00, MeOH). MS (ESI) *m/z* calculated for $[C_{24}H_{35}N_3O_5Na]^+$ ([M+Na]$^+$): 468.3, found: 468.3, Purity: 99 %.

44, *N*-((*S*)-1-(((*S*)-1-(Benzyloxy)-3-oxo-4-(phenylsulfonyl)butan-2-yl) amino)-3-cyclohexyl-1-oxopropan-2-yl)morpholin-4-carboxamid

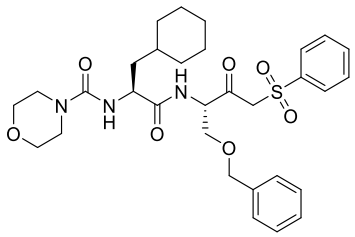

(1) To a solution of methylphenyl sulfone (151 mg; 0.97 mmol, 2.0 eq) in dry THF (5 mL) was added *n*-BuLi (0.78 mL, 1.94 mmol, 2.5 M) at –5 °C. The mixture was stirred at this temperature for 30 min and boc protected *O*-benzylserine-methylester (150 mg, 0.49 mmol, 1.0 eq) dissolved in THF (5 mL) was added dropwise at –78 °C. The mixture was stirred for 3 h while allowing to reach rt. After quenching with water and extracting the crude product with EtOAc (3x 25 mL), the combined organic extracts were washed with brine (25 mL) and water (20 mL), dried over anhydrous Na_2SO_4, and concentrated. After purification of the crude product via column chromatography on silica gel (CH/ EtOAc 3:1), *tert*-butyl (*S*)-(1-(benzyloxy)-3-oxo-4-(phenylsulfonyl)butan-2-yl)carbamate was obtained as a colorless oil (150 mg, 0.35 mmol, 72 %). Removing the boc-protecting group with HCl (4.0 M, 3 mL) led to the free amino-ketone, which was subsequently used in the next step.

(2) Coupling of the deprotected aminoketone (40 mg, 0.11 mmol, 1.0 eq) with **XX** (31 mg, 0.11 mmol, 1.0 eq) according to general procedure C, yielded the title compound as a colorless solid (20 mg, 0.03 mmol, 31 %) after purification via HPLC. ^{1}H-NMR (300 MHz, $CDCl_3$): δ/ppm = 7.78 (d, *J* = 7.4 Hz, 2H), 7.55 (d, *J* = 7.4 Hz, 1H), 7.43 (t, *J* = 7.7 Hz, 2H), 7.28 – 7.13 (m, 5H), 4.70 (s, 1H), 4.51 – 4.22 (m, 4H), 4.15 (d, *J* = 13.5 Hz, 1H), 3.87 – 3.79 (m, 1H), 3.56 (s, 5H), 3.28 (s, 4H), 1.75 – 1.34 (m, 7H), 1.26 (s, 1H), 1.11 (q, *J* = 10.9, 8.5 Hz, 3H), 0.97 – 0.73 (m, 2H). ^{13}C-NMR (75 MHz, $CDCl_3$): δ/ppm = 195.7, 174.2, 157.6, 138.7, 137.3, 134.3, 129.3, 128.6, 128.1, 127.9, 73.6, 68.6, 66.5, 64.1, 59.3, 52.8, 44.2, 40.0, 34.3, 33.7, 32.8, 26.4, 26.2, 26.1. Mp: 67–68 °C. $[\alpha]_D^{22}$ = –3 (*c* 1.00, MeOH). MS (ESI) *m/z* calculated for $[C_{31}H_{41}N_3O_7SNa]^+$ ([M+Na]$^+$): 622.3, found: 622.2, Purity: 99 %.

46, *N*-((2*S*)-1-((1-(benzyloxy)-4-mercapto-3-oxobutan-2-yl)amino)-3-cyclohexyl-1-oxopropan-2-yl)morpholine-4-carboxamide

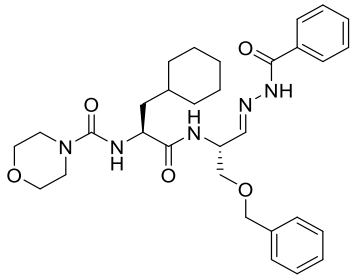

46 was prepared from **45** (20 mg, 0.05 mmol, 1.0 eq.) which was dissolved in MeOH (5 mL) and mixed with benzohydrazide (6 mg, 0.05 mmol, 1.0 eq.) and stirred overnight at rt. The solvents were evaporated, and the residue was purified on HPLC yielding the title compound as a colorless solid (20 mg, 0.04 mmol, 78 %). ^{1}H-NMR (600 MHz, DMSO-d_6): δ/ppm 7.85 (dd, J = 7.1, 1.6 Hz, 2H), 7.73 (d, J = 5.0 Hz, 1H), 7.57 (td, J = 7.3, 1.5 Hz, 1H), 7.50 (t, J = 7.8 Hz, 2H), 7.37 – 7.24 (m, 4H), 4.70 – 4.60 (m, 1H), 4.54 – 4.51 (m, 2H), 4.27 – 4.18 (m, 1H), 3.69 – 3.59 (m, 2H), 3.57 – 3.47 (m, 5H), 3.33 – 3.18 (m, 5H), 1.72 – 1.54 (m, 6H), 1.54 – 1.41 (m, 2H), 1.31 (s, 1H), 1.20 – 0.99 (m, 4H), 0.93 – 0.78 (m, 2H).^{13}C-NMR (150 MHz, DMSO-d_6): δ/ppm = 173.9, 163.5, 157.9, 149.7, 138.7, 133.8, 132.2, 128.9, 128.7, 128.6, 128.0, 127.9, 72.5. 70.3, 66.4, 52.5, 44.9, 34.0, 33.6, 32.3, 26.6, 26.2, 26.1. Mp: 59–60 °C. $[\alpha]_D^{22}$ = –11 (*c* 1.00, MeOH). MS (ESI) *m/z* calculated for $[C_{31}H_{42}N_5O_5]^+$ ($[M+H]^+$): 564.3, found: 564.2, Purity: 96 %.

47, *N*-((2*S*)-1-((1-(benzyloxy)-4-mercapto-3-oxobutan-2-yl)amino)-3-cyclohexyl-1-oxopropan-2-yl)morpholine-4-carboxamide

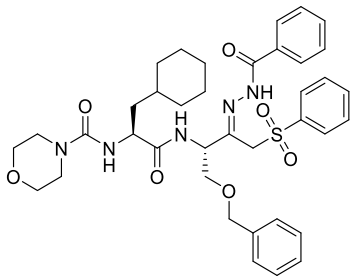

47 was prepared from **44** (20 mg, 0.03 mmol, 1.0 eq.) which was dissolved in MeOH (5 mL) and mixed with benzohydrazide (6 mg, 0.05 mmol, 1.0 eq.) and stirred overnight at rt. The solvents were evaporated, and the residue was purified on HPLC yielding the title compound as a colorless solid (10 mg, 0.014 mmol, 47 %). ^{1}H-NMR (600 MHz, DMSO-d_6) δ/ppm 8.45 (d, J = 7.3 Hz, 1H), 7.96 – 7.67 (m, 5H), 7.68 – 7.50 (m, 5H), 7.38 – 7.23 (m, 5H), 6.56 (d, J = 7.5 Hz, 1H), 4.75 (s, 1H), 4.46 – 4.40 (m, 2H), 4.18 – 4.07 (m, 1H), 3.73 – 3.58 (m, 2H), 3.55 – 3.49 (m, 5H), 3.31 – 3.15 (m, 4H), 1.71 – 1.53 (m, 5H), 1.52 – 1.36 (m, 2H), 1.34 – 1.20 (m, 2H), 1.19 – 0.98 (m, 4H), 0.90 – 0.77 (m, 2H).^{13}C-NMR (151 MHz, DMSO-d_6): δ/ppm = 174.2, 157.6, 139.6,

137.9, 129.3, 128.3, 127.6, 125.3, 80.2, 79.3, 78.3, 72.2, 67.8, 65.9, 62.1, 58.8, 44.0, 33.5, 31.9, 26.2, 25.7, 18.6. Mp: 101–102 °C. MS (ESI) *m/z* calculated for $[C_{38}H_{48}N_5O_7S]^+$ ($[M+H]^+$): 718.3, found: 718.4, Purity: 95 %.

48, *N*-((2*S*)-1-((1-(benzyloxy)-4-chloro-3-oxobutan-2-yl)amino)-3-cyclohexyl-1-oxopropan-2-yl)morpholine-4-carboxamide

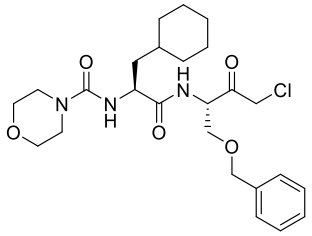

48 was synthesized according to general procedure C by coupling (*S*)-1-(benzyloxy)-4-chloro-3-oxobutan-2-amin-hydrochlorid (prepared according to literature[3]; 1.2 g; 4.60 mmol; 1.0 eq) and **19** (1.3 g, 4.60 mmol, 1.0 eq) yielding the title compound as a colorless solid (0.37 g, 0.75 mmol, 17 %) after purification via HPLC. ^{1}H-NMR (300 MHz, $CDCl_3$): δ/ppm = 7.29 – 7.13 (m, 5H), 4.72 (s, 1H), 4.52 – 4.28 (m, 3H), 4.23 – 4.11 (m, 2H), 3.84 – 3.76 (m, 1H), 3.56 (s, 5H), 3.28 (s, 4H), 1.67 – 1.41 (m, 6H), 1.32 – 1.20 (m, 1H), 1.18 – 1.00 (m, 3H), 0.95 – 0.73 (m, 3H). ^{13}C-NMR (75 MHz, $CDCl_3$): δ/ppm = 199.1, 174.3, 157.7, 137.1, 128.7, 128.2, 127.9, 73.7, 69.0, 66.5, 57.1, 52.6, 47.5, 44.4, 40.0, 34.4, 33.7, 32.8, 26.5, 26.3, 26.2. Mp: 56–57 °C. $[\alpha]_D^{22}$ = +3 (*c* 1.00, MeOH). MS (ESI) *m/z* calculated for $[C_{25}H_{36}ClN_3O_5Na]^+$ ($[M+Na]^+$): 516.2, found: 516.1, Purity: 96 %.

49, *S*-(4-(benzyloxy)-3-((*S*)-3-cyclohexyl-2-(morpholine-4-carboxamido)propanamido)-2-oxobutyl) benzothioate

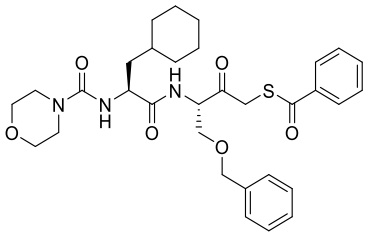

49 was prepared from **48** (100 mg, 0.20 mmol, 1.0 eq.) which was dissolved in dry THF (4 mL). At rt, K_2CO_3 (54 mg, 0.40 mmol, 2.0 eq) and thiobenzoic acid (22 µL, 0.2 mmol, 1.0 eq.) were added, and the mixture was stirred for 16 h. The solvents were removed under reduced pressure and the residue was dissolved in EtOAc (20 mL), then washed with H_2O (25 mL) and sat. NaCl-solution (20 mL), dried over anhydrous Na_2SO_4, concentrated under reduced pressure, and subsequently purified via HPLC yielding the title compound as a colorless solid 52 mg, 0.09 mmol, 45 %). ^{1}H-NMR (300 MHz, $CDCl_3$): δ/ppm = 7.89 (d, *J* = 7.9 Hz, 2H), 7.54 (t,

J = 7.1 Hz, 1H), 7.40 (t, *J* = 7.4 Hz, 2H), 7.32 – 7.16 (m, 5H), 5.30 – 4.99 (m, 1H), 4.87 – 4.76 (m, 1H), 4.49 (s, 3H), 4.13 – 3.87 (m, 3H), 3.72 (s, 1H), 3.59 (s, 4H), 3.31 (s, 4H), 1.67 – 1.58 (m, 7H), 1.32 (s, 1H), 1.22 – 0.78 (m, 6H). ^{13}C-NMR (75 MHz, $CDCl_3$): δ/ppm = 200.6, 190.3, 174.1, 157.7, 137.4, 136.1, 134.0, 128.8, 128.6, 128.0, 127.9, 127.6, 73.6, 69.1, 66.5, 58.5, 52.4, 44.2, 39.8, 37.1, 34.3, 33.7, 32.8, 26.5, 26.3, 26.1. Mp: 56–57 °C (decomposition). $[\alpha]_D^{22}$ = –3 (*c* 1.00, $CHCl_3$). MS (ESI) *m/z* calculated for $[C_{32}H_{41}N_3O_6SNa]^+$ ($[M+Na]^+$): 618.3, found: 618.2, Purity: 99 %.j

50, 4-(benzyloxy)-3-((*S*)-3-cyclohexyl-2-(morpholine-4-carboxamido)propanamido)-2-oxobutyl benzoate

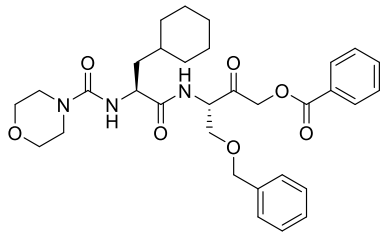

50 was prepared from **48** (100 mg, 0.20 mmol, 1.0 eq.) which was dissolved in DMF (4 mL) under argon atmosphere. At rt, CsF (70 mg, 0.46 mmol, 2.3 eq) and benzoic acid (32 mg, 0.38 mmol, 1.3 eq.) were added and the mixture was stirred for 4 h at 64 C. The solvents were removed under reduced pressure and the residue was purified on HPLC, yielding the title compound as a colorless solid (12 mg, 0.02 mmol, 10 %). ^{1}H-NMR (600 MHz, DMSO-d_6): δ/ppm = 8.02 – 7.93 (m, 2H), 7.71 – 7.64 (m, 1H), 7.59 – 7.49 (m, 2H), 7.33 (d, *J* = 4.2 Hz, 4H) 7.30 – 7.24 (m, 1H), 5.28 – 5.04 (m, 2H), 4.68 – 4.59 (m, 1H), 4.54 – 4.47 (m, 2H), 4.24 – 4.19 (m, 1H) 3.80 – 3.75 (m, 1H), 3.53 – 3.44 (m, 5H), 3.32 – 3.22 (m, 5H), 1.70 – 1.59 (m, 4H), 1.56 – 1.40 (m, 3H), 1.20 – 1.01 (m, 3H), 0.92 – 0.75 (m, 3H). ^{13}C-NMR (150 MHz, DMSO-d_6): δ/ppm = 202.1, 174.8, 165.4, 157.9, 138.1, 134.1, 129.7, 128.6, 127.9, 127.8, 72.6, 68.8, 67.9, 66.2, 56.7, 52.5, 48.9, 44.3, 33.9, 33.5, 32.1, 29.6, 26.4, 26.1, 25.9. Mp: 67–68 °C. $[\alpha]_D^{22}$ = –2 (*c* 1.00, $CHCl_3$). MS (ESI) *m/z* calculated for $[C_{32}H_{41}N_3O_7Na]^+$ ($[M+Na]^+$): 602.3, found: 602.2, Purity: 99 %.

51, *N*-((2*S*)-1-((1-(benzyloxy)-4-hydroxy-3-oxobutan-2-yl)amino)-3-cyclohexyl-1-oxopropan-2-yl)morpholine-4-carboxamide

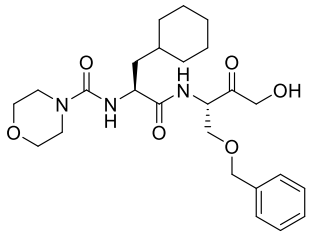

51 was prepared from **48** (70 mg, 0.14 mmol, 1.0 eq.) which was dissolved in DMF (3 mL) and a solution of $NaHCO_3$ (12 mg, 0.70 mmol, 5.0 eq.) in H_2O (3 mL). The mixture was stirred for 2 h at 40 C°. After adding EtOAc (30 mL) and water (30 mL) the phases were separated, and the aqueous phase was extracted with EtOAc (3x 20 mL). The organic extracts were washed with brine (20 mL) and dried over anhydrous Na_2SO_4. After removing the solvent under reduced pressure, the crude was purified on HPLC yielding the title compound as a colorless solid (10 mg, 0.02 mmol, 14 %). ^{1}H-NMR (600 MHz, DMSO-d_6): δ/ppm = 7.39 – 7.22 (m, 5H), 4.61 – 4.37 (m, 3H), 4.29 – 4.13 (m, 2H), 3.56 – 3.49 (m, 5H), 3.31 – 3.21 (m, 4H), 1.70 – 1.54 (m, 7H), 1.53 – 1.39 (m, 2H), 1.36 – 1.27 (m, 1H), 1.21 – 1.01 (m, 4H), 0.98 – 0.74 (m, 4H). ^{13}C-NMR (150 MHz, DMSO-d_6): δ/ppm = 207.9, 175.6, 173.9, 157.5, 138.0, 128.4, 127.6, 72.3, 68.9, 66.0, 55.8, 52.1, 51.3, 44.1, 33.4, 31.6, 29.5, 26.2, 25.7, 25.5. Mp: 59–61 °C. $[\alpha]_D^{22}$ = 14 (*c* 1.00, MeOH). MS (ESI) *m/z* calculated for $[C_{25}H_{38}N_3O_6]^+$ ($[M+H]^+$): 476.3, found: 476.2, Purity: 99 %.

5 Project 2: Reactivity and Selectivity of Protease Inhibitors with varying Warheads

5.1 Investigation of the Compatibility between Warheads and Peptidomimetic Sequences of Protease Inhibitors—A Comprehensive Reactivity and Selectivity Study

5.1.1 Context, Project Summary, and Own Contributions

The covalent binding mode of peptidomimetic protease inhibitors comprises many advantages over non-covalent inhibitors like prolonged residence times and better pharmacodynamic properties, but also some risks as toxicity and haptenization due to off-target reactions. The correct combination between a non-covalent peptidomimetic sequence suited for the target protease and a warhead with fine-tuned reactivity towards the nucleophilic amino acid in the active site is of upmost importance during drug design campaigns.

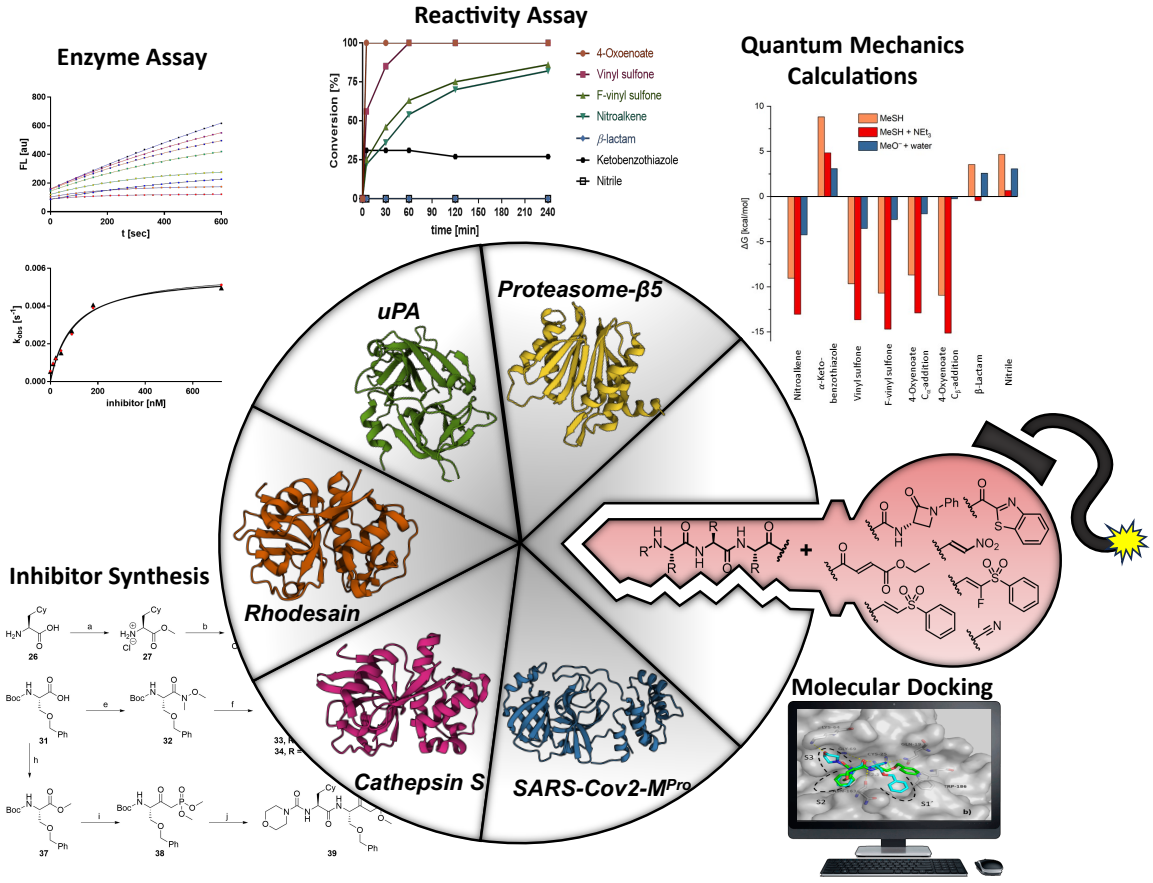

Figure 20: Aim and scope of the present publication: After successful inhibitor synthesis, a combination of enzyme assays, reactivity assays, quantum mechanics calculations and molecular docking helps revealing reactivity and selectivity profiles of several peptidomimetic inhibitors and model electrophiles.

To date, there have been several studies mainly focusing on exchanging the warhead of a model peptide and analyzing the resulting inhibition potency towards a specific target.[202,256–258] The literature lacks a comprehensive study, covering the selectivity profiles of several protease inhibitors with varying warheads against different proteases.

In this project, by selecting five medicinally relevant proteases and seven classic peptidomimetic recognition units combined with suitable warheads to address each protease individually, cross-target reactivity and the resulting selectivity were investigated. The peptidomimetic sequences were decorated with a set of warheads with at least one warhead known to react with at least one of the nucleophilic amino acids inside the active site of the selected proteases to generate covalent binders. The proteases investigated in this study consisted of two papain-like cysteine proteases (catS and rhodesain), one 3-chymotrypsin-like cysteine protease ($3CL^{pro}$), namely the SARS-CoV-2 main protease (M^{pro}), one serine protease (uPA), and a threonine protease (β-5 subunit of the human 20S proteasome).[135,259–262] The various warheads for cross reactivity assessments consisted of nitriles, nitroalkenes, (fluoro-)vinylsulfones, α-ketobenzothiazoles, 4-oxoenoates and β-lactams.[157,159,263–266]

Based on the in vitro results, the choice of the peptidomimetic sequence played an important role in the selectivity towards the tested proteases. The selectivity profiles of the M^{pro} and the uPA revealed inhibitory potency only for the inhibitors with the suited peptidomimetic sequence. Additionally, a suitable warhead was needed to generate a highly affine inhibitor while maintaining selectivity. Structurally similar proteases like rhodesain and catS did not discriminate between the used peptidomimetic sequences, resulting in inhibitors with cross-reactivity in almost all cases, if an appropriate warhead was used. For both proteases the most potent inhibitors, namely the nitrile with the peptidomimetic catS sequence and the nitroalkene with the peptidomimetic rhodesain sequence led to inhibitors with high potency while at least to some degree remaining selective towards the protease they were designed for, indicating the importance of combining a suitable peptidomimetic sequence with a fitting warhead.

The warheads were further investigated by NMR and LC-MS reactivity assays against serine / threonine and cysteine model nucleophiles to evaluate chemoselectivity. The results confirmed high reactivities for the 4-oxoenoate and (fluoro-)vinylsulfone warheads towards a deprotonated thiol model nucleophile. In agreement with the enzyme assay results, the α-ketobenzothiazole demonstrated to be a potent electrophilic trap for both cysteine and serine proteases and the nucleophilic thiol and ethanolate models.

The results of the reactivity assays were overall confirmed by quantum mechanics calculations of similar model nucelophiles MeSH/ MeS^-/ MeO^- (methanethiol/-ate and methanolate) with the isolated warheads, indicating high reactivities (exergonic reaction energies) for most warheads with MeSH and MeS^-. For the (fluoro-)vinylsulfones and the nitroalkene warhead which did not show reactivity in the reactivity assay but were calculated to react with both MeSH and MeS^-, analyzing the whole reaction

path including the activation barriers and determining the reaction kinetics was important, since for these warheads the question whether a reaction takes place could not by explained solely by thermodynamics. The differences in the reactivity between PhEtSH and $PhEtS^-$ for the (fluoro-)vinylsulfone, and nitroalkene warheads was attributed to a significant reduction in activation barriers caused by proton transfer from the nucleophile to the base prior to the nucleophilic attack.

Finally non-covalent docking simulations led to reasonable docking poses for all inhibitors, which were similar to the co-crystallized reference ligands, indicating that the peptidomimetic sequences have similar orientations inside the active sites. Except for the β-lactams, all warheads were found to be in close proximity to the nucleophilic catalytic amino acids in the active site.

Mergim Meta[‡], Patrick Müller[‡], J. Laurenz Meidner[‡], Marvin Schwickert, Jessica Meyr, Kevin Schwickert, Christian Kersten, Collin Zimmer, Stefan Hammerschmidt, Ariane Frey, Albin Lahu, Sergio de la Hoz-Rodríguez, Laura Agost-Beltrán, Santiago Rodríguez, Kira Diemer, Wilhelm Neumann, Florenci V. Gonzàlez, Bernd Engels, Tanja Schirmeister. "Investigation of the Compatibility between Warheads and Peptidomimetic Sequences of Protease Inhibitors—A Comprehensive Reactivity and Selectivity Study". *Int. J. Mol. Sci.* **2023**, *24*(8), 7226, doi: 10.3390/ijms24087226.

Own contributions: Design of the study, inhibitor synthesis (**20**, **23**, **24**, **26–49**), and reactivity probes **108**, **111** and **117** with precursors (**51**, **52**, **116**), molecular modeling and docking of all inhibitors, SAR analysis, reactivity study, fluorometric enzyme assays of all inhibitors against catS, writing of the original draft, and manuscript editing.

Contributions from other authors: Inhibitor synthesis (all other inhibitors), reactivity study, fluorometric assays against all proteases except catS, quantum mechanics simulations, writing parts of the original draft, and manuscript editing.

This work has been published in: International Journal of Molecular Sciences.

The appended Supporting Information represents an abridged version. The full Supporting Information can be accessed online at doi: 10.3390/ijms24087226.

5.1.2 Publication

The following publication quoted within "" from page 111 to page 139 is the same as the manuscript cited on page 110.

“

International Journal of *Molecular Sciences*

MDPI

Article

Investigation of the Compatibility between Warheads and Peptidomimetic Sequences of Protease Inhibitors—A Comprehensive Reactivity and Selectivity Study

Patrick Müller [1,†], Mergim Meta [1,†], Jan Laurenz Meidner [1,†], Marvin Schwickert [1], Jessica Meyr [2], Kevin Schwickert [1], Christian Kersten [1], Collin Zimmer [1], Stefan Josef Hammerschmidt [1], Ariane Frey [1], Albin Lahu [1], Sergio de la Hoz-Rodríguez [3], Laura Agost-Beltrán [3], Santiago Rodríguez [3], Kira Diemer [2], Wilhelm Neumann [2], Florenci V. Gonzàlez [3], Bernd Engels [2] and Tanja Schirmeister [1,*]

[1] Institute of Pharmaceutical and Biomedical Sciences, Johannes Gutenberg University Mainz, Staudinger Weg 5, D-55128 Mainz, Germany
[2] Institute of Physical and Theoretical Chemistry, Julius-Maximilians-University of Wuerzburg, Emil-Fischer-Straße 42 Süd, D-97074 Wuerzburg, Germany
[3] Departament de Química Inorgànica i Orgànica, Universitat Jaume I, 12080 Castelló de la Pana, Spain
* Correspondence: schirmei@uni-mainz.de; Tel.: +49-6131-39-25742
† These authors contributed equally to this work.

Abstract: Covalent peptidomimetic protease inhibitors have gained a lot of attention in drug development in recent years. They are designed to covalently bind the catalytically active amino acids through electrophilic groups called warheads. Covalent inhibition has an advantage in terms of pharmacodynamic properties but can also bear toxicity risks due to non-selective off-target protein binding. Therefore, the right combination of a reactive warhead with a well-suited peptidomimetic sequence is of great importance. Herein, the selectivities of well-known warheads combined with peptidomimetic sequences suited for five different proteases were investigated, highlighting the impact of both structure parts (warhead and peptidomimetic sequence) for affinity and selectivity. Molecular docking gave insights into the predicted binding modes of the inhibitors inside the binding pockets of the different enzymes. Moreover, the warheads were investigated by NMR and LC-MS reactivity assays against serine/threonine and cysteine nucleophile models, as well as by quantum mechanics simulations.

Keywords: covalent inhibitors; in vitro study; protease inhibitors; peptidomimetic sequence; warhead; reactivity and selectivity study

Citation: Müller, P.; Meta, M.; Meidner, J.L.; Schwickert, M.; Meyr, J.; Schwickert, K.; Kersten, C.; Zimmer, C.; Hammerschmidt, S.J.; Frey, A.; et al. Investigation of the Compatibility between Warheads and Peptidomimetic Sequences of Protease Inhibitors—A Comprehensive Reactivity and Selectivity Study. *Int. J. Mol. Sci.* **2023**, *24*, 7226. https://doi.org/10.3390/ijms24087226

Academic Editor: Raffaele Capasso

Received: 24 March 2023
Revised: 6 April 2023
Accepted: 10 April 2023
Published: 13 April 2023

1. Introduction

The human organism expresses about 600 different proteases falling into five different catalytic classes: aspartic, cysteine, metallo, serine and threonine proteases [1,2]. With their ability to catalyze irreversible protein hydrolysis, these members of the degradome manage the functions of many proteins through various mechanisms, such as activating or inactivating, e.g., growth factors, cytokines and other enzymes. As a result, they play an important role in physiological and developmental processes. These include DNA replication, cell proliferation and differentiation, but also tissue remodeling and neuronal outgrowth [3,4]. Due to their essential roles in such vital processes, dysregulation of these proteins causes severe pathologic conditions, such as cancer and neurodegenerative or cardiovascular disorders [5,6]. Furthermore, proteases play a key role in infectious diseases of, for example, parasitic or viral origin. African trypanosomiasis, also called sleeping sickness, and Chagas disease are caused by parasites and are classified as neglected tropical diseases and constitute important health issues in Latin American and Sub-Saharan African countries. For both diseases, proteases have been identified, which are essential for the

development of the parasites and the progression of the disease [7,8]. The 2019–2020 coronavirus (SARS-CoV-2) outbreak is the most recent example of a viral disease with global impact and burden. The viral replication and spreading is associated with proteases playing crucial roles in the viral life cycle, turning them into valid targets for the design of new anti-infectives [9,10].

Over the course of time, various protease inhibitors have been discovered either by targeted design or serendipity. Depending on the target binding site and inhibition mechanism, the molecular structures vary significantly. These range from small molecules to macrocyclic drugs and from non-covalent to covalent inhibition types [11–13]. Until recently, covalent modifiers which consist of an electrophilic trap (warhead) were controversially discussed as therapeutics due to the possibility of unselective reactions with off-target proteins and associated immunogenicity and toxicity. These compounds are emerging as potential drugs due to various inherent advantages, such as longer residence times and an accompanying lower drug dosage necessary for effective therapy [14]. There are many covalent drugs that have been approved, including some protease inhibitors, such as the proteasome inhibitors bortezomib or carfilzomib, for treatment of multiple myeloma, which inhibit the proteasome's β5-subunit in an irreversible manner, due to the permanent covalent bond to the catalytically active Thr-1. On the other hand, the nitriles saxagliptin and vildagliptin for treatment of type 2 diabetes and the recent first-approved cysteine protease inhibitor nirmatrelvir for treatment of COVID-19 bind covalent-reversibly to their target proteases, due to the decomposition of the (thio)-imidate adduct formed between the inhibitor and the amino acid of the protease, which is preferable since covalent-reversible inhibition leads to a lower risk of haptenization and binding to off-targets [15–17].

The binding of such covalent protease inhibitors proceeds in two stages. A peptidic or peptidomimetic recognition sequence is mainly responsible for the non-covalent interactions (first step) with the substrate binding pockets. It mainly determines the selectivity profile of the inhibitor towards the protease of interest, due to polar and non-polar interactions between the peptidic residues and the enzyme sub pockets. In the second step, the reaction between the warhead and an active site amino acid residue leads to the formation of a covalent bond, either reversibly or irreversibly, between the drug and the enzyme. This step mainly determines the affinity of the inhibitor to the target protease [14,18]. However, the warhead must be suitable for the respective nucleophilic amino acid residue in the active site. Depending on the type of nucleophile, different warheads can be used to target thiol or hydroxy groups of amino acid residues. Functional groups, such as β-lactams, but also boronic acids, which are all considered hard electrophiles with regard to the HSAB theory, are warheads targeting mainly serine and threonine-based proteases. Unsaturated, vinylogous Michael-acceptor-like structures, which are considered soft electrophiles, preferably react with cysteine proteases [18–21]. There are also warheads, e.g., ketones, aldehydes and nitriles, that are similarly suitable for serine-, threonine- and cysteine-based proteases [22–25]. Thus, exchanging the warhead can lead to different reactivity and affinity profiles, and alterations to the peptidomimetic/peptidic sequence may affect the selectivity of an inhibitor.

Within this extensive systematic study, we selected peptidomimetic sequences specifically to ensure a high affinity towards the protease of interest, which will be discussed below. We collected information about different kinds of warheads regarding their electrophilic properties and inhibition mechanisms to obtain a well-balanced assortment to potentially target cysteine and serine-/threonine proteases and combined them with the sequences (Figure 1) [18,21,22,24]. In vitro testing of all inhibitors on every target, first with the suited peptidomimetic sequence with differing warheads for their on-target and afterwards towards the off-target proteases, revealed the impact of the peptidomimetic sequences and the warheads on affinity and selectivity. The results indicate that, depending on the protease, every tested warhead behaved differently. The experimental results were compared with molecular docking results, visualizing putative binding modes in order to achieve a better understanding of the characteristics of the tested compounds.

Additionally, a reactivity study was carried out using model compounds containing the seven different warhead types, which were reacted with hydroxy and thiol model nucleophiles representing serine, threonine and cysteine proteases. Quantum mechanical computations of the reactions between the warheads and model nucleophiles were used to explain the experimental reactivity test data. These data highlight the preference of the warheads for specific active site residues.

To our knowledge, this is the first systematic study of this extent to evaluate the inhibition properties of peptidomimetic inhibitors with different warheads described in the literature, including in vitro testing towards a series of selected proteases, reactivity tests of the warheads in solution with model nucleophiles and in silico studies (docking and quantum mechanics and kinetic simulations) to explain the experimentally obtained data.

For our studies, the urokinase-type plasminogen activator (uPA) was chosen as a serine, the β5-subunit of the proteasome as a threonine and human cathepsin S (CatS), SARS-CoV-2 main protease (M^{pro}) and *T. brucei* rhodesain (TbCatL) as representatives of cysteine proteases.

The uPA belongs to the trypsin-like serine protease superfamily and contains a catalytic triad consisting of Ser195, His57 and Asp102 [26]. The enzyme is involved in several physiological functions, such as the degradation of the extracellular matrix (ECM), cell migration and thrombolysis [27,28]. Dysregulation of the uPA is involved in the metastasis of several cancer species [29]. We chose Ac–(L)Gly–(L)Thr–(L)Ala–(L)Arg–(warhead) as the specific peptidomimetic sequence for the uPA-inhibitors because of its high selectivity, which has been reported in the literature [30].

The 20S proteasome is responsible for most of the protein degradation in cells but can also lead to cancer by dysfunction [31]. It consists of three β-subunits (β1, β2 and β5), each containing a catalytic threonine. Here, we focus on the β5-subunit with the catalytic triad Thr1, Lys33 and Asp17, as it has the greatest impact on the proteolytic activity of the 20S proteasome. We selected the peptidomimetic sequence of bortezomib Pyz–(L)Phe–(L)Leu–(warhead) because of its clinically proven properties as a potent drug [32].

As cysteine proteases, we chose CatS, M^{pro} and rhodesain. Since CatS and rhodesain are both members of the papain family, they would allow a closer examination of the selectivity of the tested inhibitors towards related proteases [33]. CatS contains a catalytic dyad consisting of Cys25 and His164 [34]. It is partly tethered at the cell surface and involved in tissue remodeling, which can lead to cancer cell growth and spreading [35]. We utilized the peptidomimetic sequence morpholine–(L)cyAla–(L)Ser(OBn)–(warhead) which has been reported in the literature because of its described affinity and selectivity properties [36].

In contrast to the aforementioned proteases, rhodesain and M^{pro} do not originate from the human organism but play significant roles in the progression of infectious diseases. Rhodesain is essential for the development of the parasite *Trypanosoma brucei rhodesiense*, which is responsible for the sleeping sickness "Human African Trypanosomiasis". Analogously to CatS, it contains a catalytic dyad consisting of Cys25 and His159 [37]. There are various peptidomimetic sequences that have been published for rhodesain inhibitors. We decided to utilize Cbz–(L)Phe–(L)*h*Phe–(warhead), as it is a commonly used sequence with great affinity and selectivity [38]. M^{pro} originates from SARS-CoV-2 and plays a key role in the virus replication. The active site contains Cys145 and His164 as a catalytic dyad [39]. Similar to the newly published M^{pro} inhibitors, we chose 4-(OMe)-1*H*-indole–(L)Leu–3-[(3*S*)-2-oxopyrrolidin-3-yl]-(L)Ala–(warhead) as the general structure [40]. All peptidomimetic sequences and warheads are illustrated in Figure 1.

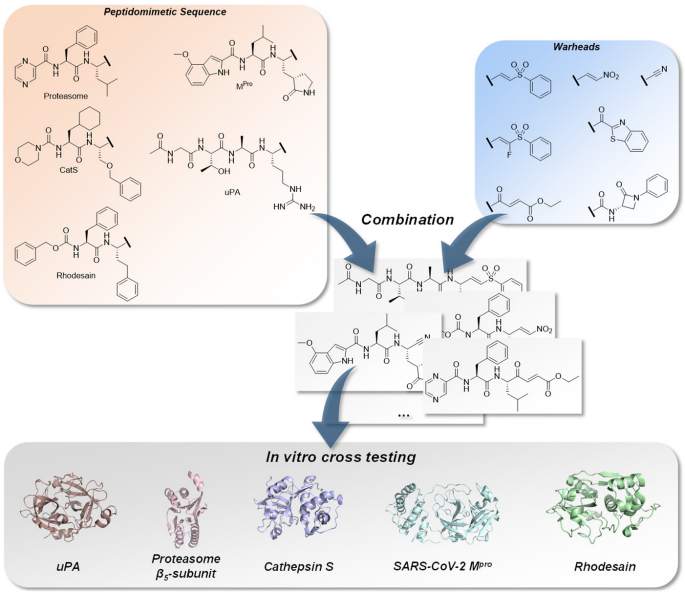

Figure 1. Combination of characteristic peptidomimetic inhibitor sequences for the targets: urokinase-type plasminogen activator (uPA), PDB-ID: 1W10 [41], proteasome β5-subunit, PDB-ID: 5LF3 [42], cathepsin S, PDB-ID: 1MS6 [43], SARS-CoV-2 main protease (M^{pro}), PDB-ID: 6XR3 [44] and rhodesain, PDB-ID: 2P7U [45], with selected warheads (vinyl sulfone, F-vinyl sulfone, nitroalkene, α-ketobenzothiazole, 4-oxoenoate, nitrile and β-lactam). The resulting compounds were tested on each target to determine affinity and selectivity.

2. Results

2.1. Chemistry

2.1.1. Synthesis of Precursors

All tested substances were synthesized in multi-step reactions [19,21]. Regarding the synthesis of the (F-)vinyl sulfone and β-lactam compounds, the same precursor molecules were used repeatedly. The preparation of these precursors is shown in Scheme 1.

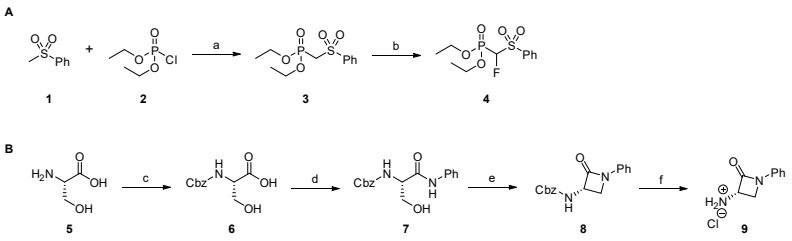

Scheme 1. Synthesis of precursor molecules. (**A**) Synthesis of phosphonate building block **4**. (**B**) Synthesis of β-Lactam building block **9**. Reaction conditions: (a) *n*-BuLi, DECP, THF, −78 °C; (b) **3**, LHMDS, Selectfluor®, THF, DMF, −78 °C, 3 h, 49%; (c) Cbz-Cl, $NaHCO_3$, H_2O, 12 h, rt, 90%; (d) aniline, TBTU, HOBt · H_2O, EtOAc, 12 h, rt, 74%; (e) $ImSO_2$, NaH, DMF, F20 °C, 1.5 h, 77%; (f) Pd/C, H_2, THF, 88%.

In a substitution reaction on diethyl chlorophosphate (DECP) **2** using methyl phenyl sulfone **1** and *n*-butyllithium (*n*-BuLi), the phosphonate **3** was prepared. Subsequent fluorination of **3** with Selectfluor® led to phosphonate **4**. These precursors were used for the synthesis of vinyl sulfone warheads.

The synthesis of the *β*-lactam precursor **9** was conducted from L-serine. Benzyloxycarbonyl (Cbz) protection followed by amide coupling of the free carboxylic acid moiety with aniline led to the intermediate **7**. The following cyclisation was performed using 1,1′-sulfonyldiimidazol ($ImSO_2$) and sodium hydride (NaH). Cbz deprotection with hydrogen and palladium on carbon (Pd/C) yielded precursor **9**.

2.1.2. Rhodesain Inhibitors

The synthesis of substances with the targeting structure designed for rhodesain was conducted according to Scheme 2.

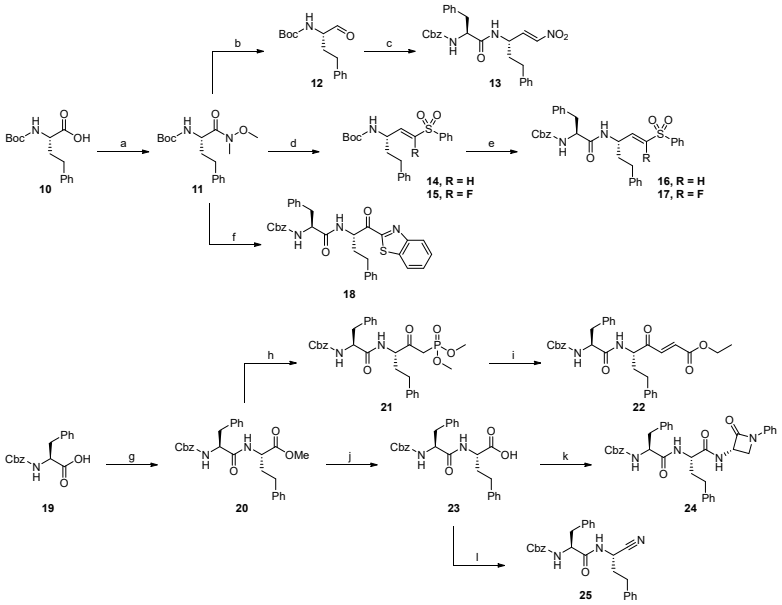

Scheme 2. Synthesis of rhodesain compounds. Reaction conditions: (a) *N*,*O*-dimethylhydroxylamine · HCl, DCC, HOBt · H_2O, DIPEA, THF, rt, 12 h, 46%; (b) LAH, THF, 0 °C, 2 h, 67%; (c) 1. $MeNO_2$, Et_3N, DCM, rt, 8 h, 2. TFA, DCM, rt, 0.5 h, 3. Cbz-(L)Phe-OH, EDC · HCl, TEA, DCM, rt, 12 h, 4. MsCl, DIPEA, DCM, rt, 2 h, 75%; (d) **3**/**4**, LiHMDS, THF, −80 °C, 12 h, 59% (**14**), 57% (**15**); (e) TFA, DCM, Cbz-(L)Phe-OH, T3P, DIPEA, DMF, rt, 12 h, 65% (**16**), 48% (**17**); (f) 1. benzothiazole, *n*-BuLi, THF, −78 °C, 3 h, 2. TFA, DCM, rt, 2 h, 3. Cbz-(L)Phe-OH, EDC · HCl, HOBt · H_2O, Et_3N, DCM, rt, 8 h, 56%; (g) H-(L)*h*Phe-OMe, HATU, 2,4,6-collidine, DCM/DMF, rt, 16 h, quant.; (h) DMMP, *n*-BuLi, THF, –70 °C, 2 h, 98%; (i) ethyl glyoxylate, K_2CO_3, EtOH, rt, 2 h, 76%; (j) LiOH, THF/H_2O, rt, 16 h, quant.; (k) **9**, HATU, 2,4,6-collidine, DCM/DMF, rt, 16 h, 67%; (l) 1. EDC · HCl, HOBt · H_2O, NH_4OH, DMF, rt, 12 h, 2. TFAA, pyridine, DMF, 0 °C, 0.1 h, 40%.

The first step of the synthesis of rhodesain inhibitors was the conversion of Boc-(L)*h*Phe-OH **10** into Weinreb amide **11**. From this intermediate, the nitroalkene inhibitor **13** was accessible by reduction to aldehyde **12** and subsequent Henry reaction followed by standard deprotection and amide coupling to connect the P2-P3 residues. In a similar way, the vinyl sulfone **16** and F-vinyl sulfone **17** were obtained, whereby the aldehyde **12** was used in a Horner–Wadsworth–Emmons (HWE) reaction with the precursors **3** and **4**

followed by the attachment of the P2-P3 residues. The α-ketobenzothiazole inhibitor **18** was prepared by alkylation of the Weinreb amide **11** with benzothiazole and subsequent attachment of the P2-P3 residues. Starting from Boc-(L)*h*Phe-OH, the methyl ester **20** was prepared by amide coupling. A following alkylation with dimethyl methylphosphonate (DMMP) and HWE reaction with ethyl glyoxylate led to the 4-oxoenoate **22**. For the synthesis of β-lactam **24**, hydrolysis of methyl ester **20** and amide coupling with precursor **9** yielded the desired product. Nitrile **25** was prepared from carboxylic acid **23** via amide coupling with ammonia followed by dehydration.

2.1.3. Cathepsin S Inhibitors

Compounds designed for the inhibition of cathepsin S were synthesized according to Scheme 3.

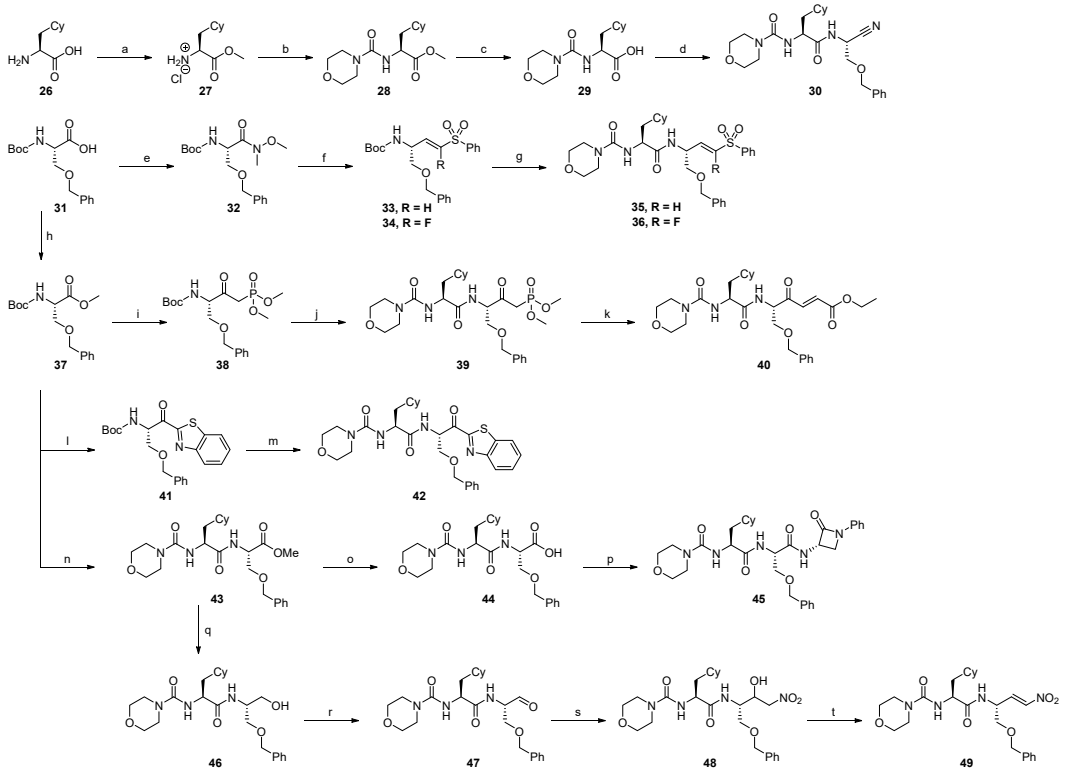

Scheme 3. Synthesis of cathepsin S compounds. Reaction conditions: (a) $SOCl_2$, MeOH, –10 °C, 16 h, 91%; (b) morpholine, triphosgene, $NaHCO_3$, $CHCl_2$, 0 °C; 16 h, 98%; (c) LiOH, THF/H_2O, 3 h, 97%; (d) 1. NaCN, NH_4Cl, NH_3, 2-(benzyloxy)acetaldehyde, Et_2O, 2. HATU, 2,4,6-collidine, DCM/DMF, rt, 16 h, 53%; (e) *N*,*O*-dimethylhydroxylamine · HCl, DCC, HOBt · H_2O, DIPEA, THF, –15–0°C, 16 h, 80%; (f) 1. LAH, Et_2O, 0 °C, 2 h, 2. **3**/**4**, KHMDS/ LHMDS, THF, –78 °C, 3 h; 75% (**33**), 44% (**34**); (g) 1. 4 N HCl in 1,4-dioxane, 2. **29**, HATU, collidine, DCM/DMF, rt, 16 h, 63% (**35**), 60% (**36**); (h) MeI, DMF,

0 °C, 16 h, 97%; (i) *n*-BuLi, DMMP, THF, –78 °C, 3 h, 79%; (j) 1. 4 N HCl in 1,4-dioxane, 2. **29**, HATU, 2,4,6-collidine, DCM/DMF, rt, 16 h, 52%; (k) LiCl, ethyl glyoxylate, DIPEA, MeCN, 0 °C, 2 h, 39%; (l) benzothiazole, *n*-BuLi, THF, –78 °C, 3 h, 38%; (m) 1. 4 N HCl in 1,4-dioxane, 2. **29** HATU, 2,4,6-collidine, DCM/DMF, rt, 16 h, 43%; (n) 1.4 N HCl in 1,4-dioxane, 2. **29**, HATU, collidine, DCM/DMF, rt, 16 h, 90%; (o) LiOH, THF/H_2O, rt, 3 h, 99%; (p) **9**, HATU, 2,4,6-collidine, DCM/DMF, rt, 16 h, 81%; (q) $NaBH_4$, MeOH, THF, 0 °C, 16 h, 91%; (r) Dess–Martin–Periodinan, DCM, rt, 16 h, 70%; (s) NaH, $MeNO_2$, THF, 0 °C, 1 h, 58%; (t) MsCl, Et_3N, DCM, 0 °C, 3 h, 45%.

For the synthesis of cathepsin S inhibitors, the P2–P3 intermediate **29** was used repeatedly. It was prepared by attaching a morpholino-urea residue to cyclohexyl alanine **26** followed by hydrolysis of the methyl ester. In a direct conversion from **29**, the nitrile inhibitor **30** was prepared by amide coupling with ammonia and dehydration. From Boc-(L)Ser(OBn)-OH **31**, the vinyl sulfone **35** and F-vinyl sulfone **36** were obtained by conversion into Weinreb amide **32** followed by reduction, HWE reaction with the precursors **3** and **4** and subsequent standard deprotection and amide coupling with intermediate **29**. Boc-(L)Ser(OBn)-OH **31** was also converted into the methyl ester **37**, which was used for the synthesis of the 4-oxoenoate **40**. Therefore, an alkylation with DMMP and subsequent introduction of the P2 and P3 residues by deprotection and amide coupling led to the phosphonate intermediate **39**, which was converted into the desired product by HWE reaction with ethyl glyoxylate. The α-ketobenzothiazole **42** was prepared from methyl ester **37** in an alkylation reaction with benzothiazole and attachment of the P2-P3 residues by deprotection and amide coupling with intermediate **29**. Starting from methyl ester **37**, deprotection and amide coupling with intermediate **29** led to the methyl ester intermediate **43**, which was converted into the β-lactam **45** by hydrolysis and amide coupling with precursor **9**. The nitroalkene **49** also was prepared from methyl ester **43** by firstly converting it to the alcohol **46** and then to aldehyde **47**, which was used in a Henry reaction with nitromethane and subsequent dehydration.

2.1.4. Proteasome β5-Subunit Inhibitors

Compounds designed for the inhibition of the proteasome β5-subunit were synthesized according to Scheme 4.

The synthesis of proteasome β5-subunit targeting compounds started from Boc-(L)Leu-OH **50**, which was converted into the Weinreb amide **51**. From this, the F-vinyl sulfone **55** was prepared by reduction to aldehyde **52** and subsequent HWE reaction followed by a standard deprotection and amide coupling procedure connecting the P2 and P3 residues. For the vinyl sulfone inhibitor **58**, a different route was taken. First, the Weinreb amide intermediate **56** containing the P2 and P3 residues was prepared by standard amide coupling. Subsequent reduction and HWE reaction led to the desired inhibitor. The Weinreb amide **57** was also the intermediate for nitroalkene **59**, which was prepared by reduction and Henry reaction with subsequent dehydration. From Weinreb amide **51**, the α-ketobenzothiazole moiety was introduced by alkylation. The attachment of the P2 and P3 residues by standard deprotection and amide coupling yielded the α-ketobenzothiazole **62**.

The 4-oxoenoate inhibitor **68** was prepared by HWE reaction of ethyl glyoxylate with the phosphonate intermediate **67**. The latter was synthesized by starting with the Boc protection of H-(L)Leu-OMe · HCl **63**, followed by alkylation of the methyl ester with DMMP and successive deprotection/amide coupling to introduce the P2 and P3 residues. In the same way, the introduction of the P2 and P3 residues to H-(L)Leu-OMe · HCl **63** led to the methyl ester intermediate **70**, from which the β-lactam **72** was prepared by hydrolysis and subsequent amide coupling with precursor **9**. Methyl ester **70** was also converted into the nitrile **74** by ammonolysis and dehydration.

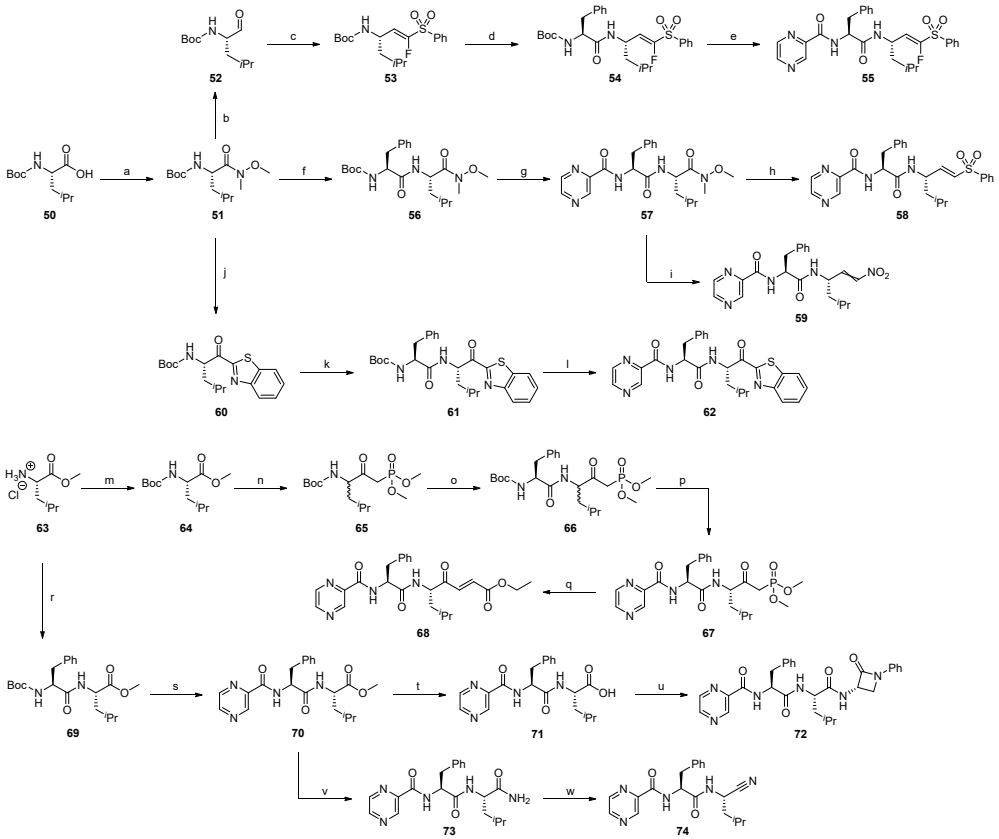

Scheme 4. Synthesis of proteasome β5-subunit compounds. Reaction conditions: (a) *N*,*O*-dimethylhydroxylamine · HCl, TBTU, HOBt · H_2O, 2,4,6-collidine, DCM, 0–20 °C, 16 h, 86%; (b) LAH, THF, 0 °C, 30 min, 29%; (c) **4**, LiCl, DBU, MeCN, 0 °C, 1 h, 80%; (d) 1. 4 N HCl in 1,4-dioxane, rt, 1 h, 2. Boc-Phe-OH, TBTU, HOBt · H_2O, 2,4,6-collidine, DCM, 0 °C, 16 h, 97%; (e) 1. 4 N HCl in 1,4-dioxane, rt, 1.5 h, 2. pyrazinoic acid, TBTU, HOBt · H_2O, 2,4,6-collidine, DCM, 0 °C, 16 h, 67%; (f) 1. 4 N HCl in 1,4-dioxane, rt, 1 h, 2. Boc-(L)Phe-OH, TBTU, HOBt · H_2O, 2,4,6-collidine, DCM, 0–20 °C, 16 h, 97%; (g) 1. 4 N HCl in 1,4-dioxane, rt, 1 h, 2. pyrazinoic acid, TBTU, HOBt · H_2O, 2,4,6-collidine, DCM, 0–20 °C, 16 h, 88%; (h) 1. LAH, THF, 0 °C, 1 h, 2. **3**, LiCl, DBU, MeCN, 0 °C, 1.5 h, 11%; (i) 1. LAH, THF, 0 °C, 1 h, 2. $MeNO_2$ Et_3N, DCM, 0–20 °C, 16h, 3. MsCl, DIPEA, DCM, rt, 3 h, 19%; (j) benzothiazole, *n*-BuLi, THF, –78 °C, 6 h, 65%; (k) 1. 4 N HCl in 1,4-dioxane, rt, 1 h, 2. Boc-(L)Phe-OH, TBTU, HOBt · H_2O, 2,4,6-collidine, DCM, 0–20 °C, 16 h, 68%; (l) 1. 4 N HCl in 1,4-dioxane, rt, 1 h, 2. pyrazinoic acid, TBTU, HOBt · H_2O, 2,4,6-collidine, DCM, 0–20 °C, 16 h, 53%; (m) Boc_2O, $NaHCO_3$, water, 1,4-dioxane, 3 h, rt, 99%; (n) *n*-BuLi, THF, –78 °C, 6 h, 88%; (o) 1. 4 N HCl in 1,4-dioxane, rt, 1 h, 2. Boc-(L)Phe-OH, TBTU, HOBt · H_2O, 2,4,6-collidine, DCM, DMF, 0–20 °C, 16 h, 72%; (p) 1. 4 N HCl in 1,4-dioxane, rt, 1 h, 2. pyrazinoic acid, TBTU, HOBt · H_2O, 2,4,6-collidine, DCM, DMF, 0–20 °C, 16 h, 66%; (q) ethyl glyoxylate, LiCl, DIPEA, MeCN, 1 h, 0 °C, 79%; (r) Boc-(L)Phe-OH, TBTU, HOBt · H_2O, 2,4,6-collidine, DCM, 0–20 °C, 16 h, 82%; (s) 1. 4 N HCl in 1,4-dioxane, rt, 1 h, 2. pyrazinoic acid, TBTU, HOBt · H_2O, 2,4,6-collidine, DCM, 0–20 °C, 16 h, 82%; (t) LiOH, water, THF, rt, 17 h, quant.; (u) **9**, TBTU, HOBt · H_2O, 2,4,6-collidine, DCM, 0–20 °C, 16 h, 65%; (v) 7 N NH_3 in MeOH, rt, 48 h, 89%; (w) cyanuric chloride, DMF, 0 °C, 48 h, 47%.

2.1.5. SARS-CoV-2 M^{pro} Inhibitors

Compounds designed for the inhibition of SARS-CoV-2 M^{pro} were synthesized according to Scheme 5.

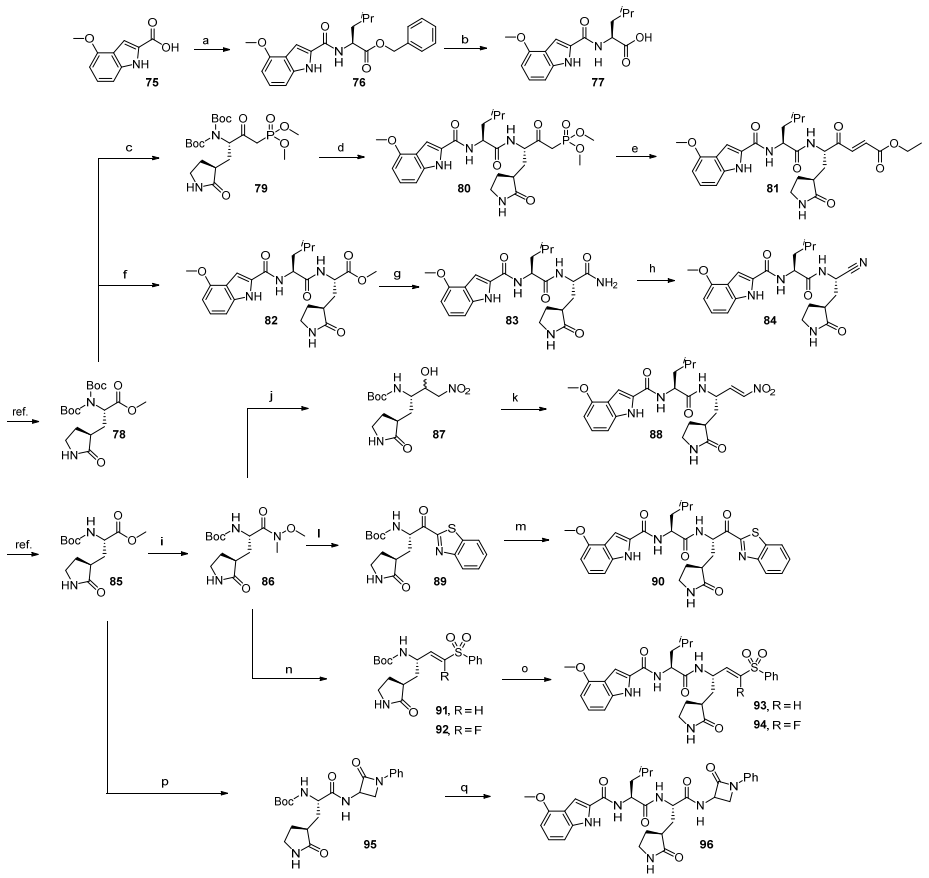

Scheme 5. Synthesis of SARS-CoV-2 M^{pro} compounds. Reaction conditions: (a) H-(L)Leu-OBn · *p*TsOH, TBTU, DIPEA, DCM, 0–20 °C, 16 h, 93%; (b) H_2, Pd/C (10%), EtOH, quant.; (c) DMMP, *n*-BuLi, THF, –78 °C, 5 h, 24%; (d) 1. TFA, DCM, 0 °C, 3 h, 2. **77**, EtOCOCl, NMM, THF, –20 °C, 2 h, 40%; (e) ethyl glyoxylate, LiCl, DIPEA, MeCN, 0 °C, 2 h, 47%; (f) 1. TFA, DCM, 0 °C, 3 h, 2. **77**, HATU, 2,4,6-collidine, DMF, 0–20 °C, 16 h, 83%; (g) 1. LiOH, THF/H_2O, 0–4 °C, 16 h, 2. NH_4OH, HATU, OxymaPure®, 2,4,6-colllidine, DMF, 0–20 °C, 16 h, 65%; (h) burgess reagent, DCM, rt, 2 h, 67%; (i) 1. LiOH, THF/MeOH/H_2O, 0–4 °C, 16 h, 2. *N*,*O*-dimethylhydroxylamine · HCl, HATU, 2,4,6-colllidine, DMF, 0–20 °C, 16 h, 76%; (j) 1. LAH, THF, −20 °C, 2 h, 2. $MeNO_2$, EtN_3, DCM, rt, 15 h, 71%; (k) 1. TFA, DCM, 0 °C, 3 h, 2. **77**, EDC · HCl, HOBt · H_2O, DIPEA, DCM, 0–20 °C, 16 h, 3. MsCl, DIPEA, DCM, 0–20 °C, 16 h, 50%; (l) benzothiazole, *n*-BuLi, THF, –78 °C, 5 h, 59%; (m) 1. TFA, DCM, 0 °C, 3 h, 2. **77**, EtOCOCl, NMM, THF, –20 °C, 2 h, 54%; (n) 1. LAH, THF, −20 °C, 2 h, 2. **3**/**4**, LiCl, DBU, MeCN, 0 °C, 2 h, 65% (**89**), 35% (**90**); (o) 1. TFA, DCM, 0 °C, 3 h, 2. **77**, EtOCOCl, NMM, THF, –20 °C, 2 h, 18% (**91**), 15% (**92**); (p) 1. LiOH, water, THF, 16 h, 2. **9**, TBTU, HOBt · H_2O, DIPEA, DCM, 0–20 °C, 48 h, 39%; (q) TFA, DCM, 0 °C, 3 h, 2. **77**, EtOCOCl, NMM, THF, –20 °C, 2 h, 80%.

Potential SARS-CoV-2 M^{pro} inhibitors were synthesized, starting from the rigidized glutamine analogs **78** and **85**, which had been prepared according to methods reported in the literature [46,47]. The P2–P3 residues fragment of the potential inhibitors was prepared by standard amide coupling with **75** and subsequent deprotection, yielding the intermediate **77**. From glutamine analog **78**, the 4-oxoenoate **81** was prepared by alkylation with DMMP and subsequent deprotection and amide coupling with **77** followed by HWE reaction with ethyl glyoxylate. Also starting from **78**, deprotection and amide coupling with **77** followed by hydrolysis and coupling with ammonia and subsequent dehydration yielded the nitrile inhibitor **84**. Starting with the preparation of Weinreb amide **86** from glutamine analog **85**, the nitroalkene **88** was accessible through reduction, a subsequent Henry reaction with nitromethane followed by dehydration and final deprotection and amide coupling with **77**. Introduction of the *α*-ketobenzothiazole moiety to **86** and connection of the P2–P3 residues by deprotection and coupling with **77** led to *α*-ketobenzothiazole **90**. Similarly, the reduction of **86** and HWE reaction with the precursors **3** and **4** and subsequent attachment of the P2–P3 residues yielded the vinyl sulfone **93** and F-vinyl sulfone **94**. For the *β*-lactam **96**, hydrolysis of **85** and amide coupling with precursor **9** followed by attachment of the P2–P3 residues yielded the desired product.

2.1.6. uPA Inhibitors

Compounds designed for the inhibition of the uPA were synthesized according to Scheme 6.

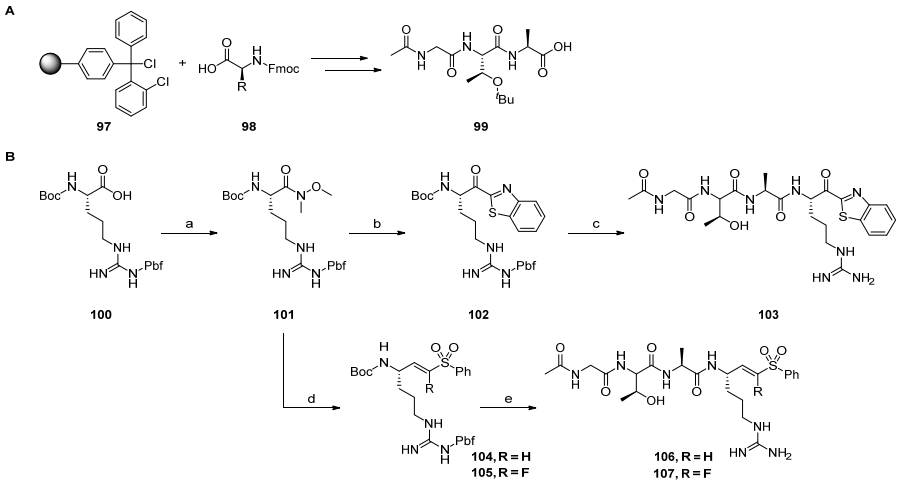

Scheme 6. Synthesis of the uPA compounds. (**A**) solid phase peptide synthesis of building block **99**. (**B**) combined synthesis of the final uPA compounds. Reaction conditions: (a) *N*,*O*-dimethylhydroxylamine· HCl, TBTU, DIPEA, DCM, rt, 12 h, 95%; (b) benzothiazole, *n*-BuLi, THF, –78 °C, 2 h, 76%; (c) 1. TFA, DCM, rt, 0.5 h, 2. HATU, DIPEA, DMF, DCM, rt, 12 h, 3. TFA, DCM, rt, 2 h, 10%; (d) 1. LAH, THF, 0 °C, 2. **3**/**4**, LiCl, DBU, MeCN, 0 °C, 1 h, 72% (**104**), 31% (**105**); (e) 1. TFA, DCM, rt, 0.5 h, 2. **99,** HATU, DIPEA, DMF, DCM, rt, 12 h, 3. TFA, DCM, rt, 2 h, 16% (**106**), 11% (**107**).

The potential uPa inhibitors are based on a peptide sequence which was synthesized via a standard Fmoc solid-phase peptide synthesis (SPPS) protocol. The obtained peptide **99** was coupled to the *α*-ketobenzothiazole intermediate **102**, which had been prepared from Boc- (L)Arg(Pbf)-OH **100** by alkylation of its Weinreb amide with benzothiazole to yield the *α*-ketobenzothiazole **103**, after deprotection. The vinyl sulfone **106** and F-vinyl sulfone **107** were prepared by reduction of Weinreb amide **101**, followed by a subsequent

HWE reaction with the precursors **104** and **105**, which were then coupled with **99** and finally deprotected. The inhibitors with the β-lactam, nitrile and 4-oxoeonoate moiety were not synthetically accessible due to the acidic conditions for the Pbf-deprotection to obtain the final inhibitors.

2.1.7. Synthesis of Reactivity Probes

Substances designed for reactivity assay were synthesized according to Scheme 7.

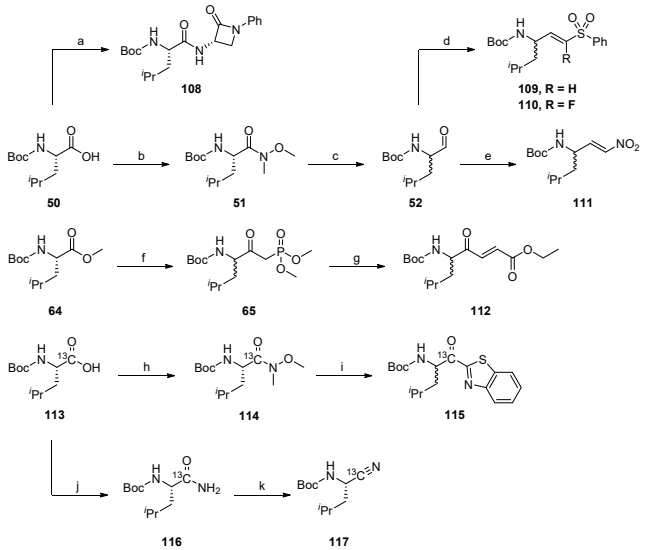

Scheme 7. Synthesis of the reactivity probes. Reaction conditions: (a) **9**, HATU, collidine, DCM, DMF, rt, 16 h, 97%; (b) TBTU, HOBt · H_2O, *N*,*O*-dimethylhydroxylamine · HCl, 2,4,6-collidine, rt, 12 h, quant.; (c) 1. LAH, Et_2O, 0 °C, 1 h, 89%; (d) **3**/**4**, LiCl, DBU, MeCN, 0 °C, 1 h, 50% (**109**), 30% (**110**); (e) 1. NaH, $MeNO_2$, THF, 0 °C, 1 h, 2. MsCl, Et_3N, DCM, 0 °C, 1 h, 15%; (f) DMMP, *n*-BuLi, THF, –78 °C, 1.5 h, 70%; (g) ethyl glyoxylate, LiCl, DBU, MeCN, 0 °C, 1 h, 45%; (h) TBTU, HOBt · H_2O, *N*,*O*-dimethylhydroxylamine · HCl, 2,4,6-collidine, 0–20 °C, 16 h, 95%; (i) benzothiazole, *n*-BuLi, THF, –78 °C, 3.5 h, 56%; (j) EDC · HCl, HOBt · H_2O, NH_4OH, DMF, rt, 16 h, 14%; (k) TFAA, pyridine, THF, –10 °C, 2 h, 74%.

For the synthesis of the reactivity probes, leucine was chosen as the model amino acid due to availability and to avoid side-chain reactivity. The different warheads were synthesized in the same way as described above for the full peptidic/peptidomimetic inhibitors. The β-lactam **108**, (F-)vinyl sulfone **109**, **110** and nitroalkene **111** reactivity probes were synthesized starting from Boc-(L)Leu-OH **50**, whereas the 4-oxoenoate **112** was prepared from Boc-(L)Leu-OMe **64**. Boc-(L)Leu-1-^{13}C-OH **113** was the starting material for the ^{13}C-labelled α-ketobenzothiazole **115** and nitrile **117** reactivity probes.

2.2. Reactivity Tests

To investigate the reactivity between the different warheads towards the three classes of proteases (serine, threonine and cysteine proteases), their behavior in model systems under the same reaction conditions (solvent, nucleophile and base) using either NMR or LC-MS analysis was investigated. We used reactivity probes with a Boc-L-Leu-(warhead) sequence. Leucin was chosen as a P1 amino acid to minimize influences of the side chain and due to synthetic accessibility. 2-Phenylethanethiol was used as a model nucleophile to mimic the thiol moiety of cysteine proteases, and sodium ethoxide was used as a ser-

ine/threonine replacement. DMSO-d_6 was used as solvent. Under these conditions, the nucleophile is deprotonated, simulating the activated serine or threonine in the catalytic triad of serine and threonine proteases, while ethanol as protonated alcohol species turned out to be unreactive in preliminary test reactions. The reactivity tests using 2-phenylethanthiol were carried out in the presence and absence of triethylamine as a base. This allowed for a reactivity comparison of the warheads towards protonated and deprotonated nucleophilic thiol species. Generating a deprotonated thiol species in the presence of triethylamine simulates the deprotonated cysteine in the catalytic dyad of cysteine proteases. Scheme 8 illustrates the reaction of the reactivity assay with both model nucleophiles and the vinyl sulfone moiety **109** as an example.

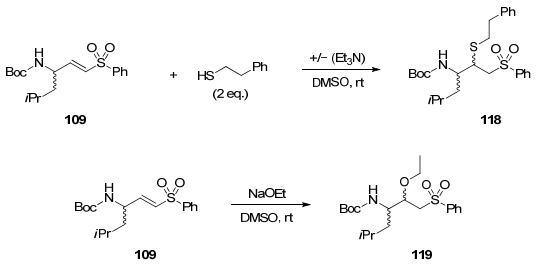

Scheme 8. Reaction scheme of the reactivity assay with both model nucleophiles under equal reaction conditions and the vinyl sulfone moiety **109**.

The reactivity tests of all Michael acceptors, **109**, **110**, **111** and **112**, the α-ketobenzothiazole **115** and nitrile **117** were investigated using an NMR-based analysis method, while the β-lactam **108** reactivity was investigated via LC-MS, due to its lack of proton signals, which could be used for evaluation of the reactivity in the ^{1}H-NMR studies, and the irreversible reaction mechanism, which allowed the LC-MS analysis. Additionally, LC-MS analyses of all reactions were performed in order to prove the formation of the expected reaction products. Formation of the expected adducts with the nitrile **117** (PhEtSH/PhEtS$^-$/EtONa), the α-ketobenzothiazole **115** (PhEtSH/PhEtS$^-$) and the nitroalkene **111** (EtONa) could not be observed. This may have been due to the covalent reversible reaction mechanism of the nitrile and α-ketobenzothiazole and the overall difficult ionization of the specific compounds by an electron spray ionization mass spectrometer.

Method A (NMR): ^{1}H-NMR spectra were recorded for the respective warhead and nucleophile mixture, before the addition of the nucleophile (0 min) and after 5, 30, 60, 120 and 240 min reaction time. For quantification, the double bond-signals (doublet/doublet of doublets, around 7.4–6.7 ppm) of the Michael acceptors were integrated relative to 1,3-dioxolane as an internal standard. The acetal CH_2 signal of the internal standard at 5.3 ppm was used as a reference.

The α-ketobenzothiazole **115** and nitrile **117** were similarly analyzed by ^{13}C-NMR. Therefore, the corresponding ^{13}C-leucin derivates were synthesized (Scheme 7). Quantifications of the reactions were carried out by using the integral of the carbonyl carbon atom signal at 195 ppm for the α-ketobenzothiazole and 120 ppm for the nitrile moiety. The reference signal of DMSO-d_6 was set to 39.52 ppm.

In Figure 2, the ^{1}H-NMR spectra of the test reaction of the 4-oxoenoate **112** with 2-phenylethanthiol **118** are shown exemplarily. After four hours, 92% conversion of the inhibitor to the product **120** was observed. LC-MS analysis confirmed the diastereomeric formation of the expected product **120**.

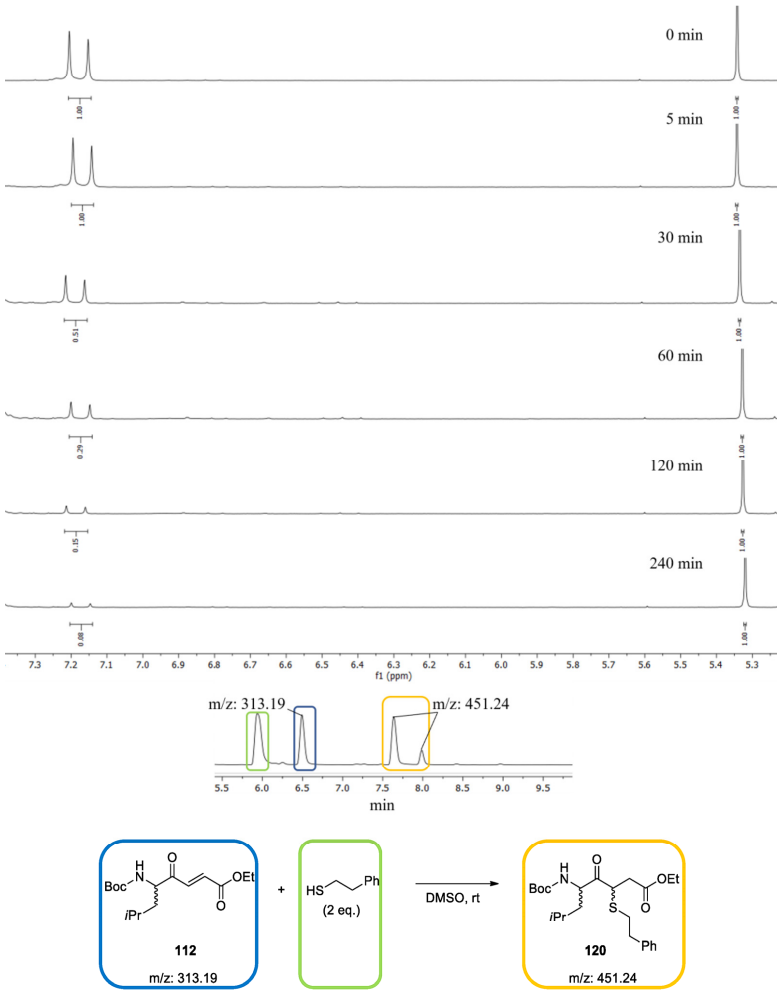

Figure 2. ^{1}H-NMR spectra of the 4-oxoenoate **112** before the addition (0 min) and after 5, 30, 60, 120 and 240 min reaction time with 2-phenylethanthiol in the absence of triethylamine. The integrals of the β-proton of the double bond at 7.17 ppm in relation to the 2-CH_2 signal of the internal standard 1,3-dioxolane at 5.3 ppm are given. LC-MS analysis of the same reaction at 30 min.

Method B (LC-MS): The reactivity of the β-lactam test compound **108** with the nucleophiles was investigated using an LC-MS-based method. To quantify the conversion, the AUCs were determined at 254 nm. In Figure 3, the UV spectra of the test reaction of the β-lactam **108** with EtONa are shown exemplarily. After one hour, complete conversion of the inhibitor to the adduct **122** was observed.

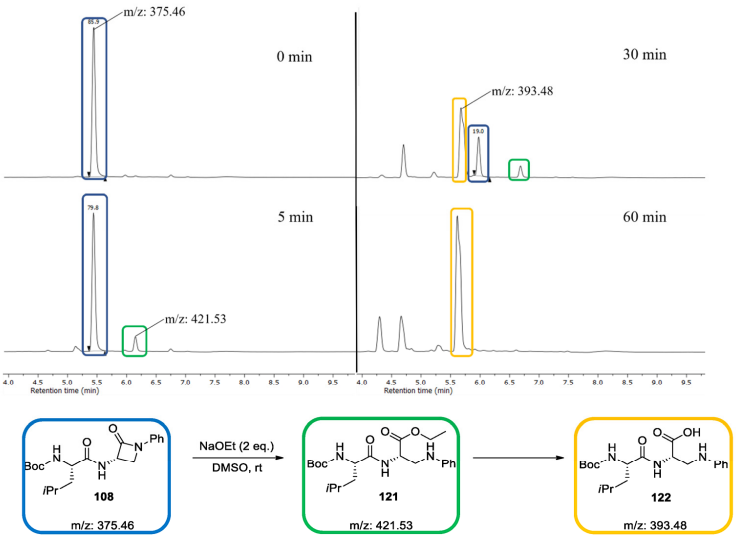

Figure 3. LC-MS spectra of the *β*-lactam **108** before (0 min) the addition and after 5, 30 and 60 min reaction time with sodium ethoxide.

All ^{1}H-NMR/^{13}C-NMR spectra and chromatograms of the reactivity tests are presented in the Supporting Information (Figures S1–S18). The reactivity test results of all warhead compounds with PhEtSH, PhEtSH + Et_3N and EtONa are shown in Figure 4.

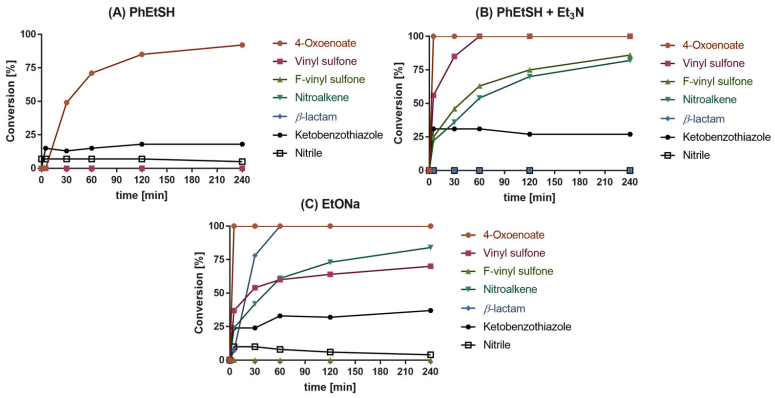

Figure 4. Progress curves of the reactions of the different warhead compounds with the model nucleophiles PhEtSH, PhEtSH + Et_3N and EtONa as measured by NMR and LC-MS analysis.

As depicted in Figure 4A, the 4-oxoenoate **112**, the *α*-ketobenzothiazole **115** and the nitrile **117** moiety did indeed react with PhEtSH under non-basic conditions. In contrast, conversion was not observed with the vinyl sulfone **109**, F-vinyl sulfone **110**, *β*-lactam **108** and nitroalkene **111** warheads. After 240 min, the 4-oxoenoate **112** had nearly completely (92%) reacted with PhEtSH, while only 18% conversion of the *α*-ketobenzothiazole **115** was observed. The equilibrium of the *α*-ketobenzothiazole **116** was reached after 5 min. Similarly, with the nitrile moiety **117**, only 7% conversion was detected, indicating that the

formed thioimidate adduct is relatively unstable (Figure 4A). With the addition of Et_3N (Figure 4B) the overall reactivity increased. Every warhead except the β-lactam **108** and the nitrile **117** reacted with the deprotonated thiol species. Full conversion of the 4-oxoenoate **112** could be observed after 5 min, followed by the vinyl sulfone **109**, which took 60 min for complete reaction. The F-vinyl sulfone **110** and nitroalkene **111** both showed similar reactivity with the thiolate species, with a maximum conversion of 86% and 82% after 240 min, respectively. The α-ketobenzothiazole **115** also showed an increased reactivity, with around 30% conversion. The reactivity tests with EtONa as nucleophile revealed the 4-oxoenoate **112** moiety as the most reactive warhead, which was completely consumed after 5 min (Figure 4C). However, LC-MS analysis did not prove the formation of the expected product but rather unspecific conversion of **112** (see Supplementary Materials, Figure S8). The nitroalkene **111** showed a similar behavior in comparison to the reactivity test with the deprotonated thiolate species, with a conversion of 84% after 240 min. The β-lactam **108** compound showed full conversion after 60 min. In contrast to the deprotonated PhEtSH species, the results indicated a much slower reactivity of the vinyl sulfone **109** with a conversion of 70% after 240 min. No conversion with EtONa was observed for the F-vinyl sulfone **110**. The α-ketobenzothiazole **115** showed a higher conversion in the presence of EtONa (37%) than with PhEtSH, but reached this maximum only after 60 min, showing a slower reaction rate compared to the deprotonated thiol species at 5 min. The equilibrium between the α-ketobenzothiazole **115** and hemiacetal shifted to 37% conversion and was higher compared to the reactivity test with the thiol nucleophiles. The nitrile **117** showed a similar conversion at 5 min with EtONa compared to the protonated thiol species, with 10% conversion, but again decreased after a period of time, which again indicates the instability of the imidate adduct under basic conditions.

The high reactivity of the 4-oxoenoate **112** warhead with the thiolate is in accordance with the high inhibitory potency of dipeptidyl 4-oxoenoate-based compounds against cysteine protease [48]. The missing reactivity of both vinyl sulfones **109** and **110** toward protonated thiol species and the high reactivity with deprotonated thiols are also in agreement with the high activity of vinyl sulfone inhibitors against cysteine proteases with a thiolate residue in the catalytic center, as reported in the literature.

Nitroalkenes are classified as cysteine targeting warheads, which is also confirmed by the observed reactivity with the model thiolate nucleophile [49].

β-lactams are commonly known as warheads in antibacterial agents with transpeptidase-inhibiting properties but have also been used in the development of serine protease inhibitors [21,50,51]. The reactivity tests demonstrate the preference for alcoholate-based nucleophiles, since they only reacted with EtONa and not with PhEtSH/$PhEtS^-$.

α-Ketobenzothiazole derivatives are used as potent serine and cysteine protease inhibitors [52,53]. Therefore, the reactivity of the α-ketobenzothiazole **115** moiety towards all three model nucleophiles was expected. In accordance with the HSAB concept, the stability of the tetrahedral (thio)hemiacetal decreased from the hard sodium ethoxide to the soft thiol/thiolate nucleophiles (EtONa>$PhEtS^-$PhEtSH) after 240 min.

The observed reaction of the nitrile **117** with both nucleophiles (PhEtSH/EtONa) is in accordance with the well-known reactivity of nitrile-based drugs. The observed instability of the (thio)-imidate adduct might have been due to the neutral or basic reaction conditions in solution [54,55]. In contrast, the (thio)imidate adduct is stabilized by interaction with amino acid residues of the enzyme pocket [56].

2.3. Quantum Mechanics Simulations

As model nucleophiles for the QM simulations, methanethiol/ate and methanolate were used. While the formed products were identical, the warheads vinyl sulfone, F-vinyl sulfone and nitroalkene exhibited varying reactivities for PhEtSH and PhEtSH in the presence of triethylamine. Only for 4-oxoenoate and α-ketobenzothiazole was significant reactivity towards PhEtSH observed, whereas for PhEtSH + Et_3N, all warheads except the nitrile and the β-lactam showed reactivity (Figure 4). Since most of the reaction energies

with both MeSH and MeSH + Et_3N were computed to be exergonic (Figure 5A), this cannot be explained merely by thermodynamics. For instance, the experimental results do not show reactivity of the warheads vinyl sulfone, F-vinyl sulfone and nitroalkene with PhEtSH, despite a computed negative free energy of reaction. Thus, to determine whether a reaction can be expected to take place, it is important to consider the whole reaction path, including the activation barriers, which determine the kinetics. Previous calculations have revealed that MeSH is often insufficiently nucleophilic to allow a reaction to occur at room temperature [57]. A base, such as triethylamine, serves as interim storage for the thiol proton before it is transferred to the warhead. By deprotonating the thiol prior to the nucleophilic attack, the nucleophilicity of MeSH is strongly increased, thereby decreasing the associated activation barriers considerably (Figures S22C, S23B and S24A–C). Following the addition of the nucleophile, the proton is transferred back from the base to the anionic intermediate. Unlike the 4-oxoenoate, vinyl sulfone, F-vinyl sulfone and nitroalkene warheads, the β-lactam warhead does not show any reactivity with PhEtSH + Et_3N. The computed reaction mechanism revealed three consecutive steps to obtain the product (Figure 5C). First, the nucleophile attacks the amide carbonyl group (TS1), resulting in a tetrahedral anionic intermediate (Int1). The rate-determining step is the opening of the lactam ring in the second step (TS2). This was computed to be about 33 kcal mol^{-1} for MeSH + NEt_3, which is in excellent agreement with the experimental data. In the last step, the former amide nitrogen is protonated by the base to yield the final product (TS3). For the nitrile warhead, a weak reaction with PhEtSH but none with PhEtSH + triethylamine was observed experimentally, which cannot be explained by reference to the computational data. As described in the reactivity tests, this might have been due to the instability of thioimidates in basic solution.

As a result of our calculations, the difference in reactivity between PhEtSH and PhEtSH + Et_3N for the vinyl sulfone, F-vinyl sulfone and nitroalkene warheads was attributed to a significant reduction in activation barriers caused by proton transfer from the nucleophile to the base prior to the nucleophilic attack. We therefore investigated the reason for the reactivity of 4-oxoenoate and α-ketobenzothiazole warheads with PhEtSH in DMSO in the absence of a base. For 4-oxoenoate, a conversion of 92% was observed experimentally, which corresponds to a computed free energy of reaction of about –9 kcal mol^{-1} for the nucleophilic attack at C_α and about –11 kcal mol^{-1} for the addition at C_β. The reaction of PhEtSH with α-ketobenzothiazole, however, showed only about 18% conversion, and the corresponding product was computed to be 8 kcal mol^{-1} (Figure 5B) and 9 kcal mol^{-1} for the thermodynamic calculation with a bigger basis set (Figure 5A). The solvent used in the experiments was not completely free of water, and, as a result, water molecules were able to catalyze the nucleophilic attack for α-ketobenzothiazole and 4-oxoenoate, as well as the keto-enol tautomerization for the latter (Figure 5B and Figure S22A,B) [58]. Our calculations demonstrate that traces of water in the solvent can function as a base to catalyze the reaction of MeSH with the warhead. The activation barrier for α-ketobenzothiazole is reduced from more than 40 kcal mol^{-1} to roughly 25 kcal mol^{-1}, and the product energy is lowered to 1 kcal mol^{-1} (Figure 5B). Similarly, water catalyzes both the nucleophilic attack of MeSH at the 4-oxoenoate warhead and the subsequent keto-enol tautomerization, leading to a decreased activation barrier of 26 kcal mol^{-1} for the first step (TS1) and one of 20–25 kcal mol^{-1} for the second step (TS2). Additionally, the product energy is even more exergonic at –17-(–18) kcal mol^{-1} (Figure S22B). Contrary to the reaction without water, the proton does not have to be transferred directly from the thiol to the atom to be protonated. Instead, it is shuffled along a chain of water molecules. The keto-enol tautomerization is favored for the C_β-addition, but the barrier associated with the rate-determining nucleophilic attack is nearly identical (Figure S22B). Thus, it is expected that both reactions should occur in solution. For the reaction with an enzyme, the conformation of the binding pocket will likely determine at which carbon atom the nucleophilic attack will occur.

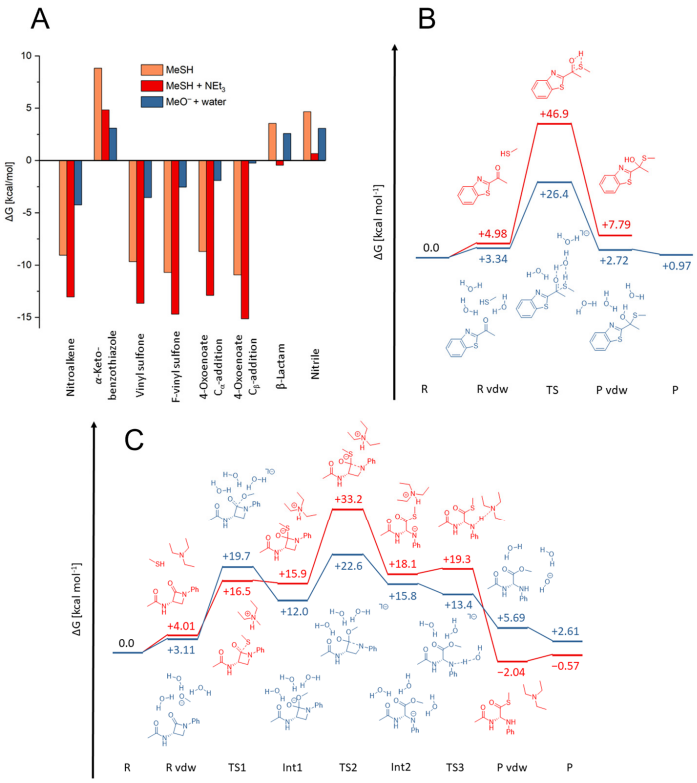

Figure 5. (**A**) Free energies of the reactions for all inhibitor warheads with MeSH, MeSH + Et_3N and MeO^- + $3H_2O$, computed as described in the Supplementary Materials section and Figures S24 by ωB97X−D/6−311++G**//ωB97X−D/6-31+G* calculations. (**B**) Free energy reaction paths of the α-ketobenzothiazole warhead with MeSH (red) and with MeSH in the presence of three water molecules (blue). For MeSH (red), the van der Waals complex (P vdw) and separated product molecules (P) are identical since the reaction yields only a single product molecule. For MeSH + water (blue), the energies are referenced on MeSH + $2H_2O$ and the α-ketobenzothiazole warhead + H_2O (R). (**C**) Free energy reaction paths of the β-lactam warhead with MeSH + NEt_3 (red) and with MeO^- in the presence of three water molecules (blue). The reaction proceeds in three consecutive steps: first, nucleophilic attack at the amide carbonyl group (TS1); second, the opening of the lactam ring (TS2); and third, the proton transfer from the base (NEt_3 or H_2O) to the former amide nitrogen (TS3).

To mimic the reaction of the warheads with NaOEt, we calculated the reaction path with MeO^- and included three water molecules to allow for protonation of the intermediates to obtain the final products and stabilize the reactive anionic species (Figures 5C, S22D, S23D and S24A–C). The reaction can either terminate at the anionic intermediate or proceed to the neutral adduct by transferring one proton from a water molecule, depending on the basicity of the intermediate, i.e., the intermediate carbanion is poorly stabilized for the vinyl sulfone, hence the reaction progresses to form the neutral addition product (Figure S24A). The nitroalkene carbanion, however, is strongly stabilized, and our calculations suggest that the reaction might stop at the intermediate (Figure S24C). Analogously, the α-ketobenzothiazole forms a deprotonated hemiacetal (Figure S23B). Experimentally, no reactivity of the F-vinyl sulfone warhead with NaOEt was observed, which was not supported by our calculations

and is contradictory to chemical intuition (Figure S24B). As previously stated, the barrier for the β-lactam ring opening in reaction with MeSH + Et_3N was computed to be over 30 kcal mol^{-1}, explaining the lack of reactivity in the experiments. Since the anionic species and ring opening are better stabilized in the reaction with $MeO^- + 3H_2O$, only 23 kcal mol^{-1} is required in this step, which is consistent with the experimental data (Figure 5C).

2.4. In Vitro Evaluation of the Synthesized Compounds

Inhibition of the target enzymes was tested via fluorometric assays. Therefore, fluorogenic AMC- or FRET-based substrates with appropriate peptide sequences for the different proteases were used (see Supplementary Materials, Figures S19–S20).

The potential inhibitors were initially screened against all five target enzymes at 20 µM. A cut-off value of 80% inhibition at this concentration was set to differentiate the non-active (n.a.) compounds from active ones.

For the reversible inhibitors (α-ketobenzothiazole, nitroalkene, F-vinyl sulfone and nitrile), the IC_{50} values were determined and converted to corresponding K_i values using the Cheng–Prusoff equation [56]. Regarding the irreversible inhibitors (vinyl sulfone, 4-oxoenoate and β-lactam) the K_i, k_{inact} and k_{2nd} values were determined (see Table S1) [56]. For a better overview, the pK_i values were calculated and are presented in Figure 6.

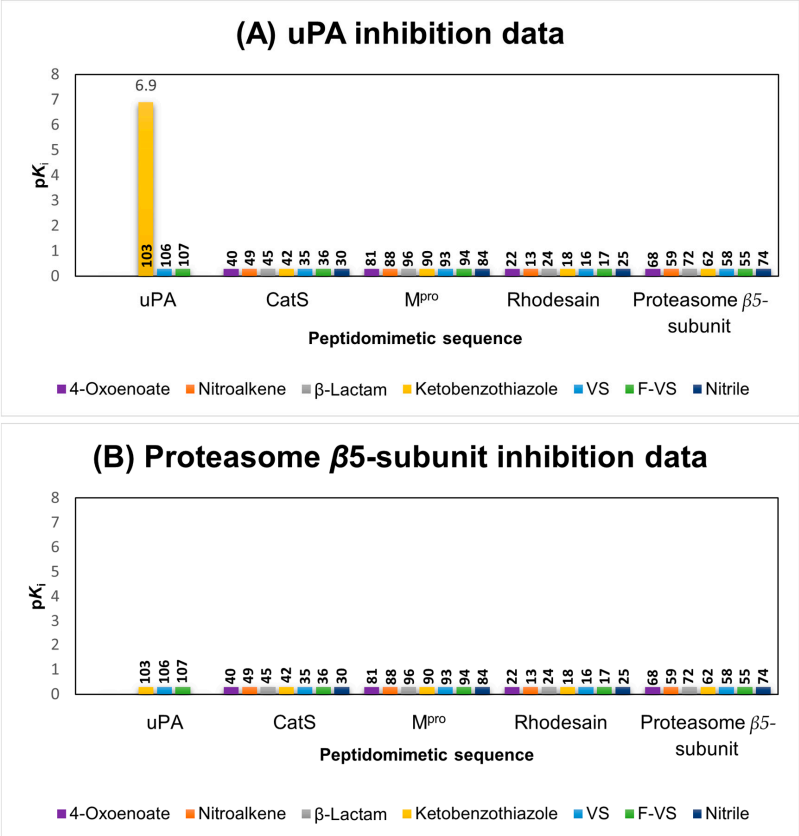

Figure 6. *Cont.*

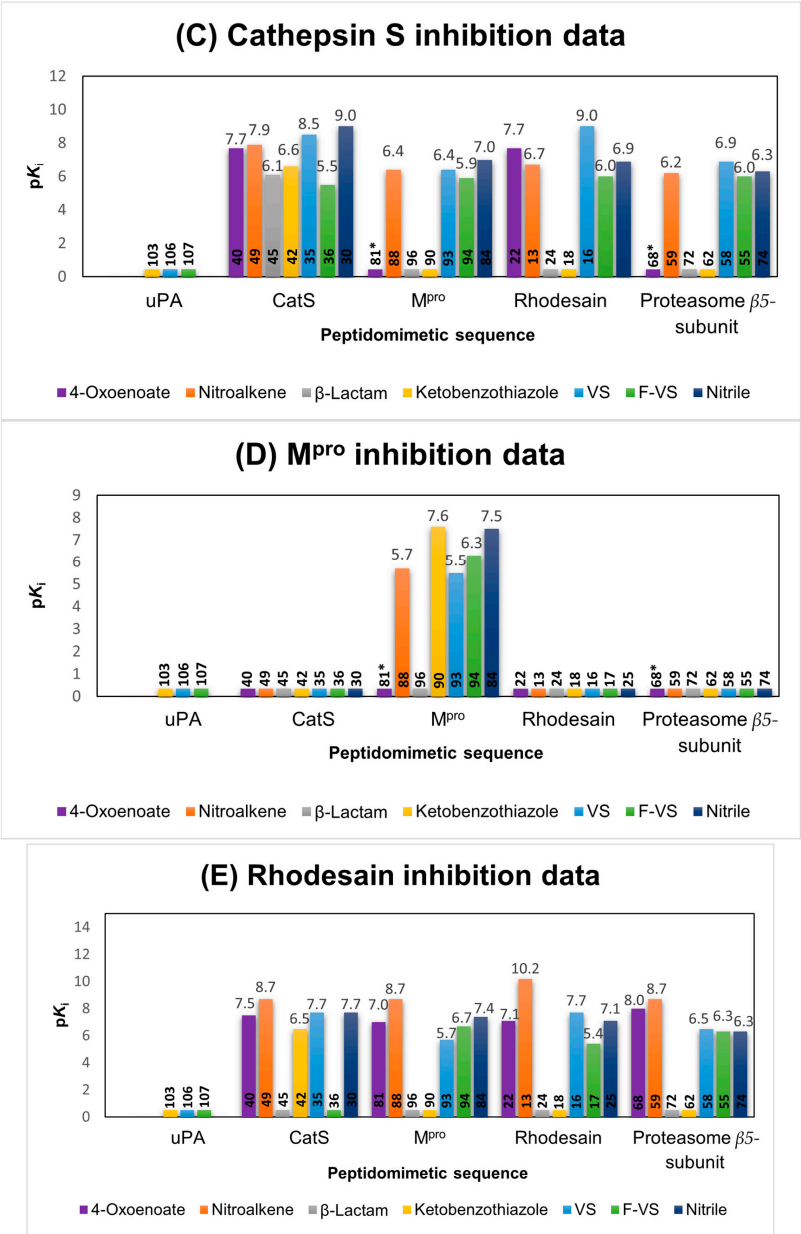

Figure 6. Inhibition data for the assays with uPA (**A**), proteasome β5-subunit (**B**), cathepsine S (**C**), SARS-CoV-2 M^{pro} (**D**) and rhodesain (**E**). pK_i values were calculated from the K_i values ($-\log_{10}(K_i/M)$) [59]. The height of a bar indicates the inhibitory potency of an inhibitor towards the target enzyme, and the color of a bar indicates the warhead of the inhibitor; the peptidomimetic sequence is indicated by the enzyme name under the bars, e.g., the purple bar with the height value

of 7.5 for rhodesain inhibition (Figure 6E) by inhibitor **40** with the oxoenoate warhead and the CatS sequence. * Respective compounds were inactive in the in vitro assay due to instability towards DTT in the buffer.

In the following, the inhibition data will be analyzed for each enzyme, first with their suited peptidomimetic sequences (Figure 6, parts A, B, C, D and E), followed by cross testing against the other enzymes.

uPA. Only the α-ketobenzothiazole inhibitor **103** was found to be active. The combination of the appropriate sequence for uPA with the α-ketobenzothiazole warhead resulted in a potent inhibitor with a pK_i value of 6.9. Other enzymes were not inhibited (Figure 6A).

Proteasome β5-subunit. None of the compounds with the Pyz–(L)Phe–(L)Leu sequence (**55**, **85**, **59**, **62**, **68**, **72** and **74**), which is well-known from the potent boronic acid-based inhibitor bortezomib, showed inhibition of the proteasome at 20 µM, independently of the warhead used (Figure 6B). Moreover, none of the other compounds with any of the other peptidomimetic sequences showed any inhibition. This highlights the general difficulty of addressing this protease with peptidomimetic inhibitors [56]. An alternative warhead which reacts preferably with Ser or Thr proteases is the epoxide functionality, which is also present in the approved proteasome inhibitor carfilzomib. Although very potent, due to its unpredictable reaction mechanism, this warhead was not included in this study [60].

CatS. Regarding the in vitro testing of the cysteine protease CatS, a total of 20 hits were detected (Figure 6C). The most potent inhibitors with the fitting CatS sequence were the nitrile **30** (pK_i = 9) and the vinyl sulfone **35** (pK_i = 8.5). The nitroalkene **49** (pK_i = 7.9) also showed high affinity towards CatS, followed by the 4-oxoenoate **40** (pK_i = 7.7), the α-ketobenzothiazole **42** (pK_i = 6.5), β-lactam **45** (pK_i = 6.1) and F-vinyl sulfone **36** (pK_i = 5.5). Since CatS and rhodesain are both papain-like cysteine proteases with similar active sites, cross reactivity between these two series was expected and has been well described in the literature [61]. The vinyl sulfone with the rhodesain-targeting sequence **16** (pK_i = 9) showed the same inhibition constant as the corresponding inhibitor with the CatS sequence. The vinyl sulfones with the proteasome and the M^{Pro} sequences inhibited CatS to lower degrees (pK_i = 6.9 and 5.5). A comparison of the 4-oxoenoates of the CatS and rhodesain series yielded the same results, since both exhibited the same pK_i value of 7.7 for inhibition of CatS. The 4-oxoenoates designed for targeting the proteasome **68** and the M^{Pro} **81** were essentially inactive against CatS (no inhibition in the initial screening at 20 µM). This can be explained by the instability of these compounds in the CatS assay buffer containing dithiothreitol (DTT).

The F-vinyl sulfones, which are reversibly reacting counterparts of the vinyl sulfones, inhibited CatS to a lower degree, and exchange of the peptidomimetic sequence (**36**, pK_i = 5.5 vs. **17**, pK_i = 6 vs. **55**, pK_i = 6 vs. **94**, pK_i = 5.9) had little to no effect, except for the compounds with the uPA sequence (**103**, **106** and **107**), which was not active at 20 µM against CatS.

The nitroalkene inhibitor which contains the CatS sequence showed a high on-target affinity but changing the sequence to any of the other targeting sequences led to less potent inhibitors (**13**, pK_i = 6.7 vs. **88**, pK_i = 6.4 µM vs. **59**, pK_i = 6.2). Interestingly, the α-ketobenzothiazole- (**42**, pK_i = 6.6) and β-lactam- (**45**, pK_i = 6.1) based inhibitors showed only significant inhibition of CatS if connected to the respective CatS sequence, indicating the strong dependency of a suitable peptidomimetic sequence combined with one of these warheads.

M^{pro}. In comparison to the M^{pro} inhibitors α-ketobenzothiazole **90** (pK_i = 7.6) and nitrile **84** (K_i = 7.5) described in the literature, vinyl sulfone **93** (pK_i = 5.5), F-vinyl sulfone **94** (pK_i = 6.3) and nitroalkene **88** (pK_i = 5.7), all of which contain the appropriate M^{pro} peptidic sequence, showed weaker inhibition (Figure 6D) [40,62]. A clear preference of the protease for specific warheads could be observed. The vinylogous warheads (vinyl

sulfone, F-vinyl sulfone and nitroalkene) showed significantly weaker inhibition than the α-ketobenzothiazole- and nitrile-based compounds. As also observed in the model reactivity studies, the in vitro studies with CatS and both 4-oxoenoate inhibitors with the M^{pro} **81** and the proteasome β5-subunit **68** sequences revealed instability in the buffer with DTT. The β-lactam **96** as well as all compounds containing a targeting structure designed for other proteases were inactive at 20 μM. This indicates a high specificity of the M^{pro} towards its peptidomimetic sequence.

Rhodesain. The results showed similar trends to those found for CatS, with 20 compounds active in the assays (Figure 6E). The most potent was the nitroalkene **13** which contains the corresponding rhodesain peptidic sequence (pK_i = 10.2), followed by the vinyl sulfone **16**, 4-oxoenoate **22** and nitrile **25**, which showed similar inhibition constants (pK_i-= 7.1–7.7). The F-vinyl sulfone **17** showed moderate inhibition (pK_i = 5.4), and the β-lactam **24** and α-ketobenzothiazole **18** were inactive at 20 μM, indicating a preference of rhodesain for vinylogous warheads. Comparable to the CatS study, inhibitors lacked selectivity between rhodesain and CatS due to the structural similarity of the proteases. This is evident through the high pK_i values of the synthesized CatS inhibitors with 4-oxoenoate- **40** (pK_i = 7.5), nitroalkene- **49** (pK_i = 8.7), vinyl sulfone- **35** (pK_i = 7.7) and nitrile- **30** (pK_i = 7.7) moieties. Surprisingly, the α-ketobenzothiazole **42** designed for targeting CatS showed significant inhibition (pK_i = 6.5), whereas the α-ketobenzothiazole with the rhodesain peptidic sequence **18** was inactive. Among the compounds designed for M^{pro} and the proteasome, the nitroalkene derivatives **88** and **59** showed the same potency as the CatS analogue **49**, both with a pK_i value of 8.7. Interestingly, the vinyl sulfones with the M^{pro} **93** (pK_i = 5.7) and the proteasome sequence **58** (pK_i = 6.5) showed significantly lower affinity compared to the vinyl sulfone designed for rhodesain **16** (pK_i = 4.7). Differently, the F-vinyl sulfones **55** (pK_i = 6.3) and **94** (pK_i = 7.7) showed higher affinities than the analogue with the rhodesain sequence **17** (pK_i = 5.4). The 4-oxoenoate inhibitor **68** (pK_i-= 8.0) designed for the proteasome and the one designed for the M^{pro} **81** (pK_i = 7.0) also showed strong inhibition. All other inhibitors with the β-lactam and α-ketobenzothiazole moiety were inactive, as well as the compounds containing the uPA sequence (**103**, **106** and **107**).

2.5. Molecular Docking

To further elucidate the impact of the different warhead types on the binding modes of the inhibitors, protease–inhibitor complexes were investigated with non-covalent and covalent docking [63,64]. For the non-covalent docking, special emphasis was laid on the distances between the reactive nucleophilic carbon atoms of the corresponding warheads to the thiol(ate) or hydroxyl(ate) side chains of the cysteine/serine(threonine) active site amino acids, respectively, as estimates for covalent-bond-formation likeliness. Additionally, the impact of the different warhead moieties on the binding conformation of the inhibitors with otherwise identical peptidomimetic recognition sequences was analyzed. The covalent docking setup was used to investigate whether realistic poses for the covalent complexes could be generated and whether larger conformational rearrangements of the ligand may occur after the covalent reaction.

Conventional non-covalent docking yielded generally reasonable binding modes for all complexes resembling interactions of the crystallographic reference ligands and peptidomimetic recognition sequences in their expected subpockets. Additionally, electrophilic warheads were regularly found in close proximity to the nucleophilic catalytic amino acids (Figure 7, Tables S2 and S3).

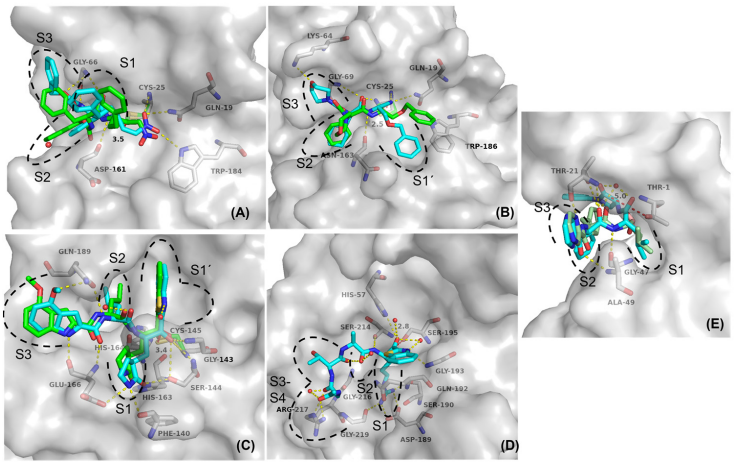

Figure 7. Predicted binding modes and polar interactions (yellow dashed lines) of different inhibitor classes with different enzymes (white carbon atoms and surface). For non-covalent docking poses, the distance between electrophilic carbon and nucleophilic sulfur or oxygen is shown as a red dashed line, with the distance measured in Å. For a clear view, only amino acids that form polar interactions with the ligands are shown as sticks and labelled. Black dashed lines indicate subpocket locations. Non-covalent docking poses are shown with cyan C-atoms and the covalent docking poses with green C-atoms. (**A**) Superposition of the non-covalent and the covalent docking pose of **13** with rhodesain, PDB-ID (2P7U). (**B**) Superposition of the non-covalent and the covalent docking pose of **30** with CatS, PDB-ID (1MS6). (**C**) Superposition of the non-covalent and the covalent docking pose of **90** with SARS-CoV-2-M^{pro}, PDB-ID (6XR3). (**D**) Predicted binding mode of non-covalently docked **103** with uPA, PDB-ID (1W10). (**E**) Superposition of the non-covalent docking pose of **72** and bortezomib (palegreen C-atoms) with the β-5 subunit of human 20S-proteasome, PDB-ID (5LF3).

The docking with rhodesain (pdb entry 2P7U) indicated that the introduction of a Michael-acceptor system as the warhead led to binding poses similar to the co-crystallized reference ligand, with all the essential interactions between inhibitor and enzyme being nearly identical, as exemplified for the docking poses of the nitroalkene inhibitor **13** (Figure 7a). The poses of the covalent and the non-covalent docking showed that the overall orientation of the inhibitor inside the active site should not change much after the covalent reaction, since the final covalent enzyme–inhibitor complex is very similar to the non-covalent complex (Figure 7a). The corresponding electrophilic C-atoms of all warheads were predicted to be in close proximity to the sulfur atom of Cys25 (2.54–3.50 Å), suggesting a high probability for a nucleophilic attack. High docking scores were also found for the nitroalkene inhibitor **13** (FlexX score: –24.03 kJ/mol; MOE score: –2.66), indicating that it should form very favorable non-covalent interactions while correctly placing the electrophilic warhead (distance to Cys25 sulfur: 3.50 Å). This is consistent with the in vitro data, showing that the nitroalkene moiety represents the most potent inhibitor class for rhodesain. Since the α-ketobenzothiazole designed for CatS (**42**) surprisingly inhibited rhodesain with a submicromolar affinity, we compared the non-covalent docking poses between **42** and the ketobenzothiazole with the rhodesain sequence (**18**) (Figure S21). Superposition of the non-covalent docking poses showed that both inhibitors have almost the same positioning with the warhead close to Cys-25 (2.5 Å) inside the active site of rhodesain, indicating that both compounds should have similar affinities towards rhodesain. This makes it hard to explain why inhibitor **42** had a significantly higher affinity for rhodesain in the in vitro testing. Since molecular docking is an inaccurate method, flawed docking

poses are no rarity. The non-covalent docking method used in this case might not be suited to explaining this in vitro result. The results of the docking with CatS (1MS6) showed similar trends, since the distances between the electrophilic C-atoms of the warheads and the sulfur atom of Cys25 were again in close proximity in all cases (2.69–3.37 Å). The vinyl sulfone **35** and the nitrile **25** had high scores (FlexX score: –27.35/–26.22 kJ/mol; MOE score: –5.32/–3.00 kcal/mol) combined with similar binding geometries for the covalent and the non-covalent docking poses (shown for nitrile inhibitor **25**, Figure 7b). These data are in accordance with the in vitro data showing that the nitrile warhead was the most potent one, but other warheads also led to productive enzyme inhibition.

For SARS-CoV-2 M^{pro} (6XR3), the distances between the electrophilic C-atoms and the Cys145 sulfur atom were overall slightly higher (2.90–4.91 Å) compared to the papain-like cysteine proteases. The α-ketobenzothiazole warhead seems to have a very favorable positioning in the binding pocket, as illustrated by the close proximity (3.41 Å) of the electrophilic C-atom to the thiol of the enzyme Cys145 (Figure 7c). Superposition of the covalent and non-covalent docking poses of **90** showed almost identical positioning of the inhibitor inside the enzyme, with most of the polar interactions retained.

Out of all the investigated warheads in this series, only the nitrile, the α-ketobenzothiazole and the β-lactam warheads are known to react with oxygen containing amino acid residues in serine (uPA) or threonine (proteasome) proteases.

For the uPA, which was the only target with only one hit in the enzymatic assay, non-covalent docking revealed a large distance between the electrophilic C-atom and the hydroxy-group in the active site for the β-lactam (5.07Å) as a known serine warhead. Only the α-ketobenzothiazole inhibitor **103**, which had one of the highest scores out of all the inhibitors (FlexX score: –51.59 kJ/mol), was in close proximity to the oxygen of Ser195 (2.84 Å distance to the electrophilic C-atom). This inhibitor also showed a high potency in the in vitro study (Figure 7d). Finally, docking of the β-lactam containing inhibitor **72** designed for the proteasome revealed that the warhead position was, again, too far away from the threonine oxygen (4.95 Å), possibly preventing a covalent reaction (Figure 7e). This could be explained by the shifted positioning of the lactam moiety compared to the other warheads. Although the docking of the nitrile and α-ketobenzothiazole inhibitors **74** and **62** might suggest that these compounds should inhibit their target sufficiently since the warheads are positioned correctly and in close proximity (2.27 Å/3.16 Å) to the Thr-1 oxygen atom, there was still no inhibition with these warheads in the in vitro study. This might have been due to wrongly generated binding poses, since docking approaches are not always reliable and cannot be considered flawless in all cases. A possible explanation why none of the compounds designed to address the β5-subunit of the proteasome showed any inhibition might be the catalytic dyad in the active site consisting of Lys33 and Thr1 compared to the catalytic dyads or even triads in the other enzymes, where the deprotonation of the active site residue is assisted by histidine and/or asparagine. The lysine residue might not always be able to deprotonate the threonine in the active site, depending on the inhibitor, and thus facilitate the covalent reaction step with a warhead [65].

2.6. Comparison of the Reactivity Assay Results with the In Vitro Study

Based on the reactivity assay, all Michael acceptors (4-oxoenoate **112**, (F-) vinyl sulfone **109**/**110** and nitroalkene **111**) showed high reactivity toward the deprotonated cysteine model nucleophile, which is congruent with the observed behavior of the synthesized compounds designed for CatS and rhodesain inhibition in the in vitro studies. Furthermore, the α-ketobenzothiazole warhead **115** showed a strong reactivity for both model nucleophiles ($PhEtS^-$/EtONa), which is consistent with the correspondent uPA and M^{pro} inhibitors **103** and **90** in the protease assays. However, the nitrile **117** showed no reaction with the deprotonated cysteine but with the serine model nucleophile, which contradicts the high inhibitory activity against the cysteine proteases and the missing inhibition by the proteasome β5-subunit inhibitor **74**. This might have been due to the aforementioned

instability of the thioimidate adduct in basic conditions compared to the stabilized adduct in the enzyme pocket and the overall difficulty of addressing the proteasome β5-subunit. The β-lactam **108** showed only a strong reactivity towards the serine model nucleophile, but the corresponding bortezomib derivative **72** did not inhibit the proteasome β5-subunit, which might have been due to the shift of the electrophilic center of the β-lactam moiety into the S1' pocket and the resulting increase in distance. The 4-oxoenoate moiety **112** was the only warhead that showed high reactivity toward the protonated cysteine model nucleophile, which might hint at non-selective reactivity behavior toward thiol species under physiological conditions. This could also be observed in the in vitro studies. The 4-oxoenoate compounds designed for the M^{pro} **81** and proteasome-β5-subunit **68** both reacted quickly with DTT in the respective buffer solutions and appeared to be inactive.

3. Discussion

Covalent targeting has become a popular and powerful concept in drug discovery, and great efforts have been devoted to developing and repurposing different warheads [66]. In this first extensive systematic study, we aimed to achieve a deeper insight into the reactivities and selectivities of a selection of electrophilic traps combined with established peptidomimetic sequences for the uPA, CatS, β5-subunit of the proteasome, SARS-CoV-2 M^{pro} and rhodesain, which represent cysteine, serine and threonine proteases. Based on these peptidomimetic sequences, we synthesized compounds decorated with warheads of different specificities. We chose the Michael acceptors ((F-)vinyl sulfone, nitroalkene and 4-oxoenoate) as cysteine-targeting and β-lactam as serine/threonine-targeting representatives. Furthermore, nitriles and α-ketobenzothiazoles were used, as they are applicable for both hydroxy- and thiol-containing nucleophiles. The compounds were tested on each target to analyze their affinities as well as their selectivity profiles.

Based on the in vitro studies, it is evident that the peptidomimetic sequences of the synthesized compounds play a crucial role in the selectivity towards the tested on-target and off-target proteases. This could be observed by the selectivity profile towards the cysteine protease M^{pro} and serine protease uPA. Only the inhibitors with the suited peptidomimetic sequence for M^{pro} (**84**, **88**, **90**, **93** and **94**) and for uPA (**103**) displayed inhibitory activity towards their targeted protease. Furthermore, the selection of a suitable warhead for the specific type of protease nucleophile ensures high affinity to the target or even activity in the first place, as demonstrated with the bortezomib congeners and the α-ketobenzothiazole inhibitor **103** as the only affine compound towards the uPA. The structurally similar papain-like proteases CatS and rhodesain showed that cross reactivity can occur, despite the design of well-defined peptidomimetic sequences. Therefore, the combination of both a highly reactive warhead towards the target protease, for example, the nitrile **30** group for CatS or the nitroalkene **13** for rhodesain, with a suitable peptidomimetic sequence can lead to potent inhibitors with promising pharmacodynamic properties.

Non-covalent docking yielded reasonable binding modes for all compounds resembling interactions of the crystallographic reference ligands and peptide recognition sequences in their expected subpockets. Additionally, electrophilic warheads were regularly found in close proximity to the nucleophilic catalytic amino acids, except for the β-lactams.

A reactivity test system with tool compounds of the used warheads and model nucleophiles was established to evaluate chemoselectivity. The findings confirmed the high reactivity of the 4-oxoenoate, the (F-)vinyl sulfones and the nitroalkene moieties towards the deprotonated thiol nucleophile/cysteine model, and high affinity of the Michael acceptor inhibitors towards the cysteine proteases was observed. Analogously to the in vitro studies of the uPA and M^{pro} target, the α-ketobenzothiazole warhead was found to be a potent electrophilic trap for both cysteine and serine proteases. Nevertheless, some major differences in reactivity could be observed, which might have been due to different conditions used in the chemical test system and the biochemical in vitro studies. To the best of our knowledge, this is the first extensive study in which different warhead types were combined with different peptidic recognition units and in which the resulting compounds

were cross tested against different protease types. Similar published studies limited their focus to testing different warheads on one target or exchanging the peptidic backbone while retaining the same warhead [37,59,67,68].

4. Material and Methods

The material as well as the methods used for this study are described in the Supporting Information. The authors have cited additional references within the Supporting Information [21,42,43,46,47,63,64,69–89] (Supplementary Figures of the reactivity study (Figures S1–S18), of the fluorometric inhibition assays (Figures S19 and S20), of molecular docking (Figure S21), of quantum mechanics simulation (Figures S22–S25) and of the NMR-spectra and HPLC-chromatograms of the final inhibitors (Figures S26–S137) can be accessed in the supporting information).

Supplementary Materials: The following supporting information can be downloaded at: https://www.mdpi.com/article/10.3390/ijms24087226/s1.

Author Contributions: P.M.: synthesis, reactivity assay and in vitro investigation, writing—original draft; M.M.: synthesis, molecular docking and in vitro investigation, writing—original draft; J.L.M.: synthesis and in vitro investigation, writing—original draft; M.S.: synthesis, review and editing; J.M.: quantum mechanics simulations, review and editing; K.S.: synthesis; C.K.: review and editing; C.Z.: rhodesain expression; S.J.H.: SARS-CoV-2 M^{pro} expression; A.F.: synthesis, A.L.: synthesis, S.d.l.H.-R.: synthesis, L.A.-B.: synthesis, S.R.: synthesis, K.D.: quantum mechanics simulations, W.N.: quantum mechanics simulations, F.V.G.: validation, review and editing; B.E.: validation, review and editing; T.S.: validation, review and editing. All authors have read and agreed to the published version of the manuscript.

Funding: Financial support from the DFG (Deutsche Forschungsgemeinschaft) in the framework of the CRC 1066 (Nanodimensional Polymeric Therapeutics for Tumor Therapy) project Q5 (Targeting and Immunomodulator Structures and their Coupling to Therapeutic Nanosystems for Oncological Application) is gratefully acknowledged. This research was also funded by the Generalitat Valenciana (PROMETEO with ref. CIPROM/2021/079) and Universitat Jaume I (UJI-B2021-71 and SomUJIcontracovid crowdfunding campaign). L.A-B. thanks the Ministerio de Universidades for funding a PhD fellowship (ref. FPU19/04913).

Institutional Review Board Statement: Not applicable.

Informed Consent Statement: Not applicable.

Data Availability Statement: Not applicable.

Acknowledgments: We thank Sabine Maehrlein for the in vitro testing of all synthesized compounds against the proteasome β5-subunit and Katrina Schorstein for help in the synthesis. The authors wish to thank the Serveis Centrals d'Instrumentació Científica of Universitat Jaume I for technical support. The authors gratefully acknowledge the computing time provided to them on the high-performance computer Noctua2 at the NHR Center PC2. This system is funded by the Federal Ministry of Education and Research and the state governments participating on the basis of the resolutions of the GWK for national high-performance computing at universities (www.nhr-verein.de/unsere-partner, accessed on 23 March 2023). The authors gratefully acknowledge the computational and data resources provided by the Leibniz Supercomputing Centre (www.lrz.de, accessed on 9 April 2023).

Conflicts of Interest: The authors declare no conflict of interest.

References

1. López-Otín, C.; Overall, C.M. Protease degradomics: A new challenge for proteomics. *Nat. Rev. Mol. Cell Biol.* **2002**, *3*, 509–519. [CrossRef] [PubMed]
2. Grozdanić, M.; Vidmar, R.; Vizovišek, M.; Fonović, M. Degradomics in Biomarker Discovery. *Proteom. Clin. Appl.* **2019**, *13*, 1800138. [CrossRef] [PubMed]
3. Ruggiano, A.; Ramadan, K. DNA–protein crosslink proteases in genome stability. *Commun. Biol.* **2021**, *4*, 11. [CrossRef]
4. Lee, C.W.; Stankowski, J.N.; Chew, J.; Cook, C.N.; Lam, Y.W.; Almeida, S.; Carlomagno, Y.; Lau, K.F.; Prudencio, M.; Gao, F.B.; et al. The lysosomal protein cathepsin L is a progranulin protease. *Mol. Neurodegener.* **2017**, *12*, 55. [CrossRef] [PubMed]

5. Eatemadi, A.; Aiyelabegan, H.T.; Negahdari, B.; Mazlomi, M.A.; Daraee, H.; Daraee, N.; Eatemadi, R.; Sadroddiny, E. Role of protease and protease inhibitors in cancer pathogenesis and treatment. *Biomed. Pharmacother.* **2017**, *86*, 221–231. [CrossRef] [PubMed]
6. Liu, C.L.; Guo, J.; Zhang, X.; Sukhova, G.K.; Libby, P.; Shi, G.P. Cysteine protease cathepsins in cardiovascular disease: From basic research to clinical trials. *Nat. Rev. Cardiol.* **2018**, *15*, 351–370. [CrossRef]
7. Previti, S.; Ettari, R.; Calcaterra, E.; Di Chio, C.; Ravichandran, R.; Zimmer, C.; Hammerschmidt, S.; Wagner, A.; Bogacz, M.; Cosconati, S.; et al. Development of Urea-Bond-Containing Michael Acceptors as Antitrypanosomal Agents Targeting Rhodesain. *ACS Med. Chem. Lett.* **2022**, *13*, 1083–1090. [CrossRef]
8. Rocha, D.A.; Silva, E.B.; Fortes, I.S.; Lopes, M.S.; Ferreira, R.S.; Andrade, S.F. Synthesis and structure-activity relationship studies of cruzain and rhodesain inhibitors. *Eur. J. Med. Chem.* **2018**, *157*, 1426–1459. [CrossRef]
9. Kincaid, J.R.A.; Caravez, J.C.; Iyer, K.S.; Kavthe, R.D.; Fleck, N.; Aue, D.H.; Lipshutz, B.H. A sustainable synthesis of the SARS-CoV-2 Mpro inhibitor nirmatrelvir, the active ingredient in Paxlovid. *Commun. Chem.* **2022**, *5*, 156. [CrossRef]
10. Müller, P.; Maus, H.; Hammerschmidt, S.J.; Knaff, P.M.; Mailänder, V.; Schirmeister, T.; Kersten, C. Interfering with Host Proteases in SARS-CoV-2 Entry as a Promising Therapeutic Strategy. *Curr. Med. Chem.* **2022**, *29*, 635–665. [CrossRef]
11. Knaff, P.M.; Müller, P.; Kersten, C.; Wettstein, L.; Münch, J.; Landfester, K.; Mailänder, V. Structure-Based Design of High-Affinity and Selective Peptidomimetic Hepsin Inhibitors. *Biomacromolecules* **2022**, *23*, 2236–2242. [CrossRef] [PubMed]
12. Tsantrizos, Y.S.; Bolger, G.; Bonneau, P.; Cameron, D.R.; Goudreau, N.; Kukolj, G.; LaPlante, S.R.; Llinàs-Brunet, M.; Nar, H.; Lamarre, D. Macrocyclic inhibitors of the NS3 protease as potential therapeutic agents of hepatitis C virus infection. *Angew. Chemie Int. Ed.* **2003**, *42*, 1356–1360. [CrossRef] [PubMed]
13. Maus, H.; Barthels, F.; Hammerschmidt, S.J.; Kopp, K.; Millies, B.; Gellert, A.; Ruggieri, A.; Schirmeister, T. SAR of novel benzothiazoles targeting an allosteric pocket of DENV and ZIKV NS2B/NS3 proteases. *Bioorg. Med. Chem.* **2021**, *47*, 116392. [CrossRef] [PubMed]
14. Martin, J.S.; MacKenzie, C.J.; Fletcher, D.; Gilbert, I.H. Characterising covalent warhead reactivity. *Bioorg. Med. Chem.* **2019**, *27*, 2066–2074. [CrossRef] [PubMed]
15. Wang, Y.-H.; Zhang, F.; Diao, H.; Wu, R. Covalent Inhibition Mechanism of Antidiabetic Drugs—Vildagliptin vs Saxagliptin. *ACS Catal.* **2019**, *9*, 2292–2302. [CrossRef]
16. Lamb, Y.N. Nirmatrelvir Plus Ritonavir: First Approval. *Drugs* **2022**, *82*, 585–591. [CrossRef]
17. Robak, P.; Robak, T. Bortezomib for the Treatment of Hematologic Malignancies: 15 Years Later. *Drugs R D* **2019**, *19*, 73–92. [CrossRef]
18. Johe, P.; Jung, S.; Endres, E.; Kersten, C.; Zimmer, C.; Ye, W.; Sönnichsen, C.; Hellmich, U.A.; Sotriffer, C.; Schirmeister, T.; et al. Warhead Reactivity Limits the Speed of Inhibition of the Cysteine Protease Rhodesain. *ACS Chem. Biol.* **2021**, *16*, 661–670. [CrossRef]
19. Santos, M.; Moreira, R. Mini-Reviews. *Med. Chem.* **2007**, *7*, 1040–1050.
20. Adams, J.; Kauffman, M. Development of the Proteasome Inhibitor Velcade^{TM} (Bortezomib). *Cancer Investig.* **2004**, *22*, 304–311. [CrossRef]
21. Dražić, T.; Kopf, S.; Corridan, J.; Leuthold, M.M.; Bertoša, B.; Klein, C.D. Peptide-β-lactam Inhibitors of Dengue and West Nile Virus NS2B-NS3 Protease Display Two Distinct Binding Modes. *J. Med. Chem.* **2020**, *63*, 140–156. [CrossRef] [PubMed]
22. Fleming, F.F.; Yao, L.; Ravikumar, P.C.; Funk, L.; Shook, B.C. Nitrile-Containing Pharmaceuticals: Efficacious Roles of the Nitrile Pharmacophore. *J. Med. Chem.* **2010**, *53*, 7902–7917. [CrossRef] [PubMed]
23. Bullock, T.L.; Breddam, K.; Remington, J.S. Peptide Aldehyde Complexes with Wheat Serine Carboxypeptidase II: Implications for the Catalytic Mechanism and Substrate Specificity. *J. Mol. Biol.* **1996**, *255*, 714–725. [CrossRef] [PubMed]
24. Hu, X.; Lin, C.; Xu, Q.; Zhou, X.; Zeng, P.; McCormick, P.J.; Jiang, H.; Li, J.; Zhang, J. Structural Basis for the Inhibition of Coronaviral Main Proteases by a Benzothiazole-Based Inhibitor. *Viruses* **2022**, *14*, 2075. [CrossRef] [PubMed]
25. Akiyama, Y.; Tsutsumi, S.; Hatsushiba, E.; Ohuchi, S.; Okonogi, T. Peptidyl α-keto thiazole as potent thrombin inhibitors. *Bioorg. Med. Chem. Lett.* **1997**, *7*, 533–538. [CrossRef]
26. Vincenza Carriero, M.; Patrizia Stoppelli, M. The Urokinase-type Plasminogen Activator and the Generation of Inhibitors of Urokinase Activity and Signaling. *Curr. Pharm. Des.* **2011**, *17*, 1944–1961. [CrossRef] [PubMed]
27. Ismail, A.A.; Shaker, B.T.; Bajou, K. The plasminogen–activator plasmin system in physiological and pathophysiological angiogenesis. *Int. J. Mol. Sci.* **2021**, *23*, 337. [CrossRef] [PubMed]
28. Smith, H.W.; Marshall, C.J. Regulation of cell signalling by uPAR. *Nat. Rev. Mol. Cell Biol.* **2010**, *11*, 23–36. [CrossRef]
29. Kumar, A.A.; Buckley, B.J.; Ranson, M. The Urokinase Plasminogen Activation System in Pancreatic Cancer: Prospective Diagnostic and Therapeutic Targets. *Biomolecules* **2022**, *12*, 152. [CrossRef]
30. Li, C.Y.; de Veer, S.J.; Law, R.H.P.; Whisstock, J.C.; Craik, D.J.; Swedberg, J.E. Characterising the Subsite Specificity of Urokinase-Type Plasminogen Activator and Tissue-Type Plasminogen Activator using a Sequence-Defined Peptide Aldehyde Library. *ChemBioChem* **2019**, *20*, 46–50. [CrossRef]
31. Collins, G.A.; Goldberg, A.L. The Logic of the 26S Proteasome. *Cell* **2017**, *169*, 792–806. [CrossRef] [PubMed]
32. Kisselev, A.F.; van der Linden, W.A.; Overkleeft, H.S. Proteasome Inhibitors: An Expanding Army Attacking a Unique Target. *Chem. Biol.* **2012**, *19*, 99–115. [CrossRef] [PubMed]

33. Kerr, I.D.; Wu, P.; Marion-Tsukamaki, R.; Mackey, Z.B.; Brinen, L.S. Crystal Structures of TbCatB and Rhodesain, Potential Chemotherapeutic Targets and Major Cysteine Proteases of Trypanosoma brucei. *PLoS Negl. Trop. Dis.* **2010**, *4*, e701. [CrossRef] [PubMed]
34. Pauly, T.A.; Sulea, T.; Ammirati, M.; Sivaraman, J.; Danley, D.E.; Griffor, M.C.; Kamath, A.V.; Wang, I.K.; Laird, E.R.; Seddon, A.P.; et al. Specificity determinants of human cathepsin S revealed by crystal structures of complexes. *Biochemistry* **2003**, *42*, 3203–3213. [CrossRef] [PubMed]
35. Wilkinson, R.D.A.; Williams, R.; Scott, C.J.; Burden, R.E. Cathepsin S: Therapeutic, diagnostic, and prognostic potential. *Biol. Chem.* **2015**, *396*, 867–882. [CrossRef] [PubMed]
36. Chen, J.-C.; Uang, B.-J.; Lyu, P.-C.; Chang, J.-Y.; Liu, K.-J.; Kuo, C.-C.; Hsieh, H.-P.; Wang, H.-C.; Cheng, C.-S.; Chang, Y.-H.; et al. Design and Synthesis of α-Ketoamides as Cathepsin S Inhibitors with Potential Applications against Tumor Invasion and Angiogenesis. *J. Med. Chem.* **2010**, *53*, 4545–4549. [CrossRef] [PubMed]
37. Jung, S.; Fuchs, N.; Johe, P.; Wagner, A.; Diehl, E.; Yuliani, T.; Zimmer, C.; Barthels, F.; Zimmermann, R.A.; Klein, P.; et al. Fluorovinylsulfones and -Sulfonates as Potent Covalent Reversible Inhibitors of the Trypanosomal Cysteine Protease Rhodesain: Structure-Activity Relationship, Inhibition Mechanism, Metabolism, and in Vivo Studies. *J. Med. Chem.* **2021**, *64*, 12322–12358. [CrossRef]
38. Previti, S.; Ettari, R.; Cosconati, S.; Schirmeister, G.; Chouchene, K.; Wagner, A.; Hellmich, U.A.; Ulrich, K.; Krauth-Siegel, R.L.; Wich, P.R.; et al. Development of Novel Peptide-Based Michael Acceptors Targeting Rhodesain and Falcipain-2 for the Treatment of Neglected Tropical Diseases (NTDs). *J. Med. Chem.* **2017**, *60*, 6911–6923. [CrossRef]
39. Jin, Z.; Du, X.; Xu, Y.; Deng, Y.; Liu, M.; Zhao, Y.; Zhang, B.; Li, X.; Zhang, L.; Peng, C.; et al. Structure of Mpro from SARS-CoV-2 and discovery of its inhibitors. *Nature* **2020**, *582*, 289–293. [CrossRef]
40. Owen, D.R.; Allerton, C.M.N.; Anderson, A.S.; Aschenbrenner, L.; Avery, M.; Berritt, S.; Boras, B.; Cardin, R.D.; Carlo, A.; Coffman, K.J.; et al. An oral SARS-CoV-2 M pro inhibitor clinical candidate for the treatment of COVID-19. *Science* **2021**, *374*, 1586–1593. [CrossRef]
41. Zeslawska, E.; Jacob, U.; Schweinitz, A.; Coombs, G.; Bode, W.; Madison, E. Crystals of urokinase type plasminogen activator complexes reveal the binding mode of peptidomimetic inhibitors. *J. Mol. Biol.* **2003**, *328*, 109–118. [CrossRef] [PubMed]
42. Schrader, J.; Henneberg, F.; Mata, R.A.; Tittmann, K.; Schneider, T.R.; Stark, H.; Bourenkov, G.; Chari, A. The inhibition mechanism of human 20S proteasomes enables next-generation inhibitor design. *Science* **2016**, *353*, 594–598. [CrossRef] [PubMed]
43. Ward, Y.D.; Thomson, D.S.; Frye, L.L.; Cywin, C.L.; Morwick, T.; Emmanuel, M.J.; Zindell, R.; McNeil, D.; Bekkali, Y.; Marc Girardot, M.; et al. Design and synthesis of dipeptide nitriles as reversible and potent Cathepsin S inhibitors. *J. Med. Chem.* **2002**, *45*, 5471–5482. [CrossRef] [PubMed]
44. Hattori, S.-I.; Higashi-Kuwata, N.; Hayashi, H.; Allu, S.R.; Raghavaiah, J.; Bulut, H.; Das, D.; Anson, B.J.; Lendy, E.K.; Takamatsu, Y.; et al. A small molecule compound with an indole moiety inhibits the main protease of SARS-CoV-2 and blocks virus replication. *Nat. Commun.* **2021**, *12*, 668. [CrossRef] [PubMed]
45. Kerr, I.D.; Lee, J.H.; Farady, C.J.; Marion, R.; Rickert, M.; Sajid, M.; Pandey, K.C.; Caffrey, C.R.; Legac, J.; Hansell, E.; et al. Vinyl sulfones as antiparasitic agents and a structural basis for drug design. *J. Biol. Chem.* **2009**, *284*, 25697–25703. [CrossRef] [PubMed]
46. Vuong, W.; Vederas, J.C. Improved Synthesis of a Cyclic Glutamine Analogue Used in Antiviral Agents Targeting 3C and 3CL Proteases Including SARS-CoV-2 M pro. *J. Org. Chem.* **2021**, *86*, 13104–13110. [CrossRef]
47. Tian, Q.; Nayyar, N.K.; Babu, S.; Chen, L.; Tao, J.; Lee, S.; Tibbetts, A.; Moran, T.; Liou, J.; Guo, M.; et al. An efficient synthesis of a key intermediate for the preparation of the rhinovirus protease inhibitor AG7088 via asymmetric dianionic cyanomethylation of N-Boc-l-(+)-glutamic acid dimethyl ester. *Tetrahedron Lett.* **2001**, *42*, 6807–6809. [CrossRef]
48. Royo, S.; Rodríguez, S.; Schirmeister, T.; Kesselring, J.; Kaiser, M.; González, F.V. Dipeptidyl Enoates As Potent Rhodesain Inhibitors That Display a Dual Mode of Action. *ChemMedChem* **2015**, *10*, 1484–1487. [CrossRef]
49. Latorre, A.; Schirmeister, T.; Kesselring, J.; Jung, S.; Johé, P.; Hellmich, U.A.; Heilos, A.; Engels, B.; Krauth-Siegel, R.L.; Dirdjaja, N.; et al. Dipeptidyl Nitroalkenes as Potent Reversible Inhibitors of Cysteine Proteases Rhodesain and Cruzain. *ACS Med. Chem. Lett.* **2016**, *7*, 1073–1076. [CrossRef]
50. Shah, S.K.; Finke, P.E.; Brause, K.A.; Chandler, G.O.; Ashe, B.M.; Weston, H.; Maycock, A.L.; Mumford, R.A.; Doherty, J.B. Monocyclic β-lactam inhibitors of human leukocyte elastase. Stereospecific synthesis and activity of 3,4-disubstituted-2-azetidinones. *Bioorg. Med. Chem. Lett.* **1993**, *3*, 2295–2298. [CrossRef]
51. Han, W.T.; Trehan, A.K.; Kim Wright, J.J.; Federici, M.E.; Seiler, S.M.; Meanwell, N.A. Azetidin-2-one derivatives as inhibitors of thrombin. *Bioorg. Med. Chem.* **1995**, *3*, 1123–1143. [CrossRef] [PubMed]
52. Steert, K.; Berg, M.; Mottram, J.C.; Westrop, G.D.; Coombs, G.H.; Cos, P.; Maes, L.; Joossens, J.; Van der Veken, P.; Haemers, A.; et al. α-Ketoheterocycles as Inhibitors of Leishmania mexicana Cysteine Protease CPB. *ChemMedChem* **2010**, *5*, 1734–1748. [CrossRef] [PubMed]
53. Costanzo, M.J.; Almond, H.R.; Hecker, L.R.; Schott, M.R.; Yabut, S.C.; Zhang, H.-C.; Andrade-Gordon, P.; Corcoran, T.W.; Giardino, E.C.; Kauffman, J.A.; et al. In-Depth Study of Tripeptide-Based α-Ketoheterocycles as Inhibitors of Thrombin. Effective Utilization of the S1 'Subsite and Its Implications to Structure-Based Drug Design. *J. Med. Chem.* **2005**, *48*, 1984–2008. [CrossRef] [PubMed]
54. DiNinno, F.; Ernest, V.L. Facile Synthesis of β-Thioxo Esters from β-Enamino Esters. *J. Org. Chem.* **1979**, *44*, 3271–3273. [CrossRef]

55. Delprino, L.; Giacomotti, M.; Dosio, F.; Brusa, P.; Ceruti, M.; Grosa, G.; Cattel, L. Toxin-Targeted Design for Anticancer Therapy. I: Synthesis and Biological Evaluation of New Thioimidate Heterobifunctional Reagents. *J. Pharm. Sci.* **1993**, *82*, 506–512. [CrossRef] [PubMed]
56. Brogi, S.; Ibba, R.; Rossi, S.; Butini, S.; Calderone, V.; Gemma, S.; Campiani, G. Covalent Reversible Inhibitors of Cysteine Proteases Containing the Nitrile Warhead: Recent Advancement in the Field of Viral and Parasitic Diseases. *Molecules* **2022**, *27*, 2561. [CrossRef]
57. Barthels, F.; Meyr, J.; Hammerschmidt, S.J.; Marciniak, T.; Räder, H.-J.; Ziebuhr, W.; Engels, B.; Schirmeister, T. 2-Sulfonylpyrimidines as Privileged Warheads for the Development of S. aureus Sortase A Inhibitors. *Front. Mol. Biosci.* **2022**, *8*, 804970. [CrossRef]
58. Paasche, A.; Schiller, M.; Schirmeister, T.; Engels, B. Mechanistic Study of the Reaction of Thiol-Containing Enzymes with α,β-Unsaturated Carbonyl Substrates by Computation and Chemoassays. *ChemMedChem* **2010**, *5*, 869–880. [CrossRef]
59. Silva, D.G.; Ribeiro, J.F.R.; De Vita, D.; Cianni, L.; Franco, C.H.; Freitas-Junior, L.H.; Moraes, C.B.; Rocha, J.R.; Burtoloso, A.C.B.; Kenny, P.W.; et al. A comparative study of warheads for design of cysteine protease inhibitors. *Bioorg. Med. Chem. Lett.* **2017**, *27*, 5031–5035. [CrossRef]
60. Kim, K.B.; Crews, C.M. From epoxomicin to carfilzomib: Chemistry, biology, and medical outcomes. *Nat. Prod. Rep.* **2013**, *30*, 600. [CrossRef]
61. Cianni, L.; Feldmann, C.W.; Gilberg, E.; Gütschow, M.; Juliano, L.; Leitão, A.; Bajorath, J.; Montanari, C.A. Can Cysteine Protease Cross-Class Inhibitors Achieve Selectivity? *J. Med. Chem.* **2019**, *62*, 10497–10525. [CrossRef] [PubMed]
62. Konno, S.; Kobayashi, K.; Senda, M.; Funai, Y.; Seki, Y.; Tamai, I.; Schäkel, L.; Sakata, K.; Pillaiyar, T.; Taguchi, A.; et al. 3CL Protease Inhibitors with an Electrophilic Arylketone Moiety as Anti-SARS-CoV-2 Agents. *J. Med. Chem.* **2022**, *65*, 2926–2939. [CrossRef] [PubMed]
63. Chemical Computing Group ULC. *Molecular Operating Environment (MOE)*; Chemical Computing Group ULC: Montreal, QC, Canada, 2020; Available online: https://www.chemcomp.com/. (accessed on 23 March 2022).
64. *LeadIT/FlexX*, Version 2.3.2; GmbH, BioSolveIT: Sankt Augustin, Germany, 2017.
65. Serrano-Aparicio, N.; Moliner, V.; Świderek, K. Nature of Irreversible Inhibition of Human 20S Proteasome by Salinosporamide A. The Critical Role of Lys–Asp Dyad Revealed from Electrostatic Effects Analysis. *ACS Catal.* **2021**, *11*, 3575–3589. [CrossRef]
66. Gehringer, M.; Laufer, S.A. Emerging and Re-Emerging Warheads for Targeted Covalent Inhibitors: Applications in Medicinal Chemistry and Chemical Biology. *J. Med. Chem.* **2019**, *62*, 5673–5724. [CrossRef]
67. Chenna, B.C.; Li, L.; Mellott, D.M.; Zhai, X.; Siqueira-Neto, J.L.; Calvet Alvarez, C.; Bernatchez, J.A.; Desormeaux, E.; Alvarez Hernandez, E.; Gomez, J.; et al. Peptidomimetic Vinyl Heterocyclic Inhibitors of Cruzain Effect Antitrypanosomal Activity. *J. Med. Chem.* **2020**, *63*, 3298–3316. [CrossRef]
68. Vankadara, S.; Dawson, M.D.; Fong, J.Y.; Oh, Q.Y.; Ang, Q.A.; Liu, B.; Chang, H.Y.; Koh, J.; Koh, X.; Tan, Q.W.; et al. A Warhead Substitution Study on the Coronavirus Main Protease Inhibitor Nirmatrelvir. *ACS Med. Chem. Lett.* **2022**, *13*, 1345–1350. [CrossRef] [PubMed]
69. Ludewig, S.; Kossner, M.; Schiller, M.; Baumann, K.; Schirmeister, T. Enzyme Kinetics and Hit Validation in Fluorimetric Protease Assays. *Curr. Top. Med.Chem.* **2010**, *10*, 368–382. [CrossRef] [PubMed]
70. Barthels, F.; Marincola, G.; Marciniak, T.; Konhäuser, M.; Hammerschmidt, S.; Bierlmeier, J.; Distler, U.; Wich, P.R.; Tenzer, S.; Schwarzer, D.; et al. Irreversible and Selective Inhibitors of Staphylococcus aureus Sortase A. *ChemMedChem* **2020**, *15*, 839–850. [CrossRef]
71. Amendola, G.; Ettari, R.; Previti, S.; Di Chio, C.; Messere, A.; Di Maro, S.S.; Hammerschmidt, J.; Zimmer, C.; Zimmermann, R.A.; Schirmeister, T.; et al. Lead Discovery of SARS-CoV-2 Main Protease Inhibitors through Covalent Docking-Based Virtual Screening. *J. Chem. Inf. Model.* **2021**, *61*, 2062–2073. [CrossRef]
72. Schirmeister, T.; Kesselring, J.; Jung, S.; Schneider, T.H.; Weickert, A.; Becker, J.; Lee, W.; Bamberger, D.; Wich, P.R.; Distler, U.; et al. Engels, Quantum Chemical-Based Protocol for the Rational Design of Covalent Inhibitors. *J. Am. Chem. Soc.* **2016**, *138*, 8332–8335. [CrossRef]
73. Caffrey, C.R.; Hansell, E.; Lucas, K.D.; Brinen, L.S.; Hernandez, A.A.; Cheng, J.; Roush, W.R.; Stierhof, Y.-D.; Bogyo, M.; Steverding, D.; et al. Active site mapping, biochemical properties and subcellular localization of rhodesain, the major cysteine protease of Trypanosoma brucei rhodesiense. *Mol. Biochem. Parasitol.* **2001**, *118*, 61–73. [CrossRef]
74. Berman, H.M. The Protein Data Bank. *Nucleic Acids Res.* **2000**, *28*, 235–242. [CrossRef]
75. Berman, H.; Henrick, K.; Nakamura, H. Announcing the worldwide Protein Data Bank. *Nat. Struct. Mol. Biol.* **2003**, *10*, 980. [CrossRef] [PubMed]
76. Halgren, T.A. MMFF94s option for energy minimization studies. *J. Comput. Chem.* **1999**, *20*, 720–729. [CrossRef]
77. *The PyMOL Molecular Graphics System*, version 2.5.2; Schrödinger, LLC: New York, NY, USA, 2021.
78. Reulecke, I.; Lange, G.; Albrecht, J.; Klein, R.; Rarey, M. Towards an Integrated Description of Hydrogen Bonding and Dehydration: Decreasing False Positives in Virtual Screening with the HYDE Scoring Function. *ChemMedChem* **2008**, *3*, 885–897. [CrossRef] [PubMed]
79. Frisch, M.J.; Trucks, G.W.; Schlegel, H.B.; Scuseria, G.E.; Robb, M.A.; Cheeseman, J.R.; Scalmani, G.; Barone, V.; Peterson, G.A.; Nakatsuji, H.; et al. *Gaussian 16 (Revision A.03)*; Gaussian Inc.: Wallingfort, CT, USA, 2016.

80. Chai, J.-D.; Head-Gordon, M. Long-range corrected hybrid density functionals with damped atom–atom dispersion corrections. *Phys. Chem. Chem. Phys.* **2008**, *10*, 6615. [CrossRef]
81. Marenich, A.V.; Cramer, C.J.; Truhlar, D.G. Universal Solvation Model Based on Solute Electron Density and on a Continuum Model of the Solvent Defined by the Bulk Dielectric Constant and Atomic Surface Tensions. *J. Phys. Chem. B* **2009**, *113*, 6378–6396. [CrossRef]
82. Pliego, J.R., Jr.; Riveros, J.M. Gibbs energy of solvation of organic ions in aqueous and dimethyl sulfoxide solutions. *Phys. Chem. Chem. Phys.* **2002**, *4*, 1622–1627. [CrossRef]
83. Ben-Naim, A. Standard Thermodynamics of Transfer. Uses and Misuses. *J. Phys. Chem.* **1978**, *82*, 792–803. [CrossRef]
84. Spina, R.; Colacino, E.; Martinez, J.; Lamaty, F. Poly(ethylene glycol) as a Reaction Matrix in Platinum- or Gold-Catalyzed Cycloisomerization: A Mechanistic Investigation. *Chem.-A Eur. J.* **2013**, *19*, 3817–3821. [CrossRef]
85. Ho, A.; Cyrus, K.; Kim, K.-B. Towards Immunoproteasome-Specific Inhibitors: An Improved Synthesis of Dihydroeponemycin. *Eur. J. Org. Chem.* **2005**, *2005*, 4829–4834. [CrossRef]
86. St-Georges, C.; Désilets, A.; Béliveau, F.; Ghinet, M.; Dion, S.P.; Colombo, É.; Boudreault, P.-L.; Najmanovich, R.J.; Leduc, R.; Marsault, É. Modulating the selectivity of matriptase-2 inhibitors with unnatural amino acids. *Eur. J. Med. Chem.* **2017**, *129*, 110–123. [CrossRef] [PubMed]
87. Costanzo, M.J.; Yabut, S.C.; Almond, H.R.; Andrade-Gordon, P.; Corcoran, T.W.; de Garavilla, L.; Kauffman, J.A.; Abraham, W.M.; Recacha, R.; Chattopadhyay, D.; et al. Potent, Small-Molecule Inhibitors of Human Mast Cell Tryptase. Antiasthmatic Action of a Dipeptide-Based Transition-State Analogue Containing a Benzothiazole Ketone. *J. Med. Chem.* **2003**, *46*, 3865–3876. [CrossRef]
88. Engel-Andreasen, J.; Wellhöfer, I.; Wich, K.; Olsen, C.A. Backbone-Fluorinated 1,2,3-Triazole-Containing Dipeptide Surrogates. *J. Org. Chem.* **2017**, *82*, 11613–11619. [CrossRef] [PubMed]
89. Dutton, F.E.; Lee, B.H.; Johnson, S.S.; Coscarelli, E.M.; Lee, P.H. Restricted Conformation Analogues of an Anthelmintic Cyclodepsipeptide. *J. Med. Chem.* **2003**, *46*, 2057–2073. [CrossRef]

"

Supporting information

Investigation of the compatibility between warheads and peptidomimetic sequences of protease inhibitors - a comprehensive reactivity and selectivity study

Patrick Müller[1†], Mergim Meta[1†], J. Laurenz Meidner[1†], Marvin Schwickert[1], Jessica Meyr[2], Kevin Schwickert[1], Christian Kersten[1], Collin Zimmer[1], Stefan Hammerschmidt[1], Ariane Frey[1], Albin Lahu[1], Sergio de la Hoz-Rodríguez[3], Laura Agost-Beltrán[3], Santiago Rodríguez[3], Kira Diemer[2], Wilhelm Neumann[2], Florenci V. Gonzàlez[3], Bernd Engels[2] and Tanja Schirmeister[1*]

[1] Institute of Pharmaceutical and Biomedical Sciences, Johannes Gutenberg University Mainz, Mainz, Germany

[2] Institute of Physical and Theoretical Chemistry, Julius-Maximilians-University of Wuerzburg, Wuerzburg, Germany

[3] Departament de Química Inorgànica I Orgànica, Universitat Jaume I, 12080 Castello, Spain

[*] Author to whom correspondence should be addressed.

[†] These authors contributed equally to this work.

Content

***In vitro* results of the synthesized compounds**…… S2–4

Reactivity assay……... S5–20

Fluorometric inhibition assays……. S21–23

Protein Expression……. S23–25

Molecular Docking……..…….…… S26–30

Quantum mechanics simulations / kinetics…….... S31–34

Synthesis……. S35–98

Spectra and chromatograms…….....…….…… S99–172

References…….…….…… S173–174

In vitro results of the synthesized compounds

Table S1. *In vitro* results of the tested compounds against the corresponding protease. The peptidic sequence targeting the protease is shown on top.

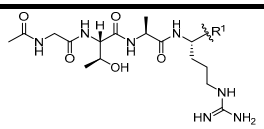

K_i (µM)/ k_{inact} (s^{-1})/ k_{2nd} (M^{-1} s^{-1})					
R^1	**uPA**	**Proteasome β5-subunit**	**CatS**	**M^{Pro}**	**Rhodesain**
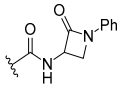 **103**	0.141 ± 0.027 [a]	n.a.	n.a.	n.a.	n.a.
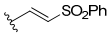 **106**	n.a.	n.a.	n.a.	n.a.	n.a.
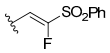 **107**	n.a.	n.a.	n.a.	n.a.	n.a.

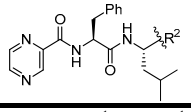

K_i (µM)/ k_{inact} (s^{-1})/ k_{2nd} (M^{-1} s^{-1})					
R^2	**uPA**	**Proteasome β5-subunit**	**CatS**	**M^{Pro}**	**Rhodesain**
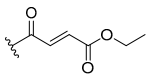 **68**	n.a.	n.a.	n.a.*	n.a.	0.009 ± 0.001/ 0.006 ± 0.001/ 6.65 x 10^5 ± 1.57 x10^4
 **59**	n.a.	n.a.	0.619 ± 0.054 [a]	n.a.	0.002 ± 0.005 [a]
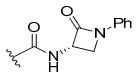 **72**	n.a.	n.a.	n.a.	n.a.	n.a.
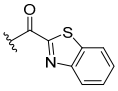 **62**	n.a.	n.a.	n.a.	n.a.	n.a.
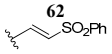 **58**	n.a.	n.a.	0.126 ± 0.071/ 0.013 ± 0.002/ 1.00 x 10^5 ± 1.25 x10^4	n.a.	0.331 ± 0.041/ 0.019 ± 0.001/ 5.85 x 10^4 ± 1.66 x10^3
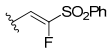 **55**	n.a.	n.a.	0.934 ± 0.138 [a]	n.a.	0.462 ± 0.039 [a]
 **74**	n.a.	n.a.	0.238 ± 0.023[a]	n.a.	0.560 ± 0.267

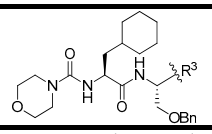

	K_i (µM)/ k_{inact} (s^{-1})/ k_{2nd} (M^{-1} s^{-1})				
R^3	**uPA**	**Proteasome β5-subunit**	**CatS**	**M^{Pro}**	**Rhodesain**
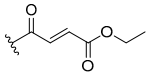 **40**	n.a.	n.a.	0.022 ± 0.004/ 0.0023 ± 0.00007/ 1.04 x 10^5 ± 1.04 x10^4	n.a.	0.035 ± 0.009/ 0.003 ± 0.0001/ 1.03 x 10^5 ± 1.09 x10^4
 **49**	n.a.	n.a.	0.012 ± 0.001 [a]	n.a.	0.002 ± 0.0002 [a]
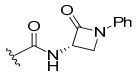 **45**	n.a.	n.a.	0.86 ± 0.13/ 0.00046 ± 0.00002/ 5.34 x 10^5 ± 8.29 x10^4	n.a.	n.a.
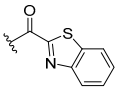 **42**	n.a.	n.a.	0.233 ± 0.024 [a]	n.a.	0.324 ± 0.089 [a]
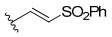 **35**	n.a.	n.a.	0.003 ± 0.0006/ 0.02022 ± 0.0006/ 7.24 x 10^6 ± 2.36 x10^5	n.a.	0.022 ± 0.002/ 0.006 ± 0.0004/ 2.57 x 10^5 ± 1.04 x10^3
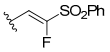 **36**	n.a.	n.a.	3.215 ± 0.612 [a]	n.a.	n.a.
 **30**	n.a.	n.a.	0.001 ± 0.0001 [a]	n.a.	0.021 ± 0.002

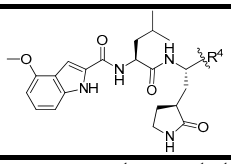

	K_i (µM)/ k_{inact} (s^{-1})/ k_{2nd} (M^{-1} s^{-1})				
R^4	**uPA**	**Proteasome β5-subunit**	**CatS**	**M^{pro}**	**Rhodesain**
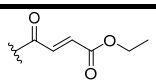 **81**	n.a.	-	n.a*	n.a*	0.099 ± 0.024/ 0.006 ± 0.0009/ 6.41 x 10^4 ± 3.00 x10^3-
 **88**	n.a.	n.a.	0.388 ± 0.277 [a]	2.197 ± 0.184 a)	0.002 ± 0.0001 [a]
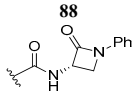 **96**	n.a.	n.a.	n.a.	n.a.	n.a.
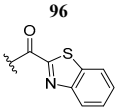 **90**	n.a.	n.a.	n.a.	0.026 ± 0.003 a)	n.a.
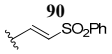 **93**	n.a.	n.a.	0.330 ± 0.065/ 0.0087 ± 0.0001/ 2.62 x 10^4 ± 2.41 x10^3	3.531 ± 1.112/ 0.0137 ± 0.0061/ 2.79 x 10^3 ± 3.12 x10^2	2.002 ± 0.604/ 0.029 ± 0.008/ 1.49 x 10^4 ± 1.09 x10^4

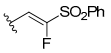 **94**	n.a.	n.a.	1.351 ± 0.09 [a]	0.517 ± 0.033 [a]	0.217 ± 0.031 [a]
 **84**	n.a.	n.a.	0.104 ± 0.009	0.031 ± 0,005 [a])	0.042 ± 0.005

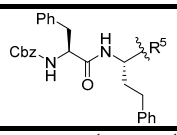

K_i (µM)/ k_{inact} (s^{-1})/ k_{2nd} (M^{-1} s^{-1})

R^5	uPA	Proteasome β-5-subunit	CatS	M^{Pro}	Rhodesain
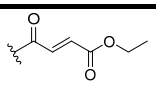 **22**	n.a.	n.a.	0.018 ± 0.003/ 0.0022 ± 0.0001/ 1.24 x 10^5 ± 1.86 x10^4	n.a.	0.079 ± 0.007/ 0.008 ± 0.001/ 1.06 x 10^5 ± 4.57 x10^2
 **13**	n.a.	n.a.	0.201± 0.093 [a]	n.a.	0.060 ± 0.006 nM [a]
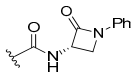 **24**	n.a.	n.a.	n.a.	n.a.	n.a.
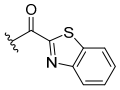 **18**	n.a.	n.a.	n.a.	n.a.	n.a.
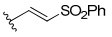 **16**	n.a.	n.a.	0.001 ± 0.0006/ 0.0037 ± 0.0006/ 2.88 x 10^6 ± 8.56 x10^5	n.a.	0.020 ± 0.002/ 0.005 ± 0.0001/ 2.90 x 10^5 ± 3.17 x10^3
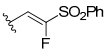 **17**	n.a.	n.a.	0.966 ± 0.104)	n.a.	3.565 ± 0.437 [a]
 **25**	n.a.	n.a.	0.136 ± 0.012 [a]	n.a.	0.088 ± 0.0174 [a]

a) Calculated from IC_{50} value with the Cheng–Prusoff equation.
n.d. not determined.
n.a. not active.

Reactivity assay

Method A (^{1}H-NMR):

The corresponding Michael-acceptor (0.07 mmol, 1 eq) and the reference compound 1,3-dioxolan (0.5 eq) were dissolved in DMSO-d_6 (0.5 mL). The reaction was measured in time intervals before (0 min) and 5, 30, 60, 120 and 240 mins after the addition of the corresponding nucleophile (PhEtSH/EtONa, 2 eq) in presence or absence of Et_3N (2 eq). The CH_2-signal of 1,3-dioxlan was set at 5.3 ppm to get uniform shifts of the olefin signals in the ^{1}H-NMR spectra.

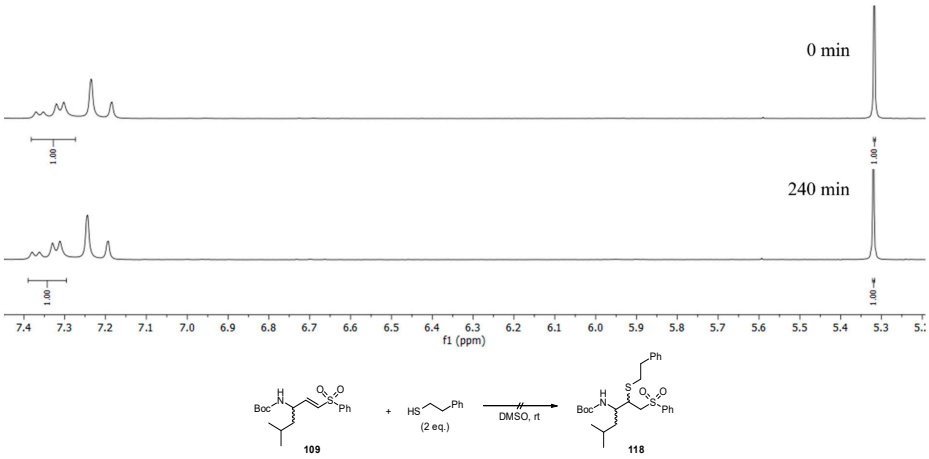

Figure S1. ^{1}H-NMR spectra of **109** after certain time intervals. Reaction of 2-phenylethanthiol with the vinyl sulfone moiety.

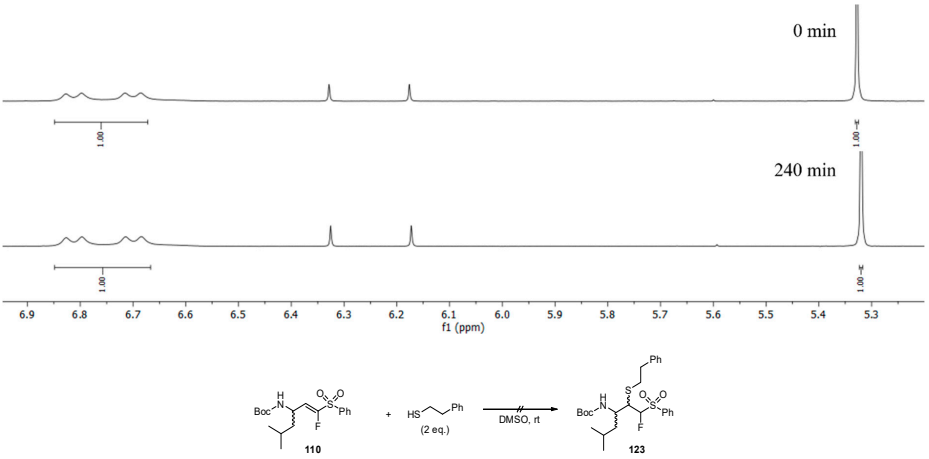

Figure S2. ^{1}H-NMR spectra of **110** after certain time intervals. Reaction of 2-phenylethanthiol with the F-vinyl sulfone moiety.

Method A (^{13}C-NMR):

The α-ketobenzothiazole or nitrile **115**, **117** (0.07 mmol, 1 eq) was dissolved in DMSO-d_6 (0.5 mL). The reaction was measured in time intervals before (0 min), 5, 30, 60, 120 and 240 mins after the addition of the corresponding nucleophile (PhEtSH/EtONa, 2 eq) in presence or absence of Et_3N (2 eq). The reference signal of DMSO-d_6 was set at 39.52 ppm.

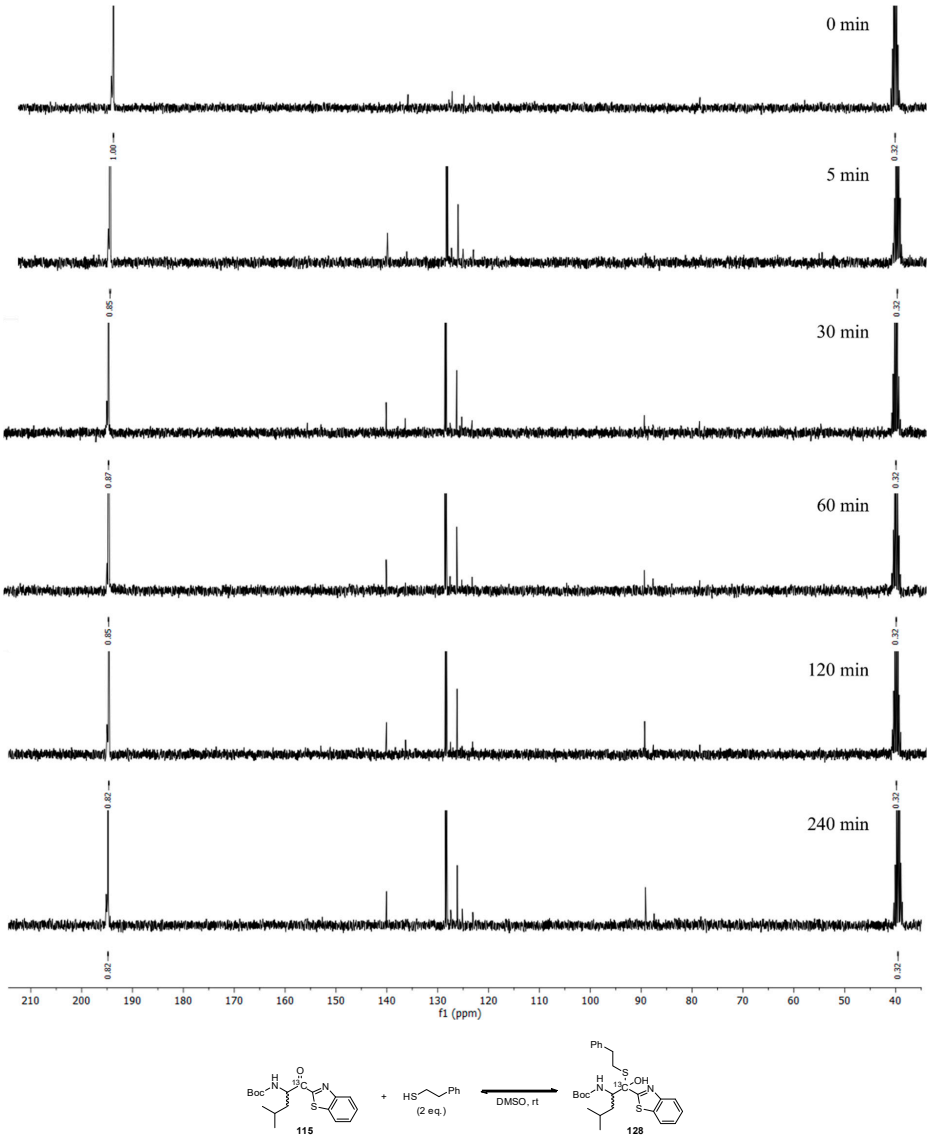

Figure S12. ^{13}C-NMR spectra of **115** after certain time intervals. Reaction of 2-phenylethanthiol with the ketobenzothiazole moiety.

Method B (LC/MS):

The *β*-lactam **108** (0.07 mmol, 1eq) was solved in DMSO-d_6 (0.5 mL). The reaction was measured in time intervals before (0 min), 5, 30, 60, 120 and 240 mins after the addition of the corresponding nucleophile (PhEtSH/EtONa, 2 eq) in presence of Et_3N (2 eq) or not. In case of PhEtSH as the nucleophile the reaction got quenched by pouring 10 µL of the reaction mixture into a solution of 25 mM TRIS (pH 7.00) and 27 mM maleimide in a 1:1 mixture of acetonitrile/H_2O (990 µL). For the reaction with EtONa as the nucleophile, the reaction solution got quenched by pouring 10 µL of the mixture in 990 µL of a acetonitrile/Tris (50 mM) solution. The quenched reaction mixtures were measured and analyzed via LC-MS.

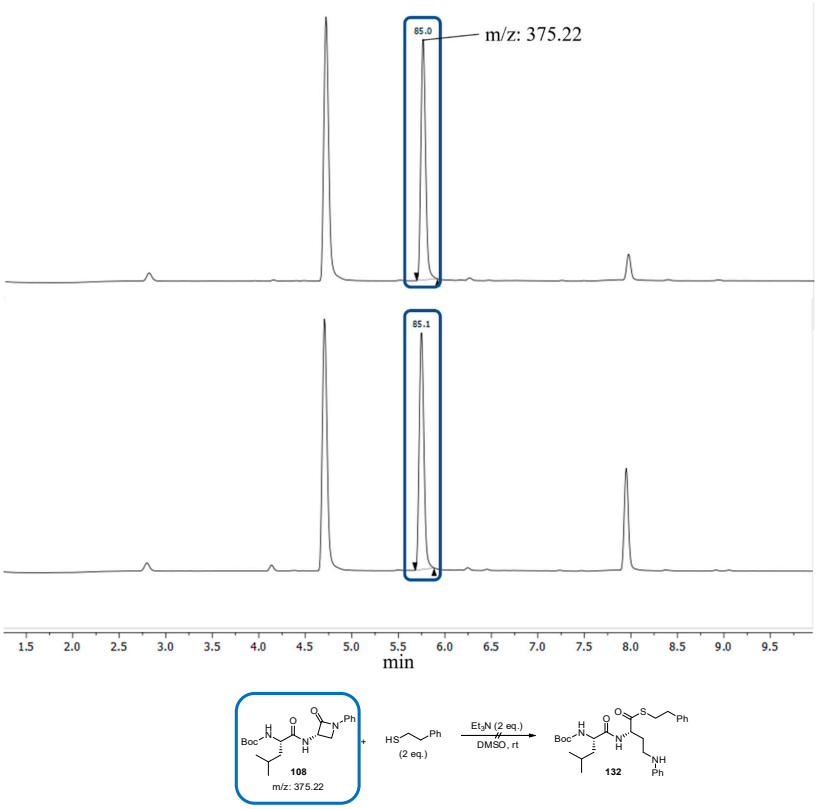

Figure S18. UV chromatogram of **108** after certain time intervals. Reaction of 2-phenylethanthiol with the *β*-lactam moiety in presence of Et_3N and without Et_3N.

Fluorometric inhibition assays

The inhibitory activities of the compounds against the proteases were determined with assays based on fluorogenic or FRET-based substrates. The fluorescence was measured in a white flat-bottom 96-well plate from Greiner Bio-One using a Tecan Infinite F2000 Pro plate reader. Measurements were performed as triplicates. The substrate and the compounds were prepared as stock solutions in DMSO. Each well contained a total volume of 200 µL, consisting of 185 µL buffer, 5 µL inhibitor in DMSO or pure DMSO as negative control, 5 µL substrate in DMSO and 5 µL enzyme solution in buffer. Dilution series between 200 µM and 50 pM were prepared for the determination of the inhibition constants. The fluorescence signal was measured every 30 s for 10 min at 25 °C with the corresponding excitation and emission wavelengths. IC_{50} values for the reversible inhibitors were calculated by fitting the remaining enzymatic activity to the four parameter IC_{50} equation with Y [ΔF/min] as the substrate hydrolysis rate, Y_{max} as the maximum value of the dose response curve at inhibitor concentrations [I] = 0 µM, Y_{min} as the minimum value at high inhibitor concentrations and *s* as the hill coefficient.[1] The sigmoidal dose-response curves of the compounds **30** and **94** against rhodesain are shown exemplary in Figure **S19**.

$$y = \frac{y_{\max} - y_{\min}}{1 + \left(\frac{[\mathrm{I}]}{\mathrm{IC}_{50}}\right)^{s}} + y_{\min}$$

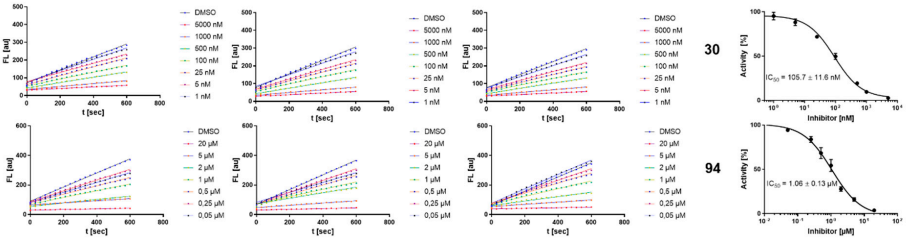

Figure S19. (left) Fluorescence progress curves for **30** and **94** against rhodesain. (right) Plots showing the respective IC_{50} values from sigmoidal fits.

Due to the dependence of the IC_{50} value on the substrate affinity and concentration, the K_i values were calculated with the Cheng-Prusoff equation (1) for appropriate comparison of the inhibitory activities to the other enzymes and inhibitors.[1]

$$K_I = \frac{\mathrm{IC}_{50}}{1 + \frac{[S]}{K_\mathrm{M}}} \qquad 1$$

To evaluate the inhibitory activities of the irreversible inhibitors, reporting IC_{50} values is less suitable, because the IC_{50} values are heavily depending on the incubation time of the enzyme and inhibitor. Therefore, the dissociation constant of the reversible enzyme-inhibitor complex K_I, the maximum inactivation rate k_{inact} and the second-order rate constants of inhibition k_{2nd} were determined. The substrate-conversion plots in presence of the compounds **16**, and **35** against rhodesain are indicating a time-dependent inhibition as shown exemplary in Figure **S20**. It is shown, that the apparent first-order rate constant k_{obs} changed hyperbolically with the inhibitor concentration. A limiting value was approached at higher inhibitor concentrations, indicating a two-step inhibition-mechanism.[1,2]

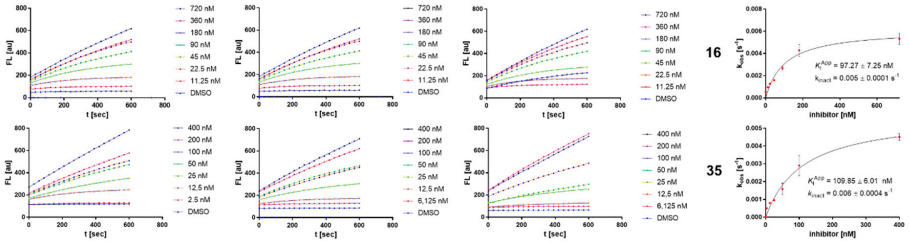

Figure S20. (left) Fluorescence progress curves for **16** and **35** against rhodesain. (right) k_{obs} against [I] plots showing the respective K_I^{App} and k_{inact} values from hyperbolic fits.

For determination of the k_{obs} values, progress curves were analyzed by non-linear regression analysis up to 10 min with the exponential equation (2). F represents the fluorescence intensity, which is proportional to the product concentration [P] and offset represents the background fluorescence.

$$F = [P]^{\propto}(1 - e^{-k_{obs} \cdot t}) + \text{offset} \qquad 2$$

The received k_{obs} values were fitted against the inhibitor concentrations using the hyperbolic equation (3) to get the k_{inact} and K_I^{app} values. For compound **93** no k_{obs} saturation was observed. A Lineweaver-Burk linearization (4) was used to receive K_I^{app} and $k_{inact.}$

$$k_{obs} = \frac{k_{inact}[I]}{K_I^{App} + [I]} \qquad 3$$

$$\frac{1}{k_{obs}} = \frac{K_I^{App}}{k_{inact}[I]} \frac{1}{[I]} + \frac{1}{k_{inact}} \qquad 4$$

The K_I^{app} values were corrected to the K_I values by the Cheng-Prussoff equation (5), for better comparison of the inhibitory constants to the other enzymes and compounds.

$$K_I = \frac{K_I^{App}}{1 + \frac{[S]}{K_M}} \quad 5$$

The second-order rate constant of inhibition k_{2nd} were calculated from the equation (6).[1]

$$K_{2nd} = \frac{k_{inact}}{K_I} \quad 6$$

Buffers and substrates

The following buffers and substrates were used for the respective assays: Rhodesain (50 mM Na-acetate pH 5.5, 5 mM EDTA, 200 mM NaCl, 50 µM DTT, 0.005% Brij 10 µM Cbz-Phe-Arg-AMC, 1 nM rhodesain), Cathepsin S (50 mM KH_2PO_4, pH 6.5, 50 mM K_2HPO_4, 2.5 mM DTT, 2.5 mM EDTA, Z-Val-Arg-Arg-AMC, 10 nM CatS), β-5-subunit of the proteasome (50 mM Tris HCl, 25 mM NaCl, 10 mM NaCl, $MgCl_2 \cdot 6\ H_2O$, 100 µM Succ-Leu-Leu-Val-Tyr-AMC, 0.02 mg/mL proteasome β5-subunit), Sars-Cov-2 M^{Pro} (20 mM TRIS, pH 7.5, 0.1 mM, NaCl 200 mM, DTT 1 mM, 50 nm M^{Pro}), an internally quenched 14-mer fluorogenic (FRET) peptide (DABCYL-KTSAVLQSGFRKME-EDANS)), uPA (50 mM Tris HCl, 150 mM pH 7.5, NaCl, 10 mM $CaCl_2$, 0.005% TX-100, 240µM Cbz-Gly-Gly-Arg-AMC, 2.5 U uPA). As positive controls, several well-known inhibitors have been used for the respective enzymes and their biological activity was reproduced.

The human uPa and recombinant CatS were purchased from Sigma Aldrich, and the proteasome β5-subunit from Enzo Life sciences. Rhodesain and SARS-CoV-2 M^{pro} were expressed under the conditions described below.

Protein Expression and purification

SARS-CoV-2 M^{pro}.

The expression of SARS-CoV-2 Mpro was performed as described previously.[3] Briefly, the pMal-c2 plasmid (New England Biolabs, Ipswich, MA, USA), harboring the DNA of the entire SARS-CoV-2 M^{pro} coding sequence framed by a short sequence specifying the 5 *C*-terminal residues of nonstructural protein 4 (nsp4/nsp5 cleavage site) at the 5' end and the sequence of a hexahistidine tag at the 3' end. The presence of the nsp4/nsp5 cleavage site between the plasmid's MBP and the M^{pro} sequence together with the native nsp5/nsp6 cleavage site between

Computational studies

Molecular docking

Since the inhibitors were designed to react covalently with the cysteine or the serine-/ threonine-proteases two different docking approaches were followed. First, a conventional non-covalent docking was performed, to estimate affinity and geometry of the pre-organized enzyme-inhibitor complex, secondly a covalent docking was used to determine the final covalent enzyme-inhibitor complex.

In both docking setups crystallographic reference ligands were used for validation *via* redocking (Table S2), all inhibitors with the same peptidic recognition sequence with varying warheads were docked against their corresponding target enzyme.

Molecular docking experiments were performed using the following crystal structures freely available in the protein data bank (PDB)[6]: rhodesain covalently bound to K11777 (PDB entry 2P7U)[7]; cathepsin S covalently bound to morpholine-4-carboxylic acid [1s-(2-benzyloxy-1r-cyano-ethylcarbamoyl)-3-methyl-butyl]amide (PDB entry 1MS6)[8]; urokinase type plasimogen activator covalently bound to *N*-(Isobutoxycarbonyl)-D-seryl-N-((1s)-4-{[amino(imino)methyl]amino}-1-formylbutyl)-L-alanineamide (pdb entry 1W10)[9]; Main Protease of SARS-Cov-2 covalently bound to GRL-024-20 (pdb entry 6XR3)[10]; Chain K of the human 20 S proteasome covalently bound to bortezomib (pdb entry: 5LF3)[11]. All ligands were energetically minimized prior docking with Molecular operating environment (MOE 2020.09)[12] using the MMF94x force field.[13]

Docking approach A: non-covalent docking with LeadIT

The non-covalent docking was performed with LeadIT-2.3.2.[14] The receptors were prepared in MOE with the protonate3D functionality and the covalent bonds between the co-crystallized ligands and the corresponding proteases were untethered *via* the Builder tool in MOE. In case of the proteasome the *β*-5-subunit (chain K) was extracted with PyMOL-2.5.2[15] and used for all subsequent docking operations. For all receptors the binding site was defined as a 6.5 Å shell around the bound reference ligand. Water molecules that form at least three hydrogen bonds with the receptor and ligand were kept as part of the binding site. The docking was performed under default settings using the enthalpy-entropy hybrid approach with 2000 solutions *per* iteration and fragmentation. Only the top pose of the initial docking was kept and re-scored using the HYDE scoring function.[16] For the *β*-5 subunit of the proteasome, pharmacophore constraints needed to be included to obtain reasonable binding modes. The nitrogen atoms of the peptide backbone were therefore defined as h-bond donors with a 1 Å sphere radius.

Docking approach B: covalent docking with MOE

Covalent docking was performed with MOE. The receptors were prepared using the 3D protonation tool inside MOE. For the covalent reaction of the different warheads, the already existing template reactions were used or customized using the combinatorial library tool of MOE. Initial 30 poses from the triangle match placement with London ΔG scoring were re-scored using the Affinity ΔG scoring function and induced fit refinement implemented in MOE. 10 Poses were kept and visually inspected for binding geometry the interactions matching between the docked inhibitor pose and co-crystallized ligand with the enzyme. The poses best matching inspected interaction patterns are further discussed.

Table S2. Redocking.

Enzyme (pdb entry)	Reference ligand ID	Redocking FlexX (RMSD/ Å)	FlexX score (kJ/mol)
UPA (1W10)	SJ1	0.97	–41.8
β-5-subunit 20S-Proteasome (5LF3)	BO2	0.91	–21.7
Cathepsin S (1MS6)	BLN	0.94	–18.0
SARS-Cov-2 M^{pro} (6XR3)	V7G	0.53	–49.1
Rhodesain (2P7U)	D1R	1.48	–20.2

Table S3. Results of molecular docking analysis.

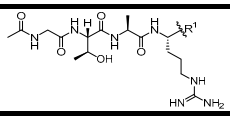			Target (pdb entry) uPA (1W10)	
R^1	Distance (electrophilic C-Ser195-O) / Å	FlexX score (kJ/mol)	Hyde score (kJ/ mol)[a]	Covalent docking score (Affinity ΔG, MOE/ kcal/mol)
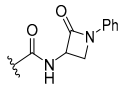 **103**	2.84	–51.59	17	–5.97
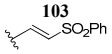 **106**[b]	2.74	–48.96	3	–5.01
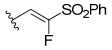 **107**[b]	4.04	–40.11	5	–5.37
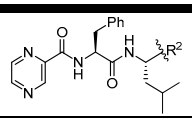			Target (pdb entry) *β*-5-subunit of 20S-Proteasome (5LF3)	
R^2	Distance (electrophilic C-Ser195-O) / Å	FlexX score (kJ/mol)	Hyde score (kJ/ mol)[a]	Covalent docking score (Affinity ΔG, MOE/ kcal/mol)
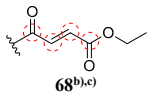 **68**[b],[c]	2.56	–16.64	–14	–4.32

 **59**	2.52	–21.67	–22	–2.93
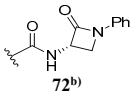 **72**[b]	4.95	–21.48	–13	–3.08
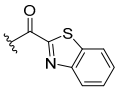 **62**	3.16	–23.97	–2	–3.40
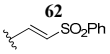 **58**[b]	6.77	–12.33	–25	–2.73
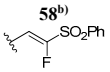 **55**[b]	5.90	–9.76	–4	–2.44
 **74**	2.27	–22.96	–22	–3.17

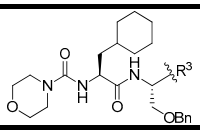			Target (pdb entry) Cathepsin S (1MS6)	
R[3]	Distance (electrophilic C-Ser195-O) / Å	FlexX score (kJ/mol)	Hyde score (kJ/ mol)[a]	Covalent docking score (Affinity ΔG, MOE/ kcal/mol)
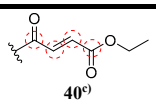 **40**[c]	3.37	–21.56	–51	–5.44
 **49**	2.69	–22.88	–32	–4.38
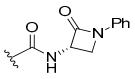 **45**	3.03	–30.80	–24	–4.61
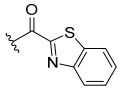 **42**	2.96	–30.67	–30	–6.29
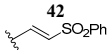 **35**	3.07	–27.35	–48	–5.32
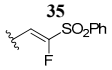 **36**	3.30	–25.17	–45	–5.19
 **30**	2.87	–26.22	–40	–3.00

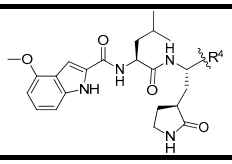			Target (pdb entry) Sars-Cov-2 MPro (6XR3)	
R[4]	Distance (electrophilic C-Ser195-O) / Å	FlexX score (kJ/mol)	Hyde score (kJ/ mol)[a]	Covalent docking score (Affinity ΔG, MOE/ kcal/mol)
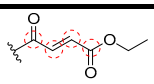	3.81	–44.50	–11	–5.38

81[c]				
 **88**	2.90	–42.80	–9	–3.56
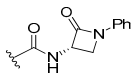 **96**	4.91	–43.37	–9	–5.89
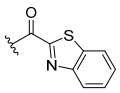 **90**	3.41	–46.96	–8	–4.88
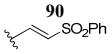 **93**	3.02	–36.04	–8	–4.66
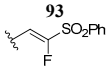 **94**	3.58	–37.95	–21	–5.50
 **84**	3.04	–44.38	–27	–4.42

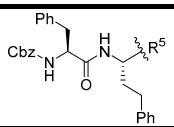

Target (pdb entry) Rhodesain (2P7U)

R^5	Distance (electrophilic C-Ser195-O) / Å	FlexX score (kJ/mol)	Hyde score (kJ/ mol)[a]	Covalent docking score (Affinity ΔG, MOE/ kcal/mol)
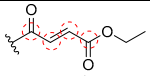 **22**[c]	2.70	–23.18	–33	–4.53
 **13**	3.50	–24.03	–12	–2.66
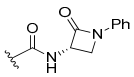 **24**	2.93	–28.88	–21	–4.22
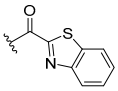 **18**	2.54	–25.62	–28	–3.91
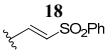 **16**	3.00	–27.11	–17	–2.96
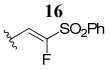 **17**	2.76	–26.92	–23	–3.58
 **25**	2.60	–26.35	–17	–3.04

a) The HYDE-scores were in the negative range for all inhibitors except the UPA inhibitors. This could be due to the high polarity of these inhibitors with calculated log P values below 0 and TPSA values above 200 Å2 which could hamper the desolvation term of the HYDE rescoring function.

b) A covalent reaction between the inhibitor and the active site is unlikely/ not expected.

c) The four possible reaction sites of the 4-oxo-enoate warhead are depicted in red dashed circles. Only one distance between the nucleophilic residue in the active site and the 4-oxo-enoate warhead was measured.

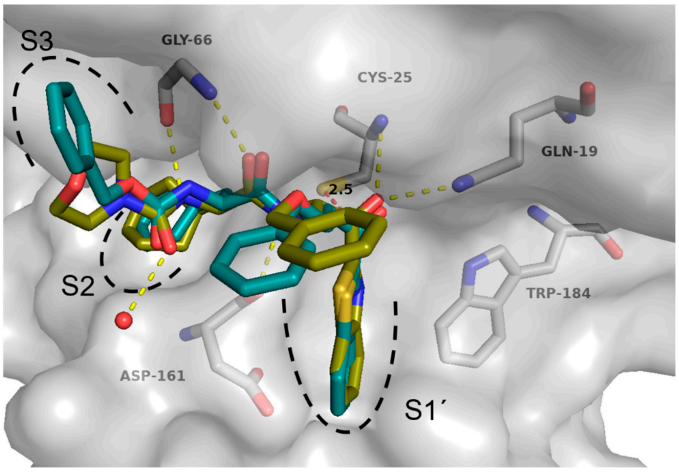

Figure S21. Superposition of the non-covalent docking poses of *α*-ketobenzothiazole **42** (deepolive C-atoms) and **18** (deepteal C-atoms) inside the active site of rhodesain (pdb entry: 2P7U). Polar interactions between **42** and the enzyme are depicted as yellow dashed lines. The distance between the sulfur atom of Cys25 and the electrophilic C-atom of **42** is depicted as red dashed line and the distance is given in Å.

Synthesis

General Methods and Materials:

All reagents and solvents were purchased commercially and used as provided by the supplier without further purification. Solvents for synthesis, extraction, and chromatography were of analytical grade. Moisture-sensitive reactions were carried out under argon atmosphere, and anhydrous solvents were used as provided by the commercial supplier. Reaction progress was monitored by thin-layer chromatography using Alugram Xtra F254 silica plates from Macherey-Nagel and/or LC-MS. Therefore, an Agilent 1100 series HPLC system and an Agilent Poroshell 120 EC-C18, 150 x 2.10 mm, 4 μm column coupled to an Agilent 1100 series LC/MSD Trap with electron spray ionization (ESI), was used. The identities and purities of compounds were determined by the same LC-MS system with a gradient of acetonitrile and water (+0.1% formic acid). Signals were detected at 210/254 nm with quantitation by AUC and masses were determined in positive ionization mode (ESI). HPLC purification was performed with the Agilent 1290 II Infinity Preparative LC System using an InfinityLab Pursuit XRs C18, 30 x 250mm, 5 µm, preparative LC column. Flash chromatography was performed with the Biotage Isolera^{TM} One system using prepacked columns from Biotage. Silica gel (0.040 – 0.063 mm) from Macherey-Nagel was used for column chromatography. Optical rotations $[\alpha]_D^{22}$ were measured on an P3000 polarimeter from Krüss at 22 °C and are reported in ml·dm^{-1}·g^{-1} with the concentration c being g/100 ml. Fourier-transformed ATR-corrected IR spectra were measured on an Avatar 330 single crystal spectrometer from ThermoNicolet. Melting points (uncorrected) were measured with an MPM-H3 using semi-open capillaries. NMR spectra were recorded as stated individually on Bruker Fourier 300 MHz, Bruker Avance DSX 400 MHz and Bruker Avance III 600 MHz. Chemical shifts are indicated in parts per million (ppm), with the solvent resonance ($CDCl_3$, DMSO-d_6 or CD_3OD from Deutero GmbH) as internal standard. The purity of all compounds tested in biological assays was ≥95% as determined by LC-MS.

Synthesis of the vinyl sulfone precursors[4]

3, Diethyl ((phenylsulfonyl)methyl)phosphonate

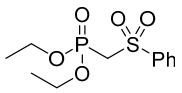

Methyl phenyl sulfone (1.5 g, 9.9 mmol, 1 eq) was dissolved in dry THF (30 mL) under argon atmosphere and cooled to 0 °C. Subsequently, *n*-BuLi (2.5 M in hexanes, 9.6 mL, 24 mmol, 2.5 eq) was added dropwise and the reaction mixture stirred for one hour at 0 °C. Afterwards, diethyl chlorophosphate (2.4 mL, 16 mmol 1.2 eq) was added and stirring was continued for one hour. The reaction was quenched with the addition of saturated NH_4Cl (10 mL) and diluted with DCM (30 mL). The aqueous phase was extracted with DCM (3x 20 mL) and the combined organic layers were dried over anhydrous Na_2SO_4. The solvent was removed under reduced pressure and the crude product was purified by column chromatography (CH/EA 4:1) to yield the desired product as a colorless solid (1.47 g, 5 mmol, 51%). ^{1}H NMR (300 MHz, $CDCl_3$): δ/ppm = 8.01 – 7.95 (m, 2H), 7.70 – 7.63 (m, 1H), 7.61 – 7.53 (m, 2H), 4.20 – 4.09 (m, 4H), 3.75 (d, J = 16.9 Hz, 2H), 1.28 (td, J = 7.1, 0.6 Hz, 6H). ^{13}C NMR (75 MHz, $CDCl_3$): δ/ppm = 140.0, 134.2, 129.2, 128.4, 63.5, 54.8, 52.9 (d, J = 6.5 Hz), 23.6 16.3. FT-IR: ν/cm^{-1} = 2988, 2898, 1324, 1257, 1155, 1018, 970, 796, 751, 683, MS (ESI) *m/z* calculated for $[C_{11}H_{18}O_5PS]^+$ ($[M+H]^+$): 293.1, found 293.0.

4, Diethyl (fluoro(phenylsulfonyl)methyl)phosphonate

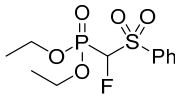

3 (1 g, 4.45 mmol, 1 eq) was dissolved in dry THF (15 mL) and cooled to −78 °C. LiHMDS (1 M in THF, 5.6 mL, 5.56 mmol, 1.25 eq) was added and stirring was continued for 30 min at −78 °C. Afterwards, Selectfluor® (2.4 g, 6.66 mmol, 1.5 eq) in DMF (10 mL) was added dropwise and the mixture stirred for two hours. The reaction was quenched with saturated NH_4Cl solution (15 mL) and diluted with EtOAc (30 mL). The aqueous phase was extracted with EtOAc (3x 20 mL) and the combined organic phases were dried over anhydrous Na_2SO_4 and the solvent was removed under reduced pressure. The crude product was purified by column chromatography (CH/EA 4:1) to yield the desired product as a colorless solid (0.81 g, 2.6 mmol, 58%). ^{1}H NMR (300 MHz, $CDCl_3$): δ/ppm = 8.03 – 7.96 (m, 1H), 7.75 – 7.68 (m, 1H), 7.60 (dd, J = 8.3, 6.9 Hz, 2H), 5.38 (dd, J = 45.5, 6.6 Hz, 1H), 4.35 – 4.19 (m, 4H), 1.34 (t, J = 7.1 Hz, 6H). ^{13}C NMR (75 MHz, $CDCl_3$): δ/ppm = 136.3, 135.0, 129.9, 129.3, 100.0, 97.9, 97.0, 94.9, 65.0 (t, J = 7.1 Hz), 16.41 (d, J = 5.9 Hz). mp: 61 – 65 °C. FT-IR: ν/cm^{-1} = 2990, 2907, 1449, 1331, 1263, 1221, 1159, 1061, 1006, 967, 852, 784, 755, 716, 699, 680. MS (ESI) *m/z* calculated for $[C_{11}H_{17}FO_5PS]^+$ ($[M+H]^+$): 311.0, found 311.0.

Synthesis of the *β*-lactam precursor[22]

6, (*S*)-2-(((Benzyloxy)carbonyl)amino)-3-hydroxypropanoic acid

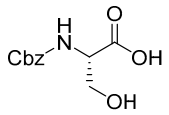

H-Ser-OH (1 g, 9.6 mol, 1 eq) and $NaHCO_3$ (2 g, 24 mmol, 2.5 eq) were dissolved in water (20 mL) and cooled to 0 °C. Benzyl chloroformate (2.01 mL, 14.4 mmol, 1.5 eq) was added dropwise. The reaction mixture was stirred for two hours at 0 °C and overnight at room temperature. The aqueous solution was acidified to pH = 2 with hydrochloric acid (1 M) and then extracted with EtOAc (3x, 10 mL). The combined organic layers were dried over Na_2SO_4, filtered and the solvent was removed under reduced pressure to yield the desired product as a colorless solid (2 g, 8.64 mmol, 90%). ^{1}H NMR (300 MHz, DMSO-d_6): δ/ppm = 7.40 – 7.25 (m, 5H), 5.04 (s, 2H), 4.06 (dt, J = 8.2, 5.1 Hz, 1H), 3.66 (d, J = 5.1 Hz, 2H). ^{13}C NMR (75 MHz, DMSO-d_6): δ/ppm = 172.2, 156.1, 137.0, 128.4, 127.8, 65.5, 61.3, 56.7. mp: 115 – 116 °C. $[\alpha]_D^{20}$ = +9 (c 1.00, DMSO). FT-IR: ν/cm^{-1} = 3320, 2935, 1710, 1690, 1567, 1477, 1285, 996, 821, 755. MS (ESI) *m/z* calculated for $[C_{11}H_{14}NO_5]^+$ ($[M+H]^+$): 240.1, found 262.1.

7, (*S*)-Benzyl (3-hydroxy-1-oxo-1-(phenylamino)propan-2-yl)carbamate

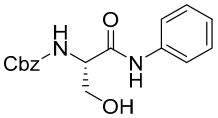

6 (3.26 g, 13.6 mmol, 1 eq) was dissolved in EtOAc (50 mL) under argon atmosphere and cooled to 0 °C. NMM (1.65 mL, 15 mmol, 1.1 eq) and TBTU (5.3 g, 16.3 mmol, 1.2 eq) were added and stirring was continued for 30 min at 0 °C. Afterwards, aniline (1.4 mL, 15 mmol, 1.1 eq) was added and the reaction mixture stirred for 12 h. The mixture was evaporated under reduced pressure and the crude product was purified by column chromatography (CH/EA 1:1) to yield the desired product as a colorless oil (3.32 g, 10.06 mmol, 74%). ^{1}H NMR (300 MHz, DMSO-d_6): δ/ppm = 7.65 – 7.58 (m, 2H), 7.39 – 7.25 (m, 7H), 7.09 – 7.01 (m, 1H), 5.07 – 5.03 (m, 2H), 4.94 (dt, J = 10.7, 5.8 Hz, 1H), 4.24 (dt, J = 7.9, 5.8 Hz, 1H), 3.66 (dq, J = 10.7, 5.5, 4.8 Hz, 2H). ^{13}C NMR (75 MHz, DMSO-d_6): δ/ppm = 169.1, 155.9, 138.9, 136.9, 128.6, 128.3, 127.8, 127.7, 123.3, 119.2, 65.5, 61.7, 57.7. $[\alpha]_D^{20}$ = +11 (c 1.00, DMSO). FT-IR: ν/cm^{-1} = 2241, 2108, 1740, 1689, 1510, 1341, 1049, 1015, 832, 754, MS (ESI) *m/z* calculated for $[C_{17}H_{19}N_2O_4]^+$ ($[M+H]^+$): 315.1, found 315.1.

8, (S)-Benzyl (2-oxo-1-phenylazetidin-3-yl)carbamate

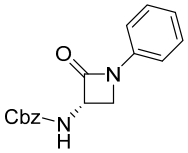

7 (1.5 g, 4.8 mmol, 1 eq) was dissolved in DMF (25 mL) under argon atmosphere and cooled to 0 °C. 1,1-sulfonyldiimidazole (1.42 g, 7.20 mmol, 1.5 eq) was added and stirred for 30 min at 0 °C. Afterwards, the reaction mixture was cooled to –20 °C and NaH (60%, 0.20 g, 7.20 mmol, 1.5 eq) was added portion wise. After additional 30 min of stirring, mixture of MeOH (0.04 mL) and water (20 mL) were added. The precipitate was filtered under reduced pressure and washed with cold water (15 mL) to yield the desired product as a white solid (1.1 g, 3.70 mmol, 77%). ^{1}H NMR (300 MHz, DMSO-d_6): δ/ppm = 8.09 (d, J = 8.4 Hz, 1H), 7.39 – 7.33 (m, 9H), 7.13 – 7.07 (m, 1H), 5.06 (s, 2H), 4.88 (ddd, J = 8.8, 5.8, 2.9 Hz, 1H), 3.94 (dt, J = 8.8, 5.8 Hz, 1H), 3.60 (dd, J = 5.8, 2.9 Hz, 2H). ^{13}C NMR (75 MHz, DMSO-d_6): δ/ppm = 164.7, 155, 138.0, 136.7, 129.2, 128.3, 127.9, 127.8, 123.6, 116.2, 65.7, 56.2, 46.4. $[\alpha]_D^{20}$ = –5 (c 1.00, DMSO). FT-IR: ν/cm^{-1} = 1754, 1512, 1501, 1380, 1341, 1254, 1023, 1004, 813, 756. MS (ESI) *m/z* calculated for $[C_{17}H_{17}N_2O_3]^+$ ($[M+H]^+$): 297.1, found 297.4.

9, (*S*)-3-Amino-1-phenylazetidin-2-one hydrochloride

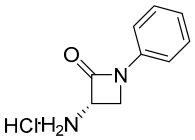

9 (0.5 g, 1.7 mmol, 1 eq) was dissolved in THF (5 mL). Subsequently, Pd/C (50 mg, 10%) was added, and the reaction mixture was stirred for two hours under a H_2 atmosphere (3 bar). Afterwards, the solution was filtered through Celite® 545 and acidified with hydrochloric acid (1 M, 7 mL). The desired product was obtained after removing the solvent under reduced pressure as a white solid (0.3 g, 1.5 mmol, 88%). ^{1}H NMR (300 MHz, DMSO-d_6): δ/ppm = 9.14 (s, 1H), 7.44 – 7.36 (m, 4H), 7.16 (ddt, J = 6.3, 5.2, 2.9 Hz, 1H), 4.67 (dd, J = 5.6, 2.5 Hz, 1H), 4.0 (dd, J = 6.7, 5.6 Hz, 1H), 3.74 (dd, J = 6.7, 2.6 Hz, 1H). ^{13}C NMR (75 MHz, DMSO-d_6): δ/ppm = 160.3, 137.4, 129.4, 124.5, 116.5, 53.5, 44.0. $[\alpha]_D^{20}$ = +17 (c 1.00, MeOH). FT-IR: ν/cm^{-1} = 1749, 1532, 1509, 1368, 1339, 1244, 1025, 1000, 813, 756. MS (ESI) *m/z* calculated for $[C_9H_{11}N_2O]^+$ ($[M+H]^+$): 163.1, found 163.0.

Synthesis of rhodesain targeting compounds

11, *tert*-Butyl (*S*)-(1-(methoxy(methyl)amino)-1-oxo-4-phenylbutan-2-yl) carbamate

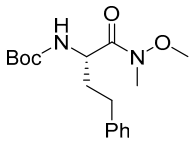

Boc-*h*Phe-OH **10** (8.07 g, 29.53 mmol, 1 eq) was dissolved in THF (165 mL) and the solution was cooled to 0 °C. DCC (7.20 g, 34.55 mmol, 1.17 eq), HOBt · H_2O(4.669 g, 34.557 mmol, 1.17 eq) and DIPEA (22 mL, 127.01 mmol, 4.3 eq) were added and the mixture was stirred for 15 min before *N*,*O*-dimethylhydroxylamine · HCl (3.439 g, 34.557 mmol, 1.17 eq) was added. The mixture was allowed to warm up to room temperature and was stirred overnight. Filtration of side product DCU was carried out several times (immersion of the solution in an ice bath to favour precipitation of DCU is recommended). The solvent was removed under reduced pressure, DCM was added (50 mL) and the organic phase was washed with hydrochloric acid (1 M, 3x 50 mL), saturated $NaHCO_3$ solution (3x 50 mL), H_2O (50 mL) and brine (50 mL). The organic phase was dried over anhydrous $MgSO_4$ and concentrated under vacuum. The crude product was purified by column chromatography (CH/EA 7:3) to obtain the pure product as a transparent oil (4.37 g, 13.58 mmol, 46%). ^{1}H NMR (300 MHz, $CDCl_3$): δ/ppm = 7.26 (m, 5H), 5.34 (m, 1H), 4.65 (m, 1H), 3.57 (s, 3H), 3.12 (s, 3H), 2.79 – 2.55 (m, 2H), 2.04 – 1.93 (m, 1H), 1.82 (m, 1H), 1.42 (s, 9H). ^{13}C NMR (101 MHz, $CDCl_3$): δ/ppm = 173.1, 155.7, 141.3, 128.6, 128.4, 126.1, 61.6, 53.5, 50.2, 34.7, 32.2, 31.8, 28.4. $[\alpha]_D^{20}$ =–7° (c = 10 mg/ mL, $CHCl_3$) . FT-IR: ν/cm^{-1} = 3321, 3050, 2974, 2933, 1707, 1655, 1495, 1454, 1445, 1390, 1245, 1163, 992, 701. MS (ESI) *m/z* calculated for $[C_{17}H_{26}N_2O_4Na]^+$ ($[M+Na]^+$): 345.2, found: 345.2.

12, *tert*-Butyl (*S*)-(1-oxo-4-phenylbutan-2-yl) carbamate

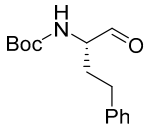

A solution of **11** (1.97 g, 6.13 mmol, 1 eq) in THF (40 mL) was placed in an ice bath. $LiAlH_4$ (0.73 g, 18.41 mmol, 3 eq) was slowly added. The reaction mixture was stirred for two hours and subsequently quenched by addition of aqueous saturated Rochelle salt solution (50 mL). The organic phases were extracted with EtOAc (3x 50 mL), washed with brine (50 mL), dried over anhydrous $MgSO_4$ and the solvent was removed under reduced pressure. Purification by column chromatography (CH/EA 8:2) was performed and the pure product was obtained as a transparent oil (1.08 g, 4.11 mmol, 67%). ^{1}H NMR (300 MHz, $CDCl_3$): δ/ppm = 9.45 (s, 1H), 7.17 (m, 5H), 5.33 – 4.80 (m, 1H), 4.35 – 2.59 (m, 1H), 2.62 (t, J = 7.9 Hz, 2H), 2.21 – 2.04 (m, 1H), 1.79 (m, 1H), 1.38 (s, 9H). ^{13}C NMR (101 MHz, $CDCl_3$): δ/ppm = 199.6, 155.6, 140.6, 128.6, 128.5, 126.4, 59.6, 31.5, 30.9, 28.3, FT-IR: ν/cm^{-1} = 3347, 3027, 2978, 2930, 2863,

23, (*S*)-2-((*S*)-2-(((benzyloxy)carbonyl)amino)-3-phenylpropanamido)-4-phenylbutanoic acid

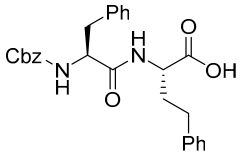

20 (5.0 g, 10 mmol, 1.0 eq) with LiOH (1.26 g, 30.0 mmol, 3.00 eq) in a mixture of water and THF (1:1, 30 mL). was stirred for 18 h at room temperature. After the reaction was complete as indicated by TLC, the solvent was evaporated under reduced pressure and to the resulting crude product was added hydrochloric acid (1.0 M) until pH = 3 was reached. The mixture was then extracted with EtOAc (3x 20 mL) and after phase separation, the combined organic layers were dried over anhydrous Na_2SO_4. The solvent was evaporated under reduced pressure yielding the target carboxylic acid as a colorless solid (4.57 g, 9.92 mmol, quant.). ^{1}H-NMR (300 MHz, $CDCl_3$): δ/ppm = 8.37 (d, J = 7.9 Hz, 1H), 7.60 – 7.39 (m, 1H), 7.41 – 6.95 (m, 15H), 5.09 – 4.81 (m, 2H), 4.42 – 4.31 (m, 1H), 4.26 – 4.14 (m, 1H), 3.05 (dd, J = 13.9, 3.8 Hz, 1H), 2.84 – 2.72 (m, 1H), 2.71 – 2.56 (m, 2H), 2.13 – 1.76 (m, 2H). ^{13}C-NMR (75 MHz, $CDCl_3$): δ/ppm = 173.5, 171.8, 55.9, 141.0, 138.1, 137.0, 129.3, 128.4, 2 × 128.3, 128.2, 128.1, 127.7, 127.4, 126.3, 125.9, 65.2, 56.0, 51.3, 37.3, 32.9, 31.3. $[\alpha]_D^{22}$ = +16 (c 1.00, ACN). FT-IR: ν/cm^{-1} = 3299, 3029, 2359, 1699, 1643, 1497, 1243, 1028, 744, 698. MS (ESI) *m/z* calculated for $[C_{27}H_{29}N_2O_5]^+$ ($[M+H]^+$): 461.2, found: 461.2.

24, Benzyl ((*S*)-1-oxo-1-(((*S*)-1-oxo-1-(((*S*)-2-oxo-1-phenylazetidin-3-yl)amino)-4-phenylbutan-2-yl)amino)-3-phenylpropan-2-yl)carbamate

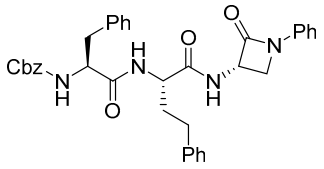

23 (138 mg, 0.30 mmol, 1.0 eq) was coupled with **9** (60 mg, 0.3 mmol, 1.0 eq), HATU (136.9 mg, 0.360 mmol, 1.2 eq) and 2,4,6-collidine (0.12 mL; 0.91 mmol; 3.0 eq). After stirring overnight, water (30 mL) was added, and the aqueous phase was extracted with EtOAc (3x 25 mL). The combined organic extracts were washed with brine (15 mL) and water (20 mL), dried over anhydrous $NaSO_4$ and concentrated under reduced pressure. The crude product was purified by preparative HPLC yielding the desired product as a colorless solid (120 mg, 0.20 mmol, 67%). ^{1}H-NMR (300 MHz, DMSO-d_6): δ/ppm =8.65 (d, J = 8.4 Hz, 1H), 8.25 (d, J = 7.8 Hz, 1H), 7.56 (d, J = 8.5 Hz, 1H), 7.44 – 6.99 (m, 20H), 5.15 – 5.01 (m, 1H), 4.96 (s, 2H), 4.49 – 4.26 (m, 2H), 3.95 (t, J = 5.8 Hz,1H), 3.65 – 3.53 (m, 1H), 3.15 – 3.00 (m, 1H), 2.89 – 2.74 (m, 1H), 2.73 – 2.57 (m, 2H), 2.10 – 1.83 (m, 2H). ^{13}C-NMR, HSQC, HMBC (75.5 MHz, DMSO-d_6): δ/ppm = 164.5, 155.9, 141.3, 138.1, 137.0, 126.3, 125.9, 123.7, 116.2, 65.3, 56.1, 54.9, 52.2, 46.2, 37.2, 33.9, 31.2. mp: 240°C (decomposition). $[\alpha]_D^{22}$ = +13 (c 1.00, DMSO). FT-IR: ν/cm^{-1} = 3305, 2925, 1744, 1685, 1650, 1528, 1389, 1285, 1226, 1037. MS (ESI) *m/z* calculated for $[C_{36}H_{36}N_4O_5Na]^+$ ($[M+Na]^+$): 627.3 , found: 627.3. Purity: 98%.

Synthesis of Cathepsin S targeting compounds

General procedures

A Boc deprotection

The Boc-protected amino acid or dipeptide (1.0 eq) was dissolved in 2 mL 1,4-Dioxan and 3 mL of a 4.0 M HCl-solution in 1,4-Dioxan was added dropwise. The mixture was stirred at room temperature until completion of the deprotection could be observed via TLC monitoring. The solvent was then removed under reduced pressure and the deprotected target compound could be obtained and was used in the next step without further purification and characterization.

B Ester cleavage with LiOH

The ester (1.0 eq) was dissolved in THF (20 mL) and mixed with a solution of LiOH (3.0 eq) in water (20 mL). The resulting mixture was stirred for 18 h at room temperature. After the reaction was complete as indicated by TLC, the solvent was evaporated under reduced pressure and to the resulting crude product was added hydrochloric acid (1.0 M) until pH = 3 was reached. The mixture was then extracted with EtOAc (3x 20 mL) and after phase separation, the combined organic layers were dried over anhydrous Na_2SO_4. The solvent was evaporated under reduced pressure yielding the target carboxylic acid as a colorless oil or a colorless solid.

C: Peptide coupling with HATU

The carboxylic acid (1.0 eq) was dissolved in a mixture of DCM/DMF (9:1) at 0 °C. Under stirring HATU (1.2 eq) was added in portions. Afterwards 2,4,6- collidine (3.0 eq) was added and stirred for an additional 10 min at 0 °C. The amine (1.0 eq) was added in portions or dropwise diluted in DCM and the reaction mixture was allowed to reach room temperature and stirred overnight. H_2O (30 mL) was added, and the organic phase separated. The aqueous phase was extracted with EtOAc (3x 20 mL). The combined organic extracts were washed with brine (40 mL) and dried over anhydrous $NaSO_4$. The solvent was evaporated under reduced pressure to give a crude product that was purified using either column chromatography or via preparative HPLC.

27, Cyclohexylalanine methylester hydrochloride

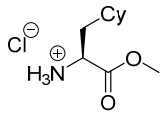

H-Cha-OH **26** (0.51 g, 2.92 mmol, 1.0 eq) was dissolved in dry MeOH (20 mL) and cooled to 10 °C. $SOCl_2$ was added dropwise, and the mixture was allowed to reach room temperature and was stirred overnight. After completion of the reaction, indicated by TLC monitoring, the solvent was evaporated under reduced pressure. EtOAc (20 mL) was added to the residue and

after filtration the methyl ester was obtained as a colorless solid (0.59 g, 2.65 mmol, 91%). ^{1}H NMR (300 MHz, $CDCl_3$): δ/ppm = 8.81 (s, 3H), 4.10 (s, 1H), 3.79 (s, 3zH), 1.84 (dd, J = 33.5, 16.6 Hz, 4H), 1.72 – 1.55 (m, 4H), 1.42 – 1.03 (m, 3H), 0.92 (p, J = 11.7 Hz, 2H). ^{13}C NMR (75 MHz, $CDCl_3$): δ/ppm = 170.3, 53.2, 51.2, 38.2, 33.4, 32.9, 32.6, 26.4, 26.0, 25.8. mp: 152–153 °C. $[\alpha]_D^{22}$ = +20 (c 1.00, $CHCl_3$). FT-IR: ν/cm^{-1} = 2929, 2855, 1730, 1483, 1227, 1209, 1156, 1046, 844, 753. MS (ESI) *m/z* calculated for $[C_{10}H_{21}NO_2]^+$ ($[M+H]^+$): 187.15, found: 187.21.

28, (4-Morpholine-1-carbonyl)-L-cyclohexyl alanine-methyl ester

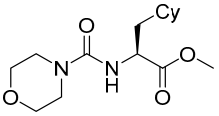

27 (0.55 g, 2.48 mmol, 1.0 eq) was dissolved in DCM and saturated $NaHCO_3$ solution (40 mL) and cooled to 0°C. Triphosgene (0.25 g, 0.83 mmol, 0.33 eq) was added and the mixture was stirred for 30 min. The mixture was extracted with DCM (2x 40 mL) and the combined organic layers were washed with saturated $NaHCO_3$ solution (2x 30 mL), and brine (2x 30 mL), then dried over anhydrous Na_2SO_4 and concentrated under reduced pressure, resulting in a crude product that was dissolved in THF (30 mL) and cooled to 0 °C. Morpholine (1.0 eq, 2.48 mmol, 0.22 g) was added and the mixture stirred for one hour. The solvent was removed under reduced pressure. Water (30 ml) to the crude residue, which was then extracted with EtOAc (3x 20 mL). The combined organic layers were washed with brine (2x 20 mL), dried over anhydrous Na_2SO_4, and concentrated under reduced pressure to yield a colorless oil (0.75 g, 2.46 mmol, 98%). ^{1}H NMR (300 MHz, $CDCl_3$): δ/ppm = 4.96 – 4.83 (m, 1H), 4.58 – 4.40 (m, 1H), 4.09 (q, J = 7.1 Hz, 1H), 3.70 (s, 3H), 3.69 – 3.61 (m, 4H), 3.41 – 3.28 (m, 4H), 2.01 (s, 1H), 1.76 (d, J = 12.8 Hz, 1H), 1.70 – 1.55 (m, 6H), 1.53 – 1.43 (m, 1H), 1.38 – 1.28 (m, 1H), 1.28 – 1.10 (m, 4H), 1.02 – 0.75 (m, 2H). ^{13}C NMR (75 MHz, $CDCl_3$): δ/ppm = 175.1, 157.4, 66.5, 52.3, 51.6, 44.1, 40.4, 34.2, 33.6, 32.7, 26.4, 26.2, 26.1, 21.1, 14.3. $[\alpha]_D^{22}$ = –9 (c 1.00, $CHCl_3$). FT-IR: ν/cm^{-1} = 3317, 3015, 2929, 1707, 1655, 1460, 1260, 1159, 910, 700. MS (ESI) *m/z* calculated for $[C_{15}H_{26}N_2O_4Na]^+$ ($[M+Na]^+$): 321.18, found: 321.18.

29, (4-Morpholin-1-carbonyl)-L-cyclohexyl alanine

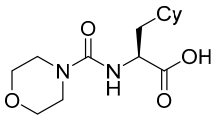

29 was prepared according to procedure B using **28** (1.0 eq, 0.7 g, 2.35 mmol), resulting in a colorless solid (0.65 g, 2.29 mmol, 97%).^{1}H NMR (300 MHz, $CDCl_3$): δ/ppm = 9.37 (s, 1H), 5.27 – 5.07 (m, 1H), 4.41 (s, 1H), 3.75 – 3.55 (m, 4H), 3.46 – 3.28 (m, 4H), 1.83 – 1.47 (m, 6H), 1.44 – 1.30 (m, 1H), 1.26 – 1.04 (m, 4H), 1.04 – 0.79 (m, 2H). ^{13}C NMR (75 MHz, $CDCl_3$): δ/ppm = 176.9, 158.1, 66.5, 51.9, 44.2, 39.6, 34.3, 33.6, 32.6, 26.6, 26.2, 26.1. 176.9, 158.1, 66.5, 51.9, 44.2, 39.6, 34.3, 33.6, 32.6, 26.5, 26.2, 26.1. mp: 96–97 °C. $[\alpha]_D^{22}$ = –22 (c 1.00,

$CHCl_3$). FT-IR: ν/cm^{-1} = 3320, 2978, 1707, 1655, 1460, 1368, 126, 1051, 910, 700. MS (ESI) *m/z* calculated for $[C_{14}H_{24}N_2O_4Na]^+$ ($[M+Na]^+$): 307.2, found: 307.2.

30, *N*-((*S*)-1-((*R*-2-(Benzyloxy)-1-cyanoethyl) amino)-3-cyclohexyl-1-oxopropan-2-yl) morpholine-4-carboxamideL-Cyclohexylalanine-methylester-hydrochloride

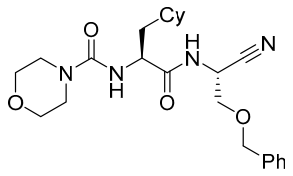

To a solution of NaCN (0.45 g, 9.11 mmol, 1.0 eq) and NH_4Cl (0.58 g, 10.87 mmol, 1.48 eq) in 35% aq. NH_4OH at 0°C, 2-(benzyloxy)acetaldehyde (1.0 eq, 7.35 mmol, 1.0 g) was added dropwise. The mixture was stirred for 48 h at room temperature after which a brown precipitate was formed. DCM (20 mL) and water (20 mL) were added and extracted with DCM (2x 30 mL). The organic extracts were washed with brine (1x 20 mL) and dried over anhydrous $NaSO_4$. The solvent was removed under reduced pressure yielding the intermediate aminonitrile as a pale-brown oil that was used in the next step without further purification. Coupling of the aminonitrile (31 mg, 0.18 mmol, 1.0 eq) with **29** (50 mg, 0.18 mmol, 1.0 eq) according to general procedure C followed by preparative HPLC purification yielded **30** as a colorless solid (20 mg, 0.05 mmol, 26%). ^{1}H NMR (300 MHz, $CDCl_3$): δ/ppm = 7.34 – 7.20 (m, 5H), 5.00 – 4.83 (m, 1H), 4.49 (d, J = 4.1 Hz, 2H), 4.39 (d, J = 7.2 Hz, 1H), 3.71 – 3.44 (m, 4H), 3.34 – 3.15 (m, 4H), 1.73 – 1.38 (m, 8H), 1.33 – 1.02 (m, 6H), 0.96 – 0.70 (m, 3H).^{13}C NMR (75 MHz, $CDCl_3$): δ/ppm = 173.8, 157.5, 136.9, 128.7, 128.3, 127.9, 117.3, 73.7, 68.9, 66.4, 52.3, 44.2, 40.9, 40.1, 34.3, 33.6, 32.9, 26.4, 26.3, 26.2. mp: 140–141 °C. $[\alpha]_D^{22}$ = –20 (c 1.00, $CHCl_3$). FT-IR: ν/cm^{-1} = 2920, 2850, 1666, 1619, 1521, 1447, 1247, 1114, 999, 698. MS (ESI) *m/z* calculated for $[C_{24}H_{34}N_4O_4Na]^+$ ($[M+Na]^+$): 465.3, found: 465.2. Purity: 99%.

32, *tert*-Butyl (*S*)-(3-(benzyloxy)-1-(methoxy(methyl)amino)-1-oxopropan-2-yl) carbamate

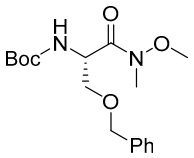

Boc-Ser(Bzl)-OH **31** (3.0 g, 10.2 mmol, 1.0 eq) was dissolved in DCM (20 mL) and cooled to –15 °C. *N*,*O*-dimethylhydroxyalmine · HCl (1.0 g, 10.26 mmol, 1.01 eq) and NMM (1.1 mL, 10.26 mmol, 1.01 eq) were added and after stirring for 5 min at this temperature EDC · HCl (1.97 g, 10.26 mmol, 1.01 eq) was added. The mixture was stirred overnight at room temperature and after consumption of the starting material, the solvent was removed under reduced pressure. Water (20 mL) and DCM (20 mL) were added, and the aqueous phase was extracted with DCM (3x 25 mL). The combined organic extracts were washed with brine (15 mL) and water (20 mL) dried over anhydrous $NaSO_4$ and concentrated under reduced

pressure. The crude product was purified by column chromatography (CH/EA 3:1), giving a colorless oil (3.4 g, 10.15 mmol, 98%). ^{1}H NMR (300 MHz, $CDCl_3$): δ/ppm = 7.37 – 7.11 (m, 5H), 5.48 – 5.25 (m, 1H), 4.84 (s, 1H), 4.58 – 4.40 (m, 2H), 3.66 (s, 3H), 3.65 – 3.57 (m, 2H), 3.16 (s, 3H), 1.39 (s, 9H). ^{13}C NMR (75 MHz, $CDCl_3$): δ/ppm = 170.8, 155.5, 137.9, 128.4, 127.7, 79.8, 73.2, 69.9, 61.5, 50.9, 32.4, 28.4. $[\alpha]_D^{22}$ = +5° (*c* 1.00, $CHCl_3$). FT-IR: ν/cm^{-1} = 2976, 1710, 1662, 1496, 1459, 1390, 1248, 1104, 1022, 986. MS (ESI) *m/z* calculated for $[C_{17}H_{26}N_2O_5Na]^+$ ([M+Na]$^+$): 361.2, found: 361.1.

33, *tert*-Butyl (*S*,*E*)-(1-(benzyloxy)-4-(phenylsulfonyl)but-3-en-2-yl) carbamate

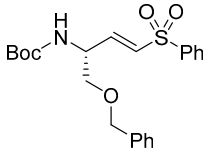

32 (0.5 g, 1.48 mmol, 1.0 eq) was dissolved in dry Et_2O (20 mL) at 0 °C. $LiAlH_4$ (72.9 mg, 1.92 mmol, 1.2 eq) was added and the mixture was stirred for 2 h at this temperature. The reaction was then quenched by adding hydrochloric acid (1 M, 15 mL). After phase separation, the organic phase was washed with hydrochloric acid (1 M, 15 mL) and brine (15 mL), dried over $NaSO_4$ and concentrated under reduced pressure yielding a colorless oil as crude product that was used in the next step without further characterization. To a solution of **3** (430 mg, 1.47 mmol, 1.0 eq) in dry THF at −78 °C, LiHMDS (1.0 M in THF, 1.62 mL) was added dropwise. After stirring for 30 min at this temperature the crude aldehyde (410 mg, 1.47 mmol, 1.0 eq) in THF (5 mL) was added. The mixture was stirred for 2.5 h at −78 °C. Saturated NH_4Cl-solution (15 mL) and EtOAc (5 mL) were added. After separating the phases, the aqueous phase was extracted with EtOAc (2x 15 mL) and the combined organic extracts were washed with water (15 mL) and brine (15 mL). The organic extract was dried over anhydrous Na_2SO_4 and concentrated under reduced pressure. The crude product was purified via column chromatography (CH/EA 3:1), yielding the desired product as a colorless oil (463 mg, 1.11 mmol, 75%). ^{1}H NMR (300 MHz, $CDCl_3$): δ/ppm = 7.90 – 7.81 (m, 2H), 7.65 – 7.46 (m, 3H), 7.39 – 7.21 (m, 4H), 6.98 (dd, *J* = 15.1, 4.8 Hz, 1H), 6.48 (dd, *J* = 15.1, 1.7 Hz, 1H), 5.01 (s, 1H), 4.64 – 4.42 (m, 2H), 3.58 (d, *J* = 4.1 Hz, 2H), 1.41 (s, 9H). ^{13}C NMR (75 MHz, $CDCl_3$): δ/ppm = 154.9, 144.5, 140.3, 137.3, 133.4, 131.5, 129.3, 128.5, 128.0, 127.7, 127.6, 80.3, 73.4, 70.7, 28.2. $[\alpha]_D^{22}$ = +10 (*c* 1.00, $CHCl_3$). FT-IR: ν/cm^{-1} = 2978, 1711, 1497, 1447, 1307, 1249, 1086, 1024, 751, 688. MS (ESI) *m/z* calculated for $[C_{22}H_{27}NO_5SNa]^+$ ([M+Na]$^+$): 440.2, found: 440.1.

34, *tert*-Butyl (*R*,*E*)-(1-(benzyloxy)-4-fluoro-4-(phenylsulfonyl) but-3-en-2-yl) carbamate

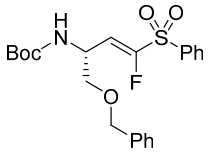

To a solution of **4** (170 mg, 0.55 mmol, 1.0 eq) in dry THF at −78 °C, KHMDS (1.0 M in THF, 0.55 mL) was added dropwise. After stirring for 30 min at this temperature the crude aldehyde (155 mg, 0.55 mmol, 1.0 Äq.) dissolved in THF (5 mL) was added. The mixture was stirred for 2.5 h at −78 °C. Saturated NH_4Cl-solution (15 mL) and EtOAc (5 mL) were added. Saturated NH_4Cl solution (15 mL) and EtOAc (5 mL) were added. After separating the phases, the aqueous phase was extracted with EtOAc (2x 15 mL) and the combined organic extracts were washed with water (15 mL) and brine (15 mL). The combined organic layers were dried over anhydrous Na_2SO_4 and concentrated in under reduced pressure. The crude product was purified via column chromatography (CH/EA 5:1), yielding the desired product as a colorless oil (105 mg, 0.24 mmol, 44%). ^{1}H NMR (300 MHz, $CDCl_3$): δ/ppm = 8.03 (s, 2H), 7.62 – 7.52 (m, 1H), 7.49 – 7.39 (m, 2H), 7.32 – 7.14 (m, 5H), 5.84 (dd, J = 21.2, 9.7 Hz, 1H), 5.48 (s, 1H), 5.15 (d, J = 8.2 Hz, 1H), 4.45 (s, 2H), 3.72 – 3.51 (m, 2H), 1.36 (s, 9H). ^{13}C NMR (75 MHz, $CDCl_3$): δ/ppm = 155.0, 137.5, 134.6, 129.4, 128.5, 127.9, 119.9, 119.8, 73.4, 72.8, 46.3, 28.4. $[\alpha]_D^{22}$ = –64 (c 1.00, $CHCl_3$). FT-IR: ν/cm^{-1} = 3390, 2978, 2929, 1711, 1497, 1366, 1335, 1166, 1081, 735. MS (ESI) *m/z* calculated for $[C_{22}H_{26}FNO_5SNa]^+$ ($[M+Na]^+$): 458.1, found: 458.1.

35, *N*-((*S*)-1-(((*S*,*E*)-1-(benzyloxy)-4-(phenylsulfonyl) but-3-en-2-yl) amino)-3-cyclohexyl-1-oxopropan-2-yl) morpholin-4-carboxamide

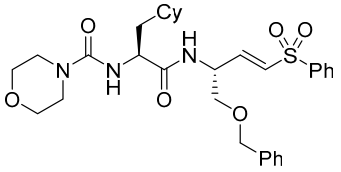

Deprotection of **33** (88 mg, 0.21 mmol, 1.0 eq) was performed following general procedure A. The deprotected amino acid was then coupled with **29** (60 mg, 0.21 mmol, 1.0 eq) following general procedure C. After purification via column chromatography ($CHCl_3$/MeOH 75:1) the desired product was obtained as a colorless solid (74 mg, 0.13 mmol, 62%). ^{1}H NMR (300 MHz, $CDCl_3$): δ/ppm = 7.86 – 7.74 (m, 2H), 7.64 – 7.52 (m, 1H), 7.51 – 7.41 (m, 2H), 7.36 – 7.15 (m, 6H), 6.96 (dd, J = 15.1, 4.6 Hz, 1H), 6.48 (dd, J = 15.1, 1.8 Hz, 1H), 5.03 (d, J = 7.7 Hz, 1H), 4.89 – 4.74 (m, 1H), 4.53 – 4.21 (m, 3H), 3.65 – 3.40 (m, 5H), 3.35 – 3.16 (m, 4H), 1.72 – 1.36 (m, 8H), 1.31 – 0.73 (m, 6H). ^{13}C NMR (75 MHz, $CDCl_3$): δ/ppm = 173.4, 157.4, 144.0, 140.3, 137.4, 133.5, 131.7, 129.3, 128.6, 127.9, 127.7, 127.7, 73.4, 70.6, 66.4, 52.6, 49.4, 44.1, 40.1, 34.3, 33.5, 32.9, 26.4, 26.2, 26.1. mp: 74–75 °C. $[\alpha]_D^{22}$ = +5 (c 1.00, $CHCl_3$). FT-IR: ν/cm^{-1} = 3756, 2921, 2851, 1659, 1537, 1446, 1261, 1147, 1117, 999. MS (ESI) *m/z* calculated for $[C_{31}H_{42}N_3O_6S]^+$ ($[M+H]^+$): 584.1, found: 584.2. Purity: 98%.

36, *N*-((*S*)-1-(((*S*,*E*)-1-(Benzyloxy)-4-fluoro-4-(phenylsulfonyl) but-3-en-2-yl) amino)-3-cyclohexyl-1-oxopropan-2-yl) morpholine-4-carboxamide

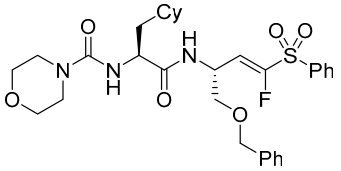

Deprotection of **38** (90 mg, 0.21 mmol, 1.0 eq) was performed following the general procedure A. The deprotected amino acid was then coupled with **29** (60 mg, 0.21 mmol, 1.0 eq) following general procedure C. After purification via preparative HPLC using a **36** was obtained as an amorphous glass (80 mg, 0.13 mmol, 63%). ^{1}H NMR (300 MHz, $CDCl_3$): δ/ppm = 8.08 – 8.02 (m, 2H), 7.71 – 7.62 (m, 1H), 7.60 – 7.46 (m, 2H), 7.38 – 7.21 (m, 5H), 5.97 – 5.82 (m, 1H), 5.81 – 5.66 (m, 1H), 5.28 (d, J = 7.9 Hz, 1H), 4.66 – 4.44 (m, 2H), 4.37 (td, J = 8.3, 5.9 Hz, 1H), 3.79 – 3.54 (m, 5H), 3.39 – 3.23 (m, 4H), 1.74 – 1.40 (m, 6H), 1.34 – 0.74 (m, 9H). ^{13}C NMR (75 MHz, $CDCl_3$): δ/ppm = 173.62, 170.03, 157.56, 154.85, 150.95, 137.51 (d, J = 6.3 Hz), 134.7, 129.5, 128.9, 128.6, 127.9, 127.8, 119.2, 119.0, 73.4, 72.3, 66.5, 52.4, 45.2, 44.1, 39.9, 34.3, 33.6, 32.8, 29.7, 26.4, 26.2, 23.2. mp: 78–79 °C. $[\alpha]_D^{22}$ = –22 (c 1.00, $CHCl_3$). FT-IR: ν/cm^{-1} = 3274, 3064, 2922, 2852, 1661, 1541, 1448, 1334, 1116, 735. MS (ESI) *m/z* calculated for $[C_{31}H_{41}FN_3O_6S]^+$ ($[M+H]^+$): 602.3, found: 602.2. Purity: 97%.

37, Methyl *O*-benzyl-*N*- (tert-butoxy carbonyl)-L-serinate

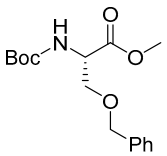

To a solution of Boc-Ser(Bzl)-OH **31** (3.0 g, 10.16 mmol, 1.0 eq) in DMF (40 mL) at 0°C, K_2CO_3 (2.8 g, 20.3 mmol, 2.0 eq) and MeI (1.26 mL, 20.3 mmol, 2.0 eq) were added. The mixture was stirred overnight at room temperature and subsequently diluted with saturated NH_4Cl solution (30 mL). The aqueous phase was extracted with EtOAc (3x 25 mL). The combined organic layers were dried over anhydrous Na_2SO_4 and concentrated under reduced pressure to yield **37** as a pale-orange oil (3.05 g, 9.85 mmol, 97%). ^{1}H NMR (300 MHz, $CDCl_3$): δ/ppm = 7.38 – 7.09 (m, 5H), 5.38 (d, J = 8.8 Hz, 1H), 4.59 – 4.35 (m, 3H), 3.84 (dd, J = 9.4, 3.3 Hz, 1H), 3.72 (s, 3H), 3.66 (dd, J = 9.4, 3.4 Hz, 1H), 1.43 (s, 9H). ^{13}C NMR (75 MHz, $CDCl_3$): δ/ppm = 171.2, 155.6, 137.7, 128.5, 127.9, 127.7, 80.1, 73.3, 70.1, 54.1, 52.5, 28.4. $[\alpha]_D^{22}$ = +33 (c 1.00, $CHCl_3$). FT-IR: ν/cm^{-1} = 2978, 2360, 1750, 1714, 1497, 1365, 1296, 1208, 1062, 739. MS (ESI) *m/z* calculated for $[C_{11}H_{16}NO_3]^+$ ($[M-Boc+H]^+$): 210.1, found: 210.0.

38, *tert*-Butyl (*S*)-(1-(benzyloxy)-4-(dimethoxy phosphoryl)-3-oxobutan-2-yl) carbamate

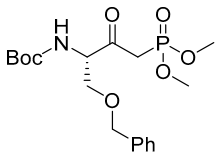

To a solution of dimethyl methylphosphonate (2.2 g, 18.4 mmol, 4.0 eq) in dry THF (12 mL) at −78 °C under an argon-atmosphere, *n*-BuLi (2.5 M in hexanes, 7.36 mL) was added dropwise. After stirring for one hour, **37** (1.5 g, 4.6 mmol, 1.0 eq) was added and the mixture stirred for an additional 2.5 h at this temperature. The reaction was then stopped by adding water (30 mL) and EtOAc (30 mL). After extraction with EtOAc (3x 20 mL) the organic extracts were dried over anhydrous Na_2SO_4 and the mixture concentrated under reduced pressure to give a crude product that was purified via column chromatography (CH/EA 1:3) yielding a pale-yellow oil (1.46 g, 3.64 mmol, 79%). ^{1}H NMR (300 MHz, $CDCl_3$): δ/ppm = 7.36 – 7.20 (m, 5H), 5.58 (d, J = 7.7 Hz, 1H), 4.55 – 4.45 (m, 3H), 3.93 – 3.85 (m, 1H), 3.79 – 3.61 (m, 7H), 3.31 (dd, J = 22.3, 14.5 Hz, 1H), 3.10 (dd, J = 21.9, 14.5 Hz, 1H), 1.41 (s, 9H). ^{13}C NMR (75 MHz, $CDCl_3$): δ/ppm = 199.7, 155.4, 137.4, 128.5, 127.9, 127.8, 80.2, 73.4, 69.3, 60.4, 53.2, 39.2, 37.4, 28.3. $[\alpha]_D^{22}$ = +3 (c 1.00, $CHCl_3$). FT-IR: ν/cm^{-1} = 2976, 1708, 1496, 1454, 1366, 1251, 1166, 1068, 866, 809. MS (ESI) *m/z* calculated for $[C_{13}H_{21}NO_5P]^+$ ($[M-Boc+H]^+$): 302.1, found: 302.1.

39, Dimethyl ((*S*)-4-(benzyloxy)-3-((*S*)-3-cyclohexyl-2-(morpholine-4-carboxamido) propanamido)-2-oxobutyl) phosphonate

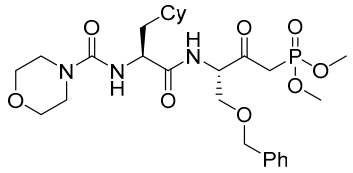

Deprotection of **38** (0.83 g, 2.07 mmol, 1.0 eq) was performed following the general procedure A. The deprotected amino acid was then coupled with **29** (0.59 g, 2.07 mmol, 1.0 eq) following general procedure C. After Purification via preparative HPLC **39** was obtained as a colorless oil (0.68 g, 1.2 mmol, 58%). ^{1}H NMR (300 MHz, $CDCl_3$): δ/ppm = 7.66 (d, J = 8.3 Hz, 1H), 7.34 – 7.20 (m, 5H), 4.72 (dt, J = 8.0, 3.8 Hz, 1H), 4.54 – 4.38 (m, 3H), 3.97 (dd, J = 9.7, 3.8 Hz, 1H), 3.78 – 3.53 (m, 11H), 3.49 – 3.26 (m, 1H), 3.04 (dd, J = 22.5, 14.0 Hz, 4H), 1.84 – 1.56 (m, 6H), 1.55 – 1.41 (m, 1H), 1.40 – 1.26 (m, 1H), 1.24 – 0.78 (m, 6H). ^{13}C NMR (75 MHz, $CDCl_3$): δ/ppm = 199.7, 199.6, 173.8, 157.6, 137.5, 128.5, 127.9, 127.7, 73.5, 68.7, 66.5, 59.1, 59.1, 53.4, 53.3, 53.2, 52.5, 44.2, 40.1, 39.7, 37.9, 34.3, 33.8, 32.7, 26.5, 26.3, 26.1. $[\alpha]_D^{22}$ = –21 (c 1.00, $CHCl_3$). FT-IR: ν/cm^{-1} = 3278, 2920, 2850, 2360, 1627, 1533, 1449, 1249, 1115, 999. MS (ESI) *m/z* calculated for $[C_{27}H_{43}N_3O_8P]^+$ ($[M+H]^+$): 568.3, found: 568.2.

Ethyl (*S*,*E*)-6-(benzyloxy)-5-((*S*)-3-cyclohexyl-2-(morpholine-4-carboxamido) propanamido)-4-oxohex-2-enoate

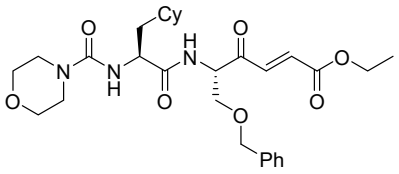

In a schlenk tube containing LiCl (8 mg, 0.19 mmol, 1.2 eq), a solution of **39** (90 mg, 0.16 mmol, 1.0 eq) in MeCN was added. At 0 °C, over P_2O_{10}, freshly distilled ethyl glyoxylate (33 µL, 0.32 mmol, 2.0 eq) and DIPEA (36 µL, 0.21 mmol, 1.3 eq) were added and the mixture was stirred for 2 h. After adding a saturated NH_4Cl solution (30 mL) and extracting with EtOAc (3x 20 mL), the organic extracts were washed with brine (20 mL), dried over anhydrous Na_2SO_4 and concentrated under reduced pressure to yield a crude which was purified via preparative HPLC. **40** could be obtained as a colorless solid (34 mg, 0.06 mmol, 10%). ^{1}H NMR (300 MHz, $CDCl_3$): δ/ppm = 7.48 – 7.14 (m, 5H), 6.96 – 6.69 (m, 1H), 4.56 – 3.88 (m, 9H), 3.71 – 3.57 (m, 4H), 3.38 – 3.25 (m, 4H), 1.80 – 1.55 (m, 6H), 1.36 – 1.23 (m, 3H), 1.20 – 1.07 (m, 6H), 1.01 – 0.79 (m, 3H). ^{13}C NMR (75 MHz, $CDCl_3$): δ/ppm = 192.6, 192.2, 165.4, 165.1, 157.2, 137.0, 133.8, 133.3, 131.7, 128.6, 128.0, 73.9, 70.7, 66.5, 62.2, 61.6, 52.5, 44.2, 34.2, 33.7 32.9, 32.7, 14.3, 14.0. mp: 62–63 °C. $[\alpha]_D^{22}$ = –23 (*c* 1.00, $CHCl_3$). FT-IR: ν/cm^{-1} = 2923, 1735, 1632, 1526, 1449, 1370, 1250, 1187, 1115, 752 cm^{-1}. MS (ESI) *m/z* calculated for $[C_{29}H_{42}N_3O_7]^+$ ($[M+H]^+$): 544.3, found: 544.2. Purity: 99%.

41, *tert*-Butyl (*S*)-(1-(benzo[*d*]thiazol-2-yl)-3-(benzyloxy)-1-oxopropan-2-yl) carbamate

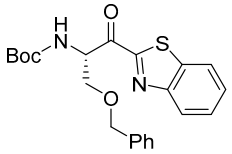

To a solution of benzothiazole (0.87 mL, 8.08 mmol, 10.0 eq) in THF (25 mL) at −78 °C under argon, *n*-BuLi (2.5 M in hexanes, 3.23 mL, 8.08 mmol, 10.0 eq) was added dropwise. The mixture was stirred for 30 min at this temperature and subsequently **37** (250 mg, 0.81 mmol, 1.0 eq) was added and stirred for an additional three hours. After consumption of the starting material, the mixture was diluted with a saturated NH_4Cl solution (30 mL). The aqueous phase was extracted with EtOAc (3x 25 mL). The organic extracts were dried over anhydrous Na_2SO_4 and concentrated to give a crude product that was purified via column chromatography (CH/EA 10:1) which gave access to **41** as a pale-yellow oil (215 mg, 0.52 mmol, 64%). ^{1}H NMR (300 MHz, $CDCl_3$): δ/ppm = 8.15 – 8.04 (m, 1H), 8.03 – 7.92 (m, 1H), 7.62 – 7.49 (m, 2H), 7.20 – 7.05 (m, 5H), 5.78 – 5.60 (m, 2H), 4.58 – 4.35 (m, 2H), 4.35 – 4.28 (m, 1H), 4.01 – 3.84 (m, 1H), 1.47 (s, 9H). ^{13}C NMR (75 MHz, $CDCl_3$): δ/ppm = 191.4, 163.9, 155.5, 153.5, 137.5, 137.3, 128.3, 128.0, 127.7, 127.6, 127.1, 125.8, 122.5, 80.1, 73.3, 70.5, 57.9, 28.5. $[\alpha]_D^{22}$ = +1 (*c* 1.00, $CHCl_3$). FT-IR: ν/cm^{-1} = 2978, 2359, 1698, 1485, 1454, 1367, 1216, 1165, 1102, 744. MS (ESI) *m/z* calculated for $[C_{22}H_{24}N_2O_4SNa]^+$ ($[M+H]^+$): 435.1, found: 435.1.

42, *N*-((*S*)-1-(((*S*)-1-(benzo[*d*]thiazol-2-yl)-3-(benzyloxy)-1-oxopropan-2-yl) amino)-3-cyclohexyl-1-oxopropan-2-yl) morpholine-4-carboxamide

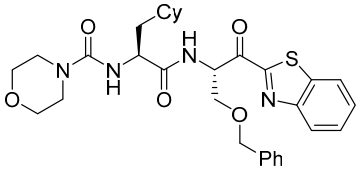

Deprotection of **41** (56 mg, 0.14 mmol, 1.0 eq) was performed following general procedure A. The deprotected amino acid was then coupled with **29** (40 mg, 0.14 mmol, 1.0 eq) following general procedure C. After purification via preparative HPLC **42** could be obtained as a colorless solid (33 mg, 0.06 mmol, 44%). ^{1}H NMR (300 MHz, $CDCl_3$): δ/ppm = 8.15 – 8.05 (m, 1H), 8.03 – 7.92 (m, 1H), 7.63 – 7.47 (m, 2H), 7.10 (d, J = 6.9 Hz, 5H), 5.95 – 5.78 (m, 1H), 4.64 – 4.44 (m, 2H), 4.41 – 4.25 (m, 2H), 4.02 – 3.86 (m, 1H), 3.65 (q, J = 4.7 Hz, 4H), 3.45 – 3.28 (m, 4H), 1.89 – 1.34 (m, 9H), 1.30 – 0.80 (m, 5H). ^{13}C NMR (75 MHz, $CDCl_3$): δ/ppm = 190.4, 173.5, 163.7, 157.6, 153.5, 137.4, 137.3, 137.2, 128.3, 128.1, 127.7, 127.6, 127.6, 127.2, 125.8, 122.4, 73.2, 70.0, 66.6, 56.7, 52.5, 52.3, 44.3, 40.8, 40.2, 34.4, 33.8, 32.9, 26.5, 26.3, 26.2. mp: 95–96 °C. $[\alpha]_D^{22}$ = –12 (c 1.00, $CHCl_3$). FT-IR: ν/cm^{-1} = 3275, 2920, 2850, 1648, 1541, 1485, 1249, 1116, 998, 761. MS (ESI) *m/z* calculated for $[C_{31}H_{39}N_4O_5S]^+$ ($[M+H]^+$): 579.3, found: 580.1. Purity: 97%

43, Methyl *O*-benzyl-*N*-((*S*)-3-cyclohexyl-2-(morpholine-4-carboxamido) propanoyl)-L-serinate

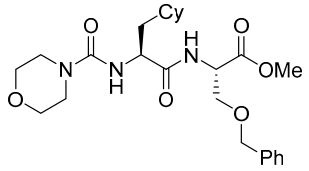

Deprotection of **37** (217 mg, 0.7 mmol, 1.0 eq) was performed following general procedure A. The deprotected amino acid was then coupled with **29** (200 mg, 0.7 mmol, 1.0 eq) following general procedure C. After purification via column chromatography (CH/EA 1:3), **43** could be obtained as a colorless oil (253 mg, 0.53 mmol, 76%). ^{1}H NMR (300 MHz, $CDCl_3$): δ/ppm = 7.36 – 7.19 (m, 5H), 4.69 (dt, J = 8.2, 3.4 Hz, 1H), 4.58 – 4.37 (m, 3H), 3.86 (dd, J = 9.6, 3.4 Hz, 1H), 3.71 (s, 3H), 3.68 – 3.52 (m, 5H), 3.41 – 3.24 (m, 4H), 1.86 – 1.58 (m, 6H), 1.57 – 1.31 (m, 3H), 1.29 – 0.80 (m, 6H). ^{13}C NMR (75 MHz, $CDCl_3$): δ/ppm = 173.7, 170.5, 157.5, 137.6, 128.5, 127.9, 127.7, 73.4, 69.6, 66.5, 52.8, 52.6, 52.4, 44.2, 40.6, 34.2, 33.7, 32.9, 26.5, 26.3, 26.2. $[\alpha]_D^{22}$ = +13 (c 1.00, $CHCl_3$). FT-IR: ν/cm^{-1} = 3276, 2920, 2850, 2360, 1748, 1662, 1538, 1449, 1261, 1116. MS (ESI) *m/z* calculated for $[C_{25}H_{37}N_3O_6Na]^+$ ($[M+Na]^+$): 498.3, found: 498.2.

44, *O*-benzyl-*N*-((*S*)-3-cyclohexyl-2-(morpholine-4-carboxamido) propanoyl)-L-serine

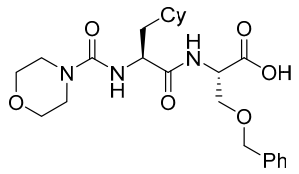

The methyl ester **43** (252 mg, 0.53 mmol, 1.0 eq) was cleaved according to the general procedure B. **44** was obtained as a colorless solid (250 mg, 0.52 mmol, 98%). ^{1}H NMR (300 MHz, $CDCl_3$): δ/ppm = 7.43 – 7.18 (m, 5H), 4.75 – 4.24 (m, 2H), 3.98 – 3.64 (m, 2H), 3.63 – 3.44 (m, 4H), 3.44 – 3.19 (m, 4H), 2.60 (s, 2H), 2.46 (s, 1H), 1.77 – 1.48 (m, 7H), 1.44 – 0.68 (m, 8H). ^{13}C NMR (75 MHz, $CDCl_3$): δ/ppm = 174.4, 172.9, 157.7, 153.0, 137.7, 128.5, 127.9, 127.8, 127.7, 125.1, 73.4, 69.6, 66.5, 53.5, 52.9, 44.2, 39.9, 34.2, 33.7, 32.7, 26.5, 26.3, 26.2, 21.9, 19.5. mp: 75–76 °C. $[\alpha]_D^{22}$ = +19 (c 1.00, $CHCl_3$). FT-IR: ν/cm^{-1} = 3304, 2922, 2852, 2359, 1725, 1622, 1532, 1450, 1260, 1116. MS (ESI) *m/z* calculated for $[C_{24}H_{36}N_3O_6]^+$ ($[M+H]^+$): 462.3 found: 462.4.

45, *N*-((2*S*)-1-(((2*S*)-3-(benzyloxy)-1-oxo-1-((2-oxo-1-phenylazetidin-3-yl) amino) propan-2-yl) amino)-3-cyclohexyl-1-oxopropan-2-yl) morpholine-4-carboxamide

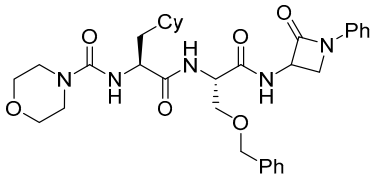

Coupling of **44** (185 mg, 0.4 mmol, 1.0 eq) with **9** (80 mg, 0.4 mmol, 1.0 eq) was performed following general procedure C. After purification via preparative HPLC **45** could be obtained as a colorless solid (169 mg, 0.28 mmol, 70%). ^{1}H NMR (300 MHz, $CDCl_3$): δ/ppm = 8.15 (d, J = 7.3 Hz, 1H), 7.35 – 7.12 (m, 10H), 7.08 – 6.95 (m, 2H), 5.10 (s, 2H), 5.00 – 4.80 (m, 1H), 4.61 – 4.51 (m, 1H), 4.43 (q, J = 11.8 Hz, 2H), 4.14 – 4.03 (m, 1H), 3.94 (dd, J = 9.6, 4.1 Hz, 1H), 3.81 (t, J = 5.6 Hz, 1H), 3.63 – 3.49 (m, 2H), 3.48 – 3.31 (m, 4H), 3.25 – 2.99 (m, 4H), 1.70 – 1.37 (m, 6H), 1.35 – 0.68 (m, 9H).^{13}C NMR (75 MHz, $CDCl_3$): δ/ppm = 173.5, 170.6, 163.7, 157.9, 138.0, 137.8, 129.3, 128.6, 128.0, 127.9, 124.4, 166.7, 73.5, 69.4, 66.3, 55.8, 53.8, 53.2, 47.1, 44.1, 39.3, 34.5, 33.8, 32.5, 26.4, 26.2, 26.1. mp: 91–92 °C. $[\alpha]_D^{22}$ = +11 (c 1.00, $CHCl_3$). FT-IR: ν/cm^{-1} = 3271, 2922, 2850, 2340, 1754, 1626, 1502, 1386, 115, 866. MS (ESI) *m/z* calculated for $[C_{33}H_{43}N_5O_6Na]^+$ ($[M+Na]^+$): 628.3, found: 628.4. Purity: 99%.

46, *N*-((*S*)-1-(((*R*)-1-(benzyloxy)-3-hydroxypropan-2-yl) amino)-3-cyclohexyl-1-oxopropan-2-yl) morpholine-4-carboxamide

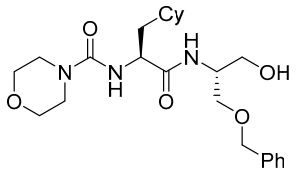

To a solution of **43** (132 mg, 0.28 mmol, 1.0 eq) in THF (15 mL) at 0 °C, $NaBH_4$ (42 mg, 1.11 mmol, 4.0 eq) and MeOH (1.2 mL) were added. The mixture was stirred for 16 h at room temperature and upon completion, diluted with saturated NH_4Cl solution (30 mL). After extraction with EtOAc (3x 25 mL) the combined organic layers were washed with saturated NH_4Cl solution (20 mL) and brine (20 mL), dried over anhydrous Na_2SO_4 and concentrated under reduced pressure to yield **46** as a colorless solid (114 mg, 0.25 mmol, 91%). ^{1}H NMR (300 MHz, $CDCl_3$): δ/ppm = 7.34 – 7.18 (m, 5H), 6.98 (d, J = 7.5 Hz, 1H), 5.26 (d, J = 7.7 Hz, 1H), 4.55 – 4.40 (m, 2H), 4.33 (td, J = 8.4, 6.3 Hz, 1H), 4.08 – 3.91 (m, 2H), 3.67 – 3.41 (m, 7H), 3.33 – 3.07 (m, 4H), 1.78 – 1.43 (m, 6H), 1.32 – 0.71 (m, 9H). ^{13}C NMR (75 MHz, $CDCl_3$): δ/ppm = 174.1, 171.2, 157.5, 137.8, 135.9, 128.5, 127.9, 127.7, 125.6, 73.5, 69.6, 66.5, 62.9, 60.5, 52.7, 51.2, 44.1, 40.4, 34.3, 33.6, 32.9, 26.3, 21.1, 14.3. mp: 89–90 °C. $[\alpha]_D^{22}$ = +14 (c 1.00, $CHCl_3$). FT-IR: ν/cm^{-1} = 33280, 2916, 2850, 2265, 2339, 1615, 1540, 1447, 1250, 1111. MS (ESI) *m/z* calculated for $[C_{24}H_{37}N_3O_5Na]^+$ ([M+Na]$^+$): 470.3, found: 470.3.

47, *N*-((*S*)-1-(((*S*)-1-(benzyloxy)-3-oxopropan-2-yl) amino)-3-cyclohexyl-1-oxopropan-2-yl) morpholine-4-carboxamide

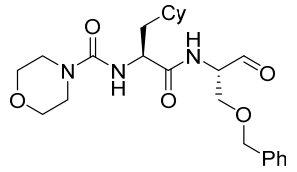

To a solution of **46** (45 mg, 0.1 mmol, 1.0 eq) in DCM (10 mL) Dess-Martin-Periodinane (51 mg, 0.12 mmol, 1.2 eq) was added and the mixture was stirred at room temperature for 12 h. After completion, indicated by TLC, the mixture was filtrated, washed a saturated $Na_2S_2O_3$ solution (15 mL), a saturated $NaHCO_3$ solution (15 mL) and brine (20 mL). The mixture was dried over anhydrous Na_2SO_4, concentrated under reduced pressure and subsequently purified via column chromatography ($CHCl_3$/MeOH 30:1), to yield **47** as a colorless solid (31 mg, 0.07 mmol, 70%). ^{1}H NMR (300 MHz, $CDCl_3$): δ/ppm = 9.56 (s, 1H), 7.43 – 7.17 (m, 5H), 5.15 – 4.96 (m, 1H), 4.76 – 4.34 (m, 3H), 4.25 (s, 1H), 3.99 (dd, J = 9.7, 3.6 Hz, 1H), 3.75 – 3.53 (m, 4H), 3.48 – 3.20 (m, 4H), 1.84 – 1.47 (m, 6H), 1.40 – 0.77 (m, 8H). ^{13}C NMR (75 MHz, $CDCl_3$): δ/ppm = 198.3, 174.1, 157.5, 137.3, 128.6 127.8, 127.7, 73.7, 67.5, 66.5, 59.0,52.4, 44.2, 40.6, 34.3, 33.7, 32.9, 26.5, 26.3. mp: 85–86 °C. $[\alpha]_D^{22}$ = +20 (c 1.00, MeOH).

FT-IR: ν/cm^{-1} = 3291, 2921, 2851, 2363, 2341, 1624, 1541, 1448, 1261, 1117. MS (ESI) *m/z* calculated for $[C_{24}H_{25}N_3O_5Na]^+$ ($[M+Na]^+$): 468.3, found: 468.3.

48, *N*-((2*S*)-1-(((2*S*)-1-(benzyloxy)-3-hydroxy-4-nitrobutan-2-yl) amino)-3-cyclohexyl-1-oxopropan-2-yl) morpholine-4-carboxamide

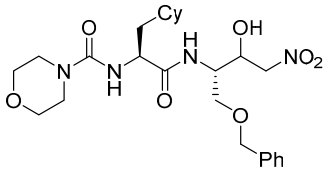

To a suspension of NaH (60% in paraffin, 23 mg, 0.56 mmol, 1.25 eq), and $MeNO_2$ (24 µL, 0.45 mmol, 1.0 eq) in THF (20 mL) at 0 °C, **48** (200 mg, 0.45 mmol, 1.0 eq) was added and the mixture was stirred for one hour. After completion, indicated by TLC, the mixture was diluted with a saturated NH_4Cl solution (20 mL). After separation of the aqueous phase, the organic phase was washed with brine (15 mL), dried over anhydrous Na_2SO_4 and concentrated to yield a crude yellowish-oil **48** (132 mg), which was used in the next step without further purification.

49, *N*-((*S*)-1-(((*R*,*E*)-1-(benzyloxy)-4-nitrobut-3-en-2-yl) amino)-3-cyclohexyl-1-oxopropan-2-yl) morpholine-4-carboxamide

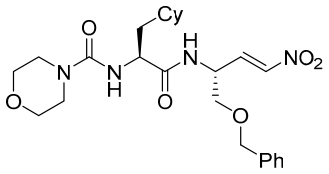

To a solution of **48** (72 mg, 0.14 mmol, 1.0 eq) and Et_3N (59 µL, 0.43 mmol, 3.0 eq) in DCM (10 mL) at 0 °C, MsCl (16 µL, 0.21 mmol, 1.5 eq) was added and the mixture was stirred for one hour at room temperature. The mixture was diluted and washed with a saturated $NaHCO_3$ solution (15 mL) and extracted with EtOAc (3x 25 mL). The mixture was dried over anhydrous Na_2SO_4, concentrated under reduced pressure and subsequently purified via preparative HPLC yielding **49** as a colorless solid (30 mg, 0.06 mmol, 44%). ^{1}H NMR (300 MHz, $CDCl_3$): δ/ppm = 7.43 – 7.27 (m, 5H), 7.25 – 7.15 (m, 1H), 7.12 – 6.99 (m, 1H), 4.95 – 4.79 (m, 1H), 4.63 – 4.45 (m, 2H), 4.44 – 4.29 (m, 1H), 3.73 – 3.52 (m, 4H), 3.44 – 3.19 (m, 4H), 1.91 – 1.45 (m, 8H), 1.40 – 0.69 (m, 9H). ^{13}C NMR (75 MHz, $CDCl_3$): δ/ppm = 173.5, 157.6, 141.2, 139.2, 137.2, 128.8, 128.3, 127.9, 73.7, 70.3, 66.5, 52.6, 47.8, 44.2, 39.9, 34.5, 33.7, 32.9, 26.5, 26.3, 26.2. mp: 71–72 °C. $[\alpha]_D^{22}$ = –4 (*c* 1.00, $CHCl_3$). FT-IR: ν/cm^{-1} = 3286, 2923, 2852, 2360, 2341, 1653, 1624, 1449, 1351, 117. MS (ESI) *m/z* calculated for $[C_{25}H_{36}N_4O_6Na]^+$ ($[M+Na]^+$): 511.3, found: 511.2. Purity: 99%.

Synthesis of reactivity test compounds

108, *tert*-Butyl ((2S)-4-methyl-1-oxo-1-((2-oxo-1-phenylazetidin-3-yl) amino) pentan-2-yl) carbamate

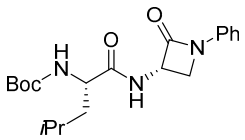

Boc-Leu-OH **50** (0.13 g, 0.67 mmol, 1.0 eq) was dissolved in a mixture of DCM/DMF (9:1) at 0 °C. Under stirring HATU (0.31 g, 0.80 mmol, 1.2 eq) was added in portions. Afterwards 2,4,6- collidine (0.24 g, 2.0 mmol, 3.0 eq) was added and stirred for an additional 10 min at 0 °C. A solution of **9** (0.14 g, 0.67 mmol, 1 eq) in DCM (5 ml) was added dropwise and the reaction mixture was allowed to reach room temperature and was stirred overnight. H_2O (30 mL) was added, and the organic phase separated. The aqueous phase was extracted with EtOAc (3 × 20 mL). The combined organic extracts were washed with aq. sat. NaCl-solution (40 mL) and dried over Na_2SO_4. The solvent was evaporated under reduced pressure to give a crude product that was purified with column chromatography (EA:Cy = 7:4) yielding the title compound as an off-white solid (0.2 g, 0.54 mmol, 81%). ^{1}H NMR (300 MHz, $CDCl_3$): δ/ppm = 7.65 – 7.45 (m, 1H), 7.38 – 7.20 (m, 4H), 7.06 (tdd, J = 5.9, 4.6, 3.0 Hz, 1H), 5.18 – 4.99 (m, 2H), 3.88 (t, J = 5.7 Hz, 1H), 3.51 (dd, J = 5.9, 2.7 Hz, 1H), 1.75 – 1.44 (m, 3H), 1.39 (s, 10H), 0.90 (dd, J = 6.3, 3.8 Hz, 6H). ^{13}C NMR (75 MHz, $CDCl_3$): δ/ppm = 173.6, 163.8, 156.0, 137.8, 129.3, 124.5, 116.8, 80.3, 65.4, 55.4, 53.1, 47.4, 41.6, 28.4, 24.8, 23.1, 21.9, 14.2. mp: 84 – 85 °C. $[\alpha]_D^{20} = -16$ (c 1.00, $CHCl_3$). MS (ESI) *m/z* calculated for $[C_{20}H_{28}N_3O_4Na]^+$ ($[M+Na]^+$): 389.2, found: 398.2. Purity: 99%.

109, *tert*-Butyl (*S,E*)-(5-methyl-1-(phenylsulfonyl)hex-1-en-3-yl)carbamate

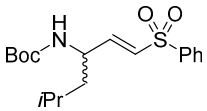

3 (0.52 g, 1.77 mmol, 1 eq) and LiCl (0.09 g, 2.21 mol, 1.25 eq) were dissolved in dry MeCN (18 mL) under argon atmosphere and cooled to 0 °C. Subsequently DBU (0.27 mL, 1.77 mmol, 1 eq) and 10 min later **52** (0.38 g, 1.77 mmol, 1 eq) in MeCN (5 mL) were added dropwise to the solution and stirred one hour at 0 °C and one hour at room temperature. The reaction mixture was quenched with citric acid solution (10%, 10 mL). The organic phase was separated, and the aqueous phase extracted with EtOAc (3x 20 mL). The combined organic extracts were dried over anhydrous Na_2SO_4 and evaporated under reduced pressure. The crude product was purified with column chromatography (CH/EA 1:6) to yield the product as colorless oil (0.18 g, 0.52 mmol, 30%). ^{1}H NMR (300 MHz, CDCl3): δ/ppm = 7.89 – 7.83 (m, 2H), 7.64 – 7.48 (m, 3H), 6.87 (dd, J = 15.0, 4.9 Hz, 1H), 6.42 (dd, J = 15.0, 1.3 Hz, 1H), 4.48 – 4.34 (m, 1H), 1.74 – 1.59 (m, 2H), 1.40 – 1.32 (m, 9H), 0.92 (d, J = 6.6 Hz, 6H). ^{13}C NMR (75 MHz, CDCl3): δ/ppm = 155.0, 147.2, 140.4, 133.5, 130.1, 129.4, 127.7, 43.4, 28.3, 24.8, 22.8, 22.1. mp: 72 –

1.00, $CHCl_3$). FT-IR: ν/cm^{-1} = 3446, 3333, 2959, 2940, 2870, 2561, 1684, 1533, 1392, 1366, 1237, 1161, 1048, 872, 757. MS (ESI) *m*/*z* calculated for $[C_{10}{}^{13}CH_{21}NO_4Na]^+$ ($[M+Na]^+$): 255.1, found: 255.0.

114, *tert*-Butyl (*S*)-(1-(methoxy(methyl)amino)-4-methyl-1-oxopentan-2-yl-1-^{13}*C*)carbamate

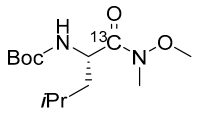

To a 0 °C cold solution of Boc-Leu-1-^{13}C-OH **113** (1.70 g, 7.32 mmol, 1 eq) in DCM (80 mL) were added HOBt · H_2O (1.12 g, 7.32 mmol, 1 eq) and 2,4,6-collidine (1.94 mL, 14.64 mmol, 2 eq). After stirring at 0 °C for 30 min, TBTU (2.35 g, 7.32 mmol, 1 eq) was added. The solution was stirred for further 30 min at 0 °C and *N*,*O*-dimethyl hydroxylamine · HCl (0.71 g, 7.32 mmol, 1 eq) was added. After stirring at room temperature overnight, the solvent was removed under reduced pressure and the residue was taken up in EtOAc (100 mL). The mixture was washed with saturated $NaHCO_3$ solution (3x 80 mL) and hydrochloric acid (1 M, 3x 80 mL) and filtered over a small silica column. The filtrate was concentrated under reduced pressure to yield the desired product as a colorless oil (1.91 g, 6.92 mmol, 95%). ^{1}H NMR (300 MHz, $CDCl_3$): δ/ppm = 5.14–4.95 (m, 1H), 4.79–4.60 (m, 1H), 3.77 (s, 3H), 3.22–3.15 (m, 3H), 1.78–1.61 (m, 1H), 1.49–1.37 (m, 11H), 0.97–0.88 (m, 6H). ^{13}C NMR (75.5 MHz, $CDCl_3$): δ/ppm = 174.0, 155.8, 79.6, 61.7, 49.10 (d, J = 54.6 Hz), 42.2, 32.3, 28.5, 24.9, 23.5, 21.0. $[\alpha]_D^{22}$ = −10 (*c* 1.00, $CHCl_3$). FT-IR: ν/cm^{-1} = 3321, 2957, 2935, 2870, 1708, 1619, 1499, 1365, 1250, 1165, 1045, 1017, 986, 875, 758. MS (ESI) *m*/*z* calculated for $[C_{12}{}^{13}CH_{26}N_2O_4Na]^+$ ($[M+Na]^+$): 298.2, found: 298.1.

115, *tert*-Butyl (1-(benzo[*d*]thiazol-2-yl)-4-methyl-1-oxopentan-2-yl-1-^{13}*C*)carbamate

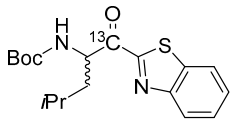

To a solution of benzothiazole (2.65 g, 19.61 mmol, 10 eq) in dry THF (50 mL) at −75 °C was added *n*-BuLi (2.5 M in hexanes, 5.5 mL, 13.73 mmol, 7 eq) dropwise over 15 min. The mixture was stirred at −75 °C for one hour and a solution of **114** (540 mg, 1.96 mmol, 1 eq) in dry THF (10 mL) was added. After stirring was continued at −75 °C for 2.5 h, saturated NH_4Cl solution (30 mL) was added. The mixture was extracted with EtOAc (3x 80 mL) and the combined organic extracts were filtered over a small silica column. The filtrate was concentrated by distillation under reduced pressure and the residue was purified by column chromatography (CH/EA 20:1) to yield the desired product as a yellowish solid (380 mg, 1.09 mmol, 56%). ^{1}H NMR (300 MHz, $CDCl_3$): δ/ppm = 8.22–8.16 (m, 1H), 8.00–7.94 (m, 1H), 7.61–7.49 (m, 2H), 5.76–5.52 (m, 1H), 5.40–5.18 (m, 1H), 1.88–1.77 (m, 2H), 1.60–1.50 (m, 1H), 1.43 (s, 9H), 1.09 (d, J = 6.0 Hz, 3H), 0.96 (d, J = 6.2 Hz, 3H). ^{13}C NMR (75.5 MHz, $CDCl_3$): δ/ppm =194.9, 164.2 (d, J = 64.8 Hz), 155.6, 153.7 (d, J = 7.8 Hz), 137.4, 128.0, 127.1,

125.9, 122.5, 80.0, 55.4 (d, J = 46.0 Hz), 42.2, 28.4, 25.4, 23.4, 21.8. mp: 108–110 °C. $[\alpha]_D^{22}$ = +40 (c 1.00, $CHCl_3$). FT-IR: ν/cm^{-1} = 3364, 3066, 2965, 2929, 2871, 1682, 1659, 1518, 1480, 1366, 1161, 876, 824, 760, 731. MS (ESI) m/z calculated for $[C_{17}{}^{13}CH_{24}N_2O_3SNa]^+$ ([M+Na]$^+$): 372.1, found: 372.0. Purity: 98%.

116, *tert*-Butyl (*S*)-(1-amino-4-methyl-1-oxopentan-2-yl-1-^{13}*C*)carbamate

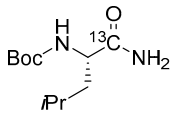

Boc-Leu-1-^{13}C-OH **113** (0.3 g, 1.5 mmol, 1.0 eq) was dissolved in DMF (10 mL) at 0 °C. Under stirring HOBt · H_2O (0.3 g, 1.9 mmol, 1.2 eq) was added in portions. After 20 min, NH_4OH solution (25% in water, 5 mL) was added, and reactions stirred overnight. After adding DCM (15 mL), a white precipitate formed, which was collected via filtration. The filtrate was washed with brine (15 mL), saturated $NaHCO_3$ solution (15 mL), dried over anhydrous N_2SO_4 and the solvent removed under reduced pressure to give a crude product that was purified with column chromatography (CH/EA 1:2) yielding the title compound as a colorless oil (51 mg, 0.22 mmol, 15%). ^{1}H NMR (300 MHz, CDCl3): δ/ppm = 6.85 – 6.50 (m, 1H), 5.42 – 5.05 (m, 1H), 4.18 (s, 1H), 1.82 – 1.57 (m, 2H), 1.42 (d, J = 4.5 Hz, 10H), 0.91 (dd, J = 6.3, 4.0 Hz, 6H). ^{13}C NMR (75.5 MHz, $CDCl_3$): δ/ppm =175.9, 155.9, 80.2, 52.4, 41.5, 28.4, 24.9, 23.1, 22.0. MS (ESI) m/z calculated for $[C_{10}{}^{13}CH_{23}N_2O_3]^+$ ([M+H]$^+$): 231.17, found: 232.22.

117, *tert*-Butyl (*S*)-(1-(cyano-^{13}*C*)-3-methylbutyl)carbamate

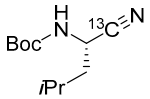

116 (50 mg, 1.5 mmol, 1.0 eq) was dissolved in dry THF (10 mL) at −78 °C and trifluoroacetic anhydride (45 µL, 0.33 mmol, 1.5 eq) and pyridine (53 µL, 0.65 mmol, 3.0 eq) were added subsequently. After stirring for 2 h, the solvent was removed in vacuum and the crude residue was diluted with EtOAc (20 mL) and washed with 1 m $KHSO_4$-solution (15 mL) and brine (15 mL). The combined organic extracts were dried over Na_2SO_4 and the solvent removed in vacuum yielding the title compound as an colorless oil (34 mg, 0.16 mmol, 74%). ^{1}H NMR (300 MHz, $CDCl_3$): δ/ppm = 1.91 – 1.75 (m, 1H), 1.74 – 1.60 (m, 2H), 1.55 – 1.43 (m, 9H), 1.04 – 0.90 (m, 6H).^{13}C NMR (75.5 MHz, $CDCl_3$): δ/ppm =172.9, 119.2, 81.5, 52.4, 42.2, 28.3, 24.9, 23.1, 22.0. Purity: 95%.

6 Conclusions and Outlook

This scientific work, divided into two projects, focused on the design and functionalization of catS inhibitors in the framework of the CRC 1066 (subproject Q5), and on the interactions between protease inhibitors containing a suitable peptidomimetic sequence in combination with various warheads and different proteases.

In the first project the goal was to develop new highly affine and selective inhibitors of the cysteine protease catS, as this enzyme is involved in a plethora of diseases, especially its involvement in several cancers makes it attractive and interesting as a potential target for novel anti-cancer drugs. The newly designed inhibitors demonstrate improvements in affinity and selectivity over closely related off-targets, with the possibility of further functionalization in several positions by either functionalizing the P3 residue or by using the warhead functionality as a linker position. The warhead functions as an electrophilic trap with high reactivity which is deactivated by attaching reversible linkers that mask and protect the highly reactive warhead from side-reactions, until the inhibitor reaches the target compartment by targeted drug delivery. Especially the highly reactive aldehyde and vinylsulfonate warheads were successfully 'tamed' by generating inhibitors with sub-nanomolar affinities for the target protease catS while retaining high selectivity towards similar off-targets and by masking the warhead in case of the aldehyde with a reversible and pH-sensitive hydrazone linker (**Figure 21**).

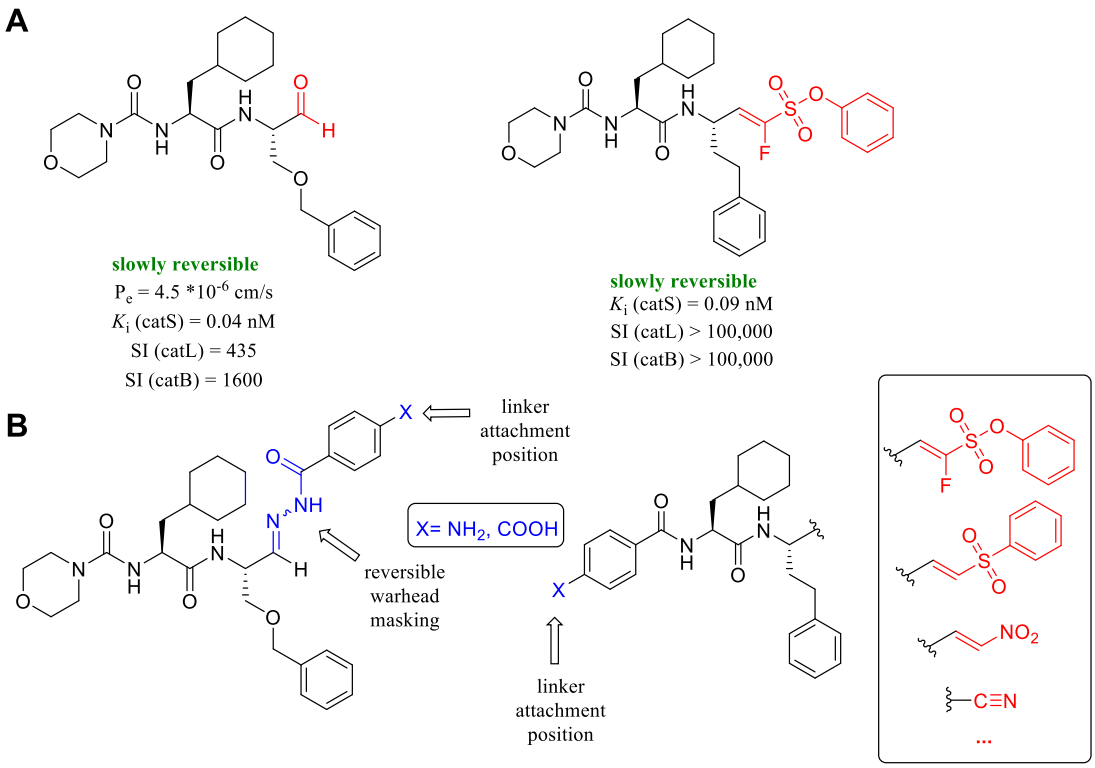

Figure 21: **A**: The most potent catS inhibitors of project 1. **B**: Linker attachment strategies. Linker attachment positions are depicted in blue and the warhead functionality in red.

The most potent inhibitors show slowly reversible tight binding modes, which is favorable and might help reduce off-target reactivities and thus minimize the risks of toxicity and haptenization in further development campaigns. The design of these highly affine new inhibitors was facilitated by in silico methods like molecular modeling and (non-)covalent docking approaches.

In the second project the goal was to investigate the selectivity profiles of several well-known warheads with different reactivity for a set of different proteases with varying nucleophilic amino acids in the active site. The warheads were combined with peptidomimetic sequences, suited for each of the different proteases and cross-testing of the warhead-decorated inhibitors in fluorometric enzyme assays against all proteases gave insight on the impact of peptidomimetic sequences and warheads on affinity and selectivity. Most of the produced inhibitors showed affinity in the sub-micromolar range towards the target protease catS. Due to structural similarity, especially between the papain-like cysteine proteases, new lead structures for inhibiting several proteases could be found, while hardly druggable targets like the subunits of the 20S proteasome didn't allow for the identification of any new potential inhibitors through this approach. This combinatorial approach demonstrated clear limits to affinity and selectivity, while revealing additional off-target data on several newly generated inhibitors on (patho-)physiologically relevant targets (**Figure 22**). The warheads were further investigated by NMR and LC-MS reactivity assays against model nucleophiles mimicking the catalytic nucleophilic amino acids of the different proteases to evaluate chemoselectivity. The results confirmed high reactivity for the 4-oxoenoate and (fluoro-)vinylsulfone warheads towards a deprotonated thiol model nucleophile. In agreement with the enzyme assay results, the α-ketobenzothiazole demonstrated to be a potent electrophilic trap for both cysteine and serine proteases and the nucleophilic thiol and ethanolate models. The results of the reactivity assays were overall confirmed by quantum mechanics calculations of similar model nucelophiles, and (non-)covalent docking approaches yielded poses with reasonable binding modes, resembling the crystallographic reference ligands of all pdb structures.

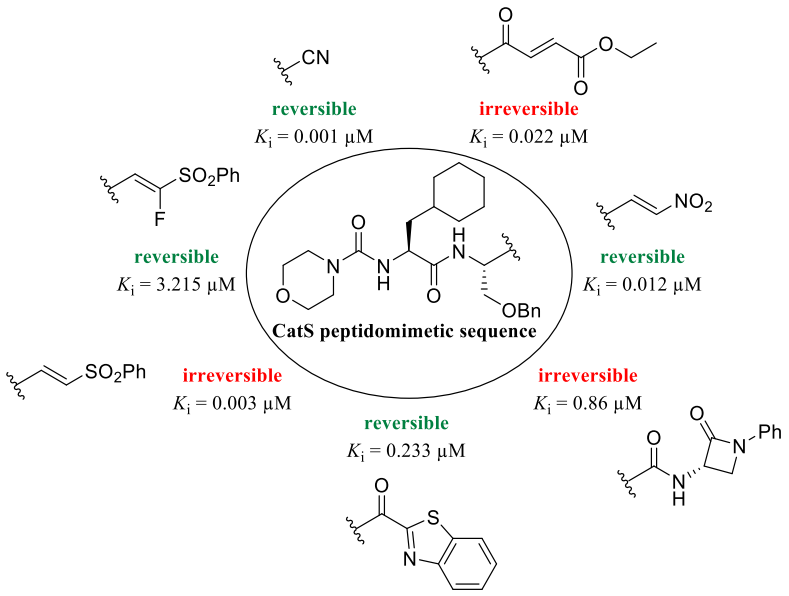

Figure 22: Inhibition data against catS for inhibitors with catS peptidomimetic sequence and various warheads.

Through a combination of molecular modeling and docking, enzyme kinetic analysis, quantum mechanics calculations and combinatorial SAR analysis, new highly affine inhibitors with different selectivity profiles were produced that can act as a foundation for future optimization campaigns. By attaching reversible linkers on either the warhead or on a side chain (e.g., the P3 residue) of an inhibitor, and by immobilizing the probe on a suitable nanocarrier, the drug delivery process could be enhanced and the transport as well as the successful release of the drug in the destination compartment could be observed by confocal microscopy or similar imaging methods if the nanocarrier is appropriately functionalized with fluorophore- or radiolabels.

Since it is known that reducing the catS expression leads to a change in the expression ratio of $CD4^+$ T cells and $CD8^+$ cytotoxic T cells towards the cytotoxic T cells, delivering the functionalized inhibitors with a nanocarrier based delivery system might shift the $CD4^+$ / $CD8^+$ ratio towards the cytotoxic T cells, thus effectively altering the TME towards an anti-tumor immune response. With cell-based catS activity assays, this effect on different tumor models is putatively directly related to the successful delivery of the catS inhibitors.[45,89,267]

7 Bibliography

[1] O. Schilling, C. M. Overall, *Nat Biotechnol* **2008**, *26*, 685–694.

[2] A. B. Marnett, C. S. Craik, *Trends Biotechnol* **2005**, *23*, 59–64.

[3] Q. Li, L. Yi, P. Marek, B. L. Iverson, *FEBS Lett* **2013**, *587*, 1155–1163.

[4] C. López-Otín, J. S. Bond, *Journal of Biological Chemistry* **2008**, *283*, 30433–30437.

[5] M. Duffy, P. McGowan, W. Gallagher, *J Pathol* **2008**, *214*, 283–293.

[6] T. E. Hugli, *Trends Biotechnol* **1996**, *14*, 409–412.

[7] G. Abbenante, D. Fairlie, *Med Chem (Los Angeles)* **2005**, *1*, 71–104.

[8] *Proteases in Human Diseases*, Springer Singapore, Singapore, **2017**.

[9] A. A. Agbowuro, W. M. Huston, A. B. Gamble, J. D. A. Tyndall, *Med Res Rev* **2018**, *38*, 1295–1331.

[10] S. Dhillon, *Drugs* **2015**, *75*, 1783–1796.

[11] E. C. Li, B. S. Heran, J. M. Wright, *Cochrane Database of Systematic Reviews* **2014**, *2014*, DOI 10.1002/14651858.CD009096.pub2.

[12] P. G. Richardson, P. Sonneveld, M. W. Schuster, D. Irwin, E. A. Stadtmauer, T. Facon, J.-L. Harousseau, D. Ben-Yehuda, S. Lonial, H. Goldschmidt, D. Reece, J. F. San-Miguel, J. Bladé, M. Boccadoro, J. Cavenagh, W. S. Dalton, A. L. Boral, D. L. Esseltine, J. B. Porter, D. Schenkein, K. C. Anderson, *New England Journal of Medicine* **2005**, *352*, 2487–2498.

[13] D. Schomburg, I. Schomburg, **2010**, pp. 113–128.

[14] N. D. Rawlings, M. Waller, A. J. Barrett, A. Bateman, *Nucleic Acids Res* **2014**, *42*, D503–D509.

[15] N. D. Rawlings, A. J. Barrett, *Biochemical Journal* **1993**, *290*, 205–218.

[16] I. Schechter, A. Berger, *Biochem Biophys Res Commun* **2012**, *425*, 497–502.

[17] H.-H. Otto, T. Schirmeister, *Chem Rev* **1997**, *97*, 133–172.

[18] H. M. Berman, *Nucleic Acids Res* **2000**, *28*, 235–242.

[19] A. L. Hughes, *Mol Phylogenet Evol* **1994**, *3*, 310–321.

[20] D. Wei, X. Huang, J. Liu, M. Tang, C.-G. Zhan, *Biochemistry* **2013**, *52*, 5145–5154.

[21] T. Vernet, D. C. Tessier, J. Chatellier, C. Plouffe, T. S. Lee, D. Y. Thomas, A. C. Storer, R. Ménard, *Journal of Biological Chemistry* **1995**, *270*, 16645–16652.

[22] S. Ma, L. S. Devi-Kesavan, J. Gao, *J Am Chem Soc* **2007**, *129*, 13633–13645.

[23] S. D. Lewis, F. A. Johnson, J. A. Shafer, *Biochemistry* **1976**, *15*, 5009–5017.

[24] S. D. Lewis, F. A. Johnson, J. A. Shafer, *Biochemistry* **1981**, *20*, 48–51.

[25] W.-G. Han, E. Tajkhorshid, S. Suhai, *J Biomol Struct Dyn* **1999**, *16*, 1019–1032.

[26] K. Brocklehurst, *International Journal of Biochemistry* **1979**, *10*, 259–274.

[27] M. J. Harrison, N. A. Burton, I. H. Hillier, *J Am Chem Soc* **1997**, *119*, 12285–12291.

[28] W. G. J. Hol, P. T. Van Duijnen, H. J. C. Berendsen, *Nature* **1978**, *273*, 443–446.

[29] M. Mladenovic, R. F. Fink, W. Thiel, T. Schirmeister, B. Engels, *J Am Chem Soc* **2008**, *130*, 8696–8705.

[30] R. MÉNARD, A. C. STORER, *Biol Chem Hoppe Seyler* **1992**, *373*, 393–400.

[31] A. Rossi, Q. Deveraux, B. Turk, A. Sali, *Biol Chem* **2004**, *385*, DOI 10.1515/BC.2004.040.

[32] K. Brix, A. Dunkhorst, K. Mayer, S. Jordans, *Biochimie* **2008**, *90*, 194–207.

[33] M. Vizovišek, E. Vidak, U. Javoršek, G. Mikhaylov, A. Bratovš, B. Turk, *Expert Opin Ther Targets* **2020**, *24*, 573–588.

[34] J. Y. Gauthier, W. C. Black, I. Courchesne, W. Cromlish, S. Desmarais, R. Houle, S. Lamontagne, C. S. Li, F. Massé, D. J. McKay, M. Ouellet, J. Robichaud, J. F. Truchon, V. L. Truong, Q. Wang, M. D. Percival, *Bioorg Med Chem Lett* **2007**, *17*, 4929–4933.

[35] D. Brömme, F. Lecaille, *Expert Opin Investig Drugs* **2009**, *18*, 585–600.

[36] T. Weitoft, A. Larsson, V. A. Manivel, J. Lysholm, A. Knight, J. Rönnelid, *Rheumatology* **2015**, *54*, 1923–1928.

[37] D. R. Sudhan, D. W. Siemann, *Pharmacol Ther* **2015**, *155*, 105–116.

[38] S. D. Mason, J. A. Joyce, *Trends Cell Biol* **2011**, *21*, 228–237.

[39] O. C. Olson, J. A. Joyce, *Nat Rev Cancer* **2015**, *15*, 712–729.

[40] M. M. Mohamed, B. F. Sloane, *Nat Rev Cancer* **2006**, *6*, 764–775.

[41] R. Dennhöfer, P. Kurschat, P. Zigrino, A. Klose, A. Bosserhoff, G. van Muijen, T. Krieg, C. Mauch, N. Hunzelmann, *Int J Cancer* **2003**, *106*, 316–323.

[42] J. Kos, A. Mitrović, B. Mirković, *Future Med Chem* **2014**, *6*, 1355–1371.

[43] J. Gora, R. Latajka, *Curr Med Chem* **2015**, *22*, 944–957.

[44] D. Bararia, J. A. Hildebrand, S. Stolz, S. Haebe, S. Alig, C. P. Trevisani, F. Osorio-Barrios, M. D. Bartoschek, M. Mentz, A. Pastore, E. Gaitzsch, M. Heide, V. Jurinovic, K. Rautter, J. Gunawardana, M. B. Sabdia, M. Szczepanowski, J. Richter, W. Klapper, A. Louissaint, C. Ludwig, S. Bultmann, H. Leonhardt, S. Eustermann, K. P. Hopfner, W. Hiddemann, M. von Bergwelt-Baildon, C. Steidl, R. Kridel, J. W. D. Tobin, M. K. Gandhi, D. M. Weinstock, M. Schmidt-Supprian, M. B. Sárosi, M. Rudelius, V. Passerini, J. Mautner, O. Weigert, *Cell Rep* **2020**, *31*, DOI 10.1016/j.celrep.2020.107522.

[45] E. Dheilly, E. Battistello, N. Katanayeva, S. Sungalee, J. Michaux, G. Duns, S. Wehrle, J. Sordet-Dessimoz, M. Mina, J. Racle, P. Farinha, G. Coukos, D. Gfeller, A. Mottok, R. Kridel, B. E. Correia, C. Steidl, M. Bassani-Sternberg, G. Ciriello, V. Zoete, E. Oricchio, *Cancer Cell* **2020**, *37*, 674-689.e12.

[46] N. Fuchs, M. Meta, D. Schuppan, L. Nuhn, T. Schirmeister, *Cells* **2020**, *9*, DOI 10.3390/cells9092021.

[47] J. R. Somoza, H. Zhan, K. K. Bowman, L. Yu, K. D. Mortara, J. T. Palmer, J. M. Clark, M. E. McGrath, *Biochemistry* **2000**, *39*, 12543–12551.

[48] G. Kopitar, M. Dolinar, B. Štrukelj, J. Pungerčar, V. Turk, *Eur J Biochem* **1996**, *236*, 558–562.

[49] O. Vasiljeva, M. Dolinar, J. R. Pungerčar, V. Turk, B. Turk, *FEBS Lett* **2005**, *579*, 1285–1290.

[50] G. P. Shi, J. S. Munger, J. P. Meara, D. H. Rich, H. A. Chapman, *Journal of Biological Chemistry* **1992**, *267*, 7258–7262.

[51] T. A. Pauly, T. Sulea, M. Ammirati, J. Sivaraman, D. E. Danley, M. C. Griffor, A. V. Kamath, I. K. Wang, E. R. Laird, A. P. Seddon, R. Ménard, M. Cygler, V. L. Rath, *Biochemistry* **2003**, DOI 10.1021/bi027308i.

[52] R. A. Kirschke H, Wiederanders B, Brömme D, *Biochemical Journal* **1989**, *264*, 467–473.

[53] G. P. Shi, A. C. Webb, K. E. Foster, J. H. M. Knoll, C. A. Lemere, J. S. Munger, H. A. Chapman, *Journal of Biological Chemistry* **1994**, *269*, 11530–11536.

[54] J. J. M. Wiener, S. Sun, R. L. Thurmond, *Curr Top Med Chem* **2010**, *10*, 717–732.

[55] R. J. Riese, P. R. Wolf, D. Brömme, L. R. Natkin, J. A. Villadangos, H. L. Ploegh, H. A. Chapman, *Immunity* **1996**, *4*, 357–366.

[56] G. P. Shi, J. S. Munger, J. P. Meara, D. H. Rich, H. A. Chapman, *Journal of Biological Chemistry* **1992**, *267*, 7258–7262.

[57] W.-H. Boehncke, E. Weber, H. Schmid, G. Schwarz, M. Braun, C. J. Schröter, T. Burster, T. Flad, D. Dressel, H. Kalbacher, *Journal of Investigative Dermatology* **2002**, *119*, 44–49.

[58] D. Caglič, U. Repnik, C. Jedeszko, G. Kosec, C. Miniejew, M. Kindermann, O. Vasiljeva, V. Turk, K. U. Wendt, B. F. Sloane, M. B. Goldring, B. Turk, *bchm* **2013**, *394*, 307–316.

[59] E. Fiebiger, P. Meraner, E. Weber, I.-F. Fang, G. Stingl, H. Ploegh, D. Maurer, *J Exp Med* **2001**, *193*, 881–892.

[60] K. Storm van's Gravesande, M. D. Layne, Q. Ye, L. Le, R. M. Baron, M. A. Perrella, L. Santambrogio, E. S. Silverman, R. J. Riese, *The Journal of Immunology* **2002**, *168*, 4488–4494.

[61] S. Weldon, P. McNally, D. F. McAuley, I. K. Oglesby, C. L. Wohlford-Lenane, J. A. Bartlett, C. J. Scott, N. G. McElvaney, C. M. Greene, P. B. McCray, C. C. Taggart, *Am J Respir Crit Care Med* **2014**, *190*, 165–174.

[62] C.-J. Chang, H.-C. Hsu, W.-J. Ho, G.-J. Chang, J.-H. S. Pang, W.-J. Chen, C.-C. Huang, Y.-J. Lai, *American Journal of Physiology-Lung Cellular and Molecular Physiology* **2019**, *317*, L1–L13.

[63] C. Ji, M. Tang, J. Harrison, A. Paciorkowski, G. V. W. Johnson, *European Journal of Neuroscience* **2018**, *48*, 3043–3051.

[64] S. J. Kim, S. Schätzle, S. S. Ahmed, W. Haap, S. H. Jang, P. K. Gregersen, G. Georgiou, B. Diamond, *Nat Immunol* **2017**, *18*, 1016–1024.

[65] Y. Wang, R. M. Baron, G. Zhu, M. Joo, J. W. Christman, E. S. Silverman, M. A. Perrella, R. J. Riese, M. Cernadas, *The Journal of Immunology* **2006**, *176*, 275–283.

[66] F. Bollmann, Z. Wu, M. Oelze, D. Siuda, N. Xia, J. Henke, A. Daiber, H. Li, D. J. Stumpo, P. J. Blackshear, H. Kleinert, A. Pautz, *Journal of Biological Chemistry* **2014**, *289*, 15653–15665.

[67] D. F. Doherty, S. Nath, J. Poon, R. F. Foronjy, M. Ohlmeyer, A. J. Dabo, M. Salathe, M. Birrell, M. Belvisi, N. Baumlin, M. D. Kim, S. Weldon, C. Taggart, P. Geraghty, *Am J Respir Crit Care Med* **2019**, *200*, 51–62.

[68] J. Yang, X. Luo, Y. Nie, Y. Su, Q. Zhao, K. Kabir, D. Zhang, R. Rabinovici, *Immunology* **2003**, *109*, 15–23.

[69] C. P. Nader, A. Cidem, N. M. Verrills, A. J. Ammit, *Respir Res* **2019**, *20*, 222.

[70] D. Pires, E. M. Bernard, J. P. Pombo, N. Carmo, C. Fialho, M. G. Gutierrez, P. Bettencourt, E. Anes, *Front Immunol* **2017**, *8*, DOI 10.3389/fimmu.2017.01819.

[71] P. Saftig, J. Klumperman, *Nat Rev Mol Cell Biol* **2009**, *10*, 623–635.

[72] B. Wiederanders, G. Kaulmann, K. Schilling, *Curr Protein Pept Sci* **2003**, *4*, 309–326.

[73] D. Yan, H.-W. Wang, R. L. Bowman, J. A. Joyce, *Cell Rep* **2016**, *16*, 2914–2927.

[74] R. L. Lackman, A. M. Jamieson, J. M. Griffith, H. Geuze, P. Cresswell, *Traffic* **2007**, *8*, 1179–1189.

[75] X. W. Cheng, M. Kuzuya, K. Nakamura, Q. Di, Z. Liu, T. Sasaki, S. Kanda, H. Jin, G.-P. Shi, T. Murohara, M. Yokota, A. Iguchi, *Am J Pathol* **2006**, *168*, 685–694.

[76] I. Potolicchio, G. J. Carven, X. Xu, C. Stipp, R. J. Riese, L. J. Stern, L. Santambrogio, *The Journal of Immunology* **2005**, *175*, 2237–2243.

[77] K. Nissler, W. Strubel, S. Kreusch, W. Rommerskirch, E. Weber, B. Wiederanders, *Eur J Biochem* **1999**, *263*, 717–725.

[78] R. Brown, S. Nath, A. Lora, G. Samaha, Z. Elgamal, R. Kaiser, C. Taggart, S. Weldon, P. Geraghty, *Respir Res* **2020**, *21*, 111.

[79] Y. Yoo, E. Choi, Y. Kim, Y. Cha, E. Um, Y. Kim, Y. Kim, Y.-S. Lee, *Biomedicine & Pharmacotherapy* **2022**, *145*, 112245.

[80] B. Turk, D. Turk, G. Salvesen, *Curr Pharm Des* **2002**, *8*, 1623–1637.

[81] E. Vidak, U. Javoršek, M. Vizovišek, B. Turk, *Cells* **2019**, *8*, 264.

[82] M. Fonović, B. Turk, *Biochimica et Biophysica Acta (BBA) - General Subjects* **2014**, *1840*, 2560–2570.

[83] E. A. Comen, R. L. Bowman, M. Kleppe, *Front Cell Dev Biol* **2018**, *6*, DOI 10.3389/fcell.2018.00056.

[84] D. M. Small, R. E. Burden, C. J. Scott, *Clin Rev Bone Miner Metab* **2011**, *9*, 122–132.

[85] R. D. A. Wilkinson, R. Williams, C. J. Scott, R. E. Burden, *Biol Chem* **2015**, *396*, 867–882.

[86] V. Gocheva, W. Zeng, D. Ke, D. Klimstra, T. Reinheckel, C. Peters, D. Hanahan, J. A. Joyce, *Genes Dev* **2006**, *20*, 543–556.

[87] D. M. Small, R. E. Burden, J. Jaworski, S. M. Hegarty, S. Spence, J. F. Burrows, C. McFarlane, A. Kissenpfennig, H. O. McCarthy, J. A. Johnston, B. Walker, C. J. Scott, *Int J Cancer* **2013**, *133*, 2102–2112.

[88] J. A. Joyce, A. Baruch, K. Chehade, N. Meyer-Morse, E. Giraudo, F.-Y. Tsai, D. C. Greenbaum, J. H. Hager, M. Bogyo, D. Hanahan, *Cancer Cell* **2004**, *5*, 443–453.

[89] V. Gocheva, H. W. Wang, B. B. Gadea, T. Shree, K. E. Hunter, A. L. Garfall, T. Berman, J. A. Joyce, *Genes Dev* **2010**, *24*, 241–255.

[90] S. H. McDowell, S. A. Gallaher, R. E. Burden, C. J. Scott, *Biochim Biophys Acta Mol Cell Res* **2020**, *1867*, DOI 10.1016/j.bbamcr.2020.118781.

[91] B. Wang, J. Sun, S. Kitamoto, M. Yang, A. Grubb, H. A. Chapman, R. Kalluri, G. P. Shi, *Journal of Biological Chemistry* **2006**, *281*, 6020–6029.

[92] G.-P. Shi, G. K. Sukhova, M. Kuzuya, Q. Ye, J. Du, Y. Zhang, J.-H. Pan, M. L. Lu, X. W. Cheng, A. Iguchi, S. Perrey, A. M.-E. Lee, H. A. Chapman, P. Libby, *Circ Res* **2003**, *92*, 493–500.

[93] D. Yan, H.-W. Wang, R. L. Bowman, J. A. Joyce, *Cell Rep* **2016**, *16*, 2914–2927.

[94] L. Sevenich, R. L. Bowman, S. D. Mason, D. F. Quail, F. Rapaport, B. T. Elie, E. Brogi, P. K. Brastianos, W. C. Hahn, L. J. Holsinger, J. Massagué, C. S. Leslie, J. A. Joyce, *Nat Cell Biol* **2014**, *16*, 876–888.

[95] R. D. A. Wilkinson, A. Young, R. E. Burden, R. Williams, C. J. Scott, *Mol Cancer* **2016**, *15*, DOI 10.1186/s12943-016-0513-7.

[96] T. Shree, O. C. Olson, B. T. Elie, J. C. Kester, A. L. Garfall, K. Simpson, K. M. Bell-McGuinn, E. C. Zabor, E. Brogi, J. A. Joyce, *Genes Dev* **2011**, *25*, 2465–2479.

[97] R. E. Burden, J. A. Gormley, T. J. Jaquin, D. M. Small, D. J. Quinn, S. M. Hegarty, C. Ward, B. Walker, J. A. Johnston, S. A. Olwill, C. J. Scott, *Clinical Cancer Research* **2009**, *15*, 6042–6051.

[98] M. Davis, *Clin J Oncol Nurs* **2016**, *20*, S2–S8.

[99] T. Flannery, D. Gibson, M. Mirakhur, S. McQuaid, C. Greenan, A. Trimble, B. Walker, D. McCormick, P. G. Johnston, *Am J Pathol* **2003**, *163*, 175–182.

[100] T. Flannery, R. S. McConnell, S. McQuaid, G. Mcgregor, M. Mirakhur, L. Martin, C. Scott, R. Burden, B. Walker, C. McGoohan, P. G. Johnston, *Br J Neurosurg* **2007**, *21*, 204–209.

[101] L. Zhang, H. Wang, J. Xu, J. Zhu, K. Ding, *Toxicol Lett* **2014**, *228*, 248–259.

[102] P. Liu, W. Jiang, H. Ren, H. Zhang, J. Hao, *Pathology & Oncology Research* **2015**, *21*, 1077–1083.

[103] E. Ryschich, P. Lizdenis, C. Ittrich, A. Benner, S. Stahl, A. Hamann, J. Schmidt, P. Knolle, B. Arnold, G. J. Hämmerling, R. Ganss, *Cancer Res* **2006**, *66*, 198–211.

[104] Xu J, Ke Z, Liu R, Maubach G, Zhuo L, *Mol Med Rep* **2009**, *2*, 713–718.

[105] X. Yan, C. Wu, T. Chen, M. M. Santos, C. L. Liu, C. Yang, L. Zhang, J. Ren, S. Liao, H. Guo, G. K. Sukhova, G. P. Shi, *Mol Immunol* **2017**, *82*, 66–74.

[106] M. Frydrychowicz, M. Boruczkowski, A. Kolecka-Bednarczyk, G. Dworacki, *Scand J Immunol* **2017**, *86*, 436–443.

[107] Y. Yixuan, L. S. Kiat, C. L. Yee, L. Huiyin, C. Yunhao, C. P. Kuan, A. Hassan, W. T. Ting, S.-T. Manuel, Y. K. Guan, L. Y. Pin, *J Proteome Res* **2010**, *9*, 4767–4778.

[108] W.-L. Liu, D. Liu, K. Cheng, Y.-J. Liu, S. Xing, P. Chi, X.-H. Liu, N. Xue, Y. Lai, L. Guo, G. Zhang, *Oncotarget* **2016**, *7*, 28124–28138.

[109] A. Lee-Dutra, D. K. Wiener, S. Sun, *Expert Opin Ther Pat* **2011**, DOI 10.1517/13543776.2011.553800.

[110] P. D. Greenspan, K. L. Clark, R. A. Tommasi, S. D. Cowen, L. W. McQuire, D. L. Farley, J. H. van Duzer, R. L. Goldberg, H. Zhou, Z. Du, J. J. Fitt, D. E. Coppa, Z. Fang, W. Macchia, L. Zhu, M. P. Capparelli, R. Goldstein, A. M. Wigg, J. R. Doughty, R. S. Bohacek, A. K. Knap, *J Med Chem* **2001**, *44*, 4524–4534.

[111] D. G. Barrett, J. G. Catalano, D. N. Deaton, A. M. Hassell, S. T. Long, A. B. Miller, L. R. Miller, L. M. Shewchuk, K. J. Wells-Knecht, D. H. Willard, L. L. Wright, *Bioorg Med Chem Lett* **2004**, *14*, 4897–4902.

[112] R. T. Shenoy, J. Sivaraman, *J Struct Biol* **2011**, *173*, 14–19.

[113] T. Sterling, J. J. Irwin, *J Chem Inf Model* **2015**, DOI 10.1021/acs.jcim.5b00559.

[114] R. L. Thurmond, M. P. Beavers, H. Cai, S. P. Meduna, D. J. Gustin, S. Sun, H. J. Almond, L. Karlsson, J. P. Edwards, *J Med Chem* **2004**, *47*, 4799–4801.

[115] D. C. Tully, H. Liu, P. B. Alper, A. K. Chatterjee, R. Epple, M. J. Roberts, J. A. Williams, K. T. Nguyen, D. H. Woodmansee, C. Tumanut, J. Li, G. Spraggon, J. Chang, T. Tuntland, J. L. Harris, D. S. Karanewsky, *Bioorg Med Chem Lett* **2006**, *16*, 1975–1980.

[116] P. K. Jadhav, M. A. Schiffler, K. Gavardinas, E. J. Kim, D. P. Matthews, M. A. Staszak, D. S. Coffey, B. W. Shaw, K. C. Cassidy, R. A. Brier, Y. Zhang, R. M. Christie, W. F. Matter, K. Qing, J. D. Durbin, Y. Wang, G. G. Deng, *ACS Med Chem Lett* **2014**, *5*, 1138–1142.

[117] M. Schade, B. Merla, B. Lesch, M. Wagener, S. Timmermanns, K. Pletinckx, T. Hertrampf, *J Med Chem* **2020**, *63*, 11801–11808.

[118] N. Fuchs, M. Meta, B. Lantzberg, M. Bros, S. Ling Kuan, T. Weil, T. Schirmeister, *ChemMedChem* **2023**, *18*, DOI 10.1002/cmdc.202300160.

[119] S. Conde, D. I. Pérez, A. Martínez, C. Perez, F. J. Moreno, *J Med Chem* **2003**, *46*, 4631–4633.

[120] K.-H. Ha, M.-S. Byun, J. Choi, J. Jeong, K.-J. Lee, D.-M. Jue, *Biochemistry* **2009**, *48*, 7271–7278.

[121] J. L. Ambroso, C. Harris, *Teratology* **1994**, *50*, 214–228.

[122] J. C. Powers, J. L. Asgian, Ö. D. Ekici, K. E. James, *Chem Rev* **2002**, *102*, 4639–4750.

[123] R. M. McConnell, J. L. York, D. Frizzell, C. Ezell, *J Med Chem* **1993**, *36*, 1084–1089.

[124] T. Sasaki, M. Kishi, M. Saito, T. Tanaka, N. Higuchi, E. Kominami, N. Katunuma, T. Murachi, *J Enzyme Inhib* **1990**, *3*, 195–201.

[125] T. E. Hughes, M. D. Mone, M. E. Russell, S. C. Weldon, E. B. Villhauer, *Biochemistry* **1999**, *38*, 11597–11603.

[126] J. Li, E. Wilk, S. Wilk, *Arch Biochem Biophys* **1995**, *323*, 148–154.

[127] A. J. Scheen, *Expert Opin Drug Saf* **2018**, *17*, 387–405.

[128] Y. N. Lamb, *Drugs* **2022**, *82*, 585–591.

[129] A. J. Scheen, *Expert Opin Pharmacother* **2015**, *16*, 43–62.

[130] J. Y. Gauthier, N. Chauret, W. Cromlish, S. Desmarais, L. T. Duong, J.-P. Falgueyret, D. B. Kimmel, S. Lamontagne, S. Léger, T. LeRiche, C. S. Li, F. Massé, D. J. McKay, D. A. Nicoll-Griffith, R. M. Oballa, J. T. Palmer, M. D. Percival, D. Riendeau, J. Robichaud, G. A. Rodan, S. B. Rodan, C. Seto, M. Thérien, V.-L. Truong, M. C. Venuti, G. Wesolowski, R. N. Young, R. Zamboni, W. C. Black, *Bioorg Med Chem Lett* **2008**, *18*, 923–928.

[131] J. H. McKerrow, *PLoS Negl Trop Dis* **2018**, *12*, e0005850.

[132] P. Ábrányi-Balogh, L. Petri, T. Imre, P. Szijj, A. Scarpino, M. Hrast, A. Mitrović, U. P. Fonovič, K. Németh, H. Barreteau, D. I. Roper, K. Horváti, G. G. Ferenczy, J. Kos, J. Ilaš, S. Gobec, G. M. Keserű, *Eur J Med Chem* **2018**, *160*, 94–107.

[133] R. Vicik, M. Busemann, K. Baumann, T. Schirmeister, *Curr Top Med Chem* **2006**, *6*, 331–353.

[134] L. Cianni, C. W. Feldmann, E. Gilberg, M. Gütschow, L. Juliano, A. Leitão, J. Bajorath, C. A. Montanari, *J Med Chem* **2019**, *62*, 10497–10525.

[135] V. Leroy, *Expert Opin Ther Pat* **2004**, DOI 10.1517/13543776.14.3.301.

[136] C. L. Cywin, R. A. Firestone, D. W. McNeil, C. A. Grygon, K. M. Crane, D. M. White, P. R. Kinkade, J. L. Hopkins, W. Davidson, M. E. Labadia, J. Wildeson, M. M. Morelock, J. D. Peterson, E. L. Raymond, M. L. Brown, D. M. Spero, *Bioorg Med Chem* **2003**, *11*, 733–740.

[137] M. Shokhen, N. Khazanov, A. Albeck, *Proteins: Structure, Function, and Bioinformatics* **2011**, *79*, 975–985.

[138] D. Yamashita, R. Dodds, *Curr Pharm Des* **2000**, *6*, 1–24.

[139] C. Gampe, V. A. Verma, *J Med Chem* **2020**, *63*, 14357–14381.

[140] L. Li, B. C. Chenna, K. S. Yang, T. R. Cole, Z. T. Goodall, M. Giardini, Z. Moghadamchargari, E. A. Hernandez, J. Gomez, C. M. Calvet, J. A. Bernatchez, D. M. Mellott, J. Zhu, A. Rademacher, D. Thomas, L. R. Blankenship, A. Drelich, A. Laganowsky, C. T. K. Tseng, W. R. Liu, A. J. Wand, J. Cruz-Reyes, J. L. Siqueira-Neto, T. D. Meek, *J Med Chem* **2021**, *64*, 11267–11287.

[141] R. A. Smith, L. J. Copp, P. J. Coles, H. W. Pauls, V. J. Robinson, R. W. Spencer, S. B. Heard, Allen. Krantz, *J Am Chem Soc* **1988**, *110*, 4429–4431.

[142] B. Bai, A. Belovodskiy, M. Hena, A. S. Kandadai, M. A. Joyce, H. A. Saffran, J. A. Shields, M. B. Khan, E. Arutyunova, J. Lu, S. K. Bajwa, D. Hockman, C. Fischer, T. Lamer, W. Vuong, M. J. Van Belkum, Z. Gu, F. Lin, Y. Du, J. Xu, M. Rahim, H. S. Young, J. C. Vederas, D. L. Tyrrell, M. J. Lemieux, J. A. Nieman, *J Med Chem* **2022**, *65*, 2905–2925.

[143] R. Manjunatha Kini, H. J. Evans, W. R. Melander, C. Horvath, R. B. Merrifield, E. Meucci, A. Mordente, G. A. D. Miggiano, G. E. Martorana, Y. Omori, Y. Matsuda, S. Aimoto, Y. Shimonishi, M. Yamamoto, J. M. Ostresh, K. Büttner, R. A. Houghten, R. Hodges, A. Ed ; Pastore, T. S. Harvey, C. E. Dempsey, I. D. Campbell, S. C. Quay, C. G. Condie, K. W. Minton, E. Schroder, K. Lübke, M. Lehmann, I. Beetz, J. F. Stocker, J. R. Traynor, J. G. Talbot, J. Dufourcq, J. De Bony, J. F. Faucon, C. Lussan, J. Tam, W. Heath, T. G. Terwilliger, D. Eisenberg, L. Weissman, . T Tosteson, S. J. Holmes, M. Razin, D. C. Tosteson, L. Caporale, *Peptidyl (Acyloxy)Methyl Ketones and the Quiescent Affinity Label Concept: The Departing Group as a Variable Structural Element in the Design of Inactivators of Cysteine Proteinases1"*, CRC Press, **1991**.

[144] K. Arafet, S. Ferrer, V. Moliner, *Biochemistry* **2015**, *54*, 3381–3391.

[145] V. Pace, L. Castoldi, M. Pregnolato, *Mini-Reviews in Medicinal Chemistry* **2013**, *13*, 988–996.

[146] H.-U. Demuth, *J Enzyme Inhib* **1990**, *3*, 249–278.

[147] S. G. Kathman, Z. Xu, A. V. Statsyuk, *J Med Chem* **2014**, *57*, 4969–4974.

[148] S. A. Thompson, P. R. Andrews, R. P. Hanzlik, *J Med Chem* **1986**, *29*, 104–111.

[149] R. P. Hanzlik, S. A. Thompson, *J Med Chem* **1984**, *27*, 711–712.

[150] S. Liu, R. P. Hanzlik, *J Med Chem* **1992**, *35*, 1067–1075.

[151] J. T. Palmer, D. Rasnick, J. L. Klaus, D. Bromme, *J Med Chem* **1995**, *38*, 3193–3196.

[152] M. Santos, R. Moreira, *Mini-Reviews in Medicinal Chemistry* **2007**, *7*, 1040–1050.

[153] J. Olson, *Bioorg Med Chem* **1999**, *7*, 633–638.

[154] M.-H. Abdulla, K.-C. Lim, M. Sajid, J. H. McKerrow, C. R. Caffrey, *PLoS Med* **2007**, *4*, e14.

[155] Y. T. Chen, L. S. Brinen, I. D. Kerr, E. Hansell, P. S. Doyle, J. H. McKerrow, W. R. Roush, *PLoS Negl Trop Dis* **2010**, *4*, e825.

[156] T. Schirmeister, J. Kesselring, S. Jung, T. H. Schneider, A. Weickert, J. Becker, W. Lee, D. Bamberger, P. R. Wich, U. Distler, S. Tenzer, P. Johé, U. A. Hellmich, B. Engels, *J Am Chem Soc* **2016**, *138*, 8332–8335.

[157] S. Jung, N. Fuchs, P. Johe, A. Wagner, E. Diehl, T. Yuliani, C. Zimmer, F. Barthels, R. A. Zimmermann, P. Klein, W. Waigel, J. Meyr, T. Opatz, S. Tenzer, U. Distler, H. J. Räder, C. Kersten, B. Engels, U. A. Hellmich, J. Klein, T. Schirmeister, *J Med Chem* **2021**, *64*, 12322–12358.

[158] J. T. Palmer, D. Rasnick, J. L. Klaus, D. Bromme, *J Med Chem* **1995**, *38*, 3193–3196.

[159] Y. D. Ward, D. S. Thomson, L. L. Frye, C. L. Cywin, T. Morwick, M. J. Emmanuel, R. Zindell, D. McNeil, Y. Bekkali, M. Giradot, M. Hrapchak, M. DeTuri, K. Crane, D. White, S. Pav, Y. Wang, M. H. Hao, C. A. Grygon, M. E. Labadia, D. M. Freeman, W. Davidson, J. L. Hopkins, M. L. Brown, D. M. Spero, *J Med Chem* **2002**, *45*, 5471–5482.

[160] H. Hilpert, H. Mauser, R. Humm, L. Anselm, H. Kuehne, G. Hartmann, S. Gruener, D. W. Banner, J. Benz, B. Gsell, A. Kuglstatter, M. Stihle, R. Thoma, R. A. Sanchez, H. Iding, B. Wirz, W. Haap, *J Med Chem* **2013**, *56*, 9789–9801.

[161] S. Ahmad, S. Bhagwati, S. Kumar, D. Banerjee, M. I. Siddiqi, *J Mol Graph Model* **2020**, *96*, 107512.

[162] D. Parisis, C. Chivasso, J. Perret, M. S. Soyfoo, C. Delporte, *J Clin Med* **2020**, *9*, 2299.

[163] C. Bissantz, B. Kuhn, M. Stahl, *J Med Chem* **2010**, *53*, 5061–5084.

[164] X. Du, Y. Li, Y.-L. Xia, S.-M. Ai, J. Liang, P. Sang, X.-L. Ji, S.-Q. Liu, *Int J Mol Sci* **2016**, *17*, 144.

[165] M. A. Williams, **2013**, pp. 3–34.

[166] S. Mandal, M. Moudgil, S. K. Mandal, *Eur J Pharmacol* **2009**, *625*, 90–100.

[167] K. J. Pacholarz, R. A. Garlish, R. J. Taylor, P. E. Barran, *Chem Soc Rev* **2012**, *41*, 4335.

[168] J. Goddard, J. Reymond, *Curr Opin Biotechnol* **2004**, *15*, 314–322.

[169] J. Sumranjit, S. Chung, *Molecules* **2013**, *18*, 10425–10451.

[170] D. Robinette, N. Neamati, K. B. Tomer, C. H. Borchers, *Expert Rev Proteomics* **2006**, *3*, 399–408.

[171] V. Canbay, U. auf dem Keller, *Curr Opin Chem Biol* **2021**, *60*, 89–96.

[172] I. L. H. Ong, K.-L. Yang, *Analyst* **2017**, *142*, 1867–1881.

[173] A. Carmel, M. Zur, A. Yaron, E. Katchalski, *FEBS Lett* **1973**, *30*, 11–14.

[174] H. Tuppy, U. Wiesbauer, E. Wintersberger, *Hoppe Seylers Z Physiol Chem* **1962**, *329*, 278–288.

[175] M. Zimmerman, E. Yurewicz, G. Patel, *Anal Biochem* **1976**, *70*, 258–262.

[176] M. Bernetti, M. Masetti, W. Rocchia, A. Cavalli, *Annu Rev Phys Chem* **2019**, *70*, 143–171.

[177] M. G. Acker, D. S. Auld, *Perspect Sci (Neth)* **2014**, *1*, 56–73.

[178] J.-P. Goddard, J.-L. Reymond, *Trends Biotechnol* **2004**, *22*, 363–370.

[179] H. Bisswanger, *Perspect Sci (Neth)* **2014**, *1*, 41–55.

[180] B. T. Burlingham, T. S. Widlanski, *J Chem Educ* **2003**, *80*, 214.

[181] C. Yung-Chi, W. H. Prusoff, *Biochem Pharmacol* **1973**, *22*, 3099–3108.

[182] R. A. Ward, N. Grimster, *The Design of Covalent-Based Inhibitors*, Academic Press, **2021**.

[183] L. Olbe, E. Carlsson, P. Lindberg, *Nat Rev Drug Discov* **2003**, *2*, 132–139.

[184] P. Savi, J. M. Pereillo, M. F. Uzabiaga, J. Combalbert, C. Picard, J. P. Maffrand, M. Pascal, J. M. Herbert, *Thromb Haemost* **2000**, *84*, 891–896.

[185] P. M. Wright, I. B. Seiple, A. G. Myers, *Angewandte Chemie International Edition* **2014**, *53*, 8840–8869.

[186] S. S. Patel, J. A. Balfour, H. M. Bryson, *Drugs* **1997**, *53*, 637–656.

[187] J. Suarez, K. Ranguelova, A. A. Jarzecki, J. Manzerova, V. Krymov, X. Zhao, S. Yu, L. Metlitsky, G. J. Gerfen, R. S. Magliozzo, *Journal of Biological Chemistry* **2009**, *284*, 7017–7029.

[188] M. Gegia, N. Winters, A. Benedetti, D. van Soolingen, D. Menzies, *Lancet Infect Dis* **2017**, *17*, 223–234.

[189] R. A. Bauer, *Drug Discov Today* **2015**, *20*, 1061–1073.

[190] P. Revill, N. Serradell, J. Bolos, E. Rosa, *Drugs Future* **2007**, *32*, 0788.

[191] A. Abdeldayem, Y. S. Raouf, S. N. Constantinescu, R. Moriggl, P. T. Gunning, *Chem Soc Rev* **2020**, *49*, 2617–2687.

[192] S. De Cesco, J. Kurian, C. Dufresne, A. K. Mittermaier, N. Moitessier, *Eur J Med Chem* **2017**, *138*, 96–114.

[193] J. Singh, R. C. Petter, T. A. Baillie, A. Whitty, *Nat Rev Drug Discov* **2011**, *10*, 307–317.

[194] R. Lonsdale, R. A. Ward, *Chem Soc Rev* **2018**, *47*, 3816–3830.

[195] T. Zhang, J. M. Hatcher, M. Teng, N. S. Gray, M. Kostic, *Cell Chem Biol* **2019**, *26*, 1486–1500.

[196] J. Engel, A. Richters, M. Getlik, S. Tomassi, M. Keul, M. Termathe, J. Lategahn, C. Becker, S. Mayer-Wrangowski, C. Grütter, N. Uhlenbrock, J. Krüll, N. Schaumann, S. Eppmann, P. Kibies, F. Hoffgaard, J. Heil, S. Menninger, S. Ortiz-Cuaran, J. M. Heuckmann, V. Tinnefeld, R. P. Zahedi, M. L. Sos, C. Schultz-Fademrecht, R. K. Thomas, S. M. Kast, D. Rauh, *J Med Chem* **2015**, *58*, 6844–6863.

[197] E. Resnick, A. Bradley, J. Gan, A. Douangamath, T. Krojer, R. Sethi, P. P. Geurink, A. Aimon, G. Amitai, D. Bellini, J. Bennett, M. Fairhead, O. Fedorov, R. Gabizon, J. Gan, J. Guo, A. Plotnikov, N. Reznik, G. F. Ruda, L. Díaz-Sáez, V. M. Straub, T. Szommer, S. Velupillai, D. Zaidman, Y. Zhang, A. R. Coker, C. G. Dowson, H. M. Barr, C. Wang, K. V. M. Huber, P. E. Brennan, H. Ovaa, F. von Delft, N. London, *J Am Chem Soc* **2019**, *141*, 8951–8968.

[198] S. G. Kathman, A. V. Statsyuk, **2019**, pp. 245–262.

[199] S. E. Dalton, S. Campos, *ChemBioChem* **2020**, *21*, 1080–1100.

[200] S. Ray, A. S. Murkin, *Biochemistry* **2019**, *58*, 5234–5244.

[201] R. Lagoutte, R. Patouret, N. Winssinger, *Curr Opin Chem Biol* **2017**, *39*, 54–63.

[202] M. Gehringer, S. A. Laufer, *J Med Chem* **2019**, *62*, 5673–5724.

[203] J. M. Bradshaw, J. M. McFarland, V. O. Paavilainen, A. Bisconte, D. Tam, V. T. Phan, S. Romanov, D. Finkle, J. Shu, V. Patel, T. Ton, X. Li, D. G. Loughhead, P. A. Nunn, D. E. Karr, M. E. Gerritsen, J. O. Funk, T. D. Owens, E. Verner, K. A. Brameld, R. J. Hill, D. M. Goldstein, J. Taunton, *Nat Chem Biol* **2015**, *11*, 525–531.

[204] C. Lee, T. N. Grossmann, *Angewandte Chemie International Edition* **2012**, *51*, 8699–8700.

[205] E. Mons, S. Roet, R. Q. Kim, M. P. C. Mulder, *Curr Protoc* **2022**, *2*, DOI 10.1002/cpz1.419.

[206] I. M. Serafimova, M. A. Pufall, S. Krishnan, K. Duda, M. S. Cohen, R. L. Maglathlin, J. M. McFarland, R. M. Miller, M. Frödin, J. Taunton, *Nat Chem Biol* **2012**, *8*, 471–476.

[207] D. R. Owen, C. M. N Allerton, A. S. Anderson, L. Aschenbrenner, M. Avery, S. Berritt, B. Boras, R. D. Cardin, A. Carlo, K. J. Coffman, A. Dantonio, L. Di, H. Eng, R. Ferre, K. S. Gajiwala, S. A. Gibson, S. E. Greasley, B. L. Hurst, E. P. Kadar, A. S. Kalgutkar, J. C. Lee, J. Lee, W. Liu, S. W. Mason, S. Noell, J. J. Novak, R. Scott Obach, K. Ogilvie, N. C. Patel, M. Pettersson, D. K. Rai, M. R. Reese, M. F. Sammons, J. G. Sathish, R. P. Shankar Singh, C. M. Steppan, A. E. Stewart, J. B. Tuttle, L. Updyke, P. R. Verhoest, L. Wei, Q. Yang, Y. Zhu, *Science (1979)* **2021**, *374*, 1586–1593.

[208] R. A. Copeland, in *Evaluation of Enzyme Inhibitors in Drug Discovery*, Wiley, **2013**, pp. 203–244.

[209] R. A. Copeland, *Evaluation of Enzyme Inhibitors in Drug Discovery*, Wiley, **2013**.

[210] R. A. Copeland, *Expert Opin Drug Discov* **2010**, *5*, 305–310.

[211] R. A. Copeland, D. L. Pompliano, T. D. Meek, *Nat Rev Drug Discov* **2006**, *5*, 730–739.

[212] G. A. Holdgate, T. D. Meek, R. L. Grimley, *Nat Rev Drug Discov* **2018**, *17*, 115–132.

[213] J. M. Strelow, *SLAS Discovery* **2017**, *22*, 3–20.

[214] P. A. Schwartz, P. Kuzmic, J. Solowiej, S. Bergqvist, B. Bolanos, C. Almaden, A. Nagata, K. Ryan, J. Feng, D. Dalvie, J. C. Kath, M. Xu, R. Wani, B. W. Murray, *Proceedings of the National Academy of Sciences* **2014**, *111*, 173–178.

[215] C. McWhirter, R. A. Ward, N. P. Grimster, **2021**.

[216] G. Jones, P. Willett, R. C. Glen, *J Mol Biol* **1995**, *245*, 43–53.

[217] J. F. Morrison, C. T. Walsh, *Adv Enzymol Relat Areas Mol Biol* **1988**, *61*, 201–301.

[218] R. A. Copeland, *Evaluation of Enzyme Inhibitors in Drug Discovery: A Guide for Medicinal Chemists and Pharmacologists*, John Wiley & Sons, **2013**.

[219] R. A. Copeland, D. L. Pompliano, T. D. Meek, *Nat Rev Drug Discov* **2006**, *5*, 730–739.

[220] R. A. Copeland, A. Basavapathruni, M. Moyer, M. P. Scott, *Anal Biochem* **2011**, *416*, 206–210.

[221] S. Ludewig, M. Kossner, M. Schiller, K. Baumann, T. Schirmeister, *Enzyme Kinetics and Hit Validation in Fluorimetric Protease Assays*, **2010**.

[222] P. T. Englund, R. B. Kelly, A. Kornberg, *Journal of Biological Chemistry* **1969**, *244*, 3045–3052.

[223] H. Bisswanger, *Enzyme Kinetics: Principles and Methods*, John Wiley & Sons, **2017**.

[224] H. Mayr, M. Patz, *Angewandte Chemie International Edition in English* **1994**, *33*, 938–957.

[225] A. D. Cox, S. W. Fesik, A. C. Kimmelman, J. Luo, C. J. Der, *Nat Rev Drug Discov* **2014**, *13*, 828–851.

[226] I. M. Serafimova, M. A. Pufall, S. Krishnan, K. Duda, M. S. Cohen, R. L. Maglathlin, J. M. McFarland, R. M. Miller, M. Frödin, J. Taunton, *Nat Chem Biol* **2012**, *8*, 471–476.

[227] C. Dubiella, R. Baur, H. Cui, E. M. Huber, M. Groll, *Angewandte Chemie International Edition* **2015**, *54*, 15888–15891.

[228] C. Lammert, S. Einarsson, C. Saha, A. Niklasson, E. Bjornsson, N. Chalasani, *Hepatology* **2008**, *47*, 2003–2009.

[229] S. Krishnan, R. M. Miller, B. Tian, R. D. Mullins, M. P. Jacobson, J. Taunton, *J Am Chem Soc* **2014**, *136*, 12624–12630.

[230] D. Basu, A. Richters, D. Rauh, *Bioorg Med Chem* **2015**, *23*, 2767–2780.

[231] A. Bandyopadhyay, J. Gao, *Curr Opin Chem Biol* **2016**, *34*, 110–116.

[232] O. C. Farokhzad, R. Langer, *ACS Nano* **2009**, *3*, 16–20.

[233] D. Peer, J. M. Karp, S. Hong, O. C. Farokhzad, R. Margalit, R. Langer, *Nano-enabled medical applications* **2020**, 61–91.

[234] A. Z. Wang, R. Langer, O. C. Farokhzad, *Annu Rev Med* **2012**, *63*, 185–198.

[235] Y. Matsumura, H. Maeda, *Cancer Res* **1986**, *46*, 6387–6392.

[236] H. Maeda, *Adv Drug Deliv Rev* **2015**, *91*, 3–6.

[237] J. Fang, W. Islam, H. Maeda, *Adv Drug Deliv Rev* **2020**, *157*, 142–160.

[238] I. Toth, M. Skwarczynski, *Nanomedicine* **2014**, *9*, 2607–2609.

[239] E. Lepeltier, L. Nuhn, C.-M. Lehr, R. Zentel, *Nanomedicine* **2015**, *10*, 3147–3166.

[240] D. J. Irvine, E. L. Dane, *Nat Rev Immunol* **2020**, *20*, 321–334.

[241] J. D. Martin, H. Cabral, T. Stylianopoulos, R. K. Jain, *Nat Rev Clin Oncol* **2020**, *17*, 251–266.

[242] L. Lybaert, K. Vermaelen, B. G. De Geest, L. Nuhn, *Journal of Controlled Release* **2018**, *289*, 125–145.

[243] D. Oelschlaegel, T. W. Sadan, S. Salpeter, S. Krug, G. Blum, W. Schmitz, A. Schulze, P. Michl, *Cancers (Basel)* **2020**, *12*, 1–22.

[244] C. S. Wong, S. Hoogendoorn, G. A. Van Der Marel, H. S. Overkleeft, J. D. C. Codée, *Chempluschem* **2015**, DOI 10.1002/cplu.201500004.

[245] X. Pang, Y. Jiang, Q. Xiao, A. W. Leung, H. Hua, C. Xu, *Journal of Controlled Release* **2016**, *222*, 116–129.

[246] Y. Xin, J. Yuan, *Polym Chem* **2012**, *3*, 3045.

[247] S. Lv, Z. Tang, D. Zhang, W. Song, M. Li, J. Lin, H. Liu, X. Chen, *Journal of Controlled Release* **2014**, *194*, 220–227.

[248] M. M. Zegota, T. Wang, C. Seidler, D. Y. Wah Ng, S. L. Kuan, T. Weil, *Bioconjug Chem* **2018**, *29*, 2665–2670.

[249] L. Xu, M. Raabe, M. M. Zegota, J. C. F. Nogueira, V. Chudasama, S. L. Kuan, T. Weil, *Org Biomol Chem* **2020**, *18*, 1140–1147.

[250] D. L. Rabenstein, K. H. Weaver, *J Org Chem* **1996**, *61*, 7391–7397.

[251] J. P. M. António, R. Russo, C. P. Carvalho, P. M. S. D. Cal, P. M. P. Gois, *Chem Soc Rev* **2019**, *48*, 3513–3536.

[252] S. J. Sonawane, R. S. Kalhapure, T. Govender, *European Journal of Pharmaceutical Sciences* **2017**, *99*, 45–65.

[253] S. Murugappan, S. Dastari, K. Jungare, N. M. Barve, N. Shankaraiah, *J Mol Struct* **2024**, *1307*, 138012.

[254] D. H. Pliura, B. J. Bonaventura, R. A. Smith, P. J. Coles, A. Krantz, *Biochemical Journal* **1992**, *288*, 759–762.

[255] Y. Dai, L. Hedstrom, R. H. Abeles, *Biochemistry* **2000**, *39*, 6498–6502.

[256] E. Mons, R. Q. Kim, B. R. van Doodewaerd, P. A. van Veelen, M. P. C. Mulder, H. Ovaa, *J Am Chem Soc* **2021**, *143*, 6423–6433.

[257] S. Vankadara, M. D. Dawson, J. Y. Fong, Q. Y. Oh, Q. A. Ang, B. Liu, H. Y. Chang, J. Koh, X. Koh, Q. W. Tan, J. Joy, C. S. B. Chia, *ACS Med Chem Lett* **2022**, *13*, 1345–1350.

[258] D. G. Silva, J. F. R. Ribeiro, D. De Vita, L. Cianni, C. H. Franco, L. H. Freitas-Junior, C. B. Moraes, J. R. Rocha, A. C. B. Burtoloso, P. W. Kenny, A. Leitão, C. A. Montanari, *Bioorg Med Chem Lett* **2017**, *27*, 5031–5035.

[259] R. Ettari, L. Tamborini, I. C. Angelo, N. Micale, A. Pinto, C. De Micheli, P. Conti, *J Med Chem* **2013**, *56*, 5637–5658.

[260] B. Bai, E. Arutyunova, M. B. Khan, J. Lu, M. A. Joyce, H. A. Saffran, J. A. Shields, A. S. Kandadai, A. Belovodskiy, M. Hena, W. Vuong, T. Lamer, H. S. Young, J. C. Vederas, D. L. Tyrrell, M. J. Lemieux, J. A. Nieman, *RSC Med Chem* **2021**, *12*, 1722–1730.

[261] M. A. Al-Sha'er, M. A. Khanfar, M. O. Taha, *J Mol Model* **2014**, *20*, 2080.

[262] L. Borissenko, M. Groll, *Chem Rev* **2007**, *107*, 687–717.

[263] A. Latorre, T. Schirmeister, J. Kesselring, S. Jung, P. Johé, U. A. Hellmich, A. Heilos, B. Engels, R. L. Krauth-Siegel, N. Dirdjaja, L. Bou-Iserte, S. Rodríguez, F. V. González, *ACS Med Chem Lett* **2016**, *7*, 1073–1076.

[264] S. Royo, S. Rodríguez, T. Schirmeister, J. Kesselring, M. Kaiser, F. V. González, *ChemMedChem* **2015**, *10*, 1484–1487.

[265] K. Bush, P. A. Bradford, *Cold Spring Harb Perspect Med* **2016**, *6*, a025247.

[266] P. C. Sharma, A. Sinhmar, A. Sharma, H. Rajak, D. P. Pathak, *J Enzyme Inhib Med Chem* **2013**, *28*, 240–266.

[267] R. D. A. Wilkinson, S. M. Magorrian, R. Williams, A. Young, D. M. Small, C. J. Scott, R. E. Burden, *Oncotarget* **2015**, *6*, 29725–29739.